TRANSFER FUNCTION APPROACHES TO THE ONE-DIMENSIONAL THERMODYNAMICS OF CLASSICAL MAGNETS, AND THE LONG-RANGE DIPOLE INTERACTION IN RARE-EARTH PYROCHLORES

by

RICHARD MASON

A thesis submitted to
The University of Birmingham
for the degree of
DOCTOR OF PHILOSOPHY

School of Physics and Astronomy
The University of Birmingham

January 5, 2015

Abstract

We work on two main topics; thermodynamics of one dimensional classical magnetic models and the long range dipolar interaction on the pyrochlore lattice. These are somewhat unconnected, and so we will summarise them separately.

We will use the transfer function technique to solve the plane rotator with nearest and next nearest neighbour interactions, the continuous spin Ising model with nearest neighbour interactions and a magnetic field, and the Heisenberg model with nearest and next nearest neighbour interactions, all exactly. For the plane rotator model and the Heisenberg, we find that the models with nearest and next nearest neighbour interactions are thermodynamically equivalent to models with nearest neighbour interactions and a magnetic field. We investigate the zero temperature phase transition in all models. For the case of the plane rotator and Heisenberg models, this is between a pure antiferromagnet and a spiral state, and for the continuous Ising model it is between a ferromagnet and an antiferromagnet. We investigate the thermal effects on the phase transition, and find a fluctuation driven crossover (rather than transition due to the dimensionality) which stabalises collinear states. We also investigate magnetisation of the models as well, and find that the continuous spin Ising model (particularly) exhibits strong field dependence, staying magnetised well beyond the associated temperature of the field.

We then move from the exact calculations to approximate solutions of the transfer function problem in order to investigate the one to two dimensional crossover for the plane rotator and the continuous spin Ising models. For the plane rotator, we use the trapezium rule, and therefore investigate the p-state clock model, a model that has been studied in its own right as it displays two phase transitions. We find two peaks in the specific heat, which are not thought to be responsible for the transition. We find a single transition for the continuous spin Ising model which we believe to be essentially the same as the Ising transition, but with a reduced critical temperature.

We then move on to the pyrochlore lattice, studying a family of compounds $R_2M_2O_7$ with R=Gd, Tb, Ho and Dy, and M= Ti or Sn. We model all these with a classical model containing nearest and third nearest neighbour Heisenberg model, crystal field interactions, and the dipolar interactions. We develop a new technique to calculate the dipole spin-spin interaction strengths directly in real space, and use a minimisation procedure to optimise the model. We find the associated phase diagram subjected to states containing no more than 32 distinct spins. We find states for all the compounds, which agree with experiment for all except $Gd_2Ti_2O_7$ which remains controversial.

Contents

List of Figures

Chapter 1

INTRODUCTION AND BASIC MAGNETISM

1.1 Thesis Overview

This thesis has two main strands, which we will deal with largely separately. We will be interested in the thermodynamics of one dimensional classical magnetism, and groundstates of long range interactions in three dimensions.

We will be concerned with condensed matter systems, in which materials are made which form fully ordered lattices. There can be many elements in these compounds which interleave in some way. The electrons in the compound can be delocalised, in which the electrons are not associated with a given element and move around forming a metal. On the other hand, they can localise, becoming bound to a particular type of atom in the compound (called an insulator), which we shall be interested in. When (at least) one of the elements has a residual magnetic moment from the localised electrons these moments can have structure. We will begin with introducing the basics of lattices and the way these moments are generated from Sec.1.2.1 onwards. It is the structure of the moments, the ordering of them, which we will be interested in. At high temperature, the moments are not correlated, and given the direction of one moment, we know very little about moments a long way away. At low temperature, the moments collectively align, and if they align across the whole system we get magnetism. We will be concerned with how this process

happens, but we will be working with a one dimensional model of this process. In three dimensions this process may occur spontaneously at some temperature, called a phase transition. This is not allowed in one dimension (at finite temperature), and so we will essentially have no phase transitions, but we may still observe the correlations that would become the order increase as we reduce the temperature. We will introduce the basics of thermodynamics, and the basics of the technique that we use in Chapter.2.

We will be studying three one-dimensional models at the same time, using related but different new techniques. Though some aspects of the technique have been used before, we extend the results found for each of the models that we study. Originally, this was motivated by trying to model $Ho_2SbGa_xCr_{1-x}O_7$, which has isotropic Cr^{3+} spins. As the concentration of chromiums is varied, we move between regimes; uncoupled chromiums, weakly coupled chains, and a fully three-dimensional (though unknown) geometry which gives us experimental access to the percolation threshold. We will not investigate the fully three dimensional geometry at all, but will exactly solve the thermodynamics for the other two regimes. We will begin by solving small clusters of chromiums, which will begin with Curie-Weiss and then is (trivially) extended beyond to include more neighbours. We show the fitting that one could do in order to extract out the density of small clusters from measuring the bulk susceptibility experimentally. We then move on to the regime where we have one dimensional chains of chromiums. Due to the isotropy of the chromium spins, we may model them with a Heisenberg interaction and attempt investigate the thermodynamics of such a model. We include a magnetic field (or second neighbour interactions) as we wish to investigate the magnetisation of the compound. Once we have our exact analysis for the Heisenberg model, we study other magnetic models in

one dimension that are related but solve in slightly different ways. We look at three one dimensional models; the plane rotator, the continuous spin Ising model, and the Heisenberg model. We exactly solve these one dimensional models in Chapters.3, 4 and 5 respectively using transfer functions. We put the Heisenberg model last in this thesis because it is more complicated than the other models, but was originally solved first due to the motivation.

The plane rotator and Heisenberg models have been solved previously, but only for nearest neighbour interactions [9, 10]. Here, we extend the result to nearest and next nearest interactions for these models, and nearest neighbour and magnetic field for all three models. We find that when the Hamiltonian and the spins exhibit the same symmetry, there exists a floating basis which maps nearest neighbour interactions on to magnetic fields, and next nearest neighbour interactions on to nearest neighbour interactions. There is very little previous work on the continuous spin Ising model. We do not find a closed form solution for the nearest neighbour model due to the anisotropy between the spin and Hamiltonian symmetry. By including two interactions, we may investigate frustration, the thermal fluctuations around a zero temperature first order transitions and the magnetisation properties of all the models, which we do in Chapter 6. To this end we find the phase diagram for all three classical models which are very similar and are entirely new. The extensions to Curie Weiss and the Heisenberg model were intended to be used to fit data for $Ho_2SbGa_xCr_{1-x}O_7$, and although that has not been done, more work has been carried out in that area elsewhere [11], along with using the exact solutions to investigate the compound. Although we investigated the model due to this specific compound, there exist other compounds that one can use the models to investigate [12, 13]. For example, the nearest and next-nearest neighbour Heisenberg model can

be used to model $SrGd_2O_4$ [14,15], in which there are chains of isotropic gadoliniums with two natural bond distances. We may use the other models to investigate this family of rare earth compounds, such as $SrTb_2O_4$ and $SrHo_2O_4$, though no further theoretical work has been done in this area [16].

This is when the motivation for studying thermodynamics takes a departure from attempting to model the compound, to trying to investigate finite temperature phase transitions. These are strictly prohibited in one dimension, and so we use the one to two dimensional crossover. There exist very few solutions to two dimensional models. The only model that has been *fully* solved in two dimensions is the Ising model (and related Potts models). We consequently use our technique to investigate other non-trivial models, though only approximately. Again, we could use the calculations to fit classical magnetism in two dimensions [17–19], but here we only investigate the theoretical side. The geometry we use is unique, though similar ones have been investigated before. In chapter 7 we will consider the one to two dimensional crossover, using similar techniques to the previous sections, though we work numerically rather than exactly. We first look at the Ising model, and find a peak in the specific heat which grows with increasing system size at the (known) transition temperature. We then look two of the continuous models. No *exact* solutions to the model exist in two dimensions, though various limits are known exactly [20]. We first investigate the clock model, which is a discrete version of the plane rotator and is thermodynamically related. We find two anomalies in the specific heat, which appear to increase in height as we enlarge the system size, but we cannot say that they diverge. We believe the lower peak is associated with the discreteness, while the upper peak is the underlying peak for the plane rotator. We use mean field theory to investigate the lower peak, using the Ising model to describe the transition, and

find good agreement. We then investigate the continuous spin Ising model which has one anomaly in the specific heat which diverges much more quickly than for the clock model. We use mean field theory to model the phase transition and find excellent agreement. More work on using the technique to get to two dimensions will appear in [21] and [22].

We now move on to the second part of the thesis. We will be looking at a family of compounds; rare earth pyrochlores, of the form $R_2M_2O_7$ where R is a rare earth compound, M is a transition metal and O is oxygen. We detail the experiments and compounds in Chapter 8. The magnetic moments align because there are *interactions* between them, which come in several styles; exchange, anisotropy and the ever present dipolar interaction, as discussed more in §.1.2.4 when we introduce the basics of magnetism. These interactions decide what the orientation of the moments should be. We will be working with the dipolar interaction, which, it turns out, causes moments at very long range to still interact. It is this long range interaction which is the difficult part, in which a single moment interacts with many others over a long range, and we will be concerned with controlling this interaction in order to find the types of ordering that the interaction requires.

This work was originally motivated by further investigations into $Gd_2Ti_2O_7$, detailed in [23], for which the dipolar interaction is the dominant interaction which can lift the degeneracy left by the geometric frustration. We study several compounds here, and attempt to model them with one classical model. This model contains several terms, one of which is the dipolar interaction, which contains long range interactions. In order to solve our model, we use a real space minimisation which maintains the spin length constraint *automatically*. We develop a new technique to calculate the dipolar interaction matrix elements, calculating them directly in real

space, which we go through in Chapter.9. Most importantly, the new technique separates out the shape anisotropy from the local dipolar spin-spin interaction. The resulting continuum problem for the shape anisotropy is left unsolved, though we work in the spherical crystal approximation which provides a known reference (which we go through in Sec.9.4.1). The usual technique of Ewald is also summarised in Chapter.9, which we use as a comparison, but it does not separate out the shape dependence which gives rise to complications at the origin in reciprocal space. We discuss the consequences of these complications, though more work is done in [24]. We find the zero temperature phase diagram of the classical model in Chapter 10, and put the compounds in the relevant regions of parameter space, finding good agreement with experiment. The phase diagram is entirely new, and also provides a prediction for the groundstates for two of the compounds that we study; $Gd_2Ti_2O_7$ and $Tb_2Ti_2O_7$.

1.2 Introduction

Spontaneously broken symmetries are an area of great interest. There are many examples of where this occurs in nature. For example, the liquid to solid transition is where the translational invariance is broken and becomes discrete spontaneously. In the liquid phase, atoms are essentially random, but form small clusters. In the solid phase the atoms form a well ordered structure, becoming long range ordered. If one knows where one atom is, one knows where the other atoms must be (on average) due to the broken symmetry. We will be studying spontaneously broken symmetries for the special case of magnetism, where the local spin symmetry on every site is broken by the magnetisation vector. We will be studying how this magnetism is formed by understanding the crystal structure and the relevant interactions which

drive the magnetism. We will also be interested in how temperature affects the magnetism; what happens when you heat a magnet up or cool it down?

We begin by introducing lattices, giving a few relevant examples and concepts. We then discuss models on lattices; how the electrons interact and the effective model we get with respect to the spin coming from open shells. We then solve the effective model that we generate in several situations, indicating the types of magnetism we may generate from our model.

We will be considering compounds made up of several elements. If one of the elements has an open shell in the compound, we have the possibility of magnetism; the electron spins which are not paired may fluctuate, generating some *collective* order which maybe the magnetism. We will only be considering insulators, in which the electrons are localised to a given site, giving us a definite magnetisation available per site.

1.2.1 Lattices

For the entirety of this work we will work with lattices, and so we introduce them here in general, before we use particular examples. The compounds that we shall study form ordered lattices, and when they have several elements these ordered lattices interpenetrate. We begin with considering one element only, and also begin with the simplest type of lattices; bipartite. To motivate this idea, we begin with the linear chain as depicted in Fig.1.1. We note that for the linear chain we can decompose the lattice into two sites, say A and B sites, and when we do this every neighbour of A is a B and vice versa; this property is known as bipartite. We call all sites which are A *sublattice* A and all sites which are B sublattice B, which means we decompose our full linear chain lattice into two sublattices. For general lattices

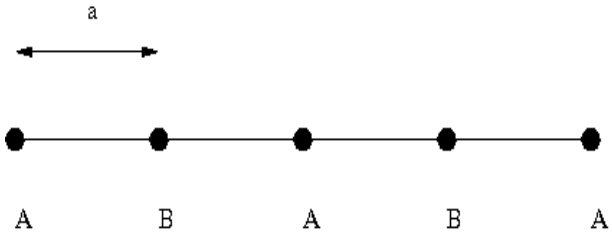

Figure 1.1: Linear chain with lattice spacing a split into A and B sublattices.

this is not possible, which causes problems for solving the magnetic (or metallic) interactions on the lattices. We now move on to other types of lattice. The square

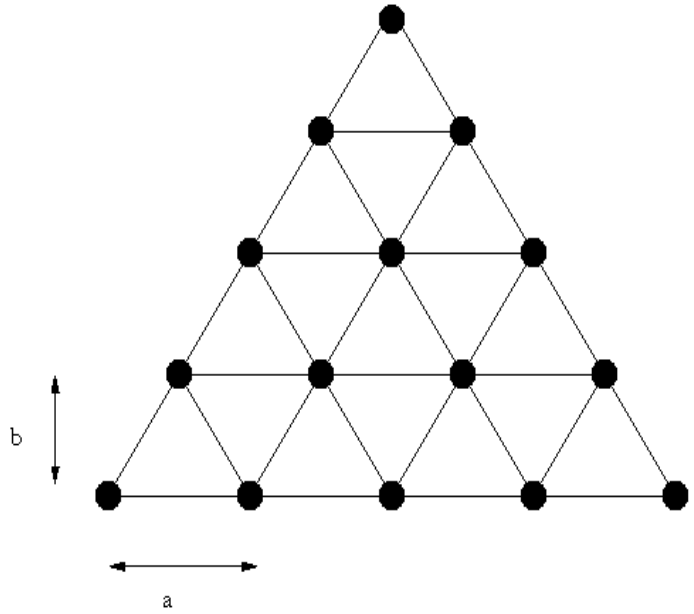

Figure 1.2: Triangular lattice with lattice spacings a in the $\hat{\mathbf{x}}$-direction and b in the $\hat{\mathbf{y}}$-direction.

lattice is clearly bipartite, and so we move on to the triangular lattice, where we cannot divide it into two sublattices seen in Fig.1.2. At this point it is useful to introduce *primitive vectors* and the *unit cell*. The unit cell is the smallest cell we can draw which we then tile to generate the full lattice and we use the primitive vectors to tell us how to tile. The unit cell is also the *largest* repeating cell that we can draw which when we tile does not overlap. For the square lattice, this is clearly

a square of equal size to the lattice parameters. For the case of the triangular lattice, the unit cell also contains one atom, and the unit vectors are given by

$$\begin{aligned} \mathbf{v}_1 &= (a, 0) \\ \mathbf{v}_2 &= \left(\frac{a}{2}, b\right), \end{aligned}$$

for the perfect triangular lattice with $b = \frac{\sqrt{3}}{2}a$. If we use the primitive vectors $\mathbf{v_i}$ then we can tile everywhere on the lattice. A Bravais lattice is one which is defined by the unit cell and the primitive vectors, such that *any* site on the lattice can be created by using

$$\mathbf{R_n} = n_1\mathbf{v}_1 + n_2\mathbf{v}_2,$$

in two dimensions, and

$$\mathbf{R_n} = n_1\mathbf{v}_1 + n_2\mathbf{v}_2 + n_3\mathbf{v}_3,$$

in three dimensions, where n_1, n_2 and n_3 are integers and $\mathbf{v}_1$, $\mathbf{v}_2$ and $\mathbf{v}_3$ are the primitive vectors. We now move on to three dimensional lattices as we will be using

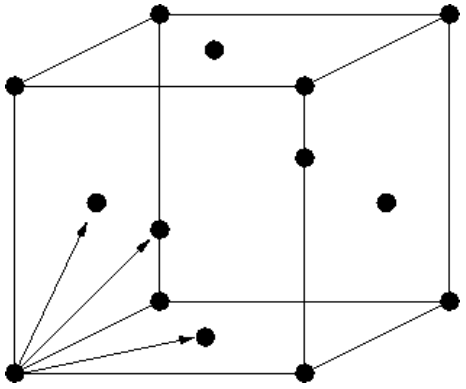

Figure 1.3: Face centered cubic lattice

these later, and we will also use $a = 1$ from now on. The simplest case is the cubic lattice, which is trivial. For the cubic lattice the unit cell is a cube around one spin,

and the primitive vectors are the Cartesian axes, just as in the square lattice. We now consider more complicated lattices, which will be relevant for later. We begin with face-centered-cubic lattice shown in Fig.1.3, which is essentially a cubic lattice but with extra atoms on each face. The primitive vectors are (as depicted in the diagram) given by

$$\begin{aligned} \mathbf{v}_1 &= \left(0, \frac{1}{2}, \frac{1}{2}\right) \\ \mathbf{v}_2 &= \left(\frac{1}{2}, 0, \frac{1}{2}\right) \\ \mathbf{v}_3 &= \left(\frac{1}{2}, \frac{1}{2}, 0\right) \end{aligned}$$

We quickly mention body centered cubic, which like face centered cubic is essentially cubic, but has an extra atom in the center of each cube. The final lattice that we mention is the pyrochlore lattice, which is fundamentally the face centered cubic, but each "atom" is made up of four; it has four atoms per unit cell. These four atoms form tetrahedra which corner share on the underlying face centered cubic lattice. The primitive vectors are the same, but there are four sublattices which are not connected by the primitive vectors, but by sublattice vectors. It is interesting to note here that face centered cubic can be regarded as a cubic lattice with four atoms per unit cell as well, which will be used later. The pyrochlore lattice is detailed much more fully in Sec.8.

We now move on to the *reciprocal lattice*, which will be essential for later calculations, although we cannot directly motivate it here. It is defined by

$$e^{i\mathbf{k}_i.\mathbf{R}_n} = 1,$$

where $\mathbf{R}_n$ is any site on the real (Bravais) lattice and $\mathbf{k}_i$ generate the reciprocal lattice. To solve this equation, we require

$$\mathbf{k}_i.\mathbf{R}_n = 2\pi \tag{1.2.1}$$

which we may solve using

$$\begin{aligned}
\mathbf{k}_1 &= 2\pi \frac{\mathbf{v}_2 \wedge \mathbf{v}_3}{\mathbf{v}_1.(\mathbf{v}_2 \wedge \mathbf{v}_3)} \\
\mathbf{k}_2 &= 2\pi \frac{\mathbf{v}_3 \wedge \mathbf{v}_1}{\mathbf{v}_1.(\mathbf{v}_2 \wedge \mathbf{v}_3)} \\
\mathbf{k}_3 &= 2\pi \frac{\mathbf{v}_1 \wedge \mathbf{v}_2}{\mathbf{v}_1.(\mathbf{v}_2 \wedge \mathbf{v}_3)},
\end{aligned}$$

where v_i are the primitive vectors for the real space lattices. If we pick on a particular example then we see that

$$e^{i\mathbf{k}_1.\mathbf{v}_1} = e^{2\pi i \frac{\mathbf{v}_1.(\mathbf{v}_2 \wedge \mathbf{v}_3)}{\mathbf{v}_1.(\mathbf{v}_2 \wedge \mathbf{v}_3)}} = 1$$

We also see that

$$\mathbf{G}_x = x_1\mathbf{k}_1 + x_2\mathbf{k}_2 + x_3\mathbf{k}_3$$

If we require that

$$e^{i\mathbf{R}_n.\mathbf{G}_x} = e^{2\pi i\left[x_1 \frac{\mathbf{v}_2 \wedge \mathbf{v}_3}{\mathbf{v}_1.(\mathbf{v}_2 \wedge \mathbf{v}_3)} + x_2 \frac{\mathbf{v}_3 \wedge \mathbf{v}_1}{\mathbf{v}_1.(\mathbf{v}_2 \wedge \mathbf{v}_3)} + x_3 \frac{\mathbf{v}_1 \wedge \mathbf{v}_2}{\mathbf{v}_1.(\mathbf{v}_2 \wedge \mathbf{v}_3)}\right][n_1\mathbf{v}_1 + n_2\mathbf{v}_2 + n_3\mathbf{v}_3]} = 1,$$

for all $\mathbf{G}_x$ and $\mathbf{R}_n$, then x_1, x_2 and x_3 must be integer, and so the reciprocal lattice of a Bravais lattice is Bravais itself, and therefore

$$e^{i\mathbf{G}_m.\mathbf{R}_n} = 1 \ \ \forall \ \ m, n$$

We could also solve Eq.1.2.1 using

$$[\mathbf{k}_1, \mathbf{k}_2, \mathbf{k}_3]^T = 2\pi[\mathbf{v}_1, \mathbf{v}_2, \mathbf{v}_3]^{-1} \tag{1.2.2}$$

if we want to work in dimensions other than 3. We introduced both the face centered cubic lattice and the body centered cubic lattice because it turns out that they are reciprocal lattices of one another.

We have provided a brief summary of the results we will use for lattices. We will use the reciprocal lattice extensively later for calculations, while understanding the lattice itself will also be part of understanding the compounds we will study. We now move on to magnetism on lattices, so far we have only dealt with the "nuclear" part.

1.2.2 Atomic Physics

We now briefly discuss atomic physics, focusing on the f-block elements as these will be studied the most. This will provide the picture of how the elements in free space behave, although this picture is complicated when we consider a lattice. Each site contains electrons, each with total spin ($\mathbf{S}$) and orbital angular momentum ($\mathbf{L}$), which leads to total angular momentum $\mathbf{J} = \mathbf{L} + \mathbf{S}$. Hund's rules control how $\mathbf{S}$, $\mathbf{L}$ and $\mathbf{J}$ order. The largest energy scale (Hund's first rule) forces the total spin of an open shell to be maximal. The second largest (Hund's second rule) forces the orbital angular momentum to be minimised, subject to Pauli exclusion. Finally, the smallest energy scale (Hund's third rule) means the total angular momentum is minimised ($\mathbf{L}$ and $\mathbf{S}$ are anti-parallel) for the first half of the series, and they are maximised (parallel) for the second half of the series.

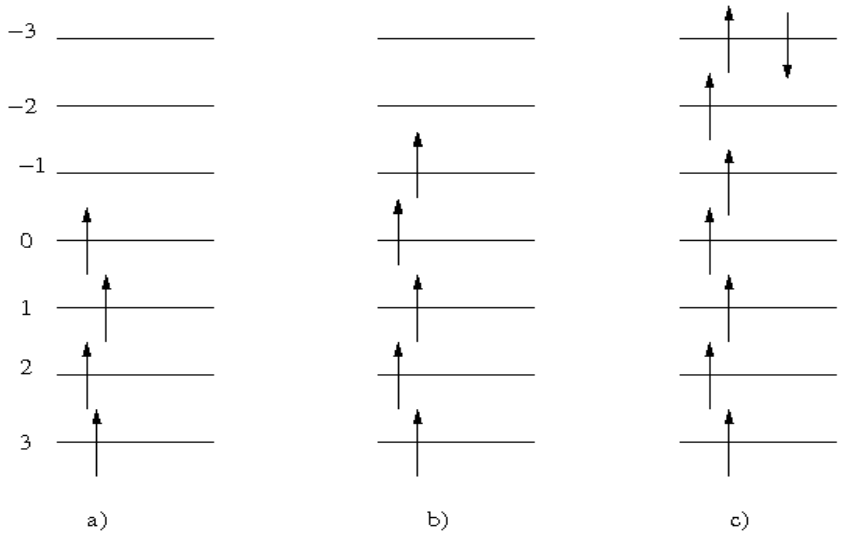

Figure 1.4: Sketch of f-electron atoms to indicate the three Hund's rules. The L^z state labels are given on the left.

To be clear, see Fig.1.4, where we sketch out the three rules. In Fig.1.4 a) we see that the spins are all aligned, maximising Hund's first rule. When we add another electron Fig.1.4 b), we see that it goes in parallel to the other spins, and in to the state with the lowest angular momentum. Finally, in Fig.1.4 c) we see that when we half fill, the next electron goes in such that **J** is maximised, that is it goes in the lowest angular momentum state to maximise the residual **L**. The f-electrons were chosen as Hund's rules are dominant in these systems; for transition metals the crystalline electric field tends to dominate so that Hund's second rule is over turned. The crystal field effect stems from the Coulomb interaction of the different orbitals between the various atoms. For example, transition metals in a cubic oxygen cage provide a crystal field interaction which splits the orbitals into two types; the t_{2g} and the e_g. The orbital *shape* notices the local charge structure surrounding it in a given compound, making some orbitals better than others (or linear combinations as is the case). For the case of f electrons, the orbital that is picked couples to the

total spin degree of freedom and makes the total spin anisotropic but it does not over turn Hund's third rule. We therefore think of the f-electron systems as large J spins, as J remains a good quantum number unlike transition metals.

1.2.3 The Hubbard Model

The Hubbard model [25,26] is a modification to the tight-binding model [27], which includes electron-electron interactions. It attempts to provide a model which gives either a localised moment (which we will be interested in) in the limit, or a band theory in the other [28]. It is given by

$$H = \sum_{<jj'>\sigma\alpha\beta} [c^{\dagger}_{j\sigma\alpha} c_{j'\sigma\beta} t^{\alpha\beta}_{jj'} + c^{\dagger}_{j'\sigma\alpha} c_{j\sigma\beta} (t^{\alpha\beta}_{jj'})^*] + \sum_{j\alpha\beta} U_{\alpha\beta;j} c^{\dagger}_{j\sigma\alpha} c_{j\sigma\alpha} c^{\dagger}_{j\bar{\sigma}\beta} c_{j\bar{\sigma}\beta}$$

Where $c^{\dagger}_{j\sigma\alpha}$ ($c_{j\sigma\alpha}$) creates (annihilates) an electron on site j, with spin σ in the orbital α, $t^{\alpha\beta}_{jj'}$ is the exchange interaction, although usually it is assumed translationally invariant, and $U_{\alpha\beta;j}$ is the coulomb interaction for two spins sitting on the site j in orbitals α and β, which again is usually approximated to be site independent. The hopping term drives the electrons to delocalise, while the coulomb term drives localisation as it seeks to prevent multiple occupation [29].

1.2.4 From Hubbard to Heisenberg

We now show how to get the basic Heisenberg interaction from the Hubbard model [30,31], following [32]. We consider the one band, translationally invariant, Hubbard model given by

$$H = -t \sum_{<jj'>\sigma} c^{\dagger}_{j\sigma} c_{j'\sigma} + U \sum_{j} c^{\dagger}_{j\uparrow} c_{j\uparrow} c^{\dagger}_{j\downarrow} c_{j\downarrow}$$

$$\equiv \quad -tH_1 + UH_0,$$

where the first sum runs over all *pairs*, and so the complex conjugate is taken care of by the sum. We will work at *exactly* half filling, where we have N sites with N electrons. We will consider the Coulomb term U to be the largest energy scale, and indeed to begin with $U = \infty$. In this situation we may only have one electron per site, though the spin degree of freedom is not chosen. We then use second order perturbation theory around this state in t to lift the spin degeneracy. However, first we offer a simple picture to suggest the type of spin interaction that we expect, before we derive the result. Consider two sites with one electron on each. If the two spins are parallel, then they cannot hop and so they can't perturbatively gain the hopping energy; Pauli exclusion. If the spins are anti-parallel, then we can virtually hop, paying the energy penalty U, but gaining the hopping energy. We therefore expect an effective interaction of the form

$$H = J \sum_{<jj'>} \hat{\mathbf{S}}_j . \hat{\mathbf{S}}_{j'}, \tag{1.2.3}$$

where $\hat{\mathbf{S}}_j$ is the spin on site j and J is the energy scale of this interaction. This model is known as the Heisenberg model, and we now derive it from the Hubbard model. We use the eigenstates of H_0 Hamiltonian, and we project out doubly occupied sites; we never have two electrons on the same site, though we will virtually excite into this state, provided we end up back with only one electron per site. Note that the hopping Hamiltonian only hops one way, and so we necessarily must have H_1^2 in

order to hop back. However, if we write second order perturbation theory we get

$$-\frac{t^2}{U}\sum_m \langle n|H_1|m\rangle\langle m|H_1\langle n| = -\frac{t^2}{U}\langle n|H_1^2|n\rangle,$$

where the last equality came from the identity operator

$$\sum_m |m\rangle\langle m| \equiv \mathbf{I},$$

which is true for our complete set of eigenstates of H_0, and we use $\epsilon_n - \epsilon_m \equiv -U$, the energy penalty for virtual double occupancy. We therefore write out H_1^2

$$H_1^2 = \sum_{<ii'>}\sum_{<jj'>}\sum_{\sigma\tau} c_{i\sigma}^\dagger c_{i'\sigma} c_{j\tau}^\dagger c_{j'\tau}$$

In order to stay in the one particle per site subspace the electrons must hop and hop back, and so we notice that we must have $i = j'$ and $i' = j$, so we get

$$H_1^2 = \sum_{<jj'>}\sum_{\sigma\tau} c_{j\sigma}^\dagger c_{j'\sigma} c_{j'\tau}^\dagger c_{j\tau} \tag{1.2.4}$$

We then use the usual commutation relations on Eq.1.2.4 to find

$$H_1^2 = \sum_{<jj'>}\sum_{\sigma\tau} c_{j\sigma}^\dagger c_{j\tau}\left[\delta_{\sigma\tau} - c_{j'\tau}^\dagger c_{j'\sigma}\right]$$

We carry out the sum over τ and write it out explicitly as

$$H_1^2 = \sum_{<jj'>\sigma} c_{j\sigma}^\dagger c_{j\sigma} + c_{j\bar{\sigma}}^\dagger c_{j\bar{\sigma}} - \underbrace{c_{j\sigma}^\dagger c_{j\sigma} c_{j'\sigma}^\dagger c_{j'\sigma}}_{1} - \underbrace{c_{j\sigma}^\dagger c_{j\bar{\sigma}} c_{j\bar{\sigma}}^\dagger c_{j\sigma}}_{2}$$

We now define the following spin operators

$$\begin{aligned} S_j^z &\equiv \frac{1}{2}[c_{j\uparrow}^\dagger c_{j\uparrow} - c_{j\downarrow}^\dagger c_{j\downarrow}] \\ S_j^\sigma &\equiv c_{j\sigma}^\dagger c_{j\bar{\sigma}}, \end{aligned}$$

from which we see that the term labelled with 2 can be written as

$$\sum_\sigma c_{j\sigma}^\dagger c_{j\bar{\sigma}} c_{j\bar{\sigma}}^\dagger c_{j\sigma} = S_j^+ S_{j'}^- + S_j^- S_{j'}^+$$

For the term labelled 1, we explicitly write out the sum over σ, and define the number operator $n_{\sigma,j} \equiv c_{j\sigma}^\dagger c_{j\sigma}$

$$\begin{aligned} \sum_\sigma c_{j\sigma}^\dagger c_{j\sigma} c_{j'\sigma}^\dagger c_{j'\sigma} &= n_{j\uparrow} n_{j'\uparrow} + n_{j\downarrow} n_{j'\downarrow} \\ &= \frac{1}{2}\left[(n_{j\uparrow} + n_{j\downarrow})(n_{j'\uparrow} + n_{j'\downarrow}) + (n_{j\uparrow} - n_{j\downarrow})(n_{j'\uparrow} - n_{j'\downarrow})\right] \\ &= 2S_j^z S_{j'}^z + \frac{1}{2} n_j n_{j'}, \end{aligned}$$

where $n_j = n_{j\uparrow} + n_{j\downarrow}$ is the occupation per site, which in the one particle per site subspace is 1. Finally, we note that

$$2\mathbf{S}_j.\mathbf{S}_{j'} = 2S_j^z S_{j'}^z + S_j^+ S_{j'}^- + S_j^- S_{j'}^+,$$

and therefore we get

$$H_1^2 = 2 \sum_{<jj'>} \mathbf{S}_j.\mathbf{S}_{j'} - \frac{1}{4},$$

and so we recognize that this is the same as the expected Heisenberg model, if we identify $J \equiv \frac{2t^2}{U}$. We now comment on this model, as it will form a central part of our

study. We considered the model for the one band Hubbard model, and indeed there can be (and are) orbital complications. It was also only derived in terms of spin-$\frac{1}{2}$, but it remains the model for large S, even though the interaction could be more complicated. Another important feature is that the model here is purely quantum, but we will mostly solve the classical limit of the model. We have the constraint $S^2 = S(S+1)$, and we shall mainly work in the limit that $S \to \infty$, where the spins become classical *vectors* in three dimensions under a constraint. It is also important to note that we derived the isotropic nearest neighbour Heisenberg model, but in fact more complicated interactions can (and will) be studied. We therefore consider the more general spin model

$$H = \sum_{jj'} \sum_{\alpha\beta} J_{jj'}^{\alpha\beta} S_j^{\alpha} S_{j'}^{\beta},$$

where the labels (j, j') represent the lattice positions, and (α, β) represent the Cartesian directions of the spins (and interaction strength).

1.3 Solutions to the Heisenberg Model

We now offer some exact solutions to the Heisenberg (some of which have been offered before [33]), though we will work in the classical limit. In this limit, the spins are taken to be commuting vectors in three dimensions, and the model is given by

$$H = \frac{J}{2} \sum_{<jj'>} \hat{\mathbf{S}}_j . \hat{\mathbf{S}}_{j'},$$

where $\hat{\mathbf{S}}_j$ is a unit vector on the site j. It is now useful to introduce an important idea; the Bloch transform which uses the translational invariance of the model to

solve it. We define the Bloch transform as

$$\hat{\mathbf{S}}_j = \frac{1}{\sqrt{N}} \sum_{\mathbf{k}} e^{i\mathbf{k}.\mathbf{R}_j} \mathbf{S}_{\mathbf{k}}, \tag{1.3.1}$$

where N is the number of sites in the system, and $\mathbf{k}$ are so called Bloch momenta. If we first consider the one dimensional Heisenberg model and substitute Eq.1.3.1 into it, we find

$$H = J \sum_{k} \cos k \;\; \mathbf{S}_k \mathbf{S}_{-k}$$

More generally, in more than one dimension we find

$$H = \frac{J}{2} \sum_{\mathbf{k}} \gamma(\mathbf{k}) \mathbf{S}_{\mathbf{k}} \mathbf{S}_{-\mathbf{k}},$$

where $\gamma(\mathbf{k})$ is called the structure factor, given by

$$\gamma(\mathbf{k}) = \sum_{\langle 0j \rangle} e^{i\mathbf{k}.\mathbf{R}_j},$$

and is a sum over the nearest neighbours to site 0. Note that the interaction is now diagonal in $\mathbf{k}$-space. For one dimension this clearly reduces to $\cos k$ as given above. In order to minimise the Hamiltonian, we find the minimum of the structure factor as a function of $\mathbf{k}$ which (can) yield the groundstate. The minimum of the structure factor is clearly also controlled by the sign of the interaction strength J. Although we have not discussed it, J can have either sign and need not only provide anti-ferromagnetism, though it is often hard to explain ferromagnetic coupling as one expects Pauli blocking to dominate. When J is positive, the minimum in the one dimensional structure factor is at $k = \pi$, while negative J puts the minimum at $k = 0$. If we now interpret these states from the Bloch transform, it is clear that

when $k = \pi$ the spins on each site are of opposite sign, while when $k = 0$ all the spins have the same sign. It is very important to note here that we have not Bloch transformed the constraint, but that these two solutions happen to be consistent with the constraint, but in general this is not true. We now consider a model where this idea fails.

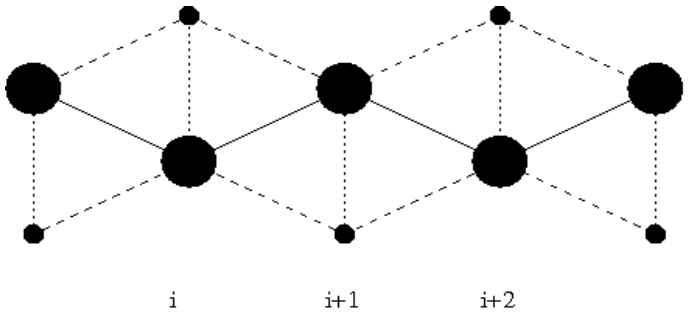

Figure 1.5: Example of two atoms per unit. The larger circles are on one sublattice, the smaller circles are on the other.

Consider the one dimensional case, but with two atoms per unit cell, depicted in Fig.1.5. Although the lines are depicted differently, they will all have the same exchange strength J. The trick is to generalise the structure factor to a *matrix* which represents each sublattice and the relative coupling. We write the Heisenberg interaction as

$$H = J \sum_{\mathbf{k}\alpha\alpha'} \gamma_{\alpha\alpha'}(\mathbf{k}) \mathbf{S}^{\alpha}_{\mathbf{k}} . \mathbf{S}^{\alpha'}_{-\mathbf{k}}$$

where α represents the sublattice index. For the model drawn above, we use a Bloch transform to find the matrix of the form

$$S^{\alpha}_{j} = \frac{1}{\sqrt{N}} \sum_{k} e^{ik(R_j + c_\alpha)} S^{\alpha}_{k},$$

where c_α is the vector connecting the sublattices (in general). Here however, we are performing a one dimensional transform where all the length scales are equivalent,

and we may therefore make the two sublattices in phase $c_\alpha = 0$, but in general one cannot. This gives us

$$\gamma_{\alpha\alpha'}(k) = \begin{pmatrix} \cos k & \frac{1}{2} + \cos k \\ \frac{1}{2} + \cos k & 0 \end{pmatrix}$$

We then minimise the eigenvalues over k to find that the minimum is at $k = 0$ and would correspond to ferromagnetism. However, this solution is inconsistent with the spin constraint, and is therefore not relevant. One needs a linear combination of both eigenvectors (which is k-dependent of the structure factor in order to maintain the constraint. For example, at $k = 0$, we get the eigenvectors

$$\propto \begin{pmatrix} 1 \pm \sqrt{10} \\ 1 \end{pmatrix},$$

whereas for $k = \pi$, we have

$$\propto \begin{pmatrix} \pm 1 \\ 1 \end{pmatrix}$$

It is important to note here that this issue is exactly the issue that we will have to deal with when it comes to solving our magnetic model. If we use reciprocal space, we must maintain the spin constraint which becomes very difficult, and so we are forced to use alternative techniques.

Other important features of magnetism are multiple-**k** and Goldstone modes. The first is best exemplified on the face centered cubic lattice, and so we focus our attention there for now. We want find the structure factor on the face centered cubic

lattice and so we define the following

$$x \equiv e^{ik_x R_x}$$
$$y \equiv e^{ik_y R_y}$$
$$z \equiv e^{ik_z R_z}$$

From this, we can set up the nearest, and next-nearest structure factor on the lattice as

$$\gamma(\mathbf{k}) = \frac{J_1}{12}\left(\left[x+\frac{1}{x}\right]\left[y+\frac{1}{y}\right]+\left[x+\frac{1}{x}\right]\left[z+\frac{1}{z}\right]+\left[y+\frac{1}{y}\right]\left[z+\frac{1}{z}\right]\right) + \frac{J_2}{6}\left[x^2+\frac{1}{x^2}+y^2+\frac{1}{y^2}+z^2+\frac{1}{z^2}\right]$$

We then use that

$$\begin{aligned} x+\frac{1}{x} &= 2\cos k_x \\ x^2+\frac{1}{x^2} &= 2(2\cos^2 k_x - 1), \end{aligned}$$

such that we get

$$\gamma(\mathbf{k}) = \frac{J_1}{3}\left(\cos k_x \cos k_y + \cos k_x \cos k_z + \cos k_y \cos k_z\right) + \frac{J_2}{3}\left(2\cos^2 k_x - 1 + 2\cos^2 k_y - 1 + 2\cos^2 k_z - 1\right)$$

We now need to minimise this, and in general solve for the J_1, J_2 phase diagram, which can be done in many ways. Here, we seek to illustrate the concept of multiple-

k, so we start with only the J_1 solution, $J_2 = 0$. This gives us

$$\gamma(\mathbf{k}) = \frac{J_1}{3}\left(\cos k_x \cos k_y + \cos k_x \cos k_z + \cos k_y \cos k_z\right)$$

We minimise this with $\cos k_x = 1$, $\cos k_y = -1$, and $\cos k_z = C$ where C is any number, and cyclic permutations, which provides a vast degeneracy. We see this degeneracy in Fig.1.6, where the red line indicate curves in parameter space which are energetically equivalent. The states which correspond to these are anti-ferromagnetic planes, which are decoupled entirely perpendicular. This is in fact more complicated than multiple-k, and we include J_2 to simplify the situation. If we include the interaction as ferromagnetic, then we minimise with $\cos^2 k_i = \pm 1$, which stabilises the points $\mathbf{k} = \{(001), (010), (100)\}$, seen at the corners of the cube in Fig.1.6. This state then allows for the formation of a multiple-**k** structure, as the three ordering vectors are orthogonal, and as such a *linear combination* can be set up. The spins can rotate freely as one of the variables is always free to minimise the structure factor. Normally a low energy mode is associated with a symmetry of the system; a

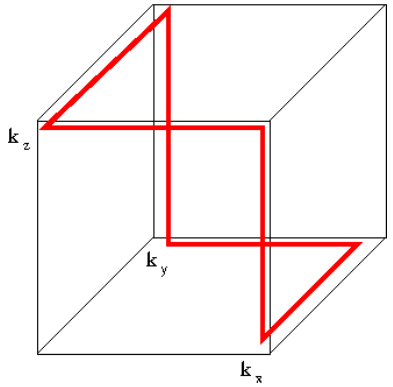

Figure 1.6: Red line showing the degeneracy in **k**-space of the face-centered-cubic lattice for J_1, indicating the possibility of multiple-**k** states

Goldstone mode. For example, an isotropic ferromagnetic Heisenberg Hamiltonian

has a well defined groundstate, but it is degenerate to global rotations of all the spins. This global rotation would then be a zero-energy Goldstone mode, which is the usual explanation for low energy-modes. However gapless modes can also be described by the transferal of magnetism between the ordering vectors. For the case of multiple-**k** moving spin density between the **k** leads to low energy modes. These gapless modes can be confused with the standard Goldstone mode idea, but it represents different underlying physics. For a multiple-**k** low energy mode, the perpendicular components of magnetism become active, and thus the spins can rotate. This is illustrated in Fig.1.7.

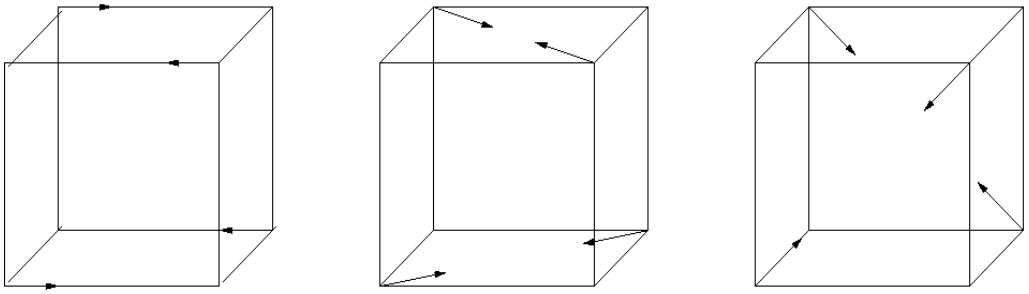

Figure 1.7: Examples of single-**q**, double-**q** and triple-**q** magnetic structures on a single tetrahedra

1.4 Neutron Scattering

The principal experiment that we study for the magnetism is neutron scattering. We simply offer the final formula for neutron scattering here, rather than derive the result. The intensity for neutron scattering Bragg peak at reciprocal wave vector **k** is given by

$$I(\mathbf{k}) = |F(\mathbf{k})|^2(1 - (\hat{\mathbf{S}}(\mathbf{k}).\mathbf{k})^2)(\mathbf{S}(\mathbf{k}))^2,$$

where $\mathbf{S}(\mathbf{k})$ is the structure factor (defined above), $F(\mathbf{k})$ is the form factor and $(1 - (\hat{\mathbf{S}}(\mathbf{k}).\mathbf{k})^2)$ is the orientational factor. The orientational factor means we only see scattering perpendicular to $\mathbf{S}(\mathbf{k})$. The form factor provides an overall envelope to the scattering, reducing the intensity of large $\mathbf{k}$ spots, and stems from the spreading of the electrons in the orbitals. The nuclear scattering only has the structure factor, and so if the magnetic scattering is at $\mathbf{k} = 0$, then the two sets of scattering are on top of one another. However, if the magnetism is anti-ferromagnetic, then new peaks appear when the magnetism orders. The anti-ferromagnetism is then characterised by some wave vector, usually chosen to be the one closest to the origin. We then see copies of this peak related by the underlying reciprocal lattice vectors.

An important feature of neutron scattering is that of domain averaging. One scatters many neutrons off a sample, and so the magnetism is "seen" in every domain structure; we therefore observe the average configuration. On the other hand, multiple-$\mathbf{k}$ magnetism is a sum of possible magnetism structures, and so once again one sees the average. It is therefore very hard to tell the difference between domain averaging and multiple-$\mathbf{k}$, though the orientational factor may allow one to deduce the structure.

1.5 Summary

We have provided a summary of some of the basic physics that we will need; lattices, atomic physics, the Hubbard and Heisenberg models, and some solutions to the Heisenberg model. The models we will be using will (at times) be more complicated than the simple nearest neighbour Heisenberg model, as will become clear, though we always essentially work classically. The notion of multiple-$\mathbf{k}$ magnetism will be present later, while Goldstone modes will be present from the start. We have also

introduced the main neutron scattering equation Eq.1.4.1, which will be used in the study of the pyrochlore compounds.

The rest of the thesis is divided in two; low dimensional magnetism and long range interactions on the pyrochlore lattice. We have introduced the magnetism which is relevant to both parts, but further ideas will be introduced in the appropriate sections.

Chapter 2

INTRODUCTION TO THERMODYNAMICS

2.1 Chapter Summary

We begin with the general model that we attempt to solve, although we only ever solve the model in certain parts of parameter space. We will introduce the basics of thermodynamics, particularly that which is relevant to the physics that will be dealt with later. We will arrive at the partition function, and then discuss magnetic phase transitions. We then move on to the Curie and Curie Weiss laws, along with some trivial extensions. These serve as the simplest examples of thermodynamic calculations for spin physics, despite being purely quantum. Then there is an overview of the models that shall be studied; the Ising model (as a reference model for transfer matrices), the plane rotator, continuous Ising, and Heisenberg model. We discuss what is already known about them, and what we shall be solving. We then motivate working in one dimension (as is mainly done here), indicating that we can have some interesting features. We then solve the nearest neighbour Ising model with an applied field in full, calculating all the thermodynamics properties that will be calculated for the later models (energy, specific heat, magnetisation and correlation functions). We will solve the thermodynamics for each of the models in Chapters

3, 4 and 5, and present the results in Chapter 6 and elect to split the calculations from the physics entirely.

2.2 Introduction to Thermodynamics

Having introduced the notion of spin physics, we now move on to the thermodynamics of such physics. We will study so called lattice models and we will only discuss thermodynamics relevant to these models. We will first restrict our attention to exactly solvable thermodynamics before we examine approximate solutions, and solve models that fall within the following general model

$$\begin{aligned} H = &- \sum_n \left[J_1^x S_n^x S_{n+1}^x + J_1^y S_n^y S_{n+1}^y + J_1^z S_n^z S_{n+1}^z \right] \\ &- \sum_n \left[J_N^x S_n^x S_{n+N}^x + J_N^y S_n^y S_{n+N}^y + J_N^z S_n^z S_{n+N}^z \right] \\ &- \sum_n \left[B^x S_n^x + B^y S_n^y + B^z S_n^z \right] \\ &- \sum_n \left[C^x (S_n^x)^2 + C^y (S_n^y)^2 + C^z (S_n^z)^2 \right] \\ &- h_p \sum_n \cos\left(p\phi_n\right) - \tilde{h}_q \sum_n \cos\left(q\theta_n\right) \end{aligned} \tag{2.2.1}$$

We consider only classical spins parametrised by

$$\hat{\mathbf{S}}_n = (\sin\theta_n \cos\phi_n, \sin\theta_n \sin\phi_n, \cos\theta_n)$$

The first and second terms are simple exchange interactions, and provide the two dimensional model in the limit $N \to \infty$. The third term is a magnetic field, while the last three terms are crystal fields. More complicated crystal fields can be studied. although here we only study models within this general model. We study several

models, which we now state including the relevant parameters, seen in Table.2.2.

Table.2.2. Table of parameters in Eq.2.2.1 for various models.

Model	J_1^x	J_1^y	J_1^z	J_N^x	J_N^y	J_N^z	B^x	B^y	B^z	C^x	C^y	C^z	h_p	h_q
Ising	0	0	α	0	0	0	0	0	β	0	0	∞	0	0
Ising	0	0	α	0	0	β	0	0	0	0	0	∞	0	0
Plane Rotator	α	α	0	0	0	0	β	0	0	0	0	$-\infty$	0	0
Plane Rotator	α	α	0	β	β	0	0	0	0	0	0	$-\infty$	0	0
Clock	α	α	0	0	0	0	β	0	0	0	0	$-\infty$	∞	0
Clock	α	α	0	β	β	0	0	0	0	0	0	$-\infty$	∞	0
Continuous Ising	0	0	α	0	0	0	0	0	β	0	0	0	0	0
Plane Ising	α	0	0	0	0	0	β	0	0	0	0	$-\infty$	0	0
Plane Ising	α	0	0	β	0	0	0	0	0	0	0	$-\infty$	0	0
Heisenberg	α	α	α	0	0	0	0	0	β	0	0	0	0	0
Heisenberg	α	α	α	β	β	β	0	0	0	0	0	0	0	0
XY	α	α	0	0	0	0	β	0	0	0	0	0	0	0

When $C^z = \infty$ we project on to only up or down, so $S_n^z \to \sigma_n$, as usual for the Ising model. When $C^z = -\infty$, we project into the plane, leaving only the ϕ degree of freedom. Including h_p discretises the ϕ angle, giving p clock ticks per site. The continuous Ising has both θ and ϕ degrees of freedom, but only interacts in the $\hat{\mathbf{z}}$-direction, while the plane Ising has only the ϕ degree of freedom, but is a related model as the energetics only depend on the "length" of spin in the $\hat{\mathbf{x}}$-direction. The Heisenberg model is isotropic, and whose spins are fully three dimensional. Finally the XY model also has isotropic spin space, but only planar interactions.

We now introduce the central quantity to the calculations. For the entirety of the calculations, we work in the canonical ensemble; we have fixed particle number

and the temperature is well specified, which in turn specifies the energy as we are in the thermodynamic. We envisage a one dimensional chain of spins weakly coupled to a heat bath (at a temperature T), with no particles exchanging. We can also apply a magnetic field which generates a magnetisation, which once again have a one to one correspondence as we are in the thermodynamic limit.

To calculate, we introduce the partition function. Let us work with discrete states first, before we move discuss classical models. We will not be working with quantum mechanics as such, and only deal with thermodynamics for which the eigenbasis is already known, or the model is automatically diagonal. Let there be a system of N spins, with t discrete states per site (this idea will have to be modified for continuous spin models). We therefore have t^N total states, an unfeasibly large number to deal with exactly and completely for any thermodynamically reasonable N. Suppose we have a Hamiltonian which acts on any given one of the t^N states and returns the energy. We will always be working in the full thermodynamic limit, and so we introduce the main ideas of thermodynamics. Firstly, we define the entropy by

$$S = -\sum_n P_n \log P_n,$$

a quantity which we seek to maximise subject to two constraints

$$\begin{aligned} \hat{1} &= \sum_n P_n \\ E &= \sum_n \epsilon_n P_n, \end{aligned}$$

where P_n is the probability of finding the state n, E is the average energy of the entire system $\hat{1}$ is the normalisation of the probabilities, and ϵ_n is the energy of the state n, which is specified by the Hamiltonian. The sum over n is over all t^N

states. We therefore optimise the entropy with these constraints, so we define two Lagrange multipliers β (which fixes the average energy) and $(\log Z - 1)$ which fixes the probability. We find

$$\beta F = S - \beta E - (\log Z - 1)\hat{1},$$

which explicitly is given by

$$\beta F = -\sum_n \left(P_n \log P_n + \beta \epsilon_n P_n + (\log Z - 1) P_n\right),$$

where we have defined the quantity F which is called the Gibbs free energy. This quantity we optimise without constraint, which optimises the probabilities under constraint. We optimise this with $\frac{\partial}{\partial P_n}\beta F = 0$ which gives us

$$\log P_n = -\beta \epsilon_n - \log Z,$$

from which we find the two main equations

$$\begin{aligned} P_n &= \frac{e^{-\beta\epsilon_n}}{Z} \\ Z &= \sum_n e^{-\beta\epsilon_n} \end{aligned}$$

The quantity Z is called the partition function, and is the central quantity to thermodynamics which we shall calculate. We can relate, for example, the average energy to the partition function, from

$$\langle E \rangle = \sum_n \epsilon_n P_n = \frac{1}{Z} \sum_n \epsilon_n e^{-\beta\epsilon_n}$$

We can trivially write this as a derivative, yielding

$$\langle E \rangle = -\frac{\partial \log Z}{\partial \beta}$$

For any quantity controlled by $\mathcal{H} = \mathcal{H}_0 + \lambda \mathcal{H}_1$, we can calculate the average as

$$\begin{aligned} \langle \mathcal{H}_1 \rangle &= \frac{1}{Z} \sum_{\{S\}} \mathcal{H}_1(S) e^{-\beta \mathcal{H}(S)} \\ &= -\frac{1}{\beta} \frac{\partial \log Z}{\partial \lambda}, \end{aligned}$$

allowing us to calculate, for example, magnetisation, or correlation functions. The Gibbs free energy is explicitly given by

$$F = E - TS,$$

which we now interpret; the entropy drives the system to disordered states, preferring fluctuations rather than order. It is the balance of the energy with the entropy which provides us with an understanding of phase transitions. It is important to note two key features of the Gibbs free energy; it is always minimised at constant temperature, and it is continuous though not necessarily smooth. Jumps in the n^{th}-derivative of the free energy provide n^{th}-order phase transitions. For first order transitions there is a discontinuity in the energy which provides a discontinuity in the specific heat. We will eventually solve the thermodynamics of (some of) these classical models, always working in one dimension, and we therefore introduce the thermodynamics of magnetism. Although, as we shall explain later, one dimension prohibits thermal phase transitions, we begin by discussing magnetic phase transitions in general. It is known that the Ising model in two or higher dimensions has a phase transition [34], a

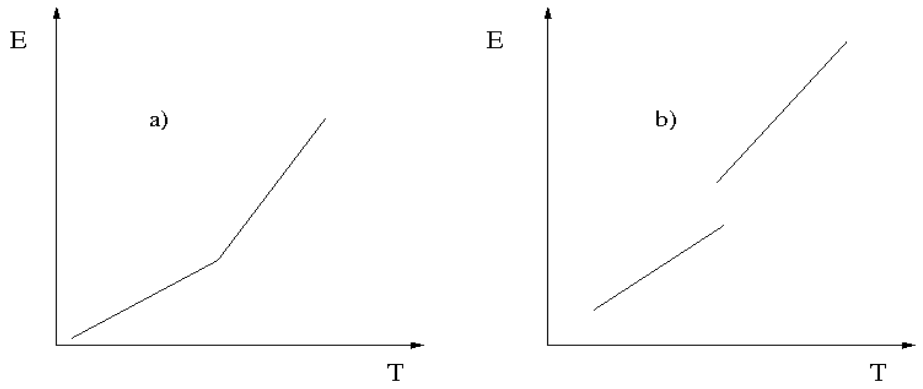

Figure 2.1: Sketch of a phase transition, with a) being second order and b) being first order

point at which a spontaneous long range correlation appears, as sketched in Fig.2.2. As we cool the system down, the correlations (that are energetically favourable)

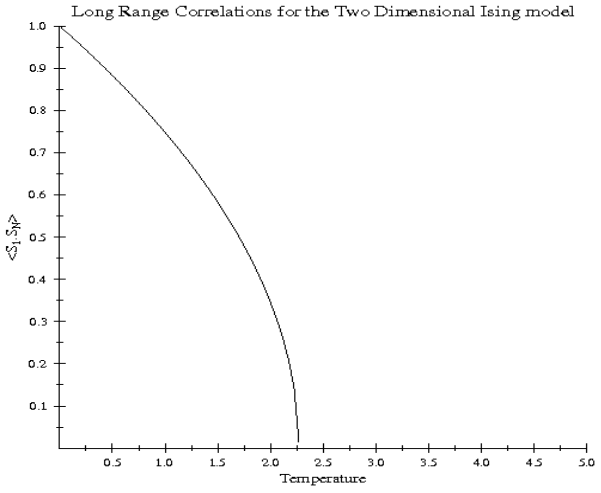

Figure 2.2: Sketch of the long range correlation function for the Ising model in two or higher dimensions

build up, until at some T_c they span the entire system, breaking some symmetry. We can see this as a degeneracy in the *free energy*; two states with different energies and entropies become degenerate at T_c, at which point one takes over from the

other. At this point, there is a huge amount of entropy available from fluctuating between the two free energy degenerate states, providing the peak in specific heat, independent of the order of the transition. There is an important aspect of this phase transition that has been skipped here. We chose the long range *correlation functions*, but in fact a spontaneous magnetisation may appear, but only if we take the thermodynamic limit carefully. We must have

$$\langle M \rangle = \lim_{B \to 0^+} \lim_{N \to \infty} \sum_{r}^{N} \langle m_r \rangle,$$

where $\langle m_r \rangle$ is the average magnetisation at the site r and $\langle M \rangle$ is the average total magnetisation. If we reverse the order of these limits, the spin inversion symmetry means that we cannot have long range order, but if we keep the limit as is, we can have spontaneously broken inversion symmetry. Note that if we took $B \to 0^-$ we would have the opposite sign for $\langle M \rangle$. A magnetic phase transition is where a global symmetry is broken and is driven by some *collective* phenomena between a *large* number of spins. If the phase transition is into long range order, then one has a macroscopic number of spins taking part in the order; a finite fraction compared to the total number of spins. For other types of order, this fraction may be zero, though a large number of spins are taking part in the order.

In principle, one can apply some other parameter and move this phase transition around in temperature, and in some cases it can be moved to zero temperature. At this point the phase transition is controlled by quantum fluctuations, and one can investigate the coexistence of quantum and thermal fluctuations near a transition. In our models, we will also have these zero temperature phase transitions, and we may therefore investigate the classical fluctuations nearby. Though it is important to note that the zero temperature transition is first order, and therefore we are not

investigating a quantum critical point.

The task we therefore set ourselves is to calculate the partition function for a given Hamiltonian. To begin with, we will calculate the simplest partition function for a magnetic system, and derive the Curie Weiss law. The Curie Weiss law is also a central component for the study of real magnetic systems, as we shall see later. It is also a quantum calculation, and will be essentially the only example of a quantum thermodynamic calculation here.

2.3 Order Parameters and Critical Exponents

An important aspect of second order (or continuous) phase transitions is that of *universality*. Many different models may have the same physics near the phase transition; we must have long range fluctuations for a phase transition, and so the details of the model can become irrelevant here. We therefore need to *characterise* the transitions in some way and put the models into "universality classes". The best way to do this is define *critical exponents*; the temperature dependence of some quantity near the phase transition. The critical exponent is the behaviour of the *order parameter* near the transition; a quantity which vanishes at and above T_C. In order to define the critical exponents, we first define the reduced temperature

$$\tau \equiv \frac{T - T_C}{T_C}$$

We expect that quantities will diverge like τ^{-x} where $x \geq 0$ is some exponent in the limit $T \to T_C$. We therefore define the following critical exponents

$$C_V \sim \tau^{-\alpha}$$

$$\chi \sim \tau^{-\gamma}$$
$$\xi \sim \tau^{-\nu},$$

where α, γ, and ν are the critical exponents for specific heat, the susceptibility and correlation length respectively. Note that these exponents are for static systems which will be the only ones we deal with. Many models have the same critical exponents. It is believed that the exponents only depend on the dimensionality of the system and of the spin space, and the range of interactions. For the two dimensional Ising model we have

$$\alpha = 0$$
$$\gamma = \frac{7}{4}$$
$$\nu = 1,$$

which is called the Ising universality class. Note that $\alpha = 0$ means that the specific heat diverges logarithmically.

For the case of our models, we note that to define the critical exponents, or even the reduced temperature, one requires T_C. For the cases where it exists, we will not know T_C, and therefore cannot calculate any critical exponents.

2.4 Curie Weiss and Generalisations

We derive the thermodynamics for a single spin in a magnetic field (Curie Law), a single spin with an average field from one neighbour and an applied field (Curie-Weiss Law). We then extend the calculation, and find the thermodynamics for a single spin with two neighbours in a triangle, and three neighbours in a tetrahedron, all with an

applied field, which is new but trivial. We work up to spin $S = \frac{3}{2}$, which amounts to the case of Cr^{3+}. We are calculating the extensions to Curie-Weiss with a particular compound in mind; $Ho_2Ga_xCr_{1-x}SbO_7$ [35], in which the chromium forms chains of magnetic atoms of spins (of length $S = \frac{3}{2}$). The style of the chains depends strongly on the doping x. For $x \to 1$ the chromiums are very dilute, and so magnetising the sample produces a weak Curie effect. When x is decreased, the chromiums may become magnetically correlated with the Heisenberg, but the coordination number is not known. One only observes the average coordination number for the entire sample. We therefore calculate the relevant Curie-Weiss laws for the geometries encountered in the compound, so that one could fit the susceptibility with four free parameters, which generate the average coordination number.

2.4.1 Curie Law and Curie-Weiss Law

We begin with a single spin in an applied magnetic field. We use the $\hat{\mathbf{z}}$-axis as the applied field, and quantise the spin in this direction. We have a spin of length S, and therefore have $2S + 1$ states to sum over. We can trivially write down the partition function for this, giving us

$$\begin{aligned} Z &= \sum_{n=-S}^{S} e^{\beta B n} \\ &= \frac{\sinh \beta B(S + \frac{1}{2})}{\sinh \frac{\beta B}{2}} \end{aligned}$$

To calculate the magnetisation we use

$$\langle M \rangle = -\frac{1}{\beta} \frac{\partial \log Z}{\partial B}$$

$$= \beta\left(S+\frac{1}{2}\right)\coth\left(\beta B\left(S+\frac{1}{2}\right)\right)-\frac{\beta}{2}\coth\left(\frac{\beta B}{2}\right) \qquad (2.4.1)$$

For the case of $B \to 0$ we expand the magnetisation, giving us

$$\langle M\rangle = \frac{\beta B S(S+1)}{3}$$

We then calculate the inverse susceptibility, yielding

$$\chi^{-1} = \frac{3T}{S(S+1)},$$

which is known as the Curie Law. We next include a mean field interaction stemming from nearest neighbours. Consider a general pairwise Hamiltonian over some range

$$H = -\sum_{\mathbf{R}\neq\mathbf{R}'}\mathbf{S}(\mathbf{R})J(\mathbf{R}-\mathbf{R}')\mathbf{S}(\mathbf{R}')$$

We use mean field theory on the interacting part. One calculates the self consistent *response* from a test spin feeling a constant field from the neighbours. We therefore choose a spin $\mathbf{S}(\mathbf{0})$ say, and calculate the *average* of the local exchange stemming from the surrounding neighbours (the exchange field)

$$\begin{aligned} H &= \mathbf{S}(\mathbf{0}).\sum_{\mathbf{R}\neq\mathbf{0}}\mathbf{S}(\mathbf{R})J(\mathbf{R}) \\ &\approx J_0\lambda\mathbf{S}(\mathbf{0}).\langle\mathbf{S}\rangle \equiv J_0\lambda\mathbf{S}(\mathbf{0}).\langle\mathbf{M}\rangle, \end{aligned}$$

where $\langle M \rangle$ is the magnetisation that we are attempting to find as a function of applied field and temperature, λ is the coordination number, and

$$J_0 = \sum_{\mathbf{R} \neq \mathbf{0}} J(\mathbf{R}),$$

the average of the interactions. For exchange interactions, we expect this to simply be sequence of interaction strengths which become exponentially small. We calculate the partition function giving

$$\begin{aligned} Z &= \sum_{n=-S}^{S} e^{\beta B n + \beta J_0 \lambda \langle M \rangle n} \\ &= \frac{\sinh \beta \tilde{B}(S + \frac{1}{2})}{\sinh \frac{\beta \tilde{B}}{2}}, \end{aligned}$$

where $\beta \tilde{B} \equiv \beta B + \beta J_0 \lambda \langle M \rangle$. We find that the magnetisation is given by the same expression as before in Eq.2.4.1, but with the substitution $B \to \tilde{B}$. At high temperature, it is clear that the magnetisation is proportional to the applied field, and so taking the limit $B \to 0$ is equivalent to $\tilde{B} \to 0$. This will not be true for all temperatures (as we shall see), but at high temperature is a valid assumption. We find (after re-arranging)

$$\langle M \rangle = \frac{BS(S+1)}{3(T - \frac{\lambda J_0 S(S+1)}{3})}$$

From this we may write the susceptibility as

$$\chi = \frac{S(S+1)}{3(T - T_c)},$$

where $T_c = \frac{\lambda J_0 S(S+1)}{3}$, the Weiss field, which provides an offset in the linear relation between inverse susceptibility and temperature. Physically, one applies a magnetic

field which polarises the sample slightly; Curie's law. Internal interactions then interfere with this. If the interactions are ferromagnetic then the response is larger than one would expect, and if they are antiferromagnetic the response is smaller. This field is called the Weiss field and we can attempt to find the *average* interaction between spins from this. Practically, one uses the slope of the inverse susceptibility to find the length of spin, and the intercept to find the mean field average interaction. However, we can calculate much more accurately the offset to the Curie law, by considering specific cases of (different geometries of) spins.

2.4.2 Extensions to the Curie Law

Let us begin by denoting the partition function for the Curie law by Z^1 as this will make generalising more obvious. We begin with a spin in a magnetic field, with one nearest neighbour. For two spins, we seek to include a Heisenberg interaction, and so we use the result

$$\mathcal{H} = J\hat{\mathbf{S}}_0.\hat{\mathbf{S}}_1 = \frac{J}{2}\left[(\hat{\mathbf{S}}_0 + \hat{\mathbf{S}}_1).(\hat{\mathbf{S}}_0 + \hat{\mathbf{S}}_1) - \hat{\mathbf{S}}_0^2 - \hat{\mathbf{S}}_1^2\right],$$

where the last two terms do not contribute to the thermodynamics, as they are cancelled out when we take $\log Z$. Thus for the partition function we have

$$Z^2 = \sum_{\{\hat{\mathbf{S}}_0, \hat{\mathbf{S}}_1\}} e^{\beta B(S_0^z + S_1^z) + \frac{\beta J}{2}(\hat{\mathbf{S}}_0 + \hat{\mathbf{S}}_1).(\hat{\mathbf{S}}_0 + \hat{\mathbf{S}}_1)},$$

where we must sum over all the *states*, and controlling this sum is the aim. For two spins, it is particularly easy. We note that the interaction is the form of $\hat{\mathbf{T}}.\hat{\mathbf{T}}$ for

some spin, and thus we use the S_z^{total} basis to represent the summation, given by

$$\begin{aligned} Z^2 &= \sum_{T=0}^{2S} \sum_{p=-T}^{T} e^{\beta B(S_1^z+S_2^z)+\frac{\beta J}{2}T(T+1)} \\ &= \sum_{T=0}^{2S} \frac{\sinh\left(\beta B\left(T+\frac{1}{2}\right)\right)}{\sinh\left(\frac{\beta B}{2}\right)} e^{\frac{\beta J}{2}T(T+1)} \end{aligned}$$

For the case of chromium, we have $S = \frac{3}{2}$, and thus four terms in the sum, explicitly

$$Z^2 = 1 + \frac{1}{\sinh\left(\frac{\beta B}{2}\right)}\left(\sinh\left(\frac{3\beta B}{2}\right)e^{\beta J} + \sinh\left(\frac{5\beta B}{2}\right)e^{3\beta J} + \sinh\left(\frac{7\beta B}{2}\right)e^{6\beta J}\right)$$

The magnetisation per spin is given by

$$m_2 = -\frac{1}{2\beta}\frac{\partial \log Z^2}{\partial B},$$

and in the limit $J \to 0$ must agree with the Curie Weiss magnetisation

$$m_1 = -\frac{1}{\beta}\frac{\partial \log Z}{\partial B}$$

Similarly one can calculate the partition function for the triangle, but more care is needed to calculate the partition function, as we have the sum of three spins, and there are therefore multiple *representations* of each S^z_{total} state. For $S = \frac{1}{2}$ we have

	0	$\frac{1}{2}$	1	$\frac{3}{2}$	2
1		1			
2	1		1		
3		2		1	
4	2		3		1

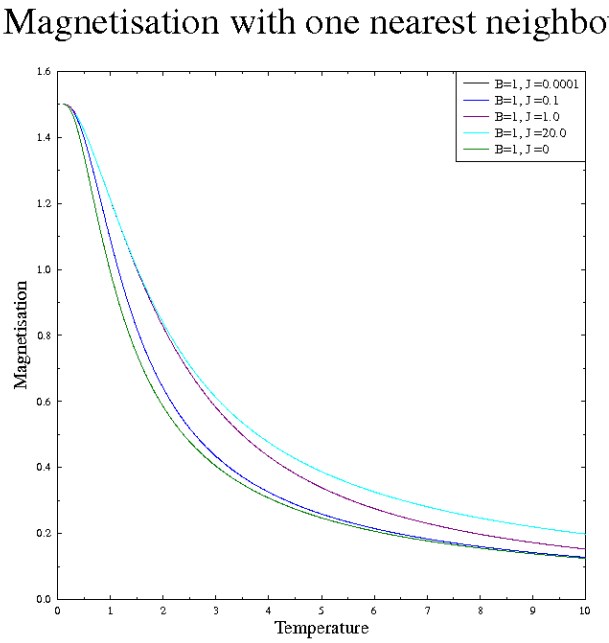

Figure 2.3: Magnetisation including one neighbour.

Along the top is S^z_{total}, and going down is the number of spins being added together, and the number is the number of representations of that particular spin state. For $S = 1$ we have

	0	1	2	3	4
1		1			
2	1	1	1	1	
3	1	3	2	1	
4	3	6	6	3	1

and for $S = \frac{3}{2}$ we have the ever more complicated

	0	$\frac{1}{2}$	1	$\frac{3}{2}$	2	$\frac{5}{2}$	3	$\frac{7}{2}$	4	$\frac{9}{2}$	5	$\frac{11}{2}$	6
1				1									
2	1		1		1		1						
3		2		4		3		2		1			
4	4		9		11		10		6		3		1

(2.4.2)

For the triangle, we have the Hamiltonian

$$\mathcal{H} = J\hat{\mathbf{S}}_0.\hat{\mathbf{S}}_1 + \hat{\mathbf{S}}_1.\hat{\mathbf{S}}_2 + \hat{\mathbf{S}}_2.\hat{\mathbf{S}}_1 = \frac{J}{2}(\hat{\mathbf{S}}_0 + \hat{\mathbf{S}}_1 + \hat{\mathbf{S}}_2).(\hat{\mathbf{S}}_0 + \hat{\mathbf{S}}_1 + \hat{\mathbf{S}}_2) - \hat{\mathbf{S}}_0^2 - \hat{\mathbf{S}}_1^2 - \hat{\mathbf{S}}_2^2,$$

which leads us to the partition function given by

$$\begin{aligned} Z^3 &= \sum_{\{\hat{\mathbf{S}}_0,\hat{\mathbf{S}}_1,\hat{\mathbf{S}}_1\}} e^{\beta B(S_0^z+S_1^z+S_2^z)+\frac{\beta J}{2}(\hat{\mathbf{S}}_0+\hat{\mathbf{S}}_1+\hat{\mathbf{S}}_2).(\hat{\mathbf{S}}_0+\hat{\mathbf{S}}_1+\hat{\mathbf{S}}_2)} \\ &= \sum_{T=\frac{1}{2}}^{3S} \sum_{p=-T}^{T} e^{\beta Bp+\frac{\beta J}{2}T(T+1)} g(T) \end{aligned}$$

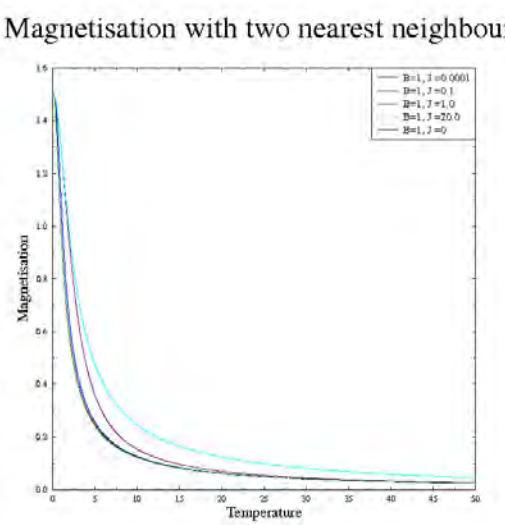

Figure 2.4: Magnetisation including two neighbours.

$$= \sum_{T=\frac{1}{2}}^{3S} \frac{\sinh\left(\beta B\left(T+\frac{1}{2}\right)\right)}{\sinh\left(\frac{\beta B}{2}\right)} e^{\frac{\beta J}{2}T(T+1)} g(T),$$

where $g(T)$ is the number of representations for each given T, given by the table above for $S = \frac{3}{2}$ in Eq.2.4.2. Once again magnetisation is obtained via

$$m_3 = -\frac{1}{3\beta}\frac{\partial \log Z^3}{\partial B},$$

and we compare to the Curie-Weiss in the limit $J \to 0$. For the tetrahedron we have essentially the same result, given by

$$Z^4 = \sum_{T=0}^{4S} \frac{\sinh\left(\beta B\left(T+\frac{1}{2}\right)\right)}{\sinh\left(\frac{\beta B}{2}\right)} e^{\frac{\beta J}{2}T(T+1)} g(T),$$

with

$$m_4 = -\frac{1}{4\beta}\frac{\partial \log Z^4}{\partial B}$$

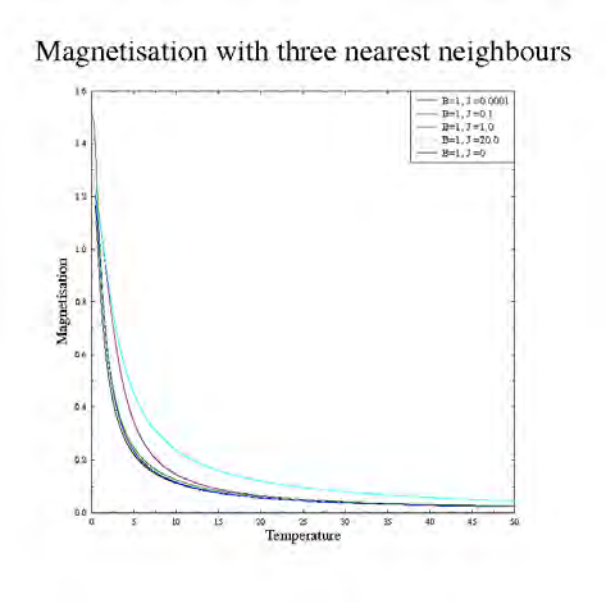

Figure 2.5: Magnetisation including three neighbours.

If we calculate the magnetisation for a given problem, we would get us the fitting procedure

$$M = m_1(\beta, B) + \alpha_2 m_2(\beta, B, J) + \alpha_3 m_3(\beta, B, J) + \alpha_4 m_4(\beta, B, J),$$

for the magnetisation, though fitting the inverse susceptibility is not as clear. Note that we can also calculate the susceptibility from these, given by

$$\chi_n = \frac{\partial m_n}{\partial B}, \tag{2.4.3}$$

and fit these term by term, but fitting the sum of contributions to the inverse susceptibility is clearly more difficult.

We have calculated the average magnetisation for a single spin in a magnetic field, two spins in a line, three spins in a triangle and four spins in a tetrahedron

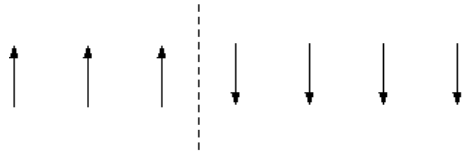

Figure 2.6: The simplest domain wall for a ferromagnetic Ising model in one dimension

all with a Heisenberg interaction. These are the simplest calculations of a partition function for magnetism, but it really serves to indicate how Curie Weiss law works. To use Curie Weiss, one simply uses high temperature in the inverse susceptibility to predict the intercept; if it is negative (positive) then we expect ferromagnetism (antiferromagnetism). The slope of the line also gives the size of the spin, indicating the average charge state on the magnetic ion under consideration.

2.5 Overview

Here we discuss the known features of the models that we solve, and attempt to motivate our study into one dimension.

2.5.1 Overview of Models

We will solve the exact thermodynamics of several one dimensional models. We will introduce the Ising model [36] to motivate the use of transfer matrices (which will become transfer functions for the continuous models) using only the standard techniques to solve the basic $J_1 - J_2$ model. The Ising model is known to have a phase transition in two dimensions, where a spontaneous magnetisation appears with only nearest neighbour interactions. It serves as the archetypal model of a magnet, whose thermodynamics are fully understood in one and two dimensions. The excitations

are well defined domain walls, as seen in Fig.2.6. In one dimension, it is clear that there are N (or $N-1$) bonds for the excitation to delocalise on, providing $-T\log N$ for the entropy. The energy penalty for one domain wall *independent* of position is $2J$. The free energy is therefore

$$F = 2J - T\log N$$

Thus the one dimensional Ising model always has domain walls in the thermodynamic limit at *any* finite temperature, destroying order. This argument is true for other one dimensional models, whose excitations are always present due to the macroscopic entropy and a finite energy penalty.

The two dimensional Ising model is the first exactly solvable model of a magnetic phase transition. It was known to have a transition at $2\beta_c = \log(1+\sqrt{2})$ [34, 37] via duality, before Onsager provided the exact solution [38] and Yang provided the formula for the spontaneous magnetisation [39]. Many generalisations of the model are exactly solvable including the n-vertex ($n = 2$ [40], $n = 8$ [41]) and the Potts model [42]. For the two dimensional Ising model, the excitations are short range domain walls, where once again the entropy scales with the number of bonds. However, the energy term does depend on the structure of the domain wall, leading to the phase transition where the temperature becomes sufficiently high to overcome the domain penalty. At low temperature we have a single dominant (macroscopic) domain which provides the magnetic order. For the particular case of the Ising model, we heat the system up, and domains of the opposite magnetisation start to grow. At the phase transition there are equal amounts of both domains, but both domains exist over the entire sample. As we heat further, the domains shrink into tiny patches, but we still have equal amounts of both such that there is no symmetry

broken overall. It is the balancing of energy penalty to entropy gain which is at the center of all phase transitions in thermodynamics.

For the continuous models, we begin with the plane rotator model, or two dimensional XY-model. It is based on the standard XY-model, but the spins are constrained to only point within a plane. This model has received a huge amount of interest in two-dimensions due to its interesting ordering properties [10,43–47]. The Mermin-Wagner theorem [48–50] prevents long range order due to the isotropy in spin space. The low energy excitations of the model are very large scale variations of the magnetisation vector due to the isotropy of the model. However, the model is proven to exhibit power law correlations for sufficiently low temperature [20], indicating that there must be a phase transition of some sort. There are three options

$$\lim_{\mathbf{r}\to\infty}\langle \mathbf{S}_0.\mathbf{S}_r\rangle = \left\{ \begin{array}{c} e^{-\frac{r}{\xi}} \\ \\ \frac{1}{r^p} \\ \\ A \end{array} \right\},$$

where A is a constant. If we get a power law then

$$\lim_{V\to\infty}\frac{1}{V}\langle \mathbf{S}(0).\int dr\ S(r)\rangle \to 0$$

Although there are an infinite number of spins involved with the correlation, there is not a *macroscopic* fraction, and so we do not get long range order. A new type of mechanism was required to produce a phase transition from the state with no long range order (power law correlations) to a state with no long range order (exponential correlations), and Kosterlitz and Thouless provided a possible explanation [50]. They showed that the low energy excitations of the effective model were vortex anti-

vortex pairs. At low temperature these vortices would be bound pairs, but at some temperature, the BKT-transition, the bound pairs would unbind and extend to infinite range, destroying order. Intuitively, the logarithmically interacting vortices provided the same free energy contribution as the free energy, viz

$$F = E_V \log r - T \log r$$

where E_V is the energy of the vortex anti-vortex pairs, and r is the separation, and so expect a transition at $T^* = E_V$ to unbound vortices, where the entropy demands that they extend to long range.

The $J_1 - B$ model has been approximately solved in one dimension and two dimensions [10]. Here, we solve the $J_1 - J_B$ and the $J_1 - J_2$ model.

We will then solve the so-called continuous-spin Ising model [51], or ("pseudo" Ising model [52]). Very little literature exists on this model [51, 53, 54], although it is known to have a phase transition in two or higher dimensions [55]. Monte Carlo analysis on this [52] finds a phase transition, and the authors believe it to be the same as the Ising model but with a reduced T_c. Here, as with all the models, we will only work in one dimension, and provide the exact solution to the $J_1 - B$ model before attempting to find approximately the two dimensional limit. This model is the same as the regular Ising model, in that the spins only interact in the $\hat{\mathbf{z}}$-direction, although the constraint $\sigma = \pm 1$ is relaxed to $\sigma \in [-1, 1]$, such that the spins are fully three-dimensional. The excitations are again local domain walls, and so one would expect a transition in two-dimensions just as in the Ising model though the fluctuations affect where the phase transition takes place. The model has the ability to weaken the magnetisation component (by fluctuating locally) as well as setting up domain walls.

We finally move on to the classical Heisenberg model. This model has received a large amount of attention as it is central to the study of isotropic magnetism [56–59]. In three-dimensions, it is proven to have a finite transition temperature [60–62], while in two-dimensions Mermin-Wagner *suggests* that there should be no phase transition [63, 64] at finite temperature. This is due to a divergent number of low energy (or low momentum) excitations which are presumed to prevent the system from finding the ground state other than at zero temperature. Frustrated $J_1 - J_2$ models are believed to have a transition if the appropriate Ising variables are examined [65]. In one dimension, the thermodynamics for some models have been exactly solved; for example, the nearest neighbour zero field partition function has been known for a long time [57]. Including a field has been done infinitesimally [56] in terms of Wigner-3j symbols, and later numerical studies have provided the calculation for finite fields [66]. Finite clusters with arbitrary internal interactions have also been solved exactly by direct integration of the partition function [67]. Here we provide the solution to the $J_1 - B$ and $J_1 - J_2$ model.

In summary, we will provide the solution to the continuous spin Ising model with nearest neighbour interactions and a field, the $J_1 - J_2$ Heisenberg and plane rotator models, along with correlation functions for all models. The continuous Ising model has never been studied in detail, and correlation functions for the two continuous models have not been found before.

2.5.2 Motivation for One Dimension

Before we motivate one dimension, first we specify what we mean by one dimension, as we use a slightly subtle definition. We will be considering models of the form

$$H = \sum_{j_1, j_1', j_2 \ldots j_d'} S_{j_1, j_2 \ldots j_d} J_{j_1, j_1', j_2 \ldots j_d'} S_{j_1', j_2' \ldots j_d'},$$

where d will define our dimensionality. We will *only* be studying short range interacting models when we study the thermodynamics, and so we only define dimensionality for short range models. We also only work in the thermodynamic limit, and therefore only discuss with reference to that here as well. There exists a way of labelling the sites such that the effective geometry has the bonds over a minimum range $|j - j'|$. We then use d and only d indices in order to label our lattice. If we use more labels, then we create a bond over an infinite range, which means we do not have the correct effective geometry. With this definition, one dimension becomes a lattice for which all bonds are short range, and there exists one infinite direction and one finite direction such that the aspect ratio is zero. Domain walls may then stretch across the side with finite length with a finite energy cost and then delocalise along the longer direction to gain from entropy, wiping out order at any finite temperature. In two dimensions, the effective geometry is two infinite directions with a constant aspect ratio, such that domain walls may not stretch across the entire system. In this way phase transitions are not strictly prohibited.

While there are no finite temperature phase transitions in these models, one dimension may still exhibit crossovers. We may therefore find phase-diagrams, where we associate phase boundaries with the one dimensional analogue of phase transitions. For example, in the fully three-dimensional compound spin-ice, one observes

a standard crossover, where entropy comes out smoothly across a temperature region, and we go from a collection of states to a smaller collection of states. For the particular case of spin-ice, this crossover is from all Ising spin states in the pyrochlore lattice to the states only satisfying the "two-in-two-out" ice rule for each tetrahedron. For these one dimensional models, a distinction should be made; we are observing what would become the phase transition in higher dimensions, but is not allowed. In one dimension, the state at high temperature is the disordered state, and at low temperature it is still a disordered state. However, at low temperature, one may have *very* large regions of the two dimensional groundstate (antiferromagnetic or ferromagnetic), but a domain wall is *necessary*, preventing full long range order. For example, the Ising model exhibits a broad peak for one dimension, which goes from the disordered state to one that mimicks the ordered state but is not allowed to have long range order.

We are also permitted zero temperature transitions, and so we can investigate how temperature affects these. These one dimensional models also offer the one- to two-dimensional crossover if we have one local and one non-local interaction. We will provide some calculations to this effect, as they provide a technique to limit to two-dimensions where phase transitions are permitted. However, most of the work is done in purely one dimension here. It is also worth noting that one dimension *may* have phase transitions, if the model is non-local (mocking up higher dimensions), and contains no continuous symmetry. For example, the Ising model with a single weak long range interaction [68], given by the Hamiltonian

$$H = -J \sum_{n} \sigma_n \sigma_{n+1} - \frac{J_2}{N} \sum_{n>m} \sigma_n \sigma_m$$

in the limit $N \to \infty$ has a finite transition temperature given by

$$\frac{J_2}{T_c} = \exp\left[\frac{-2J_1}{T_c}\right]$$

Transitions are permitted in one dimensional non-continuous models, if the excitations (and associated entropy) are non-trivial. However, given the definition of one dimension above, we would not consider this a strictly one dimensional model, and in fact using long range interactions to create non-trivial excitations is a way of investigating the one-to-two dimensional crossover (see Chap.7).

2.6 Technique overview

There are many techniques available to calculate (or approximate) the partition function and therefore the thermodynamics, such as series expansions (in some small parameter), renormalisation group, transfer functions, and Monte Carlo. We will use transfer functions, which are related to transfer matrices, but are used for continuous spin models, and Monte Carlo as a cross check for some of the calculations.

A series expansion (or high temperature) expansion is typically simply a Taylor series of the partition function

$$Z = \sum_{\{S\}} e^{-\beta H(S)} = \sum_{\{S\}} \sum_{p=0}^{\infty} \frac{(-\beta H(S))^p}{p!}$$

We then calculate the series term by term. This technique prohibits the calculation of the partition function *at* the phase transition, but it may be calculated close to the transition, and therefore may be used to get close.

Numerical simulation is used to calculate the dynamics of the system, sampling

phase space in order to "mock-up" the partition function. These techniques are often used as they are relatively easy to calculate with, but offer no exact results. We will use Monte Carlo briefly as a cross check for some of our calculations, but will not investigate using this technique.

Finally, renormalisation group is a technique which uses the idea of *universality*. Near the phase transition, it is expected that the microscopic details of the model are not important, and that the physics is only dominated by long range effects (as it must be for a phase transition to occur). Therefore, many models are controlled by the same underlying physics, and one can attempt to classify the various models into ones which behave the same; *universality classes*. Renormalisation group rescales the parameters (or variables) in such a way to indicate whether there will be a finite temperature transition, which parameters are important at the transition, and the power laws near the transition of quantities. It is usually calculated on a field theory which corresponds to the original lattice model, although for some models (like the Ising model) one can use *decimation* to calculate on the original model. We will not be using renormalisation group at all, but will use classical field theory to calculate the low energy excitations of some of our models.

2.6.1 Discrete Spin Models and Transfer Matrices

To calculate the partition function for a discrete spin model, one attempts to calculate the following

$$Z = \sum_{\{S\}} e^{-\beta H(S)},$$

where the summation is over all possible states $\{S\}$ and $H(S)$ is the Hamiltonian, which gives the energy of the state S. Quantum mechanically one would use

$$Z = \sum_n \langle n|e^{-\beta H}|n\rangle$$

for some *complete* set of states $|n\rangle$, which could be the eigenstates of the Hamiltonian. Note that one must control the operator nature of the Hamiltonian in the exponential, which means that using the eigenstate of the Hamiltonian is, as far as is known here, the best choice if available, yielding

$$Z = \sum_n e^{-\beta \epsilon_n}$$

Obviously, both here and in the classical discrete spin case, we have an *exponentially* large state space to sum over. The summation yields t^N terms in the sum for N spins with t degrees of freedom per spin. The partition function yields the relevant thermodynamic quantities via differentiation (of the partition function itself or the logarithm of the partition function) from

$$e^{-\beta F} = Z \tag{2.6.1}$$

which gives us

$$\begin{aligned} \langle E\rangle &= -\frac{\partial \log Z}{\partial \beta} \\ C_V &= \frac{\partial \langle E\rangle}{\partial T} \\ \langle M\rangle &= -\frac{1}{\beta}\frac{\partial \log Z}{\partial H}\Big|_{H\to H^*}, \end{aligned}$$

where H^* is usually 0 representing the zero field magnetisation, although H^* is general. We elect to work in one-dimension here, which yields a unique way of factorising the partition function into *transfer matrices* for finite range interactions. We can in principle solve arbitrary range interactions, though the transfer matrices themselves grow. We will go through the method of transfer matrices for the simple case of the Ising model later and only offer an outline here. The method turns the summation over states into matrix multiplication, and so, for periodic boundary conditions, we can write the partition function as

$$Z = Tr \prod_{n=0}^{N} T \to \lambda_0^N \left(1 + \left(\frac{\lambda_1}{\lambda_0} \right)^N + \left(\frac{\lambda_2}{\lambda_0} \right)^N + \dots \right),$$

where T is the transfer matrix, from which we define

$$T|n\rangle = \lambda_n |n\rangle,$$

λ_n is the nth eigenvalue, and λ_0 is the largest one. Using this decomposition, we see that if $\lambda_0 > \lambda_1 > \lambda_2 \dots > 0$ then the partition function is dominated by the largest eigenvalue. Moreover, if we are in the thermodynamic limit, then the largest eigenvalue is *exactly* the partition function, containing all the details of the thermodynamics. This will be the limit that we always work in. The free energy per spin, in the thermodynamic limit, is therefore

$$F = -\frac{1}{\beta} \log \lambda_0$$

Using the transfer matrix technique yields normalised expectation values for operators A as

$$\langle A \rangle = \frac{\langle 0|A|0\rangle}{\langle 0|0\rangle}$$

and correlations as

$$\langle S_0.S_p \rangle = \frac{\langle 0|S_0 T^{p-1} S_p|0\rangle}{\langle 0|T^{p-1}|0\rangle} \quad p > 0$$

for a given type of spin S.

2.6.2 Continuous Spin Models and Transfer Functions

When considering continuous spin models, the summation over the states in the partition function becomes an integral over parameter space. In general one has

$$Z = \int_{\mathbf{R}^{pN}} d\mathbf{r} e^{-\beta H(\mathbf{r})},$$

for an N particle system, where $\mathbf{R}^{pN}$ is the relevant N dimensional parameter space with p degrees of freedom per site, and $\mathbf{r}$ is the relevant pN dimensional vector. Historically continuous models were first studied by Fischer [9], who found that the nearest neighbour Heisenberg model was exactly solvable, which turns out to be a general result for the isotropic models that we will study. This is the first use of transfer *functions* for solving thermodynamics, which is the technique that we apply. Other nearest neighbour continuous models may be solved in one dimension using transfer functions, namely the plane rotator [10, 69]. Here we extend these calculations to the inclusion of a magnetic field, and a second neighbour interaction for some of the models.

We consider the particular case of a one dimensional lattice, with quadratic pairwise interactions of finite range (or linear interactions on single spins), with a

translationally invariant interaction (which can, in principle, be relaxed). We also consider classical spins which we parametrise via two angles to maintain the spin constraint

$$\hat{\mathbf{S}}_n \equiv (\sin\theta_n \cos\phi_n, \sin\theta_n \sin\phi_n, \cos\theta_n)$$

For the plane-rotator model the spins are two-dimensional, given by

$$\hat{\mathbf{S}}_n \equiv (\cos\phi_n, \sin\phi_n, 0),$$

where we have constrained $\theta_n = \frac{\pi}{2}$ on all sites. Using the 3-dimensional spin space for now, we find the partition function as

$$Z = \int \frac{d\hat{\mathbf{S}}_N}{4\pi} \int \frac{d\hat{\mathbf{S}}_{N-1}}{4\pi} \cdots \int \frac{d\hat{\mathbf{S}}_0}{4\pi} e^{-\beta H(g(\hat{\mathbf{S}}_n \ldots \hat{\mathbf{S}}_0))} e^{-\beta H(g(\hat{\mathbf{S}}_{n+1} \ldots \hat{\mathbf{S}}_1))} \cdots e^{-\beta H(g(\hat{\mathbf{S}}_N \ldots \hat{\mathbf{S}}_{N-n}))},$$

where the Hamiltonian $H(g(\ldots))$ is a function of a function of a finite number of spins n. We can perform the integrals one at a time if we solve the following integral equation

$$z f(\theta_1 \ldots \theta_{n+1}; \phi_1 \ldots \phi_{n+1}) = \int_0^\pi \frac{d\theta_0}{2} \int_{-\pi}^\pi \frac{d\phi_0}{2\pi} e^{-\beta \tilde{H}(\hat{\mathbf{S}}_{n+1} \ldots \hat{\mathbf{S}}_0)} f(\theta_0 \ldots \theta_n; \phi_0 \ldots \phi_n),$$

where $\tilde{H}$ is the local part of the total Hamiltonian, which has pairwise interactions up to some range $n+1$, and may have single spin interactions (like a field). We have to include appropriate boundary conditions on the eigenfunctions $f(\mathbf{x})$, although in the thermodynamic limit these are never important. In this limit, the application of the integral operator a large number of times forces the eigenvalue (and relevant eigenvector) to converge to the largest one (the power method). If the integral

operator satisfies the eigen equation

$$z_n|\psi_n\rangle = \hat{\mathbf{K}}|\psi_n\rangle,$$

then a large number of applications of the operator projects us onto the largest eigenstate. In other words

$$\hat{\mathbf{K}}^N|\psi\rangle \simeq z^N|\psi_0\rangle\langle\psi_0|\psi\rangle,$$

which in the thermodynamic limit turns into an equality. Thus we find the largest eigenvalue of the integral equation, which yields the partition function (and therefore free energy per spin) through $\frac{1}{N}\log Z \simeq \log z$ where the approximation is due to the boundary conditions (which in the thermodynamic limit becomes an equality again), and will be dealt with in more detail for the cases of particular models.

Once again, expectation values and correlation functions may be calculated. One wishes to calculate correlations in exactly the same way as Eq.2.6.2, except the spins are vectors, and so one must transfer the spin the relevant number of times to get the correlation function at range p. If we want the long range correlations, the transfer of this spin converges to the largest eigenvalue of the new operator. We will therefore use the method of transfer functions (or transfer matrices) to solve one-dimensional factorisable models.

2.7 Ising

We begin with the regular Ising model in one dimension. This has discrete energies, so the transfer integrals are not relevant, but we start here to introduce the basic

ideas. The model is given by

$$H = -J\sum_n \sigma_n\sigma_{n+1} - B\sum_n \sigma_n,$$

where $\sigma = \pm 1$, J can be positive (negative) yielding ferromagnetism (antiferromagnetism), and B is the applied magnetic field, polarising the spins. We begin with this model (despite it being very well known) to simply illustrate the calculations which will appear later for the more complicated models. There will be no improvements in understanding from applying the technique to the one dimensional Ising model. For negative J with $B \neq 0$ we can examine the simplest possible case of frustration. This model is relatively simple to solve, but serves as a useful starting point for the idea of transfer matrices. The partition function for open boundary conditions with N spins is given by

$$Z = \sum_{\{\sigma\}} e^{-\beta H(\sigma,\sigma')},$$

where $H(\sigma,\sigma')$ is the pairwise Ising Hamiltonian, and $\{\sigma\}$ means a sum over all possible *configurations* (2^N) of the spins. We notice that the Hamiltonian is factorisable (there are many choices of this, so we choose the symmetric one here).

$$\begin{aligned} H = \; & -\frac{B}{2}\sigma_0 - \left[\frac{B}{2}\sigma_0 + J\sigma_0\sigma_1 + \frac{B}{2}\sigma_1\right] - \left[\frac{B}{2}\sigma_1 + J\sigma_1\sigma_2 + \frac{B}{2}\sigma_2\right] \\ & - \ldots - \left[\frac{B}{2}\sigma_{N-1} + J\sigma_{N-1}\sigma_N + \frac{B}{2}\sigma_N\right] - \frac{B}{2}\sigma_N, \end{aligned}$$

for open boundary conditions with $N+1$ spins. The partition function, which is the exponential of the Hamiltonian is therefore a *product* over each element, given by

$$Z = \sum_{\{\sigma\}} e^{\frac{\beta B\sigma_0}{2}} \left[\prod_{n=0}^{N} V_{\sigma_n\sigma_{n+1}}\right] e^{\frac{\beta B\sigma_N}{2}},$$

where we have defined the following

$$V_{\sigma'\sigma} = e^{\frac{\beta B\sigma'}{2}} e^{\beta J\sigma'\sigma} e^{\frac{\beta B\sigma}{2}}$$

The extra terms in the partition function cater for the missing terms in the product. We now recognise that we can turn the sum over spin states into a sum over elements of a matrix if the elements of the matrix take the values from the summation.

$$Z = \sum_{\sigma_0=\pm 1} e^{-\frac{\beta B\sigma_0}{2}} \sum_{\sigma_1=\pm 1} V_{\sigma_0\sigma_1} \sum_{\sigma_2=\pm 1} V_{\sigma_1\sigma_2} \dots$$

We re-write the product as matrix multiplication as follows

$$\sum_{\sigma=\pm 1} V_{\sigma\sigma'} v_\sigma \rightarrow \begin{bmatrix} V_{++} & V_{+-} \\ V_{-+} & V_{--} \end{bmatrix} \begin{bmatrix} v_+ \\ v_- \end{bmatrix}$$

In matrix notation, we get the following transfer matrix

$$V_{\sigma\sigma'} = \begin{bmatrix} e^{\beta J+\beta B} & e^{-\beta J} \\ e^{-\beta J} & e^{\beta J-\beta B} \end{bmatrix}$$

Every time we multiply by another $V_{\sigma\sigma'}$ we perform one of the summations. We want to sum over $N+1$ variables, and so we set up N matrices, along with two vectors at the edge (due to the open boundary conditions). We now diagonalise the transfer matrix, which we shall do in general here, as the basic idea will be used extensively. We create the unitary matrix whose columns are the (normalised) eigenvectors of the transfer matrix V

$$U = \left[\mathbf{u}^0 \;\; \mathbf{u}^1 \dots \mathbf{u}^m\right],$$

for an $m \times m$ problem. We then write that

$$\begin{aligned} VU &= UD \\ \rightarrow V &= UDU^{-1}, \end{aligned}$$

where D is the diagonal matrix containing the eigenvalues z_i of V. To calculate the partition function, we need to multiply N of these matrices together, giving us

$$\begin{aligned} Z &= \mathbf{L}^\dagger \left[UDU^{-1}\right]^N \mathbf{R} \\ &= \mathbf{L}^\dagger U D^N U^{-1} \mathbf{R}, \end{aligned}$$

where $\mathbf{L}$ and $\mathbf{R}$ are the vectors which are left over when dealing with open boundary conditions. We then use that

$$D = \mathrm{diag}[z_0, z_1 \ldots z_m],$$

which, when we raise to a large power, tends towards the largest eigenvalue. For the Ising model, which is currently 2×2, we have that

$$Z = \begin{bmatrix} e^{\frac{\beta B}{2}} & e^{-\frac{\beta B}{2}} \end{bmatrix} \mathbf{U} \begin{bmatrix} z_0 & 0 \\ 0 & z_1 \end{bmatrix}^N \mathbf{U}^{-1} \begin{bmatrix} e^{\frac{\beta B}{2}} \\ e^{-\frac{\beta B}{2}} \end{bmatrix},$$

where $\mathbf{U}$ is the relevant unitary transformation to diagonalise the transfer matrix. This yields the partition function as

$$Z \approx z_0^N e^{-\beta B} \equiv z_0^N \alpha_B,$$

where z_0 and z_1 are the larger and smaller (respectively) eigenvalues of the transfer matrix, given by

$$\begin{aligned} z_0 &= e^{\beta J}\cosh\beta B + \sqrt{e^{2\beta J}(\sinh\beta B)^2 - e^{-2\beta J}} \\ z_1 &= e^{\beta J}\cosh\beta B - \sqrt{e^{2\beta J}(\sinh\beta B)^2 - e^{-2\beta J}} \end{aligned}$$

The extra term in the partition function is from the boundary, but when we calculate the free energy per spin, it does not contribute as it does not scale with N. Thus the free energy *per spin* is given by

$$F = -\frac{1}{\beta}\log\left[e^{\beta J}\cosh\beta B + \sqrt{e^{2\beta J}(\sinh\beta B)^2 - e^{-2\beta J}}\right] + \mathcal{O}\left(\frac{z_1^N}{z_0^N}\right), \qquad (2.7.1)$$

where the last term vanish completely in the thermodynamic limit. We plot the partition function in Fig.2.7 for the simple case of $J_1 = 1$ and $B = 1$. This indicates that the partition function simply exponentially grows at low temperature which is clear from Eq.2.7.1. The partition function for a periodic system is given by

$$Z = \mathrm{Tr}\; e^{-\beta H(\sigma,\sigma')} = \mathrm{Tr}T^N,$$

where $H(\sigma,\sigma')$ is the pairwise Ising Hamiltonian, and T is is the transfer matrix. Note here that we have no edge terms and so the free energy is the same as the open boundary condition case. We can now calculate thermodynamic quantities via differentiation of the free energy. We calculate these quantities now to give indications of how they look. The average energy is given by

$$\langle E\rangle = -\frac{\partial F}{\partial\beta}$$

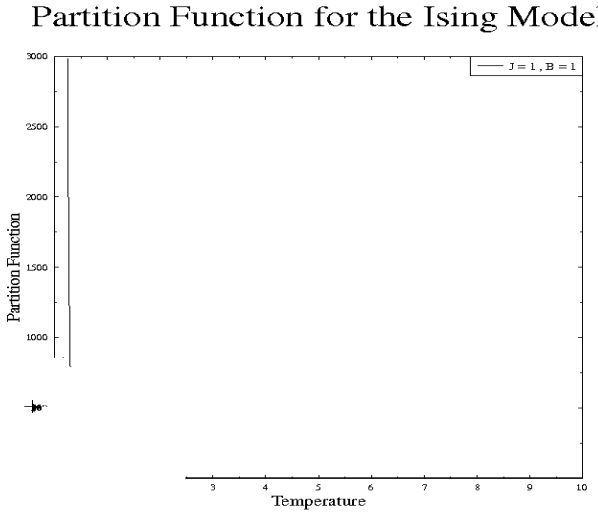

Figure 2.7: Partition function per spin for the Ising model with $J_1 = 1$ and $B = 1$.

For the case of the Ising model, we have an explicit representation of the partition function, and so direct differentiation is possible. Later on, this will not be possible. We see in Fig.2.8 the energy of the Ising model with $J_1 = 1$ and $B = 1$. We see a smooth function of temperature (as expected for one dimension). We may also find the specific heat, the derivative of the energy with respect to temperature, seen in Fig.2.9. Once again a smooth function in temperature, with a smooth peak around $T = 1$. More discussion and interpretation of the form of these graphs will be given later when we calculate them for the continuous models. We also calculate the zero field magnetisation, given by

$$\langle M \rangle = -\frac{1}{\beta} \frac{\partial \log z}{\partial B}\Big|_{B \to 0},$$

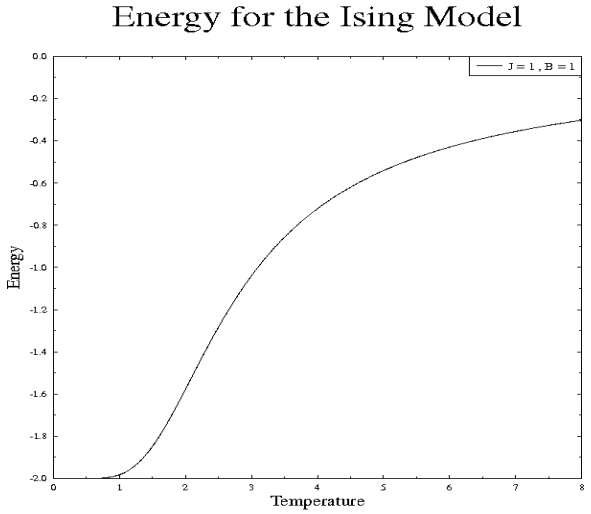

Figure 2.8: Energy for the Ising model with $J_1 = 1$ and $B = 1$.

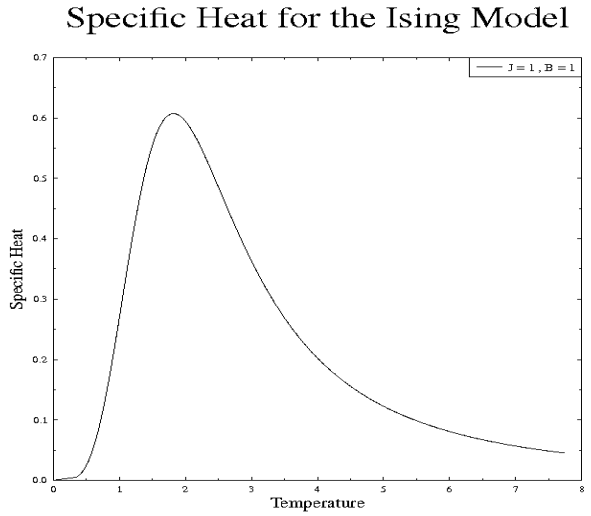

Figure 2.9: Specific heat for the Ising model with $J_1 = 1$ and $B = 1$.

which is given later on in Fig.6.27, as we will use it later. We may also want the (normalised) correlation function of the spins, given by

$$\langle \sigma_0 \sigma_n \rangle = \frac{\sum_{\{\sigma\}} \sigma_0 \sigma_n e^{-\beta H(\sigma\sigma')}}{Z},$$

which we can calculate using

$$\begin{aligned}\langle\sigma_0\sigma_n\rangle &= \frac{\langle a|T^N\sigma V^n\sigma T^N|a\rangle}{\langle a|T^{2N+n}|a\rangle} \\ &= \langle 0|\sigma\frac{V^n}{z^n}\sigma|0\rangle,\end{aligned}$$

where σ is the $\hat{\mathbf{z}}$-component Pauli matrix

$$\sigma \equiv \begin{pmatrix} 1 & 0 \\ 0 & -1 \end{pmatrix}$$

We plot the spin-spin correlations in Fig.2.10, for several values of distance. We see the expected saturation at low temperature, with the reduction in correlations as the temperature is increased as expected. Using transfer matrices, we can also

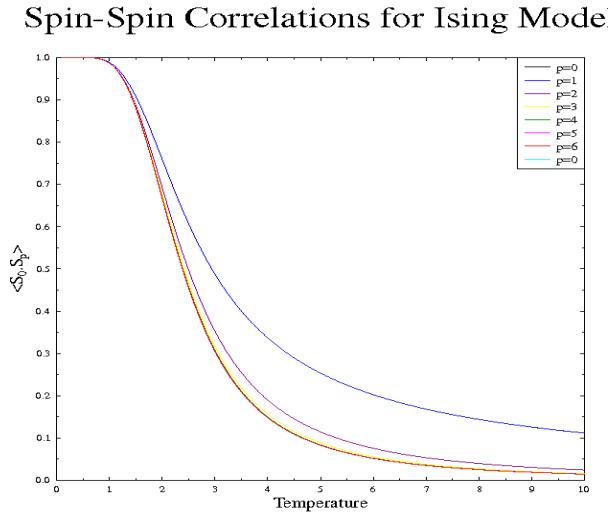

Figure 2.10: Spin-spin correlations for the Ising model with $J_1 = 1$ and $B = 1$.

consider longer range interactions, such as the $J_1 - J_2$ Ising model

$$H = -J_1 \sum_n \sigma_n \sigma_{n+1} - J_2 \sum_n \sigma_n \sigma_{n+2}$$

To solve this, we use a "floating basis", in which we use the next spin to define our local $\hat{\mathbf{z}}$-axis. As we only have Z_2 symmetry, this amounts to redefining "up" and "down" at each stage. The mapping is given by

$$\tau_n \equiv \sigma_n \sigma_{n+1}, \tag{2.7.2}$$

which makes use of the spin inversion symmetry of the Hamiltonian $\sigma \to -\sigma$. Using this mapping, we map the longer range model onto the field, if we identify $J_1 \leftrightarrow B$ and $J_2 \leftrightarrow J$. For the Heisenberg and plane rotator models, using this change of $\hat{\mathbf{z}}$-axis is very useful and allows us to solve the more complicated models in the same way. This is a generic and known feature of models where the spin symmetry and Hamiltonian symmetry are in the same class. We reduce the range of the interaction by one using this trick, so the matrix goes from $2^p \times 2^p \to 2^{p-1} \times 2^{p-1}$ for an interaction of range p, although in general this transformation is unhelpful as it generates a p-particle interaction.

We have therefore found the partition function for the Ising model in the thermodynamic limit. The importance of this is the use of transfer matrices, which will be used judiciously (although as transfer functions) in the continuous spin models. The various thermodynamic quantities (that shall be studied later) have been plotted to indicate their form, and how to calculate them. We will extend the calculations to investigate the physics, however the calculations themselves will always be the same.

2.8 Summary of Following Sections

In the next four chapters, we will solve the thermodynamics for three models and present the results. In Chapters 3, 4 and 5 we will solve the mathematics of the thermodynamics of the plane rotator model, the continuous spin Ising model, and the Heisenberg model respectively. We will provide the method of finding the partition function, and all basic thermodynamic quantities for each model in turn, though we will offer no discussion of each model. In Chapter 6 we will discuss the results of each model. We will provide the "phase diagram" for each one dimensional model (though first we clarify exactly what we mean by phase diagram in one dimensional models), and discuss the magnetisation of each model under a weak applied field.

Chapter 3

PLANE ROTATOR MODEL

3.1 Chapter Summary

Here we provide the solution to the J_1-B and J_1-J_2 plane rotator model which has not been calculated before. Although the model has been studied before using transfer functions [10], the solution was only provided for zero field and nearest neighbour. For the zero field case, the eigen function of the transfer equation becomes a constant for this model, but here we solve the equation, which allows us to solve both J_1-B and J_1-J_2. We first show how to represent the partition function as the solution to an eigenvalue problem. We provide a low and high temperature expansion of the eigenvalue problem, before solving the equation directly. For the plane rotator, we solve the eigenvalue problem in reciprocal space, expressing the problem as an infinite dimensional matrix of Bessel functions, which can be truncated due to their convergence properties. We then show how to calculate the thermodynamics properties from this eigenvalue. We provide the results from the model in Chapter 6, along with the other models, in order to separate the mathematics from the physics.

3.2 Partition Function for the Plane Rotator

3.2.1 The Transfer Equation

To introduce the idea of transfer functions, the analogue of transfer matrices for continuous spin models, we study the plane rotator model, or two-dimensional XY-model. We study the one dimensional version, with nearest neighbour and next-nearest neighbour interactions, given by

$$H = -J_1 \sum_n \left[S_n^x S_{n+1}^x + S_n^y S_{n+1}^y \right] - J_2 \sum_n \left[S_n^x S_{n+2}^x + S_n^y S_{n+2}^y \right]$$

If we had fully three dimensional spins, then this would be the XY-model. However, we elect to work with only one degree of freedom per site and investigate the plane rotator. We therefore parametrise our spins with

$$\hat{\mathbf{S}}_n = (\cos\phi_n, \sin\phi_n, 0)\,,$$

yielding

$$H = -J_1 \sum_n \cos(\phi_n - \phi_{n+1}) - J_2 \sum_n \cos(\phi_n - \phi_{n+2})$$

Note our unconventional choice of sign for the parameters. For J_1 only, we have positive (negative) J_1 yielding ferromagnetism (anti-ferromagnetism). This choice of sign simply makes the analysis easier. We wish to calculate the partition function given by

$$Z = \int \mathcal{D}\left[\phi\right] e^{-\beta H},$$

where we integrate over *all* parameter space. We can write this integral explicitly as

$$Z = \int_{-\pi}^{\pi} \frac{d\phi_0}{2\pi} \int_{-\pi}^{\pi} \frac{d\phi_1}{2\pi} \cdots \int_{-\pi}^{\pi} \frac{d\phi_N}{2\pi} e^{\beta J_1 \sum_n \cos(\phi_n - \phi_{n+1}) + \beta J_2 \sum_n \cos(\phi_n - \phi_{n+2})}$$

for an *open* chain of N spins. We begin with a change of basis, as this makes the analysis slightly easier. We introduce the *floating basis*, with

$$\psi_n = \phi_n - \phi_{n-1},$$

which is the relative angle between the spins. We can do this as the Hamiltonian only depends on this difference, and not the absolute angles, and we have a *closed* integral. We are integrating periodic functions over a closed angle, and thus we can change variables in this way without worry. This transforms the full partition function into

$$Z = \int_{-\pi}^{\pi} \frac{d\psi_0}{2\pi} \int_{-\pi}^{\pi} \frac{d\psi_1}{2\pi} \cdots \int_{-\pi}^{\pi} \frac{d\psi_{N-1}}{2\pi} e^{\beta J_1 \sum_n \cos(\psi_n) + \beta J_2 \sum_n \cos(\psi_n + \psi_{n+1})}$$

Note that the new Hamiltonian is the same as if we'd started with a nearest neighbour interaction and an applied field in the plane of the spins. This analogue is true for the Heisenberg model too, if we make the change of coefficients $J_1 \leftrightarrow B$ and $J_2 \leftrightarrow J_1$. We now notice that, just as in the regular Ising model, we can factorise the Hamiltonian as

$$H = \frac{J_1}{2} \cos\psi_0 + J_2 \cos(\psi_0 + \psi_1) + \frac{J_1}{2} \cos\psi_1 + \ldots \frac{J_1}{2} \cos\psi_{N-1}, \tag{3.2.1}$$

which allows us to factorise the partition function into

$$Z = \int_{-\pi}^{\pi} \frac{d\psi_{N-1}}{2\pi} e^{\beta \frac{J_1}{2} \cos\psi_{N-1}} \prod_{n=0}^{N-2} \left[\int_{-\pi}^{\pi} \frac{d\psi_n}{2\pi} e^{\frac{\beta J_1}{2} \cos\psi_n + \beta J_2 \cos(\psi_n + \psi_{n+1}) + \frac{\beta J_1}{2} \cos\psi_{n+1}} \right] e^{\frac{\beta J_1}{2} \cos\psi_0}$$

We then notice that we can represent this as a transfer equation. Consider the integral equation

$$\begin{aligned} f_{n+1}(\psi_{n+1}) &= \int_{-\pi}^{\pi} \frac{d\psi_n}{2\pi} e^{\frac{\beta J_1}{2} \cos\psi_n + \beta J_2 \cos(\psi_n + \psi_{n+1}) + \frac{\beta J_1}{2} \cos\psi_{n+1}} f_n(\psi_n) \\ \text{or} \quad f_{n+1} &= \hat{\mathbf{K}}(f_n), \end{aligned}$$

where the bottom notation is symbolic, meaning we have an integral operator $\hat{\mathbf{K}}$ which acts on the function f_n and transfers it. To return the partition function, we apply this integral operator $N-1$ times, and thus we have

$$Z = \int_{-\pi}^{\pi} \frac{d\psi_{N-1}}{2\pi} e^{\beta \frac{J_1}{2} \cos\psi_{N-1}} \hat{\mathbf{K}}^{N-1} f_0$$

We then use the idea that the application of this operator a large number of times will converge to the largest eigenvalue

$$\hat{\mathbf{K}}^N f = z_0^N \left[\sum_{n=0}^{p} a_n \frac{z_n^N}{z_0^N} \right],$$

with $z_0 > z_1 > \ldots z_p > 0$ for a p dimensional operator, which here is infinite dimensional for some boundary function f. The boundary conditions f_0 and f_{N-1} do not play a role in the thermodynamics, as in the regular Ising model because they do not depend upon N. Thus, we can neglect the overlap coefficients a_n, and

simply solve the eigenvalue eigenfunction problem

$$zf(\psi') = \int_{-\pi}^{\pi} \frac{d\psi}{2\pi} e^{\frac{\beta J_1}{2}\cos\psi + \beta J_2 \cos(\psi+\psi') + \frac{\beta J_1}{2}\cos\psi'} f(\psi) \tag{3.2.2}$$

This approach is *exact* in the thermodynamics limit $N \to \infty$. The boundary terms which do not play a role numerically do control the *functionality* of the eigenfunction. If we have only next nearest neighbour interactions then the eigenfunction *must* be a constant. This is clear as

$$f_0 = e^{\frac{\beta J_1}{2}\cos\psi_0},$$

and so if $J_1 = 0$, then we simply have a constant. For this case, we find a particularly trivial eigenvalue as

$$z(J_1 = 0) = \int_{-\pi}^{\pi} \frac{d\psi}{2\pi} e^{\beta J_2 \cos\psi} = B_0(\beta J_2),$$

where B_0 is the zeroth modified Bessel function of the first kind; see Appendix.A and has been found before by [10]. Note, that if we only have a nearest neighbour interaction, we have the same partition function, as we do not use the floating basis, and thus $Z(J_2 = 0) = B_0(\beta J_1)$. It should also be noted here that our choice of Hamiltonian in the transfer equation was indeed a choice, here the symmetric one. It amounts to the choice of factorisation in Eq.(3.2.1). One could actually choose

$$H = \sum_n \alpha J_1 \cos\psi_n + J_2 \cos(\psi_n + \psi_{n+1}) + (1-\alpha) J_1 \cos\psi_{n+1} \tag{3.2.3}$$

For any α, with the symmetric choice being $\alpha = \frac{1}{2}$. These other choices lead to much nicer representations for the partition function in the end, as we shall see, but lead to complications with the eigenfunctions as we have complicated the Hermiticity.

We shall deal with this when it arises.

The task we therefore have is to solve the transfer equation Eq.(3.2.2) for the largest eigenvalue and associated eigenfunction. There are many ways to solve the equation, the most obvious being to simply directly integrate it. We will use this method as a cross check, discussing it more in Sec.6.2. However, direct integration includes an error in the calculation which is not clearly under control. Instead, we solve the equation exactly, and use the underlying basis to truncate the calculation. Another naïve way one might proceed is a high temperature expansion, using the inverse temperature as a small parameter. We will provide this now, along with a low temperature expansion, before providing the exact solution to the eigenvalue equation.

3.2.2 High Temperature Expansion

We can perform a temperature expansion for the eigenvalue for the plane rotator model. We expand the eigenvalue (and eigenfunction) in powers of inverse temperature $x \equiv \beta J_1$. We consider the non-field case for the plane rotator model, which (as we have seen) has a particularly trivial partition function given by the zeroth modified Bessel-function. The transfer equation we consider is

$$zf(\cos\psi) = \int_{-\pi}^{\pi} \frac{d\phi}{2\pi} e^{x\cos(\phi+\psi)} f(\cos\phi)$$

We notice that the average of cosine on closed boundaries is zero, so we expand in quadratic order, yielding

$$\left(z_0 + x^2 z_2\right)\left(\alpha_0 f_0(\cos\psi) + \alpha_2 x^2 f_2(\cos\psi)\right) = \int_{-\pi}^{\pi} \frac{d\phi}{2\pi}\left(1 + \frac{x^2\cos^2(\phi+\psi)}{2}\right)$$

$$\times \left(\alpha_0 f_0(\cos\phi) + \alpha_2 x^2 f_2(\cos\phi)\right)$$

At $\mathcal{O}(x^0)$, we find that the eigenfunction is a constant, and that $z_0 = 1$. At $\mathcal{O}(x^2)$ we get

$$z_2 + \alpha_2 f_2(\cos\psi) = \int_{-\pi}^{\pi} \frac{d\phi}{2\pi} \left(\alpha_2 f_2(\cos\phi) + \frac{cos^2(\psi+\phi)}{2}\right)$$

We may perform the integral over the $\cos^2(\psi)$ term, yielding $\frac{1}{4}$. We are therefore left with

$$z_2 + \alpha_2 f_2(\cos\psi) = \frac{1}{4} + \int_{-\pi}^{\pi} \frac{d\phi}{2\pi} \alpha_2 f_2(\cos\phi)$$

The left hand side depends upon ψ and the right hand side does not, so we must have that f_2 is zero. To quadratic order we get

$$z \approx 1 + \frac{x^2}{4}$$

Which agrees with the numerics, as given by Fig.(3.1).

3.2.3 Low Temperature Expansion

We may also perform a low temperature expansion on the transfer function for the plane rotator model. This technique is slightly subtle, as the expansion is non-perturbative. We consider the same transfer equation as the high temperature, though for this we include the next neighbour interaction

$$z f(\psi) = \int_{-\pi}^{\pi} \frac{d\phi}{2\pi} e^{x\cos\phi + y\cos(\phi+\psi)} f(\phi),$$

where $x \equiv \beta J_1$ and $y \equiv \beta J_2$ and we use a non-Hermitian representation. We then use the *ansatz* that the eigenfunction at very low temperature tends to become a

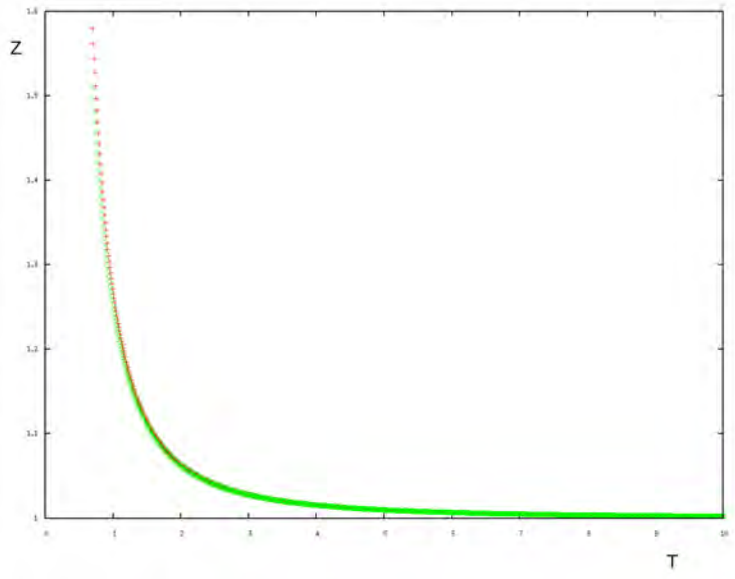

Figure 3.1: The actual calculation of the partition function (red) along with the high temperature expansion (green) for the plane rotator model with nearest neighbour interactions.

Gaussian, and at $T = 0$ it becomes a δ-function. The idea behind this is that the eigenfunction represents the thermal angle distribution of the spins. At high-temperature it is a constant (as we saw above), as the spins are random, and at low temperature the correlations are generated such that they are all parallel (for ferromagnetism). We choose the ferromagnetic groundstate to be around $\phi = 0$, and we expand the cosines as quadratics; at low temperature the spins are presumed not to fluctuate a lot, and so we expand them around some local groundstate. This gives us

$$ze^{-\frac{\alpha}{2}\psi^2} = e^{x+y}\int_{-\pi}^{\pi}\frac{d\phi}{2\pi}e^{-\frac{x}{2}\psi^2-\frac{y}{2}(\psi+\phi)^2-\frac{\alpha}{2}\psi^2}$$

In the low temperature limit, we can let the limits of the integral diverge as the Gaussian terms make the edges of the integral irrelevant in the limit. We calculate

the integral which gives us the self consistent equation

$$ze^{-\frac{\alpha}{2}\psi^2} = \frac{e^{x+y}}{\sqrt{2\pi}\sqrt{x+y+\alpha}} e^{\left(\frac{y^2}{(x+y+\alpha)^2} - \frac{y}{2}\right)\psi^2}$$

We then choose α to be consistent, which gives us the behaviour of the eigenfunction and eigenvalue. We therefore solve the cubic equation in α

$$\frac{\alpha}{2}[\beta J_1 + \beta J_2 + \alpha]^2 = (\beta J_2)^2 - \frac{\beta J_2}{2}$$

Taking the limit $\beta \to \infty$ yields that $\alpha \sim \beta$, which gives

$$z \sim \frac{e^{\gamma_1 \beta}}{\sqrt{\gamma_2 \beta}},$$

where γ_1, γ_2 are constants that depend only on J_1 and J_2. This gives the specific heat to be $\frac{1}{2}$ as $T \to 0$, as is expected.

3.2.4 Reciprocal Space Expansion

To solve Eq.(3.2.2) exactly, we need to find the natural basis for the eigenfunctions. For this problem this turns out to be Fourier space. To make this clear, we use the identity given by Eq.(A.1.16), which we write here for clarity

$$e^{x\cos\psi} = \sum_{l=-\infty}^{\infty} B_l(x) e^{il\psi},$$

where B_l is the l^{th}-modified Bessel function of the first kind. We expand the exponentials in the transfer equation using this, which gives us

$$zf(\psi') = \sum_{l_1}\sum_{l_2}\sum_{l_3} B_{l_1}\left(\frac{\beta J_1}{2}\right) B_{l_2}\left(\beta J_2\right) B_{l_3}\left(\frac{\beta J_1}{2}\right) \int_{-\pi}^{\pi} \frac{d\psi}{2\pi} e^{il_1\psi + il_2(\psi+\psi') + il_3\psi'} f(\psi)$$

We therefore expand the eigenfunctions in a Fourier basis given by

$$f(\psi) = \sum_{n=-\infty}^{\infty} \alpha_n e^{in\psi},$$

which gives us

$$z\sum_{n'} \alpha_{n'} e^{in'\psi'} = \sum_{l_1,l_2,l_3} B_{l_1}\left(\frac{\beta J_1}{2}\right) B_{l_2}\left(\beta J_2\right) B_{l_3}\left(\frac{\beta J_1}{2}\right) \int_{-\pi}^{\pi} \frac{d\psi}{2\pi} e^{il_1\psi + il_2(\psi+\psi') + il_3\psi'} \sum_{n} \alpha_n e^{in\psi}$$

We wish to turn this into a matrix equation, and so we multiply both sides by

$$e^{-im\psi'},$$

and integrate both sides with respect to ψ', yielding

$$\begin{aligned} z\alpha_m = \sum_n \alpha_n \sum_{l_1=-\infty}^{\infty}\sum_{l_2=-\infty}^{\infty}\sum_{l_3=-\infty}^{\infty} & B_{l_1}\left(\frac{\beta J_1}{2}\right) B_{l_2}(\beta J_2) B_{l_3}\left(\frac{\beta J_1}{2}\right) \\ & \times \int_{-\pi}^{\pi}\frac{d\psi}{2\pi}\int_{-\pi}^{\pi}\frac{d\psi'}{2\pi} e^{-im\psi'} e^{il_1\psi} e^{il_2(\psi+\psi')} e^{il_3\psi'} e^{in\psi}, \end{aligned}$$

which we recognise as a matrix eigenvalue eigenvector equation, given by

$$z\alpha_m = \sum_n T_{nm}\alpha_n$$

We then perform the integrals over the angles, yielding

$$\int_{-\pi}^{\pi} \frac{d\psi}{2\pi} e^{i\psi(l_1+l_2+n)} = \delta_{l_1+n=-l_2}$$
$$\int_{-\pi}^{\pi} \frac{d\psi'}{2\pi} e^{i\psi'(-m+l_2+l_3)} = \delta_{-m+l_2+l_3=0}, \tag{3.2.4}$$

which, after putting the Kronecker-delta functions into the transfer matrix gives us

$$T_{nm} = \sum_{l=-\infty}^{\infty} B_{l+n}\left(\frac{\beta J_1}{2}\right) B_l(\beta J_2) B_{l+m}\left(\frac{\beta J_1}{2}\right) \tag{3.2.5}$$

We therefore have to diagonalise this infinite dimensional matrix for the largest eigenvalue. At first sight, it seems we have not moved the problem forward, however we have represented the problem in a very useful way. For *any* non-zero temperature, the matrix has exponentially decaying elements away from the origin. Numerically, we therefore *truncate* the matrix to some range in $\pm n, m$, say N, M for which we have a numerically exact (ie. up to some numerical accuracy) answer for the matrix above some temperature, below which the truncation becomes inaccurate. Consider the high temperature limit, $\beta \to 0$. If $\beta = 0$, then $B_n(\beta J) = \delta_{n0}$, and thus the matrix becomes one element, given by $T = [B_0(0)]^3 = 1$ yielding the infinite temperature eigenvalue trivially. When we lower the temperature, we simply increase the number of elements that we include.

3.2.5 Calculating Thermodynamic Quantities

We now move on to the calculation of thermodynamic quantities; energy, specific heat, and correlation functions. To calculate thermodynamic quantities, we could use numerical differentiation of the partition function. However, the zero temper-

ature limit of the partition function is poor as it diverges, and so we use exact differentiation along with perturbation theory. The transfer matrix, for a change in any small parameter (like temperature), is given by

$$T(x+\delta x) = T(x) + \delta x \frac{dT}{dx}(x) + \dots$$

The eigenvalue is also given by

$$z(x+\delta x) = z(x) + \delta x \frac{dz}{dx}(x) + \dots$$

We therefore have

$$\langle 0|T(x+\delta x)|0\rangle = z_0(x+\delta x),$$

where $\langle 0|$ is the eigenvector of the transfer matrix associated with the eigenvalue z_0, and so we find that

$$z(x+\delta x) = z(x) + \delta x \langle 0|\frac{dz}{dx}|0\rangle$$

Note that for the models considered here, the energy (related to the first derivative with respect to β) is smooth, and so we use numerical differentiation of the energy for specific heat. We therefore only have to calculate derivatives of the Bessel function with respect to any parameter we wish to average over. For example, the energy, given by logarithmic differentiation with respect to β, gives us

$$\langle E\rangle = \frac{1}{z}\langle 0|\frac{\partial}{\partial\beta}\left[\sum_{l=-\infty}^{\infty} B_{l+n}\left(\frac{\beta J_1}{2}\right) B_l(\beta J_2) B_{l+m}\left(\frac{\beta J_1}{2}\right)\right]|0\rangle,$$

where z is the largest eigenvalue of the transfer matrix, and $\langle 0|$ is the associated eigenvector. We use the identity for differentiation of a Bessel function, given by

Eq.(A.1.17), to find

$$\begin{aligned}\langle E\rangle = \frac{1}{2z}\Big\langle 0\Big| \sum_{l=-\infty}^{\infty} \Big\{ \frac{J_1}{2}\left[B_{l+n+1}\left(\frac{\beta J_1}{2}\right) + B_{l+n-1}\left(\frac{\beta J_1}{2}\right)\right] B_l(\beta J_2) B_{l+m}\left(\frac{\beta J_1}{2}\right) \\ + J_2 B_{l+n}\left(\frac{\beta J_1}{2}\right)\left[B_{l+1}(\beta J_2) + B_{l-1}(\beta J_2)\right] B_{l+m}\left(\frac{\beta J_1}{2}\right) \\ + \frac{J_1}{2} B_{l+n}\left(\frac{\beta J_1}{2}\right) B_l(\beta J_2)\left[B_{l+m+1}\left(\frac{\beta J_1}{2}\right) + B_{l+m-1}\left(\frac{\beta J_1}{2}\right)\right] \Big\}\Big|0\Big\rangle \\ = \frac{1}{2z}\langle 0|\left[\frac{J_1}{2}\left(T_{n+1,m} + T_{n-1,m}\right) + J_2\left(T_{n+1,m+1} + T_{n-1,m-1}\right) + \frac{J_1}{2}\left(T_{n,m+1} + T_{n,m-1}\right)\right]|0\rangle,\end{aligned}$$

where the last line relates the elements back to the original transfer matrix elements that we have already calculated. We can then numerically differentiate this with respect to temperature in order to get the specific heat.

We may wish to calculate correlation functions, which once again are given by differentiation of the transfer matrix. In the transfer matrix language, correlation functions are given by

$$\langle \hat{\mathbf{S}}_p \cdot \hat{\mathbf{S}}_1 \rangle = \frac{1}{z^{n+2N}} \frac{\langle a|T^N \hat{\mathbf{S}}_p V^n \hat{\mathbf{S}}_1 T^N|a\rangle}{\langle a|0\rangle\langle 0|a\rangle},$$

where we take N to be large enough to converge left and right. This essentially means we choose $|a\rangle = |0\rangle$. The matrix V is the modification of the original matrix T by including the chosen spin. For each model, this procedure will end up differently. For the case of the plane rotator, we attempt to calculate the spin-spin correlation at range p, given by

$$\frac{\langle \hat{\mathbf{S}}_0.\hat{\mathbf{S}}_p\rangle}{z^p} = \frac{\langle \cos(\phi_0 - \phi_p)\rangle}{z^p} = \frac{\langle \cos(\psi_0 + \psi_1 + \ldots \psi_{p-1})\rangle}{z^p},$$

where ϕ is in the non-floating basis, and ψ is floating. We then write the cosine in

exponential form, which allows us to re-write the sum of the angles as a product of exponentials of the angles, viz

$$\langle S_0.S_p\rangle = \frac{1}{2}\left[\langle 0|\frac{Te^{i\psi_0}}{z}\frac{Te^{i\psi_1}}{z}\ldots\frac{Te^{i\psi_{p-1}}}{z}|0\rangle + \langle 0|\frac{Te^{-i\psi_0}}{z}\frac{Te^{-i\psi_1}}{z}\ldots\frac{Te^{-i\psi_{p-1}}}{z}|0\rangle\right],$$

where we have defined

$$\tilde{T}_\pm \equiv \frac{e^{\pm i\psi}T}{z}$$

The inclusion of the correlations simply changes the transfer matrix that we must use (in the floating basis), yielding

$$\langle S_0.S_p\rangle = \frac{1}{2}\left(\langle 0|\tilde{T}_+^{p-1}|0\rangle + \langle 0|\tilde{T}_-^{p-1}|0\rangle\right)$$

We therefore have to calculate the matrix $\tilde{T}_\pm$, which turns out to be relatively easy. It is given by

$$\begin{aligned}\tilde{T}_\pm^{nm} = &\sum_{l_1=-\infty}^{\infty}\sum_{l_2=-\infty}^{\infty}\sum_{l_3=-\infty}^{\infty} B_{l_1}\left(\frac{\beta J_1}{2}\right)B_{l_2}(\beta J_2)B_{l_3}\left(\frac{\beta J_1}{2}\right)\\ &\times\int_{-\pi}^{\pi}\frac{d\psi}{2\pi}\int_{-\pi}^{\pi}\frac{d\psi'}{2\pi}e^{-im\psi'}e^{il_1\psi}e^{il_2(\psi+\psi')}e^{il_3\psi'}e^{in\psi}e^{\pm i\psi}\end{aligned}$$

This simply changes the Kronecker-delta functions in Eq.(3.2.4) for one of the indices when we integrate over the angles, giving us

$$\begin{aligned}(\tilde{T}_+)_{nm} &= \sum_l B_{l+n+1}\left(\frac{\beta J_1}{2}\right)B_l(\beta J_2)B_{l+m}\left(\frac{\beta J_1}{2}\right)\\ &= T_{n+1,m}\end{aligned}$$

Note that $\tilde{T}_- = T_{n-1,m}$ which provides the same overlap for this Hermitian repre-

sentation, and so we only need one transfer matrix. This gives

$$\langle S_0.S_p\rangle = \langle 0|\frac{[T_+]^{p-1}}{z^p}|0\rangle$$

Note, that while one can calculate the correlation functions as posed here, in reality we use the non-Hermitian representation, (which could in principle be used for all the models). From Eq.(3.2.3), we use the choice $\alpha = 1$. As we shall see, the transfer matrix is much simpler, and would allow the one to two dimensional crossover to be analysed. We use

$$zf(\psi') = \int_{-\pi}^{\pi} \frac{d\psi}{2\pi} e^{\beta J_1 \cos\psi + \beta J_2 \cos(\psi+\psi')} f(\psi)$$

We expand the exponentials in terms of Bessel functions, and expand the eigenfunctions in reciprocal space, and use the same analysis as was used prior, to arrive at the simple expression

$$T_{nm} = B_n(\beta J_2) B_{n+m}(\beta J_1),$$

with the correlation transfer matrix being related in the same manner as previously. Care must be taken with the non-Hermiticity as there is a left and right eigenvector

$$\begin{aligned} T|v_R\rangle &= z|v_R\rangle \\ \langle v_L|T^\dagger &= \langle v_L|z, \end{aligned}$$

with the normalisation $\langle v_L|v_R\rangle = 1$. Note, that we could choose any α, which in general gives us the transfer matrix

$$T_{nm} = [B_n(\beta J_2)]^\alpha \, B_{n+m}(\beta J_1) \, [B_m(\beta J_2)]^{1-\alpha},$$

though we can only use this for ferromagnetism as the Bessel functions become negative for negative argument (antiferromagnetic interactions), which for non-integer α is a problem.

3.2.6 Summary

We have provided the solution to the plane rotator, for the partition function and various thermodynamic quantities. We have represented the partition function in terms of an integral equation using the method of transfer functions, and then reduced the problem to that of finding the largest eigenvalue of an explicit infinite dimensional matrix. The elements of this matrix become numerically irrelevant after some range for any given temperature, and we may therefore truncate it in order to diagonalise. Correlation functions have also been found in terms of this matrix, and all thermodynamic quantities may be calculated by differentiation (either exactly or numerically). We will provide the results for this model in the results section, but we use the basic ideas presented here to solve two more models first; the continuous spin Ising model and the Heisenberg model.

Chapter 4

CONTINUOUS-SPIN ISING MODEL

4.1 Chapter Summary

Here we provide the solution to the J_1-B continuous spin Ising model. This model has not been solved at all thermodynamically, and hence all of this chapter is new work. We show how to represent the partition function as the solution to an eigenvalue problem. We provide a low and high temperature expansion of the eigenvalue problem, before solving the equation directly. For the continuous spin Ising model, we solve this using recursion relations, though an "exact" solution is provided as a further cross check. We then show how to calculate the thermodynamics properties from this eigenvalue. We provide the results from the model in Chapter 6, along with the other models, in order to separate the mathematics from the physics. We also solve the so called plane Ising model, an Ising model that only has one degree of freedom per site which is continuous.

At the end of the chapter we solve a related model known as the plane Ising model. This model has also never been solved before, and we find the solution for J_1-B-Δ where Δ is anisotropy which moves between the plane Ising model and the plane rotator.

4.2 Partition Function for the Continuous Ising Model

4.2.1 The Transfer Equation

We now move on to the "continuous" version of the Ising model given by the Hamiltonian

$$H = -J\sum_n S_n^z S_{n+1}^z - B\sum_n S_n^z = -J\sum_n \cos\theta_n \cos\theta_{n+1} - B\sum_n \cos\theta_n,$$

where $S_n = (\sin\theta_n \cos\phi_n, \sin\theta_n \sin\phi_n, \cos\theta_n)$, and we have included a field in the $\hat{\mathbf{z}}$-direction which polarises the spins. Once again we have chosen the unconventional sign of the parameters to make the analysis slightly easier. The spins are fully three-dimensional, but only interact in the $\hat{\mathbf{z}}$-direction. The low temperature will be clearly dominated by maximal spin, and so we expect similarities to the Ising model. Once again however (as will be shown later) the excitations are domain walls, whose width turns out to be of order the lattice spacing, and so no order is possible. The full partition function is given by

$$\begin{aligned} Z &= \int_0^\pi \sin\theta_0 e^{\frac{\beta B}{2}\cos\theta_0}\frac{d\theta_0}{2}\int_0^\pi \sin\theta_1 \frac{d\theta_1}{2}\ldots \\ &\times \int_0^\pi \sin\theta_N e^{\frac{\beta B}{2}\cos\theta_N}\frac{d\theta_N}{2} e^{\beta J\sum_n \cos\theta_n\cos\theta_{n+1} + \frac{\beta B}{2}\sum_n(\cos\theta_n + \cos\theta_{n+1})} \end{aligned}$$

Just as in the plane rotator model, we factorise the Hamiltonian into local parts which extend over some range (here only to neighbours), and transfer them and

therefore we consider the operator equation

$$\begin{aligned} f_{n+1}(\cos\theta') &= \int_0^\pi \frac{d\theta}{2} \sin\theta e^{\beta J \cos\theta\cos\theta' + \frac{\beta B}{2}(\cos\theta+\cos\theta')} f_n(\cos\theta) \\ \text{or} \quad f_{n+1} &= \hat{\mathbf{K}}(f_n) \end{aligned}$$

We wish to use this operator a large number of times to return the partition function, and so we run it forwards and backwards. Here, we have a Hermitian representation which means that the operator is it's own inverse (going forwards and backwards are equivalent), and therefore we can write the boundary conditions as

$$f_0(\cos\theta_0) = e^{\frac{\beta B}{2}\cos\theta_0}; \quad f_N(\cos\theta_N) = e^{\frac{\beta B}{2}\cos\theta_N}$$

and therefore write the partition function as

$$Z = \int_0^\pi \sin\theta_N \frac{d\theta_N}{2} f_N^\dagger \hat{\mathbf{K}}^N f_0$$

In the large N limit, the integral operator converges to the eigenfunction associated with the largest eigenvalue, as before, while the corrections do not scale with N (stemming from boundary conditions), and so can be neglected for the thermodynamics. We therefore have the transfer equation

$$z f(\cos\theta') = \int_0^\pi \frac{d\theta}{2} \sin\theta e^{\frac{\beta B}{2}(\cos\theta+\cos\theta') + \beta J\cos\theta\cos\theta'} f(\cos\theta), \tag{4.2.1}$$

which we have to solve for the eigenvalue and eigenfunction. We then have the partition function per spin through

$$\frac{1}{N}\log Z \approx \frac{\alpha_B}{N} + \log z_0,$$

where α_B does not depend on N, and is only boundary dependent and therefore does not contribute to the thermodynamics. Once again we made a choice for the factorisation of the Hamiltonian. Here we have the symmetric version, and in fact we will only work with the symmetric version here, though once again one has the choice

$$H = \sum_m \left(\beta J \cos\theta_m \cos\theta_{m+1} + \beta B(1-\alpha)\cos\theta_m + \beta B\alpha \cos\theta_{m+1}\right)$$

for any real α. Once again, one may perform low and high temperature expansions for the transfer equation before we attempt to find the natural basis for the problem (for which new complications will arise).

4.2.2 High Temperature Expansion

We can calculate the partition function for the continuous-spin Ising model for high temperature using perturbation theory. To make the integration variable more natural, we use $u \equiv \cos\theta$ which we shall use later. We consider the case with no applied field, though for this model the eigenfunction turns out to still be non-trivial. We consider the transfer equation

$$z f(u) = \int_{-1}^{1} \frac{dv}{2} e^{xuv} f(v)$$

where $x \equiv \beta J$. We expand each term in a power series in x^2 as $x \to 0$ to get

$$\left(z_0 + x^2 z_2\right)\left(f_0(u) + x^2 f_2(u)\right) = \int_{-1}^{1} \frac{dv}{2}\left(1 + \frac{x^2u^2v^2}{2}\right)\left(f_0(v) + x^2 f_2(v)\right)$$

We first notice that $f_0(u) = \alpha_0$ and must be a constant as the kernel for this term has no u dependence at $\mathcal{O}(x^0)$. This gives us the first term in the expansion $z_0 = 1$. We next calculate the correction. For the terms in u to balance, we notice that $f_0(u) = \alpha_2 u^2$ for some constant that we shall find. Thus the $\mathcal{O}(x^2)$ term gives

$$x^2 z_2 + x^2 u^2 \alpha_2 z_0 = \int_{-1}^{1} \frac{dv}{2} \left[\frac{x^2 u^2 v^2}{2} + \alpha_2 x^2 v^2 \right]$$

from which we get

$$z_2 = \frac{u^2}{6} + \frac{\alpha_2}{3} - u^2 \alpha_2$$

We need to cancel the term in u and thus we find $\alpha_2 = \frac{1}{6}$, from which we find

$$z \approx 1 + \frac{x^2}{18},$$

which agrees with the numerics for high temperature as in Fig.(4.1).

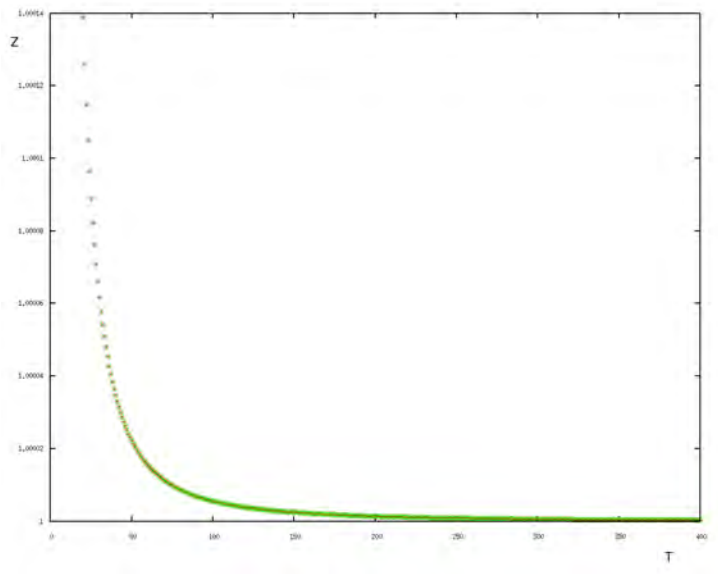

Figure 4.1: The actual calculation of the partition function (red) along with the high temperature expansion (green). for the continuous-spin Ising model

4.2.3 Low Temperature Expansion

One can also perform a low temperature expansion on the same model. Once again, we examine the same eigenvalue equation, but in the limit $x \to \infty$. For this limit, we expect the physics to be dominated by ferromagnetism which means the points $u = \pm 1$ needs to be controlled. To do this, we elect to use the variable θ rather than u. Given that the expression will be dominated by the regions around ferromagnetism, we only include the regions around these points ie. $\theta = \pi$ and $\theta = 0$. We therefore get

$$\begin{aligned} zf(\cos\theta') &= \int_0^\epsilon \frac{d\theta}{2} \sin\theta e^{x\cos\theta\cos\theta'} f(\cos\theta) + \int_{\pi-\epsilon}^{\pi} \frac{d\theta}{2} \sin\theta e^{x\cos\theta\cos\theta'} f(\cos\theta) \\ &= \int_0^\epsilon d\theta \sin\theta e^{x\cos\theta\cos\theta'} f(\cos\theta), \end{aligned}$$

where we have used the fact that the eigenfunction (and the Kernel) are symmetric with respect to $\cos\theta$. We expect the fluctuations to be small around the ferromagnetism, and therefore expand for small θ to quadratic order

$$zf(\theta'^2) = \int_0^\epsilon d\theta\theta e^{x-\frac{x}{2}(\theta^2+\theta'^2)} f(\theta^2)$$

We make θ^2 the integration variable, with the substitution $\theta^2 \equiv \frac{\psi}{x}$, and then use the ansatz

$$f\left(\frac{\psi}{x}\right) = e^{-\frac{\alpha\psi}{x}}$$

This provides us with the *self-consistent* equation for the parameter α

$$ze^{-\frac{\alpha\psi'}{x}} = e^x \int_0^{x\epsilon^2} d\psi e^{-\frac{\psi+\psi'}{2}} e^{-\frac{\alpha\psi}{x}}$$

If we choose $\alpha = \frac{x}{2}$, the equation is self-consistent, and we are simply left with the eigenvalue (in which we use the limit $x \to \infty$ to get the upper limit of the integral).

$$z = \frac{e^x}{2x} \int_0^\infty d\psi e^{-\psi} = \frac{e^x}{2x},$$

from which we see that the specific heat goes to 1 for $x \to \infty$ as expected.

4.2.4 Legendre Basis Expansion

We therefore want to find the largest eigenvalue of the integral operator. To solve this, we choose to turn it into a matrix equation, by expanding the eigenfunction in some orthogonal basis. We let $u = \cos\theta$ such that

$$\int_0^\pi \sin\theta \frac{d\theta}{2} \to \int_{-1}^1 \frac{du}{2}$$

We notice that the new measure is the natural measure for which the Legendre polynomials are orthogonal. Thus we expand the eigenfunction in this orthogonal basis as

$$f(u) = \sum_{n=0}^{\infty} \sqrt{2n+1}\alpha_n P_n(u)$$

This converts the continuous eigenfunction problem into a discreet eigenvector problem, whose eigenvalues are exactly the same. We can always recover the continuous eigenfunction by

$$f^0(\cos\theta) = \sum_{n=0}^{\infty} \sqrt{2n+1}\alpha_n^0 P_n(\cos\theta),$$

where f^0 and α^0 are the largest eigenfunction and eigenvector respectively. From this we get

$$z\sum_{l=0}^{\infty}\alpha_l\sqrt{2l+1}P_l(v)=\sum_{n=0}^{\infty}\alpha_n\sqrt{2n+1}\int_{-1}^{1}\frac{du}{2}e^{\beta Juv+\frac{\beta B}{2}(u+v)}P_n(u)$$

We multiply both sides by a Legendre polynomial, and integrate; in other words we "multiply" by

$$\sqrt{2m+1}\int_{-1}^{1}\frac{dv}{2}P_m(v),$$

to get

$$z\alpha_m=\sqrt{2m+1}\sum_{n=0}^{\infty}\sqrt{2n+1}\int_{-1}^{1}\frac{du}{2}\int_{-1}^{1}\frac{dv}{2}P_m(v)P_n(u)e^{\beta Juv+\frac{\beta B}{2}(u+v)}\alpha_n$$

We now recognise the transfer matrix, defined as

$$\begin{aligned}T_n^m &= \sqrt{2n+1}\sqrt{2m+1}H_n^m\\ H_n^m &= \int_{-1}^{1}\frac{du}{2}\int_{-1}^{1}\frac{dv}{2}P_n(u)P_m(v)e^{\beta Juv+\frac{\beta B}{2}(u+v)},\end{aligned}$$

where the subscript-superscript notation means nothing mathematically, but makes the recursion relations that we use easier to understand later. It should also be read in the order subscript-superscript which relates to row-column respectively. We can perform the integral over v using the identity given in Eq.(A.1.9) to get the integral in terms of the m-th modified Bessel function of the first kind

$$H_n^m=\int_{-1}^{1}\frac{du}{2}P_n(u)I_m\left(xu+y\right)e^{yu},$$

where $x \equiv \beta J$ and $y \equiv \beta B/2$. For the cases of the plane-rotator and the classical Heisenberg models, the limit $B \to 0$ yields a constant eigenfunction. Here the zero field case is given by

$$H_n^m(B=0) = \int_{-1}^{1} \frac{du}{2} P_n(u) I_m(xu)$$

Even the simplest term in this matrix is given by

$$H_0^0(B=0) = \int_{-1}^{1} \frac{du}{2} \frac{\sinh xu}{xu},$$

which is defined as the hyperbolic sine integral. The task is therefore to find the eigenvalue and eigenfunction of the matrix H_n^m, though the elements of this matrix are non-trivial unlike the other models. We will offer two ways of generating the matrix elements.

4.2.5 Recursion Relations

We seek to diagonalise the matrix T, but even generating the matrix elements is a non-trivial task. We therefore resort to a more subtle method; recursion relations. This method will be exact up to any numerical accuracy, as will be clear when we use the method. To generate the matrix elements, we note that the integrals are in terms of Bessel functions and Legendre polynomials which have recurrence relations. We may use these to generate recurrence relations between the integrals themselves, and so we generate three such equations given by

$$H_0^{m-2} = \left(\frac{2m-1}{m-1}\right)\left(\frac{(I_{m-1}(y+x)e^y - I_{m-1}(y-x)e^{-y} - H_0^{m-1}y)}{x}\right) - \left(\frac{m}{m-1}\right) H_0^m \tag{4.2.2}$$

$$H_1^{m-2} = \frac{\left(\frac{y-1}{y}\right) I_{m-1}(y+x)e^y - \left(\frac{y+1}{y}\right) I_{m-1}(y-x)e^{-y}}{x} \frac{2m-1}{m-1} + \frac{(m-1)H_0^{m-2} + mH_0^m}{y(m-1)} - \frac{y(2m-1)}{x(m-1)} H_1^{m-1} - \frac{m}{m-1} H_1^m \quad (4.2.3)$$

$$H_{n+1}^{m-1} = H_{n-1}^{m+1} - \frac{n-m}{n+m+1}(H_{n-1}^{m-1} - H_{n+1}^{m+1}) - \frac{y(2n+1)}{x(n+m+1)}(H_n^{m-1} - H_n^{m+1}) + \frac{y(2m+1)}{x(n+m+1)}(H_{n-1}^m - H_{n+1}^m) \quad (4.2.4)$$

where $n \neq m$. See Appendix B for the derivations. Under the assumption

$$\lim_{n\to\infty} H_n^m \to 0$$
$$\lim_{m\to\infty} H_n^m \to 0$$

which is guaranteed by the Bessel functions which have the limit

$$\lim_{n\to\infty} I_n(x) \to 0$$

exponentially, we can use the recursion relations to find the matrix to machine accuracy provided we have n and m sufficiently large at the boundary. For the case of zero field, we find the matrix has the form (for even N)

$$\begin{pmatrix} H_0^0 & 0 & H_0^2 & \dots & H_0^N \\ 0 & H_1^1 & 0 & \dots & 0 \\ H_2^0 & 0 & H_2^2 & \dots & H_2^N \\ \vdots & \vdots & \vdots & \ddots & \vdots \\ H_N^0 & 0 & H_N^2 & \dots & H_N^N \end{pmatrix}$$

The elements at the boundary tend to zero for large N and so we *truncate* the matrix to some order N. The field couples in the odd terms of this matrix. To use the recursion relations, we use that the *scale* of the relation is automatically given by the Bessel functions. We first use Eq.(4.2.2). We start with the terms furthest away from the origin as zero, and seed the next element with the Bessel functions given in the recursion relation. For large enough N, this value is close to zero and does not affect anything. We run the recursion relation *backwards* towards the origin. When we get to the origin, we do not have to rescale the first term, as the Bessel functions themselves have set the scale. We then use Eq.(4.2.3) which gives us the terms one inside from the edge, and run it in exactly the same way. Finally we use Eq.(4.2.4) which allows us to calculate everywhere in the matrix, apart from at the edges, whose terms are given by the previous two recursion relations. We then diagonalise the matrix T_n^m to find the largest eigenvalue, from which we can calculate the appropriate thermodynamic quantities.

4.2.6 Thermodynamic Quantities

Once again, we use perturbation theory to find thermodynamic quantities. For the energy, we require

$$\frac{\partial T_n^m}{\partial \beta} = \sqrt{2n+1}\sqrt{2m+1}\left[\int_{-1}^{1}\frac{du}{2}P_n(u)\left(e^{yu}\frac{\partial I_m(xu+y)}{\partial \beta}+Bue^{yu}I_m(xu+y)\right)\right],$$

from which we get

$$\left(\frac{\partial T}{\partial \beta}\right)_n^m = \frac{J}{(1+2n)(1+2m)}\Big[nmH_{n-1}^{m-1}+n(m+1)H_{n-1}^{m+1} \\ +(n+1)mH_{n+1}^{m-1}+(n+1)(m+1)H_{n+1}^{m+1}\Big]$$

$$+\frac{B}{2n+1}(nH^m_{n-1}+(n+1)H^m_{n+1})$$

Similarly we can calculate $\langle S^z\rangle$ (the magnetisation) and $\langle S^z_n S^z_{n+1}\rangle$ (the nearest neighbour correlation function), by calculating

$$\begin{aligned}\langle S^z\rangle &= \frac{2}{\beta}\frac{\left\langle 0\left|\frac{\partial z}{\partial y}\right|0\right\rangle}{z}\\ \langle S^z_n S^z_{n+1}\rangle &= \frac{1}{\beta}\frac{\left\langle 0\left|\frac{\partial z}{\partial x}\right|0\right\rangle}{z}\end{aligned}$$

To calculate longer range interactions, we wish to calculate

$$\langle S^z_0 S^z_p\rangle = \frac{1}{z^p}\langle\cos\theta_0\cos\theta_p\rangle$$

Unlike the plane rotator there is no floating basis, and so we may simply integrate over the spins that we are correlating. We get two modified transfer matrices, ie.

$$\langle S^z_0 S^z_p\rangle = \frac{1}{z^p}\langle 0|\tilde{T}^m_n (T^m_n)^{p-2}\tilde{T}^m_n|0\rangle;\quad p\geq 2$$

where $\tilde{T}$ is defined by

$$\tilde{z}\tilde{f}(v) = \int_{-1}^{1}\frac{du}{2}e^{\beta Juv+\frac{\beta B}{2}(u+v)}u\tilde{f}(u)$$

which is the modified transfer matrix for the inclusion of the spin. For the case of this model, the correlation moves us from the symmetric subspace to the anti-symmetric one, where

$$f(u) = f(-u)$$

$$\tilde{f}(u) \;=\; -\tilde{f}(-u)$$

For very long range correlations, the T^{p-2} converges to the groundstate, and so we may calculate

$$\lim_{p\to\infty} T^p \to |0\rangle z^p \langle 0|$$
$$\lim_{p\to\infty} \langle S_0.S_p\rangle \to \langle 0|\frac{\tilde{T}}{z}|0\rangle\langle 0|\frac{\tilde{T}}{z}|0\rangle$$

However, as stated before, $\tilde{T}$ is anti-symmetric, and is therefore orthogonal to the groundstate, telling us that there are no infinite range correlations (no long range order), so we must use the excited eigenstate corresponding to the new anti-symmetry, yielding

$$\lim_{p\to\infty} \langle S_0.S_p\rangle \to \langle 0|\frac{\tilde{T}}{z}|1\rangle \left(\frac{\tilde{z}}{z}\right)^{p-2} \langle 1|\frac{\tilde{T}}{z}|0\rangle,$$

where $\tilde{z}$ is the eigenvalue associated with the eigenstate $\langle 1|$. This scales away as

$$\left(\frac{\tilde{z}}{z}\right)^p,$$

which gives the correlation length for long range, given by

$$e^{-\frac{p}{\xi}} \sim \left(\frac{\tilde{z}}{z}\right)^p$$
$$\xi = \frac{1}{\log\left(\frac{z}{\tilde{z}}\right)}$$

We may use recursion relations to generate the matrix elements of the transfer matrix. However, we may cross check this by calculating the elements directly. We have also shown how to calculate various thermodynamic quantities using the

recursion relations.

4.2.7 Exact Method

We now offer an exact way of calculating the partition function for the case of zero field (although in principle a field could be added). Once again, the previous method is also exact, though not necessarily in the same sense. Here, we have a convergent summation, whereas the recursion relations rely on seeding the relations with a sufficiently small number. It turns out that these two methods are completely equivalent, and so we offer this as a cross check of the recursion method. We use the identity from scattering theory that shall be used in full for the Heisenberg model, to find

$$\begin{aligned} e^{xS_n^zS_{n+1}^z} &= e^{x[u_nu_{n+1}+(1-u_n^2)^{\frac{1}{2}}(1-u_{n+1}^2)^{\frac{1}{2}}\cos(\phi_n-\phi_{n+1})]}\Big|_{\phi_n-\phi_{n+1}=\frac{\pi}{2}} \\ &= \sum_{l=0}^{\infty}(2l+1)I_l(x)\sum_{m=-\left[\frac{l}{2}\right]}^{\left[\frac{l}{2}\right]}P_l^{2m}(u_n)P_l^{2m}(u_{n+1})(-1)^m, \end{aligned}$$

where we have used the identity

$$P_l^{2m}(x)P_l^{2m}(x) = P_l^{-2m}(x)P_l^{-2m}(x)$$

and $[\ldots]$ means integer part of. We use the same ideas as were used previously to turn the integral problem into a matrix problem to find

$$T_n^m = \sqrt{2n+1}\sqrt{2m+1}\sum_{l=0}^{\infty}(2l+1)I_l(\beta J)\sum_{p=-\left[\frac{l}{2}\right]}^{\left[\frac{l}{2}\right]}(-1)^pQ_{ln}^{2p}Q_{lm}^{2p},$$

where we have defined

$$Q_{ln}^{2p} \equiv \int_{-1}^{1} \frac{du}{2} P_n(u) P_l^{2p}(u)$$

In order to perform these integrals we use the method as given in [70]. We use the representation of of the associated Legendre polynomials of the form

$$P_l^m(u) = \frac{(-1)^m}{2^l l!} \frac{\sqrt{(l+m)!}}{\sqrt{(l-m)!}} (1-u^2)^{-\frac{m}{2}} \frac{d^{l-m}}{du^{l-m}} (u^2-1)^l$$

We then perform the differential part. We find that

$$\begin{aligned}
\frac{d^{l-m}}{du^{l-m}}(u^2-1)^l &= 2^0 (2u)^{l-m} \frac{l!}{m!}(u^2-1)^m && p=0 \\
&+ 2^1 (l-m)(2u)^{l-m-1} \frac{l!}{(m+1)!}(u^2-1)^{m-1} && p=1 \\
&+ 2^2 \frac{(l-m)(l-m-1)}{2} (2u)^{l-m-2} \frac{l!}{(m+2)!}(u^2-1)^{m-2} && p=2 \\
&+ \ldots
\end{aligned}$$

from which we find (after carrying the previous terms into the expression)

$$P_l^m(u) = \sum_{p_1=0}^{\left[\frac{l-m}{2}\right]} u^{l-m-2p_1} (1-u^2)^{p_1+\frac{m}{2}} \underbrace{\frac{(-1)^{p_1+m}\sqrt{(l+m)!}\sqrt{(l-m)!}}{2^{m+2p_1}(m+p_1)!p_1!(l-m-2p_1)!}}_{\alpha_{l,p_1}^m} \tag{4.2.5}$$

This gives us an expression for the integral

$$\begin{aligned}
Q_{l_1,l_2}^{m_1,m_2} &\equiv \int_{-1}^{1} \frac{du}{2} P_{l_1}^{m_1}(u) P_{l_2}^{m_2}(u) \\
&= \sum_{p_1=0}^{\left[\frac{l_1-m_1}{2}\right]} \sum_{p_2=0}^{\left[\frac{l_2-m_2}{2}\right]} \alpha_{l_1 p_1}^{m_1} \alpha_{l_2 p_2}^{m_2} \int_{-1}^{1} \frac{du}{2} u^{l_1-m_1-2p_1+l_2-m_2-2p_2} (1-u^2)^{p_1+p_2+\frac{m_1}{2}+\frac{m_2}{2}}
\end{aligned}$$

from this, using the identities

$$\begin{aligned}\beta(x,y) &\equiv \int_0^1 dt\; t^{x-1}(1-t)^{y-1} \\ \beta(x,y) &= \frac{\Gamma(x)\Gamma(y)}{\Gamma(x+y)}\end{aligned}$$

We find that

$$\begin{aligned}Q_{l_1,l_2}^{m_1,m_2} &= \sum_{p_1=0}^{\left[\frac{l_1-m_1}{2}\right]}\sum_{p_2=0}^{\left[\frac{l_2-m_2}{2}\right]}\frac{\alpha_{l_1p_1}^{m_1}\alpha_{l_2p_2}^{m_2}}{2} \\ &\times \underbrace{\left(\frac{\Gamma\left(\frac{1}{2}\left(l_1+l_2-m_1-m_2-2p_1-2p_2+1\right)\right)\Gamma\left(\frac{1}{2}\left(m_1+m_2+2p_1+2p_2+2\right)\right)}{\Gamma\left(\frac{1}{2}\left(l_1+l_2+3\right)\right)}\right)}_{t_{l_1,l_2,p_1,p_2}^{m_1,m_2}}\end{aligned}$$

Thus we get an expression for the transfer matrix again

$$\begin{aligned}T_n^m = \sqrt{2n+1}\sqrt{2m+1}\sum_{l=0}^{\infty}(2l+1)I_l(\beta J)\sum_{p=-\left[\frac{l}{2}\right]}^{\left[\frac{l}{2}\right]}(-1)^p \\ \sum_{p_1=0}^{\left[\frac{l-2p}{2}\right]}\sum_{p_2=0}^{\left[\frac{n}{2}\right]}\sum_{p_3=0}^{\left[\frac{l-2p}{2}\right]}\sum_{p_4=0}^{\left[\frac{m}{2}\right]}\frac{\alpha_{l,p_1}^{2p}\alpha_{n,p_2}^{0}}{2}\frac{\alpha_{l,p_3}^{2p}\alpha_{m,p_4}^{0}}{2}t_{l,n,p_1,p_2}^{2p,0}t_{l,m,p_3,p_4}^{2p,0}\end{aligned}$$

This expression is numerically much slower than the recursion relation due to the large number of summations, however, it serves as an exact calculation which we can check the recursion relation against. We get numerical accuracy, though the code runs an order of magnitude slower at low temperature in order to get the accuracy.

4.3 Plane Ising Model

We briefly introduce an alternative model to the continuous Ising model, where rather than three dimensional spins, we have planar spins, though the energetics are still only controlled by the length of the spin in some direction. We introduce it here, although it lies somewhere between the Ising model and the plane rotator. It shares the same mathematics as the plane rotator, and indeed the model we consider is a generalised plane rotator, but for for special cases it becomes an Ising model of sorts, and so we include the model here. Consider the following model

$$H = -J \sum_n S_n^x S_{n+1}^x + \Delta S_n^y S_{n+1}^y$$

For the case $\Delta = 1$ we clearly get the plane rotator model, but for $\Delta = 0$ we get an Ising like interaction but with the ϕ degree of freedom. Once again the constraint $\sigma = \pm 1$ is relaxed to $\sigma \in [-1, 1]$. The zero field solution is non-trivial (like the continuous spin Ising model), and so we begin there. It is clear that the transfer equation we must solve is

$$zf(\psi) = \int_{-\pi}^{\pi} \frac{d\phi}{2\pi} e^{\beta J \cos\phi \cos\psi} f(\phi)$$

The natural basis for the model is Fourier space, and thus we get

$$z \sum_n \alpha_n e^{in\psi} = \sum_{l_1 l_2} I_{l_1}\left(\frac{\beta J}{2}\right) I_{l_2}\left(\frac{\beta J}{2}\right) \int_{-\pi}^{\pi} \frac{d\phi}{2\pi} e^{il_1(\phi+\psi)+il_2(\phi-\psi)+im\phi},$$

which gives us the transfer matrix

$$t_{nm} = \sum_{l_1 l_2} I_{l_1}\left(\frac{\beta J}{2}\right) I_{l_2}\left(\frac{\beta J}{2}\right) \int_{-\pi}^{\pi} \frac{d\phi}{2\pi} \int_{-\pi}^{\pi} \frac{d\psi}{2\pi} e^{il_1(\phi+\psi)+il_2(\phi-\psi)+im\phi-in\psi}$$

We then find, after integrating the over angles

$$T_{nm} = I_{n+m}\left(\frac{\beta J}{2}\right) I_{n-m}\left(\frac{\beta J}{2}\right) \tag{4.3.1}$$

We may include a field in the $\hat{\mathbf{x}}$-direction, which gives us

$$zf(\psi) = \int_{-\pi}^{\pi} \frac{d\phi}{2\pi} e^{\beta J \cos\phi \cos\psi + \frac{\beta B}{2}(\cos\phi + \cos\psi)} f(\phi),$$

which, using exactly the same mathematics gives us

$$T_{nm} = \sum_{l_1,l_2} I_{l_1}\left(\frac{\beta J}{2}\right) I_{l_2}\left(\frac{\beta J}{2}\right) I_{l_1+l_2+n}\left(\frac{\beta B}{2}\right) I_{l_1-l_2-m}\left(\frac{\beta B}{2}\right)$$

If we take $B \to 0$, this yields the same result as Eq.4.3.1. We may also solve the model as a function of Δ which allows us to turn on anisotropy smoothly. We consider the Hamiltonian

$$\begin{aligned} H &= -J\sum_n S_n^x S_{n+1}^x + \Delta S_n^y S_{n+1}^y - B\sum_n S_n^x \\ &= -J\Delta\sum_n \cos(\phi_n - \phi_{n+1}) - J(1-\Delta)\sum_n \cos(\phi_n)\cos\phi_{n+1}) - B\sum_n \cos\phi_n \end{aligned}$$

which gives us the transfer equation

$$zf(\psi) = \int_{-\pi}^{\pi} \frac{d\phi}{2\pi} e^{\frac{\beta J(1+\Delta)}{2}\cos(\phi-\psi) + \frac{\beta J(1-\Delta)}{2}\cos(\phi+\psi) + \frac{\beta B}{2}(\cos\phi+\cos\psi)} f(\phi)$$

After the same mathematics again, gives us

$$T_{nm} = \sum_{l_1,l_2} I_{l_1}\left(\frac{\beta J(1+\Delta)}{2}\right) I_{l_2}\left(\frac{\beta J(1-\Delta)}{2}\right) I_{l_1+l_2+n}\left(\frac{\beta B}{2}\right) I_{l_1-l_2-m}\left(\frac{\beta B}{2}\right),$$

which once again, when $\Delta = 0$ returns the same answer as before. Moreover, $\Delta = 1$ provides the same transfer matrix as the plane rotator given in Eq.3.2.5. This representation allows us to smoothly include anisotropy to the plane rotator model, or consider the Ising model with one degree of freedom per site.

In the results section we do not discuss this model, although we expect it to be "similar" to the continuous Ising, with domain walls (of some sort) controlling the excitations, although the energy scales will be different. Including the parameter Δ drastically changes the nature of domain walls; for $\Delta = 1$ they are ill defined and infinitely long range (as will be explained in the results section). However, when $\Delta \neq 1$, (here we only consider $\Delta \leq 1$), then domain walls suddenly have finite extent, and so the model becomes Ising like.

4.3.1 Summary

We have provided the solution to the continuous spin Ising model, for the partition function and various thermodynamic quantities. We have used the method of transfer functions in order to calculate the partition function, and have demonstrated how to calculate quantities from this transfer function (matrix). We have provided two methods to find the elements of the transfer matrix in order to provide a cross check. The plane Ising model has also been solved, although very little attention will be given to this model.

Chapter 5

HEISENBERG MODEL

5.1 Chapter Summary

Here we provide the solution to the J_1-B and J_1-J_2 Heisenberg model. Once again, this is new work, and like the plane rotator, the model has only been solved when the eigenfunction is a constant [9]. Many approximate solutions exist, such as including a field [56], or directly integrating over small clusters [67]. In the same spirit as the other models, we first show how to represent the partition function as the solution to an eigenvalue problem. We solve the eigenvalue problem exactly, using a Legendre basis to represent the eigenfunction, and once again express the problem as an infinite dimensional matrix of Bessel functions, which can be truncated due to their convergence properties. We then show how to calculate the thermodynamics properties from this eigenvalue. For the J_1-J_2 Heisenberg model, the focus is on the correlation functions, which are particularly complicated due to spin space and nature of the floating basis.

5.2 Partition Function for the Heisenberg Model

Finally, we move on to the classical one-dimensional Heisenberg model. We consider the Heisenberg model with a field (or equivalently first and second nearest neighbours as will be seen later), with open boundary conditions, given by

$$H = -J\sum_n \hat{\mathbf{S}}_n \cdot \hat{\mathbf{S}}_{n+1} - B\sum_n \hat{\mathbf{B}} \cdot \hat{\mathbf{S}}_n,$$

where $\hat{\mathbf{S}}_n$ is a three dimensional unit vector on the n-th site, B is the amplitude of the field, and $\hat{\mathbf{B}}$ is the field direction, and we have chosen an unconventional minus sign to make the later analysis more natural. Clearly, the partition function is given by

$$Z = \int \frac{d\mathbf{S}_N}{4\pi}\int \frac{d\mathbf{S}_{N-1}}{4\pi}\cdots\int \frac{d\mathbf{S}_1}{4\pi} e^{-\beta H(\hat{\mathbf{S}}_N,\hat{\mathbf{S}}_{N-1}\ldots\hat{\mathbf{S}}_1;J,B)},$$

and so we can set up a transfer function given by

$$f_{n+1}(\hat{\mathbf{S}}_{n+1}) = \int \frac{d\mathbf{S}_n}{4\pi} e^{\beta\left(J\hat{\mathbf{S}}_n\cdot\hat{\mathbf{S}}_{n+1}+\frac{B}{2}\hat{\mathbf{B}}\cdot(\hat{\mathbf{S}}_n+\hat{\mathbf{S}}_{n+1})\right)} f_n(\hat{\mathbf{S}}_n)$$

We have the starting condition (stemming from the open boundary)

$$f_1(\hat{\mathbf{S}}_1) = e^{\frac{B\hat{\mathbf{B}}\cdot\hat{\mathbf{S}}_1}{2}},$$

such that the partition function is given by

$$Z = \int \frac{d\mathbf{S}_N}{4\pi} e^{\frac{B\hat{\mathbf{B}}\cdot\hat{\mathbf{S}}_N}{2}} f_N(\hat{\mathbf{S}}_N)$$

Once again, the application of the integral operator N times (in the thermodynamic limit) projects us onto the largest eigenvalue, and so we solve the eigenvalue equation

$$zf(\hat{\mathbf{S}}_{n+1}) = \int \frac{d\mathbf{S}_n}{4\pi} e^{\beta\left(J\hat{\mathbf{S}}_n\cdot\hat{\mathbf{S}}_{n+1}+\frac{B}{2}\hat{\mathbf{B}}\cdot(\hat{\mathbf{S}}_n+\hat{\mathbf{S}}_{n+1})\right)} f(\hat{\mathbf{S}}_n)$$

This yields the partition function through $Z = z^N \alpha_B$, where once again the boundary term α_B does not contribute to the thermodynamics. For this model, the $\hat{\mathbf{z}}$-axis is defined by the magnetic field (globally), as the interactions are spherically symmetric, thus we write

$$H = -J\sum_n \hat{\mathbf{S}}_n.\hat{\mathbf{S}}_{n+1} - B\sum_n S_n^z,$$

with

$$\begin{aligned}\hat{\mathbf{S}}_n &= (\sin\theta_n\cos\phi_n, \sin\theta_n\sin\phi_n, \cos\theta_n)\\ &= ((1-u_n^2)^{\frac{1}{2}}\cos\phi_n, (1-u_n^2)^{\frac{1}{2}}\sin\phi_n, u_n)\end{aligned}$$

For the case with $B = 0$, we find that the eigenfunction is a constant. The open boundary condition is clearly $f_1 = 1$, and as the interaction is isotropic, the integrand cannot depend on the next spin viz

$$\begin{aligned}zf(\hat{\mathbf{S}}_2) &= \int \frac{d\mathbf{S}}{4\pi} e^{\beta J\hat{\mathbf{S}}_1\cdot\hat{\mathbf{S}}_2}\\ &= \int_0^{2\pi}\frac{d\phi}{2\pi}\int_{-1}^{1}\frac{du}{2}e^{\beta Ju}\end{aligned}$$

We can always redefine u (the $\hat{\mathbf{z}}$-axis), which does not change the integral itself, and so $f(\hat{\mathbf{S}}_2)$ must be a constant, yielding the partition function (found originally by

Fischer [9])

$$Z(B=0) = \frac{\sinh \beta J}{\beta J} \tag{5.2.1}$$

For the case of finite field, more analysis is needed. For the case of nearest neighbour interaction, and a magnetic field, we use the magnetic field to define the global $\hat{\mathbf{z}}$-axis, and expand the dot product as follows

$$\exp\left[x\hat{\mathbf{S}}_1 \cdot \hat{\mathbf{S}}_2\right] \;=\; \exp\left[x\left(u_1u_2 + (1-u_2)^{\frac{1}{2}}(1-u_1)^{\frac{1}{2}}\cos(\phi_1-\phi_2)\right)\right]$$

We then use the plane wave expansion Eq.(A.1.10), and once again we use $u_n \equiv \cos\theta_n$. Substituting the scattering expansion into the eigenfunction equation we get

$$zf(\hat{\mathbf{S}}_{n+1}) = \sum_{l=0}^{\infty}\sum_{m=-l}^{l}\int_0^{2\pi}\frac{d\phi_n}{2\pi}\int_{-1}^{1}\frac{du_n}{2}I_l(\beta J)(2l+1)P_l^m(u_n)P_l^m(u_{n+1}) \\ \times e^{im(\phi_n-\phi_{n+1})}e^{\frac{\beta B}{2}(u_n+u_{n+1})}f(\hat{\mathbf{S}}_n)$$

We can perform the integral over the azimuthal angle, noting that the eigenfunction only depends on $\cos\theta$ (coming from the boundary condition) so that $f(\hat{\mathbf{S}}) \equiv f(S^z)$. The integration over ϕ means the only contribution is for when $m = 0$, yielding

$$zf(u_{n+1}) = \sum_{l=0}^{\infty}(2l+1)I_l(\beta J)\int_{-1}^{1}\frac{du_n}{2}f(u_n)e^{\frac{\beta B}{2}(u_n+u_{n+1})}P_l(u_n)P_l(u_{n+1})$$

We then expand the eigenfunction in the same Legendre basis, using

$$f(u) = \sum_{n=0}^{\infty}\sqrt{2n+1}\alpha_n P_n(u),$$

where we have included the extra factor $\sqrt{2n+1}$ as a convenient normalisation. Upon substitution, and "multiplying" through by

$$\sqrt{2m+1}\int_{-1}^{1} du_{n+1} P_m(u_{n+1}),$$

and using the orthogonality of the Legendre Polynomials yields the matrix representation of the transfer function, defined as

$$T_n^m = \sqrt{2n+1}\sqrt{2m+1}\sum_{l=0}^{\infty}(2l+1)I_l(\beta J)C_{nl}\left(\frac{\beta B}{2}\right)C_{ml}\left(\frac{\beta B}{2}\right),$$

where we have defined

$$C_{nl}(x) \equiv \int_{-1}^{1}\frac{du}{2}P_n(u)P_l(u)e^{xu}$$

We thus diagonalise this matrix for the largest eigenvalue, yielding the partition function. However, the function $C_{nl}(x)$ is not trivial to calculate. It has been evaluated numerically previously, and expanded and represented in terms of Wigner-3j symbols [56]. We use the identity given by Adams [71], for the expansion of a pair of Legendre polynomials in terms of one polynomial

$$P_n(x)P_m(x) = \sum_{r=0}^{\min(n,m)}\frac{\alpha(m-r)\alpha(n-r)\alpha(r)}{\alpha(n+m-r)}\left(\frac{2n+2m-4r+1}{2n+2m-2r+1}\right)P_{n+l-2r}(x),$$

where

$$\begin{aligned}\alpha(n) &= \frac{1.3.5\ldots(2n-1)}{2.4\ldots 2n}\\ &= \frac{\Gamma(2n+1)}{2^{2n}\Gamma(n+1)\Gamma(n+1)},\end{aligned}$$

where the second representation allows us to define $\alpha(0) = 1$ and for fractional arguments, though in practice we only ever use the top expression. We can check the normalisation of this expression;

$$\begin{aligned}\int_{-1}^{1} \frac{du}{2} P_n(u) P_l(u) &= \frac{\delta_{nl}}{2n+1} \\ &= \sum_{r=0}^{\min(n,l)} \frac{\alpha(l-r)\alpha(n-r)\alpha(r)}{\alpha(n+l-r)} \left(\frac{2n+2l-4r+1}{2n+2l-2r+1}\right) \\ &\times \int_{-1}^{1} \frac{du}{2} P_{n+m-2r}(u)\end{aligned}$$

The final integral, when multiplied by $P_0(u)$ is clearly $\delta_{n+m-2r,0}$, yielding

$$\alpha\left(\frac{n-l}{2}\right)\alpha\left(\frac{l-n}{2}\right)\frac{1}{n+l+1}$$

We then note that $\alpha(n)$ is zero for $n < 0$, yielding the required normalisation. We then use the identity for the Bessel function given in Eq.A.1.9 to find that

$$C_{nl}(x) = \sum_{r=0}^{\min(n,l)} \frac{\alpha(l-r)\alpha(n-r)\alpha(r)}{\alpha(n+l-r)} \left(\frac{2n+2l-4r+1}{2n+2l-2r+1}\right) I_{n+l-2r}(x)$$

We now have a way of calculating the partition function for the Heisenberg model with an applied magnetic field. Once again, we use perturbation theory to calculate thermodynamic quantities and the derivative matrices are exactly calculable using the identities for derivatives of Bessel functions. We have represented the partition function for the $J_1 - B$ model in terms of the largest eigenvalue of a transfer matrix. In principle this matrix is infinite dimensional, but the convergence of the Bessel functions makes it numerically finite. We now move on to the $J_1 - J_2$ model. For

the case of next nearest neighbour interactions, we have the model

$$H = -J_1 \sum_n \hat{\mathbf{S}}_n \cdot \hat{\mathbf{S}}_{n+1} - J_2 \sum_n \hat{\mathbf{S}}_n \cdot \hat{\mathbf{S}}_{n+2},$$

and the transfer function is given by

$$zf(\hat{\mathbf{S}}', \hat{\mathbf{S}}'') = \int \frac{d\hat{\mathbf{S}}}{4\pi} e^{\frac{J_1}{2}\hat{\mathbf{S}}\cdot\hat{\mathbf{S}}' + J_2\hat{\mathbf{S}}\cdot\hat{\mathbf{S}}'' + \frac{J_1}{2}\hat{\mathbf{S}}'\cdot\hat{\mathbf{S}}''} f(\hat{\mathbf{S}}, \hat{\mathbf{S}}')$$

The boundary condition now tells us that the eigenfunction can only depend on the dot product between the two spins. We once again expand in the Legendre basis, and notice that the nearest neighbour interaction plays the role of the magnetic field, although it can be different on every site. In fact, we are changing the local $\hat{\mathbf{z}}$-axis at each stage by defining it as the "first" spin; the one we integrate over. This becomes important when we calculate the correlation functions, as we must rotate the basis at each stage after each integration. The thermodynamics of this model are exactly the same as the one with the field. We get the same transfer matrix, but with the appropriate coefficients swapped, $J_1 \leftrightarrow B$ and $J_2 \leftrightarrow J$. This is exactly the same as when we used the floating basis in the plane rotator model, and shows that the thermodynamics of these isotropic models is the same for a field and nearest neighbour interaction, and nearest neighbour and next neighbour interactions. Although they have the same thermodynamics, they are not the same, and this is most obvious when we calculate the correlation functions for the two models. We calculate the correlation function for the nearest neighbour model first, and then the J_1-J_2 correlation functions.

5.2.1 Correlation Functions

There are two types of spin correlations; parallel and perpendicular. They have a different structure, and so we calculate them separately. We begin with the J_1-B model, for which there is a global $\hat{\mathbf{z}}$-axis. We may then calculate the correlations parallel and perpendicular to the field. To calculate the correlation function, we calculate the following

$$\langle \hat{\mathbf{S}}_n \cdot \hat{\mathbf{S}}_1 \rangle = \frac{1}{z^{n+2N}} \frac{\langle a|T^N \hat{\mathbf{S}}_n V^n \hat{\mathbf{S}}_1 T^N|a\rangle}{\langle a|0\rangle\langle 0|a\rangle}, \tag{5.2.2}$$

where N is taken to be very large such that $T^N|a\rangle$ converges to the groundstate transfer function (as before) and cancels the factor of $\frac{1}{z^{2N}}$, and V is the modified transfer function for including the chosen spin which depends on the type of correlation which is being calculated. If we simply choose $|a\rangle = |0\rangle$ then the analysis is much simpler, and we can neglect any extra factors. The parallel z-component of the correlation function yields a transfer matrix of the form

$$(T_{nn'})^{01}_{CC} = \sum_{l=0}^{\infty} \sqrt{1+2n}\sqrt{1+2n'}(1+2l) I_l(\beta J) C_{nl}\left(\frac{\beta B}{2}\right) \frac{dC_{n'l}}{dx}\left(\frac{\beta B}{2}\right),$$

where we have included the superscripts for derivatives, and we have used the representation

$$\hat{\mathbf{S}}_n = \left([1-u_n^2]^{\frac{1}{2}} \cos\phi_n, [1-u_n^2]^{\frac{1}{2}} \sin\phi_n, u_n\right)$$

We have simply included a u in the integral, which is clearly just a derivative. Thus we find the parallel component of correlation is given by

$$\langle S_p^z S_1^z \rangle = \frac{1}{z^p} \langle 0|T^{01}_{CC}(T^{00}_{CC})^{p-2} T^{01}_{CC}|0\rangle \quad p \geq 2$$

We can trivially calculate the derivative of the integral C_{nm}, which is given by

$$\frac{dC_{nl}}{dx}(x) = \frac{l}{2l+1}C_{nl-1}(x) + \frac{l+1}{2l+1}C_{nl+1}(x)$$

The perpendicular components, however, are more difficult to calculate. We have to include the extra cosine or sine in the ϕ integral, which gives $m = 1$ rather than zero as before. The extra $[1-u^2]^{\frac{1}{2}}$ must also be included, yielding

$$\tilde{T}_{nn'} = \sqrt{2n+1}\sqrt{2n'+1}\sum_{l=0}^{\infty}(2l+1)I_l(\beta J)$$
$$\times \int_{-1}^{1}\frac{du}{2}\int_{-1}^{1}\frac{du'}{2}P_n(u)P_{n'}(u')P_l^1(u)P_l^1(u')[1-u^2]^{\frac{1}{2}}e^{\frac{\beta B}{2}(u+u')},$$

which yields two integrals

$$\tilde{C}_{nl}(x) = \int_{-1}^{1}\frac{du}{2}P_n(u)[1-u^2]^{\frac{1}{2}}P_l^1(u)e^{xu}$$

And

$$\tilde{D}_{nl}(x) = \int_{-1}^{1}\frac{du}{2}P_n(u)P_l^1(u)e^{xu},$$

the first of these is, once again, trivial (using the recursion formulae), we find that

$$\tilde{C}_{nl}(x) = \frac{\sqrt{l(l+1)}}{2l+1}(C_{nl-1}(x) - C_{nl+1}(x))$$

However, $\tilde{D}$ is harder to calculate. We once again use the recursion formula for the Legendre to find

$$\tilde{D}_{nl}(x) = \frac{\sqrt{l(l+1)}}{2l+1}(D_{nl-1}(x) - D_{nl+1}(x)),$$

where

$$\begin{aligned} D_{nl}(x) &= \int_{-1}^{1} \frac{du}{2} \frac{P_n(u)P_l(u)}{\sqrt{1-u^2}} e^{xu} \\ &= \int_0^{\pi} \frac{d\theta}{2} P_n(\cos\theta)P_l(\cos\theta)e^{x\cos\theta} \end{aligned}$$

We use the identity

$$\begin{aligned} \frac{1}{\sqrt{1-2x\cos\theta+x^2}} &= \frac{1}{\sqrt{1-xe^{i\theta}}\sqrt{1-xe^{-i\theta}}} \\ &\equiv \sum_{n=0}^{\infty} x^n P_n(\cos\theta) \\ &= \sum_{n=0}^{\infty} x^n \sum_{m=0}^{n} \alpha(m)\alpha(n-m)e^{i(n-2m)\theta}, \end{aligned}$$

which yields

$$D_{nl}(x) = \frac{\pi}{2} \sum_{m_1=0}^{n} \alpha(m_1)\alpha(n-m_1) \sum_{m_2=0}^{l} \alpha(m_2)\alpha(l-m_2)$$

$$\times \sum_{m=m^*}^{\infty} \alpha(m-m_1-m_2)\alpha(m+m_1+m_2-n-l)(1+4m-2n-2l)I_{2m-n-l}(x)$$

We recognise new transfer matrices given by

$$(\tilde{T}_{nn'})^{00}_{CD} = \sum_{l=0}^{\infty} \sqrt{2n+1}\sqrt{2n'+1}(2l+1)I_l(\beta J_1)\tilde{D}_{nl}\left(\frac{\beta B}{2}\right)\tilde{C}_{n'l}\left(\frac{\beta B}{2}\right),$$

from which we find

$$\langle S^y_p S^y_1\rangle = \langle S^x_p S^x_1\rangle = \frac{1}{z^p}\langle 0|\tilde{T}^{00}_{CD}\left(\tilde{T}^{00}_{DD}\right)^{p-2}\tilde{T}^{00}_{DC}|0\rangle$$

The correlation functions for the $J_1 - J_2$ Heisenberg model are significantly more involved due to the change of basis at each stage. We wish to calculate the quantity

$$\langle \hat{\mathbf{S}}_n . \hat{\mathbf{S}}_0 \rangle = \frac{1}{z^n} \langle 0 | \hat{\mathbf{S}}_n T^n \hat{\mathbf{S}}_0 | 0 \rangle \tag{5.2.3}$$

The basic idea is to change the basis at each stage, and calculate how the distortion (due to the correlation) is transferred down the chain. The issue with the calculation is that the $J_1 - J_2$ Heisenberg model has a floating basis as there is no global $\hat{z}$ axis defined. Thus, we must rotate the basis at each stage. This idea is also in the plane rotator, but there spin space is much simpler, which means the change of basis factorises in a relatively simple manner. Here however there is no such factorisation. We begin with *representing* the chosen spin $\hat{\mathbf{S}}_n$ in the basis of the two next spins, $\hat{\mathbf{S}}_{n+1}$ and $\hat{\mathbf{S}}_{n+2}$ as follows

$$\begin{aligned} \hat{\mathbf{S}}_n &= \hat{\mathbf{S}}_{n+1} u_n + \hat{\mathbf{S}}_{n+2} [1 - u_n^2]^{\frac{1}{2}} \cos(\phi_n - \phi_{n+1}) [1 - u_{n+1}^2]^{\frac{1}{2}} \\ &- \frac{\hat{\mathbf{S}}_{n+1} - u_{n+1} \hat{\mathbf{S}}_{n+2}}{[1 - u_{n+1}^2]^{\frac{1}{2}}} \cos(\phi_n - \phi_{n+1}) u_{n+1} [1 - u_n^2]^{\frac{1}{2}} \\ &+ \frac{\hat{\mathbf{S}}_{n+1} \wedge \hat{\mathbf{S}}_{n+2}}{[1 - u_{n+1}^2]^{\frac{1}{2}}} \sin(\phi_n - \phi_{n+1}) [1 - u_n^2]^{\frac{1}{2}}, \end{aligned} \tag{5.2.4}$$

where $u_n \equiv \cos(\theta_n)$ is the angle between $\hat{\mathbf{S}}_n$ and $\hat{\mathbf{S}}_{n+1}$ which means we describe the spin $\hat{\mathbf{S}}_n$ with $\hat{\mathbf{S}}_{n+1}$ as the local $\hat{\mathbf{z}}$-axis. The crucial step is to now transfer the *basis* at each stage using this. The final term in Eq.(5.2.4) turns out to be zero when we transfer it as it is antisymmetric with respect to the ϕ integral, and so we may neglect it always. This leaves us with three terms, which we use as the natural basis

at each stage. If we set up the local basis

$$V_n^\dagger = \left(\hat{\mathbf{S}}_n, \hat{\mathbf{S}}_{n+1}, \frac{\hat{\mathbf{S}}_n - u_n \hat{\mathbf{S}}_{n+1}}{[1-u_n^2]^{\frac{1}{2}}} \right), \tag{5.2.5}$$

and then consider the transfer equation

$$V_{n+1}^\dagger = V_n^\dagger \mathcal{T},$$

where $\mathcal{T}$ is a matrix of the transfer matrices, each term in which acts on the relevant component of V_n and transfers it. If we begin with the simplest case, simply transferring the spin itself, then we start with transferring the spin along the chain with the transfer matrix T

$$T(\hat{\mathbf{S}}_n)$$

We replace the spin by the representation from Eq.(5.2.4) yielding

$$T(\hat{\mathbf{S}}_n) = \mathbf{S}_{n+1} T_{CC}^{01} + \mathbf{S}_{n+2} \tilde{T}_{CC}^{00} - \left(\frac{\hat{\mathbf{S}}_{n+1} - u_{n+1} \hat{\mathbf{S}}_{n+2}}{[1-u_{n+1}^2]^{\frac{1}{2}}} \right) \tilde{T}_{CD}^{10}$$

We wish to do this for each term in the new basis in Eq.(5.2.5), and thus we find

$$\begin{aligned} T(\hat{\mathbf{S}}_{n+1}) &= \mathbf{S}_{n+1} T_{CC}^{00} \\ T\left(\frac{\hat{\mathbf{S}}_{n+1} - u_{n+1} \hat{\mathbf{S}}_{n+2}}{[1-u_{n+1}^2]^{\frac{1}{2}}} \right) &= \mathbf{S}_{n+2} \tilde{T}_{DC}^{00} - \left(\frac{\hat{\mathbf{S}}_{n+1} - u_{n+1} \hat{\mathbf{S}}_{n+2}}{[1-u_{n+1}^2]^{\frac{1}{2}}} \right) \tilde{T}_{DD}^{10}, \end{aligned} \tag{5.2.6}$$

where we have used

$$\frac{\hat{\mathbf{S}}_n - \hat{\mathbf{S}}_{n+1} u_n}{[1-u_n^2]^{\frac{1}{2}}} = \hat{\mathbf{S}}_{n+1} u_n + \hat{\mathbf{S}}_{n+2} \cos(\phi_n - \phi_{n+1}) [1-u_{n+1}^2]^{\frac{1}{2}}$$

$$
\begin{aligned}
- \quad & \frac{\hat{\mathbf{S}}_{n+1} - u_{n+1}\hat{\mathbf{S}}_{n+2}}{[1-u_{n+1}^2]^{\frac{1}{2}}} \cos(\phi_n - \phi_{n+1}) u_{n+1} \\
+ \quad & \frac{\hat{\mathbf{S}}_{n+1} \wedge \hat{\mathbf{S}}_{n+2}}{[1-u_{n+1}^2]^{\frac{1}{2}}} \sin(\phi_n - \phi_{n+1}),
\end{aligned}
$$

which trivially comes from Eq.(5.2.4). At each stage, we may relabel the spins and thus we can represent these equations in the transfer matrix $\mathcal{T}$, yielding

$$
\mathcal{T} \equiv \begin{bmatrix} T_{CC}^{01} & \tilde{T}_{CC}^{00} & -\tilde{T}_{CD}^{10} \\ T_{CC}^{00} & 0 & 0 \\ 0 & \tilde{T}_{DC}^{00} & -\tilde{T}_{DD}^{10} \end{bmatrix}
$$

from which the correlations are given by

$$
\langle \hat{\mathbf{S}}_n . \hat{\mathbf{S}}_0 \rangle = \frac{1}{z^n} \begin{bmatrix} \langle 0| & 0 & 0 \end{bmatrix} \mathcal{T}^{n-1} \begin{bmatrix} |0\rangle \\ 0 \\ 0 \end{bmatrix}
$$

where $\frac{1}{z^n}$ normalises the correlation function. This provides us with the way to calculate the spin-spin correlation function for the $J_1 - J_2$ Heisenberg model.

Calculations of the correlation functions for J_1-J_2 are provided elsewhere [72], and will not appear in this thesis.

5.3 Summary

We have solved the thermodynamics of the $J_1 - J_2$ Heisenberg model, calculating all the standard thermodynamic quantities, and writing the partition function in terms of an infinite dimensional matrix which we must diagonalise. Once again, the matrix

has numerical convergence at any temperature due to the Bessel functions, though we are limited and cannot go to very low temperature as the matrix does become very large. We therefore truncate the matrix, and diagonalise, and do not go below $T \sim 0.1$ for this model, though in principle we can. For this, and all other models, the interesting physics that we investigate is at a temperature around $T \sim J$, while the zero temperature physics is essentially exactly solvable.

We have now offered the solutions to three one dimensional classical spin models. We will now move on to the results for all of them, as we may draw parallels between them, especially the plane rotator and the Heisenberg models. We will also offer a real space technique to solve the integral equations, which we shall use more fully in the one to two dimensional crossover chapter (7), and we also use Monte Carlo simulations for the plane rotator and Heisenberg models.

Chapter 6

RESULTS

6.1 Chapter Summary

In Chapters. 3, 4 and 5, we have reduced the calculation of the partition function of various models to that of finding the largest eigenvalue of an integral operator. The work which appears in this chapter is entirely new, apart from the summary of Monte Carlo. We provide the results of the models, starting with the continuous Ising, then the Heisenberg, and finally the plane rotator model. This order is chosen as the "discrete"-like nature of the continuous Ising model means it should be interpreted somewhat separately from the other two. Before we present the results, we offer two alternative techniques that can be used as a cross check, directly integrating the transfer equations, and Monte Carlo, which both have slightly more versatility (though are not exact). Then we offer the results, providing the one dimensional "phase"-diagram (and describe what we mean by one dimensional phase transitions which are prohibited). The phase diagram that we find has not been found before, as we have access to exact thermodynamics. We also investigate the magnetisation of the models, finding the that continuous spin Ising model exhibits very strong field dependence, while the Heisenberg and plane rotator models do not.

6.2 Integral Equation Method

As a cross check of the exact method, one may directly solve the integral equations. To do this, one discretises the integral, just as one would normally for any numerical integration, and then iteratively solve the eigen equation. In general, for the simplest problems, we have an integral equation of the form

$$zf(v) = \int_a^b duK(u,v)f(u),$$

where z and $f(x)$ are the eigenvalue and eigenfunction of the integral operator, with $K(u,v)$ being $e^{-\beta\mathcal{H}}$. We use a trapezium rule for the integral, given by

$$\int_a^b f(x)dx \approx \sum_{n=0}^{N} \alpha_n f\left(a + \frac{n}{N}\right),$$

where

$$\begin{aligned} \alpha_n &= \frac{b-a}{N} \quad n \neq 0, N \\ \alpha_0 &= \alpha_N = \frac{b-a}{2N}, \end{aligned}$$

for N steps, to write

$$zf(u_i) = \sum_j K_{ij} f(v_j),$$

where K_{ij} is the kernel of the integrand evaluated at the appropriate point (u_i, v_j). The matrix is then diagonalised using the power method, which we shall briefly explain here as a useful technique for diagonalisation problems. We have the eigenvalue problem

$$z|f\rangle = K|f\rangle$$

We start with a test state $|a_1\rangle$, which *must not* be an eigenstate of the matrix K satisfying

$$K|n\rangle = \epsilon_n|n\rangle$$

We then expand this state in the unknown eigenbasis of K,

$$|a_1\rangle = \sum_n \alpha_n|n\rangle$$

We then apply the matrix K to the starter state, finding

$$K|a_1\rangle = \sum_n \alpha_n\epsilon_n|n\rangle \equiv |a_2\rangle$$

We normalise the new state $|a_2\rangle$, with the normalisation being the first guess of the largest eigenvalue, and replace the test state with the new one $|a_1\rangle \to |a_2\rangle$. We then apply the matrix many times, repeating this process, yielding

$$K^N|1\rangle = \sum_n a_n\epsilon_n^N|n\rangle$$

Which converges exponentially to the largest eigenvalue and eigenvector, with contributions to other eigenvalues and eigenvectors scaling away as

$$\Delta_n \sim \left[\frac{\epsilon_n}{\epsilon_0}\right]^N,$$

where $\epsilon_0 > \epsilon_1 > \ldots$. We have three integral equations that we seek to solve

$$\begin{aligned} zf(v) &= \int_{-1}^{1} \frac{du}{2} e^{xuv+\frac{y}{2}(u+v)} f(u) \\ zf(\phi) &= \int_{-\pi}^{\pi} \frac{d\psi}{2\pi} e^{x\cos(\phi+\psi)+\frac{y}{2}(\cos\phi+\cos\psi)} f(\psi) \end{aligned}$$

$$zf(v) = \int_{-1}^{1} \frac{du}{2} \int_{-\pi}^{\pi} \frac{d\psi}{2\pi} \int_{-\pi}^{\pi} \frac{d\phi}{2\pi} e^{x(uv+(1-u^2)^{\frac{1}{2}}(1-v^2)^{\frac{1}{2}}\cos(\phi-\psi))+\frac{y}{2}(u+v)} f(u)$$

This provides a cross check for all our models. Note, this method (while approximate) allows many more options than the exact methods. For example, one can include crystal field interactions or longer range interactions. This technique works well, though it is limited by the ability to store either the matrix K_{ij} (if small enough) or the eigenstates. This issue manifests itself in two ways; numerical accuracy or range of interactions.

The first issue is obvious, stemming from errors in the trapezium rule. The technique is never *exact*, but it can offer solutions to more complicated Hamiltonians, where expansion in basis functions becomes too difficult. Moreover, temperature smooths the eigenfunctions such that the trapezium rule accuracy improves with temperature. The technique works like a high temperature expansion, which is exact at infinite temperature as the integrand tends to a constant

$$\lim_{\beta \to 0} e^{-\beta H} = 1,$$

for which the trapezium rule is exact. Also, the plane rotator model has no boundary in the integral so that the trapezium rule is significantly more accurate.

The second issue is slightly more subtle, and relates to how the eigenfunction scales with the range of interaction. Here we have only restricted ourselves to $J_1 - J_2$ but longer range interactions may be tackled numerically. For example, the $J_1 - J_3$ continuous spin Ising model for example has a transfer integral equation of the form

$$f(u_2, u_3, u_4) = \int_{-1}^{1} \frac{du_1}{2} e^{\frac{\beta J_1}{2}(u_1 u_2 + u_3 u_4) + \beta J_3 u_1 u_4} f(u_1, u_2, u_3)$$

The longer range the interaction, the more degrees of freedom there are which need to be described, so that the transfer matrix will become exponentially large.

We will use this real space method in the one to two dimensional crossover chapter, but we began discussing it here as it serves as a cross check of the results. We have used it to check the expansions in terms of either Bessel functions or Legendre polynomials for the various models.

6.3 Monte Carlo Simulations

The standard technique for tackling large scale thermodynamics is to use Monte Carlo simulations. Here, we will offer a brief introduction to the method, specifically the Metropolis algorithm, and show comparisons to the exact result to indicate pros and cons of each.

The basic idea behind Monte Carlo analysis is to make many random moves in some state space, calculate some quantity (like energy), and weight each move appropriately (like a Boltzmann weight). If one uses a truly random sampling, one would have to make *very* many moves, and so here we do not use a fully random move at each step. For the case of thermodynamics, one must "order" the states according to their energy. One must also *fluctuate* the state so that the moves go up and down in energy to assess the local susceptibility to fluctuations. Near a phase transition, the energy landscape becomes flatter, allowing much more large scale fluctuations. In the classical groundstate, there is a local pN-dimensional (p degrees of freedom per site, N sites) quadratic potential providing the low energy excitations.

We begin with a brief discussion of detailed balance. This is the idea of reversability; we wish all moves to be reversible, but the *probability* of going one way

verses the other need not be the same. Moving up in energy is different to moving down due to the growing of the state space; there are many more states which are higher in energy than lower, and so we must *balance* this. If we wish to consider moving state S_1 to state S_2 then we must balance this with the inverse $S_2 \to S_1$, according to

$$\begin{aligned} P(S_1)G(S_1 \to S_2) &= P(S_2)G(S_2 \to S_1) \\ \to \frac{G(S_1 \to S_2)}{G(S_2 \to S_1)} &= \frac{P(S_2)}{P(S_1)}, \end{aligned}$$

where $P(\alpha_1)$ is the probability of finding the state α_1, and $P(\alpha_1 \to \alpha_2)$ is the probability of moving from one state to the other. Next we have that

$$G(S_1 \to S_2) = g(S_1, S_2)A(S_1, S_2),$$

where $g(\alpha_1, \alpha_2)$ is the probability of selecting the new state, and $A(\alpha_1\alpha_2$ is the acceptance probability. For a finite set of states (2^N for the Ising model), then $g(S_1, S_2) = g(S_2, S_1)$, and so we are left with

$$\frac{A(S_1, S_2)}{A(S_2, S_1)} = \frac{P(S_2)}{P(S_1)}$$

If we choose $A(S_1, S_2) = \min\left(1, e^{-\beta(E_2 - E_1)}\right)$ then we have

$$\frac{A(S_1, S_2)}{A(S_1, S_2)} = \frac{\min(1, x)}{\min\left(1, \frac{1}{x}\right)} = x,$$

where $x = e^{-\beta(E_2 - E_1)}$. Thus for any $x \neq 1$ we have that the ratio of acceptance is indeed $\frac{P(S_1)}{P(S_2)}$, the Boltzmann weight. This particular choice of acceptance probability

is the Metropolis algorithm, although anything which satisfies

$$\frac{A(S_1, S_2)}{A(S_1, S_2)} = \frac{P(S_1)}{P(S_2)} \frac{g(S_1, S_2)}{g(S_2, S_1)},$$

is sufficient for detailed balance. To run Monte Carlo, we therefore start with some state. We always choose this state to be the zero temperature groundstate (or one of these groundstates) as this avoids thermalisation issues. We then choose a new state and perform the Metropolis algorithm. If we accept the new state, we throw away the old state and begin again. However, an important aspect of this procedure is the choice of the new test state; choosing a new state in the whole state space means we would seldom accept. We wish to accept states around half of the time in order to fluctuate the state sufficiently. We therefore choose a pN-dimensional hypercube

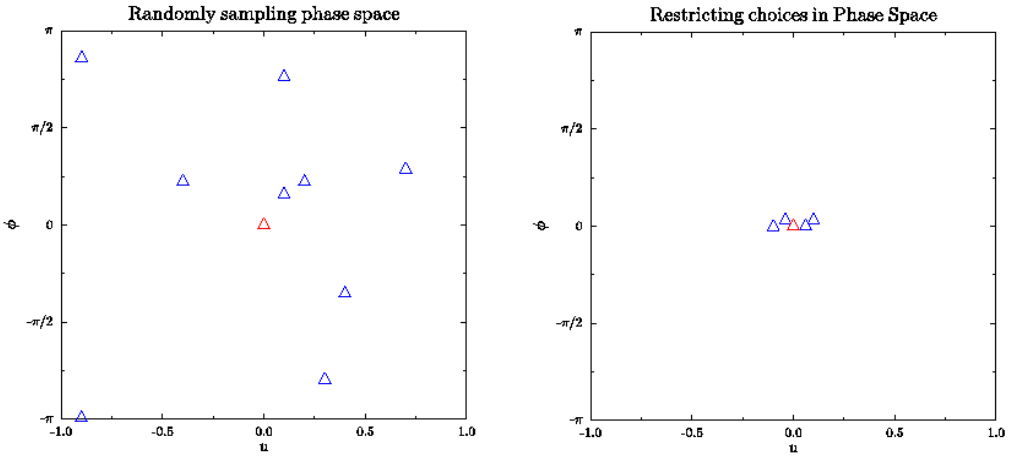

Figure 6.1: Choosing new states in from the original state (in red), either using random choices or a restricted choice.

in state space around the current space, of some size less than the whole of state space, and randomly move within this cube. We can envisage this in Fig.6.1, where

we either move randomly in phase space from the original state, or we attempt to move close to our current state. We imagine a square around the current state, in which we choose a state to attempt to move to. Note that the size of this cube has to respect the measure of the original state space, and more importantly the size is temperature dependent. Here, we use a box size of the form

$$L = \gamma T^p e^{-\frac{T}{T_0}},$$

which maintains the acceptance rate of $\frac{1}{2}$ for some temperature range. The parameters γ, p and T_0 must be chosen for each system, and also for how far in temperature one wishes to run for. To be concrete, we use $\gamma = 22$, $p = -\frac{1}{2}$ and $T_0 = 1$ for the 32 spin Heisenberg model to give an acceptance rate of roughly $\frac{1}{2}$ for $T \in [0.1, 10]$. Thermodynamic quantities can be calculated from averages in the simulation, the simplest quantity being the average total energy, given by

$$\langle E \rangle = \frac{1}{N_A} \sum_{n=1}^{N_A} E_n,$$

where E_n is the energy at each *accepted* move (to ensure we do not over count each state), and N_A is the number of accepted moves. We also have

$$\alpha = \frac{N_A}{N_T},$$

where N_T is the total number of attempted moves, and we try to ensure $\alpha \sim 0.5$ for optimal efficiency. We can calculate the specific heat as

$$C_V = \frac{\beta^2}{N} \left[\langle E^2 \rangle - \langle E \rangle^2 \right]$$

$$= \langle(\langle E\rangle - E)\rangle^2,$$

with N as the total spins. Direct differentiation of the average energy will not work here as there would be too much noise on the quantity. We may also want to calculate the magnetisation and susceptibility matrix, given by

$$\langle m_i\rangle = \frac{1}{NN_A}\sum_n (S_i)_n$$
$$\chi_{ij} = \langle[\langle m_i\rangle - m_i]\,[\langle m_j\rangle - m_j]\rangle$$

However, for the magnetisation to be thermodynamic, we must add a field, otherwise $\langle\mathbf{m}\rangle = 0$ necessarily. It is here that we find the boundary problem with the u variable. If the Monte Carlo step tries to make $u > 1$ or $u < -1$ then we must control this. The method used here is to flip the angle ϕ when this happens. When we attempt to make the move $u_n > 1$, instead we move

$$\phi_n \to \phi_n + \pi$$

We also avoid this problem if we add an infinitesimal field in the $\hat{\mathbf{x}}$-direction rather than the $\hat{\mathbf{z}}$-direction.

We now move on to the results. We simulated the Heisenberg model on a ring at first, with nearest neighbour interactions only. We compared this with the infinite chain result Eq.5.2.1, for rings of size 8, 16, 32, 64 and 128 to assess finite size effects. At each stage, we ran two simulations with 50000 and 2000000 steps to assess the noise. The "best" results are obtained with 32 spins with the larger simulation time. Note that we are comparing a periodic ring with an open chain, and thus we expect

an error of the form

$$Z_T = \frac{1}{N} z^{N-1} \rightarrow F = \frac{N-1}{N} \log z,$$

providing a $\frac{1}{N}$ correction to the results, which proved to be sufficiently small for the 32 spin system. We could compare with an open ring, however, the low temperature energy is then wrong as we miscount the number of bonds, and so we elect to use the correct bond number, and the wrong entropy. We begin with the energy, and

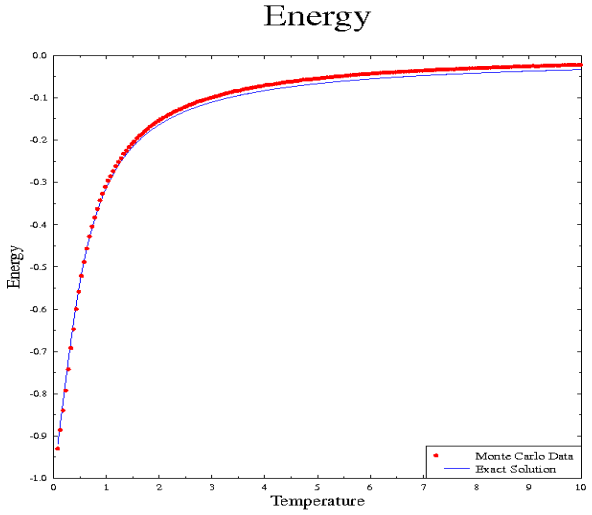

Figure 6.2: Energy for 8 spins in a ring for the Heisenberg model

for now only use the larger run size, as the noise aspect shows up in the specific heat more than the energy. In Fig.6.2 we see the energy for 8 spins. The smooth line is the exact result from Eq.5.2.1. We see good agreement until high temperature as the energy was correct at low temperature (by construction) but the entropy is wrong. There is a missing mode from the independence of the relative orientations of the end, which means that the free energy is wrong. For 16 spins, we see that this difference in Fig.6.3, we see that there is very little difference between the exact

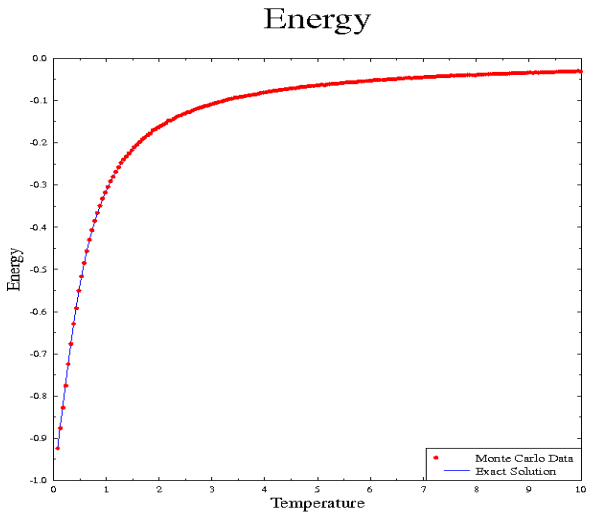

Figure 6.3: Energy for 16 spins in a ring for the Heisenberg model

curve and the Monte Carlo. For 32 spins, we see even less difference, but for 64

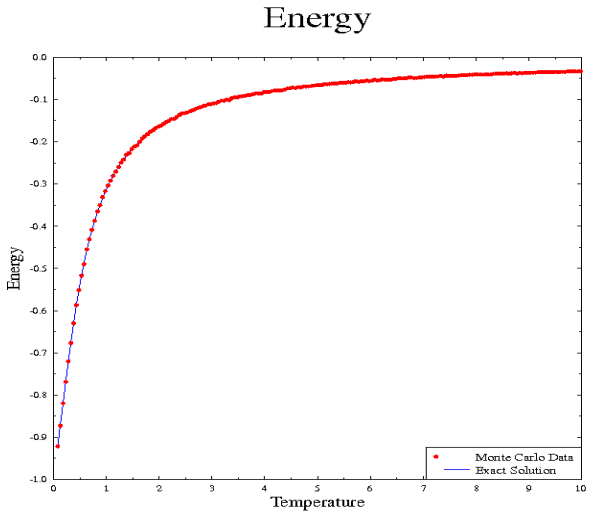

Figure 6.4: Energy for 32 spins in a ring for the Heisenberg model

spins we begin to see noise, as we have not let the simulation run long enough to

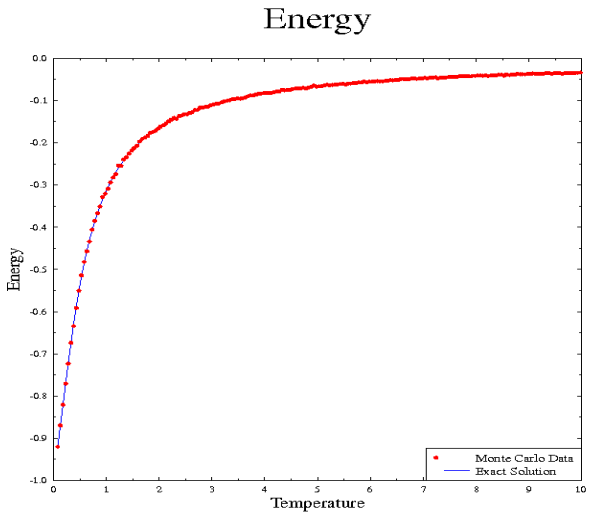

Figure 6.5: Energy for 64 spins in a ring for the Heisenberg model

thermalise. We now turn to the specific heat capacity, which inherently shows more

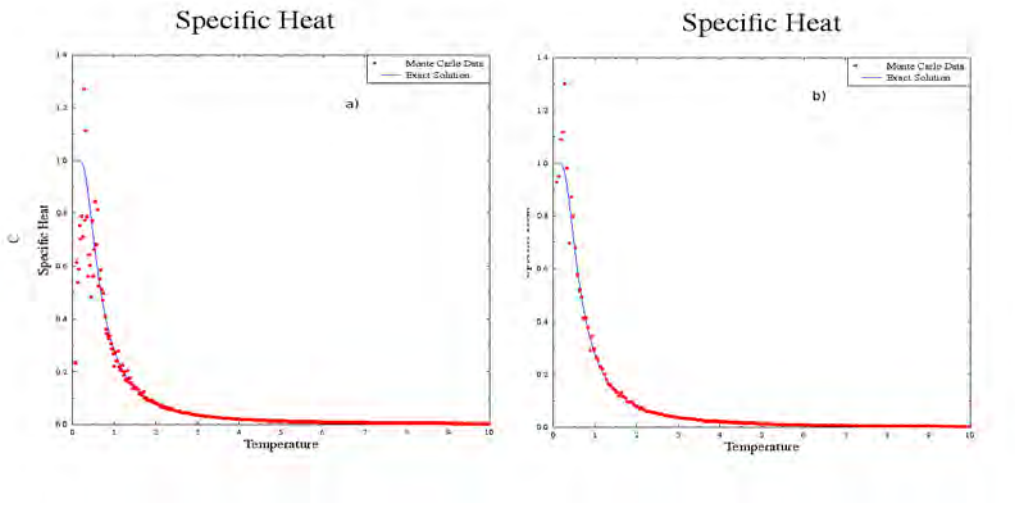

Figure 6.6: Specific Heat capacity for 128 spins with a) 50000 steps and b) 2000000 steps.

scatter. We begin with the worst example here, of 128 spins with the small and large run, seen in Fig.6.6 a) and b). We can see that Fig.6.6a) has far too much noise.

Clearly more simulation time is needed to thermalise. Even Fig.6.6b) has too much noise on to be confident in the answer, indicating that the largest system needs a very large number of steps to thermalise. For the case of 64 spins, seen in Fig.6.7

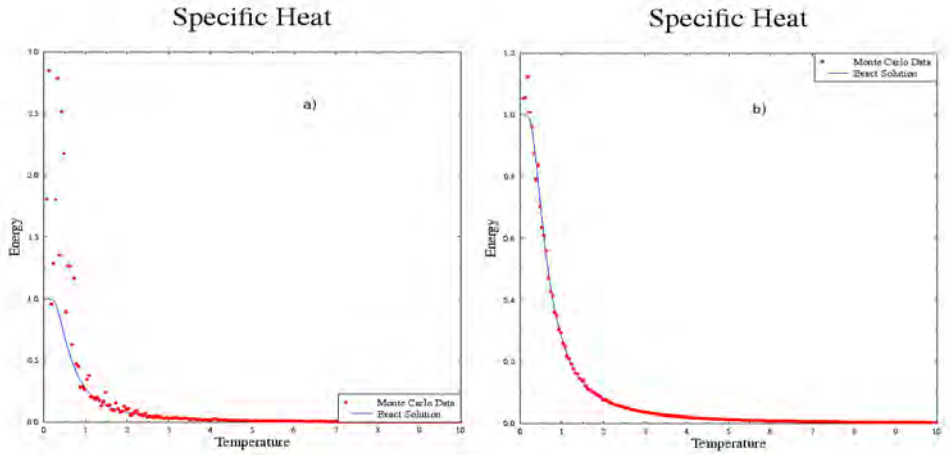

Figure 6.7: Specific Heat capacity for 64 spins with a) 50000 steps and b) 2000000 steps.

we see much less scatter on the larger run time, though the low temperature region is still poor. With less steps, the noise is very poor, as always. For the case of 32 spins in Fig.6.8, we see the best results for the larger run time, indicating that we have come close to thermalising this system at low temperature. Finally, 16 spins in Fig.6.9 has less noise, but we may observe more finite size effects.

We now move on to a non-trivial example, the $J_1 - J_2$ plane rotator, whose partition function is new. We use 128 spins and 4000000 steps to achieve good agreement between the Monte Carlo data and the exact solution. We simulated the ferromagnet as the simplest case to test the method, with $J_1 = J_2 = 1$ which is unfrustrated. The error we get as of the order $\sim 1\%$ due to the finite, periodic simulation we use. We see that the exact method and the Monte Carlo simulation

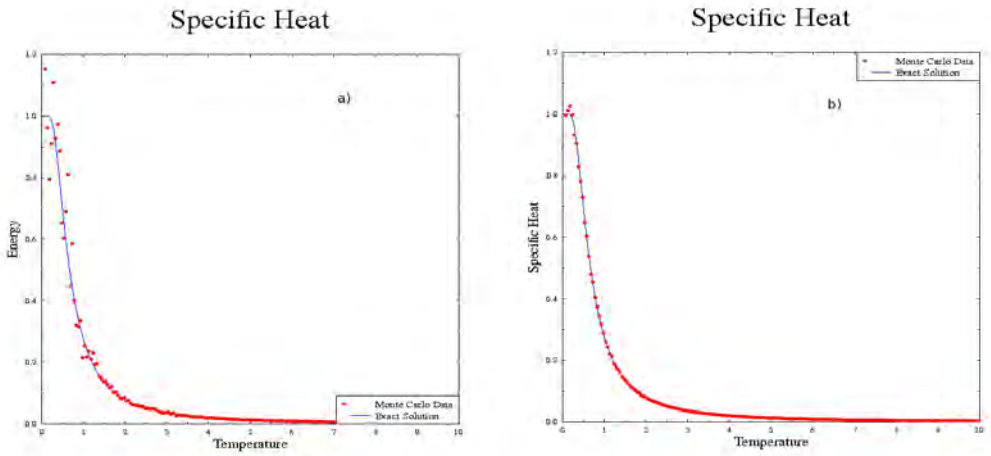

Figure 6.8: Specific Heat capacity for 32 spins with a) 50000 steps and b) 2000000 steps.

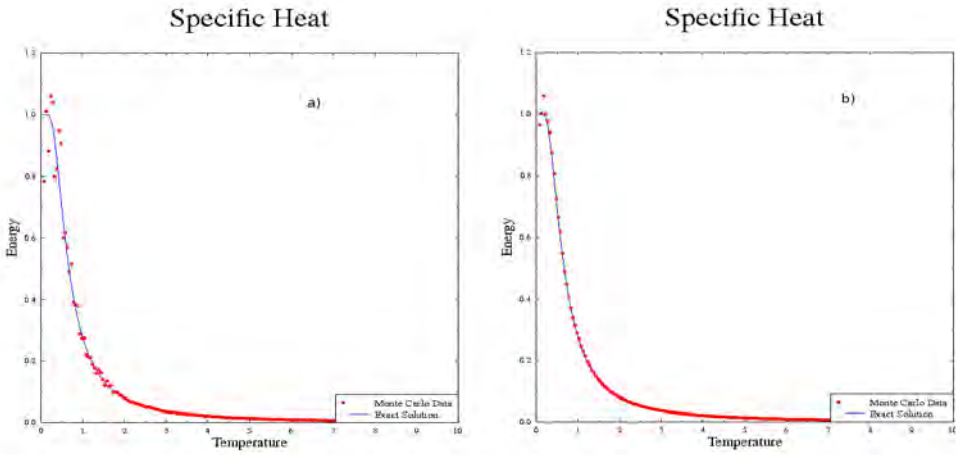

Figure 6.9: Specific Heat capacity for 16 spins with a) 50000 steps and b) 2000000 steps.

agree (for the simulated systems), but the simulation is limited by noise. Our exact solutions have no noise and therefore we will only use the transfer equation technique from now on.

We have only presented the most basic Monte Carlo simulations as a cross check,

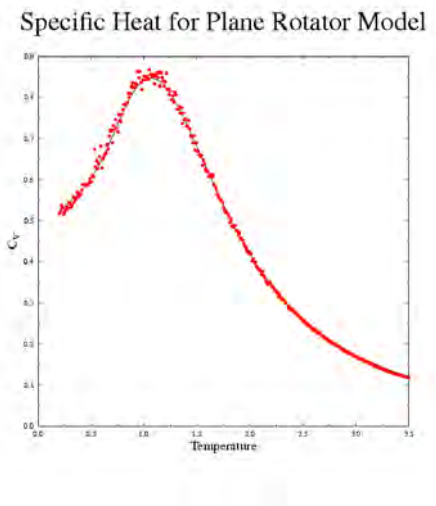

Figure 6.10: Specific heat capacity for the J_1-J_2 plane rotator model with 128 spins with 4000000 steps. We have $J_1 = J_2 = 1$

though we find that they agree with much more advanced simulations done elsewhere [73–75]. We include the discussion on Monte Carlo as we used it as a comparison, but it also allows an intuitive understanding of other Monte Carlo results, and the benefit of the exact work done here.

6.4 Results

We now provide the phase diagrams for the relevant models, and attempt to rationalise and explain them. We provide several calculations for each model; usually specific heat, magnetisation, nearest and next-nearest correlation functions, and longer range correlation functions. For each of the models there is a zero temperature phase transition, either at $\frac{B}{J} = \frac{1}{2}$ for the continuous spin Ising model, and at $\frac{J_1}{J_2} = \frac{1}{4}$ (or $\frac{B}{J} = \frac{1}{4}$) for the plane rotator and Heisenberg models. This difference stems from the first model having no continuous symmetry. Firstly we clarify what we mean by a "phase"-diagram in these one dimensional models.

We have discussed phase transitions before, and how we are not allowed them in one dimension at finite temperature. We are, however, permitted zero temperature transitions and crossovers. If we investigate the ferromagnetic nearest neighbour Ising model in one dimension, we still find a smooth peak in the specific heat. This peak would become the phase transition if we worked in two dimensions, but is prohibited from diverging. Thus the crossovers that we investigate are the remnants of the phase transition in one dimension.

These models all exhibit zero temperature phase transitions, which we may investigate. The transition is not allowed at finite temperature, and so it becomes a crossover immediately, but it may become very sharp as we near the first order zero temperature phase transition. A crossover is a smooth change of behaviour between two states, which are not symmetrically different. For example, the one dimensional Ising model exhibits a crossover from no ferromagnetic order to one in which there is no *long range* ferromagnetic order, but there are short range ferromagnetic correlations which grow as we decrease the temperature. There is a crossover in the behaviour around $T \sim \frac{J}{2}$.

We now clarify what we mean by phase diagram; we associate smooth peaks in the specific heat with crossovers and find the associated diagram of crossovers. We do this because we may observe fluctuation driven crossovers; the remnant of order from disorder in higher dimensions. One state is thermally destabalised by another, but we see no order into either state.

We will investigate the crossover between ferromagnetism and anti-ferromagnetism for the Ising models, and an anti-ferromagnet at $k = \pi$ and $k = \pi + \delta$ for the isotropic models. When we study continuous spin models, this is the first thermodynamic investigation of spiral states. Before we find the phase diagrams, we show the simplest

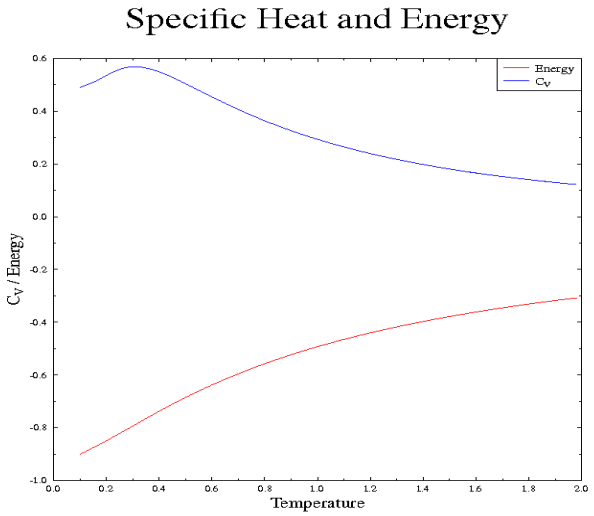

Figure 6.11: Specific heat and the energy for the plane rotator with $J_1 = -1.2$ and $J_2 = 0.25$

of calculations for each of the models to explain the details. In Fig.6.11 we see a plot of the energy (and specific heat) of the plane rotator model. We see a very smooth function, limiting to -0.95 at low energy. In Fig.6.12, we see the specific heat for the continuous spin Ising model with $J_1 = -2$ and $B = 1$. At low temperature, we have an anti-ferromagnet due to the interactions. As the temperature is increased, the remaining ferromagnetic order must be present to high temperature, and so we observe a smooth crossover to ferromagnetism, followed by a fall off in the specific heat. The low temperature limit is 1 due to the three dimensional spins, which have two degrees of freedom. They can fluctuate in two directions, perpendicular to the direction of the spin. We can expand the partition function as a local quadratic, yielding the effective partition function

$$Z_{eff} = \int dp\, dx e^{-\beta(p^2+x^2)} \tag{6.4.1}$$

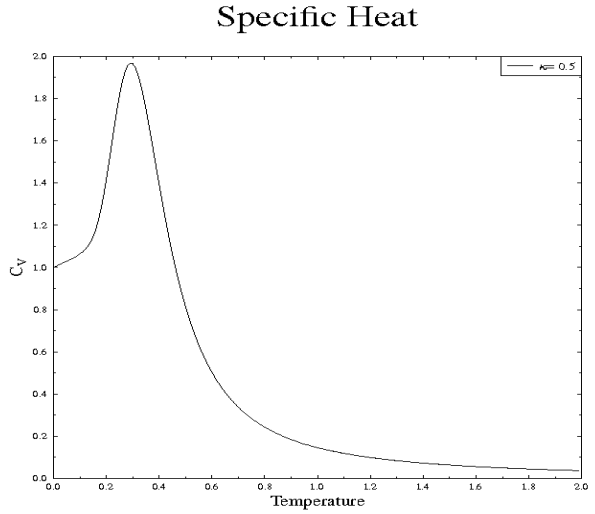

Figure 6.12: Specific heat for the continuous spin Ising model

$$\simeq \sqrt{\frac{\pi}{\beta}}\sqrt{\frac{\pi}{\beta}} \tag{6.4.2}$$

$$C_V = \beta^2 \frac{\partial^2 \log Z_{eff}}{\partial \beta^2} \to 1 \tag{6.4.3}$$

Each degree of freedom provides $\frac{1}{2}$ to the low temperature specific heat; equipartition. In Fig.6.13 we see the magnetisation for the continuous spin Ising model, with $J_1 = -1$ and $B = 0.05$. We see that the magnetisation survives to a surprisingly high temperature, roughly $T = 0.5$. This will be explored more later, but is a feature of this model. Clearly, we expect $\langle M \rangle \to 1$ for a ferromagnet at low temperature due to the classical spins, and at high temperature we expect very weak magnetisation. In Fig.6.14 we see the specific heat for the Heisenberg model, with $J_1 = 1$ and $J_2 = 1$ (or field and nearest neighbour interactions). Once again we see very smooth features, and a low temperature limit of 1 due to two degrees of freedom per spin. Note that for the Heisenberg model, we do not go down to a very low temperature. These

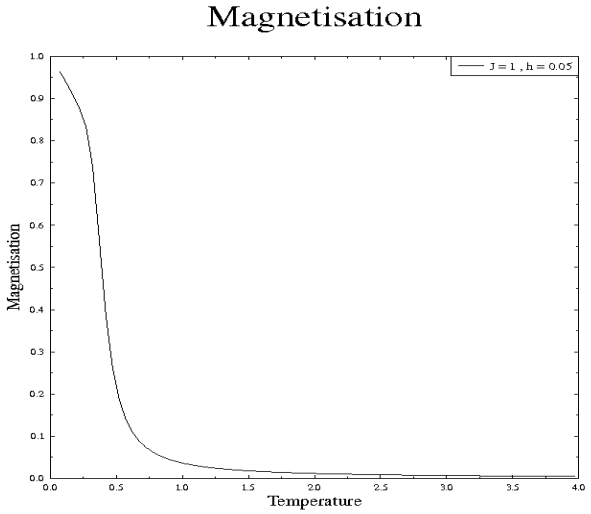

Figure 6.13: Magnetisation for the Ising model with ferromagnetic interactions

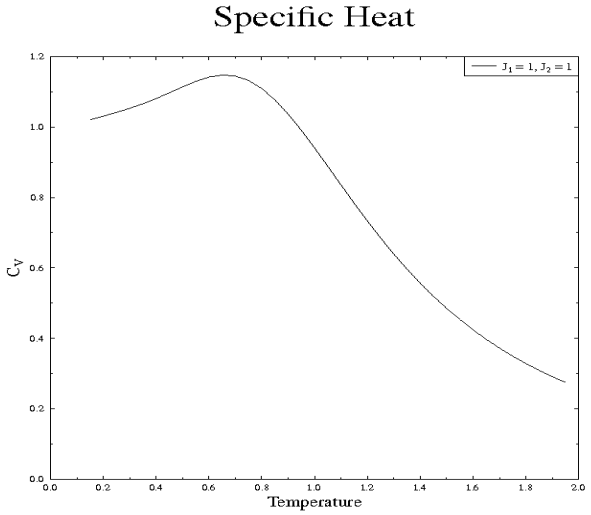

Figure 6.14: Specific heat for the Heisenberg

exact methods amount to a high temperature expansion, and are *exact* above some temperature, below which the Bessel functions themselves become numerically too large. A second important feature is that the specific heat is achieved via numerical

differentiation of the (very smooth) energy. There can be two issues here; noise and truncation errors. Noise should not be a problem with these exact methods, but truncation errors are always present. We work on a grid which is fine, but not fine enough to encounter truncation errors beyond the 6th or so decimal place, and so we have an inherent error in the specific heat. In Fig.6.15 and Fig.6.16 we provide

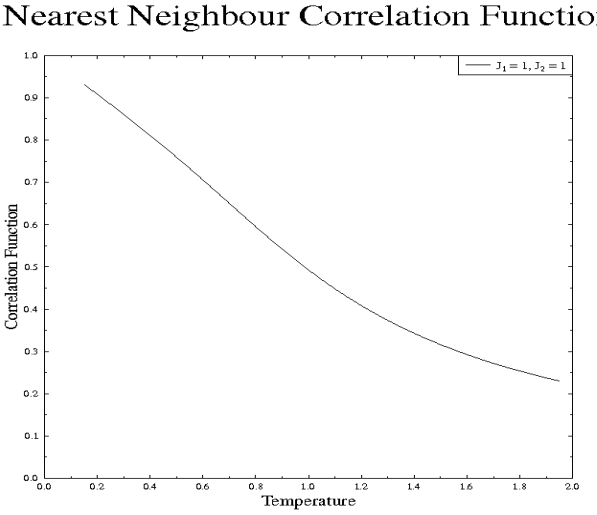

Figure 6.15: Nearest neighbour correlation function for the Heisenberg model

the nearest neighbour and next nearest neighbour correlation functions. The first two correlations occur directly in the energy, and so they are larger than one might expect, and for sufficiently long range the correlations tail off as an exponential. In Fig.6.17 we see the specific heat for the plane rotator model with $J_1 = 1.0$ and $J_2 = 1.0$. It is once again very smooth and tends to $\frac{1}{2}$ at low temperature due to the single degree of freedom at low temperature. In Fig.6.18 we see the nearest neighbour correlation function, which again is a smooth function with 1 as the low temperature limit.

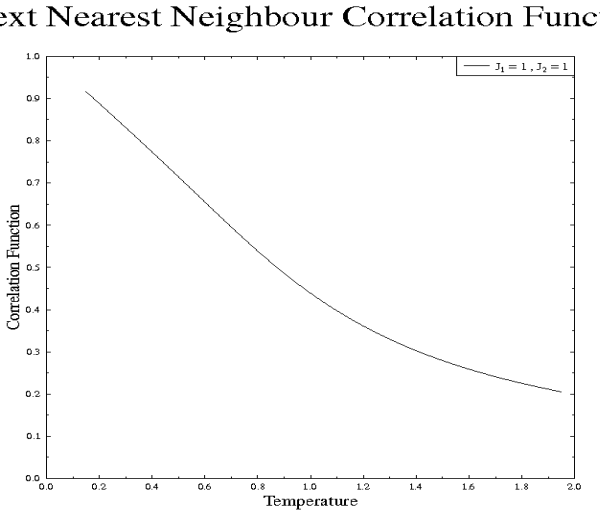

Figure 6.16: Next nearest neighbour correlation function for the Heisenberg model

6.4.1 Continuous-Spin Ising Model

We calculate several quantities in order to understand the phase diagram of the continuous-spin Ising model. To begin with we solve zero temperature. We have antiferromagnetic interactions with an applied field which are in competition. For large field we have a ferromagnet at zero temperature, and for large interaction we have an antiferromagnet. At the point $B/J = 2$ there is a transition between these two states. This comes from the local field on each spin exactly balancing the applied field. There are three relevant states at zero temperature therefore, as seen in Fig.(6.19). The two states which are well ordered will have a low temperature specific heat of 1 as they have a local quadratic potential to oscillate in. However, the special state at $\kappa \equiv B/J = 2$ will have a low temperature specific heat of $\frac{1}{2}$ as half of the spins are free to move around. The magnetisation of the ordered ferromagnet (at $T = 0$) is $\langle m \rangle = 1$, the antiferromagnet is $\langle m \rangle = 0$, while the special state is

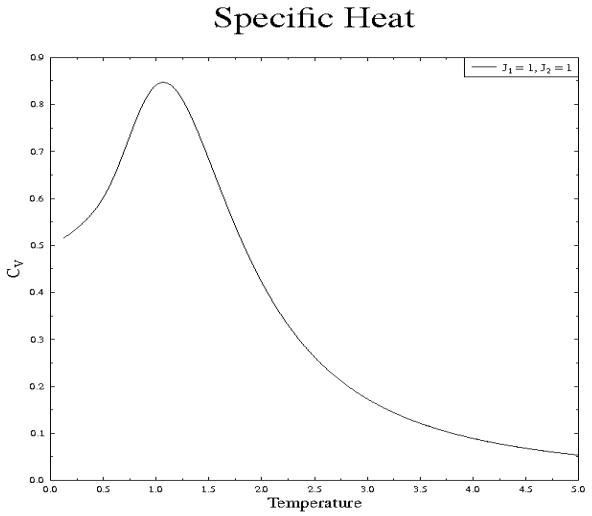

Figure 6.17: Specific heat capacity for plane rotator with $J_1 = 1.0$ and $J_2 = 1.0$

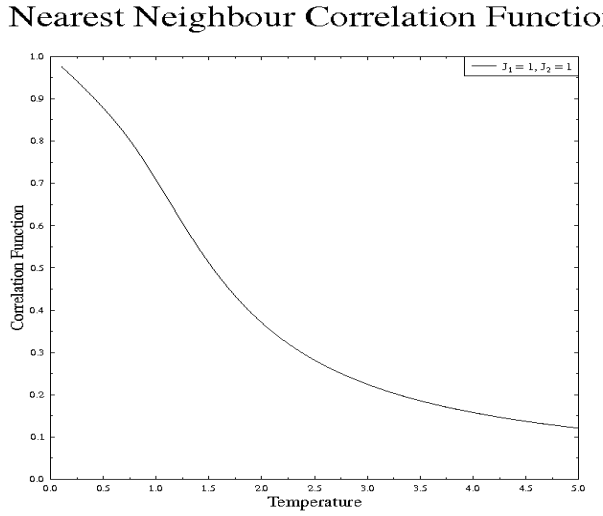

Figure 6.18: Nearest neighbour correlations for plane rotator with $J_1 = 1.0$ and $J_2 = 1.0$

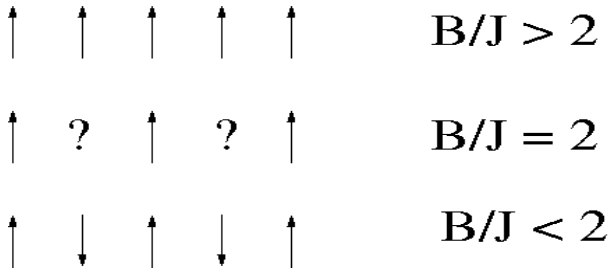

Figure 6.19: The three relevant states to the continuous-spin Ising model at zero temperature.

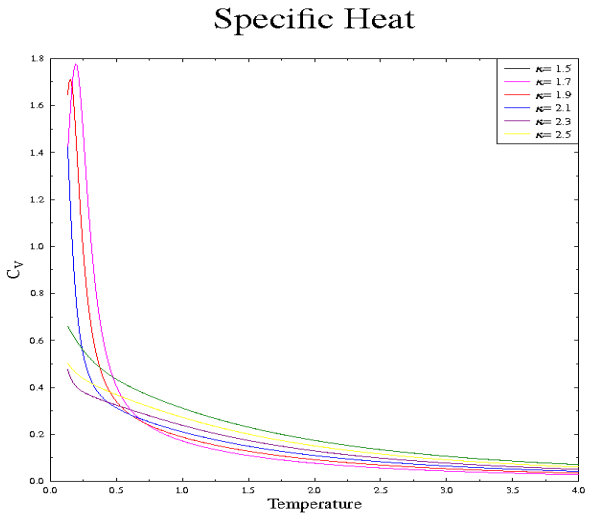

Figure 6.20: Specific heat for the continuous spin Ising model near $\kappa = 2$

$\langle m \rangle = \frac{1}{2}$. It is clear that at $\kappa = 2$, there is a macroscopic manifold (every other spin is free to be in *any* state) and therefore has more entropy associated. We might therefore expect that this special state thermally destabilises the other two. Having solved the zero temperature phase diagram, we now see how temperature affects the zero temperature transition. The specific heat for various values of κ are given in Fig.(6.20). If we associate features in the specific heat with a "phase" boundary, we get the diagram as in Fig.(6.21). The dotted line in Fig.(6.21) is the associated

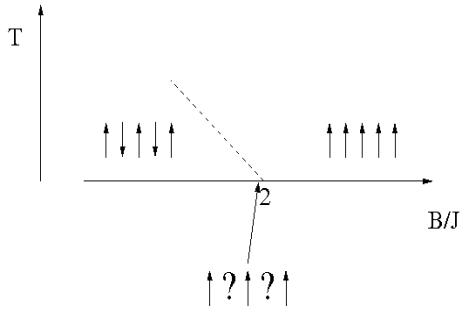

Figure 6.21: "Phase" diagram of the continuous spin Ising model as found from specific heat calculations

weak phase transition. To explain the shape of this diagram, we consider what one naïvely expects. The $\kappa = 2$ state has the most entropy, and so destabilises the other two as a function of temperature, and thus we expect a "V" shape. However, due to the applied field, there is no symmetry breaking between the $\kappa = 2$ state and the ferromagnet as they are both long range ordered ferromagnets. There is a symmetry change between the $\kappa = 2$ state and the antiferromagnet as the antiferromagnet has no long range ferromagnetic moment. Thus one sees a crossover in the specific heat between the $\kappa = 2$ state and the antiferromagnet and nothing between it and the ferromagnet. To justify the phase diagram, we use the magnetisation, as can be seen in Fig.(6.22). For small values of κ we get finite magnetisation at high temperature due to the field, then a turn over into zero magnetisation due to the antiferromagnetic interactions. At $\kappa > 2$, there are no features in the magnetisation, as we move from a partial ferromagnet to a fully ordered ferromagnet, and thus we see no signature of this.

Magnetisation

We now investigate how applying a field affects this model when it is ferromagnatic. We will use classical field theory to understand the excitations of the model, in order

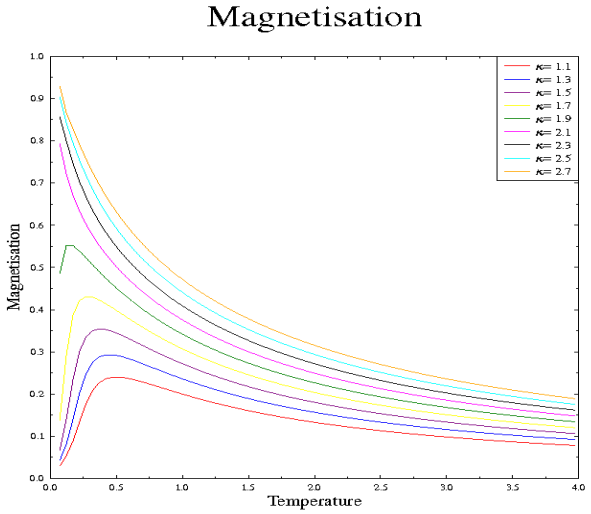

Figure 6.22: Magnetisation for the Ising model with competing interactions near $\kappa = 2$

to justify using the regular Ising model to understand the magnetisation. The field dependence in the Ising model (and this model) turns out to be very subtle, and we attempt to understand the dependence. We calculate the average domain wall separation for the ferromagnetic Ising model in an applied field in order to show that they depend on the applied field, but not strongly.

We apply an exponentially decreasing field, as seen in Fig.6.23. We reduce the field by $\frac{1}{2}$ each time, and we see that the magnetisation is reducing more slowly than this; an exponentially weak field produces a relatively large magnetisation to a surprisingly high temperature. To explain this we examine the excitations of this model, and see how they compare to the regular Ising model. To do this, we use a classical field theory, beginning with the partition function given by

$$Z = \int \mathcal{D}[\theta(x)] e^{-\beta \mathcal{L}[\theta(x)]},$$

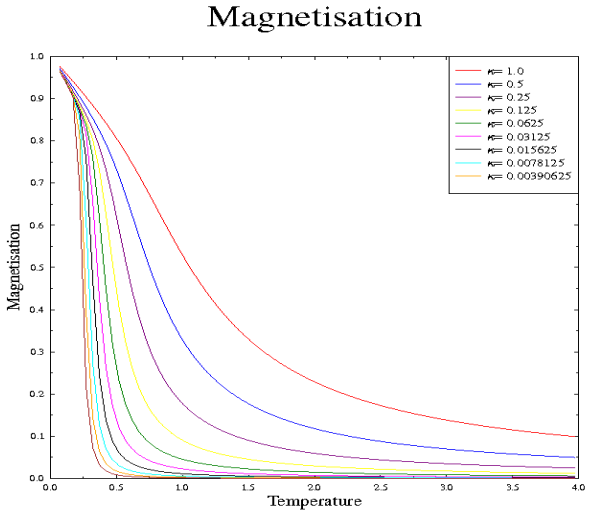

Figure 6.23: Magnetisation for the Ising model with ferromagnetic interactions with exponentially weak applied field

where the Lagrangian is given by the continuum limit of the continuous Ising model

$$\mathcal{L} = \int_{-\infty}^{\infty} dx \cos[\theta(x+\delta)] \cos[\theta(x-\delta)],$$

where x is real space position, a continuous variable, δ is the lattice separation, taken in the limit $\delta \to 0$, and θ is the classical angle field. We expand all functions to quadratic order

$$\theta(x \pm \delta) = \theta(x) \pm \delta\theta'(x) + \frac{\delta^2}{2}\theta''(x)$$
$$cos(\theta + d\theta) = \cos\theta - d\theta \sin\theta - \frac{(d\theta)^2}{2}\cos\theta,$$

where

$$d\theta \equiv \frac{\delta^2}{2}\theta''(x) \pm \delta\theta'(x)$$

This gives us

$$\mathcal{L} = \int_{-\infty}^{\infty} dx \left[\cos\theta - \sin\theta\left(\frac{\delta^2}{2}\theta''(x) + \delta\theta'(x)\right) - \cos\theta\frac{\delta^2(\theta')^2}{2}\right] \times \left[\cos\theta - \sin\theta\left(\frac{\delta^2}{2}\theta''(x) - \delta\theta'(x)\right) - \cos\theta\frac{\delta^2(\theta')^2}{2}\right],$$

and so, to quadratic order, we find

$$\mathcal{L} = \int_{-\infty}^{\infty} dx \cos^2\theta \left[1 - \delta^2(\theta')^2 - \tan\theta\delta^2\theta''\right]$$

We integrate this by parts, and there is no boundary term which affects the thermodynamics, yielding

$$\mathcal{L} = \int_{-\infty}^{\infty} dx \left[\cos^2\theta - \delta^2(\theta')^2\sin^2\theta\right]$$

We then minimise the functional which gives the dominant fluctuations to the partition function, using

$$\frac{\partial}{\partial x}\left(\frac{\partial\mathcal{L}}{\partial\theta'}\right) = \frac{\partial\mathcal{L}}{\partial\theta},$$

which gives us the equation of motion

$$\sin^2\theta(x)\theta''(x) + \sin\theta(x)\cos\theta(x)(\theta'(x))^2 = \frac{\sin\theta(x)\cos\theta(x)}{\delta^2}$$

We then solve this (by multiplying through by $2\theta'$, and rewriting as a perfect derivative) that

$$(\theta'(x))^2\sin^2\theta(x) = \frac{\sin^2\theta(x)}{2\delta^2}$$

The boundary conditions are either spin up or spin down, corresponding to $\theta = 0$

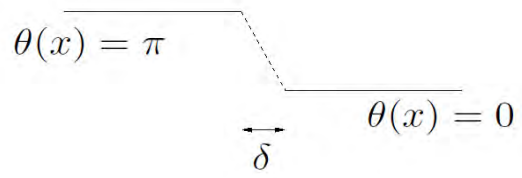

Figure 6.24: Domain wall structure for the continuous model in the continuum limit

or $\theta = \pi$, which gives $\theta'(x) \sim \frac{1}{\delta}$. This means we get a domain wall between an up domain and a down domain on the scale of one lattice spacing δ, as seen in Fig.6.24. We can calculate the average length of these domains in the $J_1 - B$ Ising model which will help us understand the field dependence of the magnetisation. We consider a background of spins which are parallel to the applied field, up. At zero temperature we only have spins parallel to the field, but as we introduce temperature, we generate some spins which are anti-parallel to the field. However, the majority of the spins are still up, and so we envisage a background of parallel spins with a small bubble of down spins. We therefore have *two* domain walls, and we can calculate the average separation of these. Each *pair* of domain walls has two entropic modes; they delocalise across the system to gain from positional entropy of the down spins, and also change the length of the domain. The entropy of the delocation is trivially $T \log L$ for a system of length L, which provides the destruction of long range order. The change of length of the domain is harder to calculate. We can calculate the effective partition function for such a domain wall

$$Z_{eff} = Le^{-2\beta J} \sum_{n=1}^{L} e^{-2\beta Bn} + 1,$$

where the term $e^{2\beta J}$ is the Boltzmann weight for the energy penalty at the boundary, and the second term sums over the length of the domain with appropriate Boltzmann weighting, and the final term is the groundstate. We have an L in front of the summation because we can delocalise the pair of domain walls across the system. We will take the upper limit of the sum to infinity, but keep the term in front of the sum as L, yielding

$$\begin{aligned} Z_{eff} &= L\frac{e^{-2\beta(J+B)}}{1-e^{-2\beta B}}+1 \\ &= \frac{Le^{-\beta(B+J)}x}{2}+1, \end{aligned}$$

where we have defined

$$x = \frac{e^{-\beta J}}{\sinh \beta B},$$

which will be used in a later calculation and is the controlling parameter for the thermodynamics here. The reason that this is the parameter is not fully understood yet, but more work will appear on this in [22], in which this parameter is derived in general. Note that we have assumed that the distance between such domains is very large, and hence we are in the low temperature limit. The L here tells us that the groundstate is never relevant, and that there is always a domain of oppositely orientated spin of some size, as it gains from the delocalising entropy. We may interpret the parameter x as the thermodynamic cost of making such a pair of domains, which can be small, but the coefficient is sufficiently large that the groundstate is never relevant at finite temperature. We may calculate the average length of these domains

$$\langle l \rangle = \frac{1}{Z_{eff}} \sum_{n=0}^{L} n e^{-2\beta B n}$$

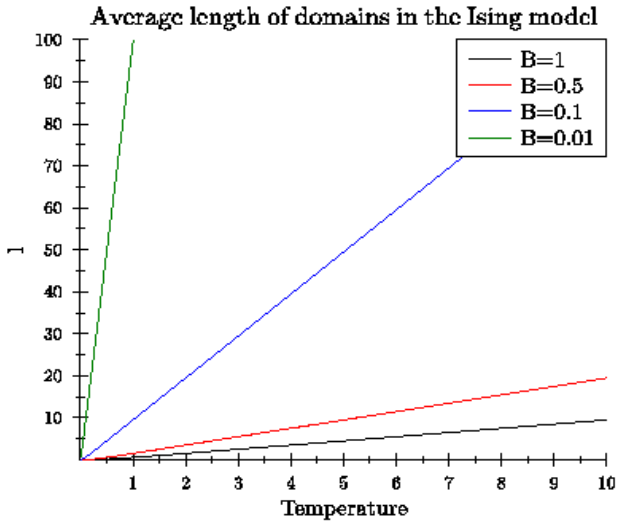

Figure 6.25: Average length of domains in the Ising model

$$\begin{aligned} &= -\frac{1}{\beta}\frac{\partial \log Z_{eff}}{\partial B} \\ &= \frac{e^{-2\beta J}}{(e^{-2\beta J}+1-e^{-2\beta B})(1-e^{-2\beta B})} \end{aligned}$$

We may take the limit that $\beta B \to 0$ to find that

$$\langle l \rangle \sim \frac{2T}{B},$$

which is the limit for small applied fields. That is, when we apply a very small field, the length of oppositely orientated domains can become *very* large as it scales with the inverse of the field. However, there is also a temperature below which βB is not small, at which point the exponential term $e^{-2\beta J}$ requires that $\langle l \rangle \to 0$ from Eq.6.4.4. We see this style of behaviour in Fig.6.25, where the temperature defeats the field and the domain size is small. This is a rather subtle limit, indicating we need to know how to order the parameters β, J and B.

In order to understand the behaviour of the magnetisation, we shall simplify our model back to the regular Ising model (whose partition function is exactly known, and whose excitations are equivalent). The partition function for the $J_1 - B$ Ising model, is given by

$$z = \left[e^{\beta J} \cosh \beta B + \sqrt{e^{2\beta J} (\sinh \beta B)^2 - e^{-2\beta J}} \right]$$

We wish to calculate the magnetisation, and so we calculate

$$\begin{aligned} \langle m \rangle &= -\frac{1}{\beta} \frac{\partial \log z}{\partial B} \\ &= \left[\frac{\tanh \beta B + \frac{1}{\sqrt{1+x^2}}}{1 + \tanh \beta B \sqrt{1+x^2}} \right] \qquad x \equiv \frac{e^{-2\beta J}}{\sinh \beta B} \end{aligned}$$

The susceptibility for this model can be calculated directly, yielding the zero field susceptibility as

$$\begin{aligned} \chi_{ij} &\equiv \left. \frac{\partial \langle m \rangle_i}{\partial B_j} \right|_{B \to 0} \\ &= \beta e^{2\beta J} + \mathcal{O}(B) \end{aligned}$$

Which only has one component for the Ising model, and diverges as $\beta \to \infty$, as can be seen in Fig.6.26. It does not show the exponential behaviour of the magnetisation however, as we have truncated this behaviour to a power series. We expand the magnetisation in powers of x, in the limit $\frac{J}{B} \to \infty$, to find

$$\begin{aligned} \langle m \rangle &= 1 - \frac{x^2}{2} + \frac{3x^4}{8} - \frac{5x^6}{8} + \mathcal{O}(x^8) \\ &= 1 - \frac{e^{-4\beta J}}{2 \sinh^2 \beta B} + \frac{3e^{-8\beta J}}{8 \sinh^4 \beta B} - \frac{5e^{-12\beta J}}{16 \sinh^6 \beta B} \end{aligned}$$

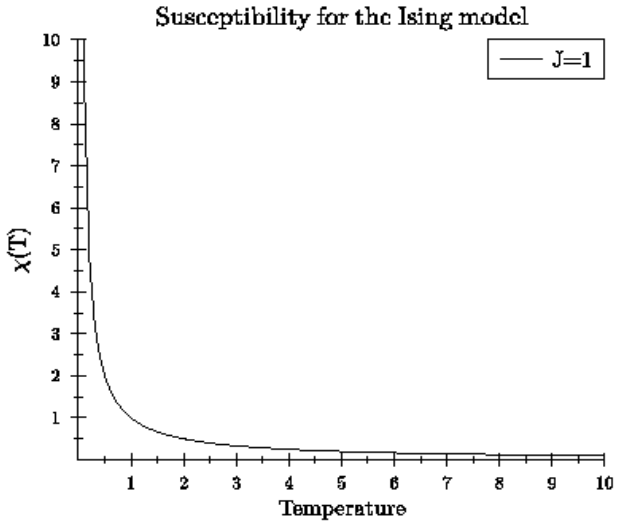

Figure 6.26: Susceptibility of the $J_1 - B$ Ising model

This produces the low temperature limit of 1 for the magnetisation, while the higher order terms produce the turn over that we wish to examine. Taking the limit $B \to 0$ is not directly possible, as this linearises the $\sinh \beta B$ terms, and causes the magnetisation to diverge. In fact, we can only consider the temperature limit where $\beta \gg B$ in order to keep the non-linearity. The parameters are therefore controlled by the sequence

$$1 \gg \beta B \gg e^{-\beta J},$$

where last term ensures that we may make the expansion in x. This also means that this expansion is only valid for large β implicitly, even though we did not explicitly expand around this. We can see the plot of this in Fig.6.27, where the exact magnetisation has been plotted for exponentially weakening fields to show the strong dependence, and the expansion is plotted. It is clear that it is only good for low temperature.

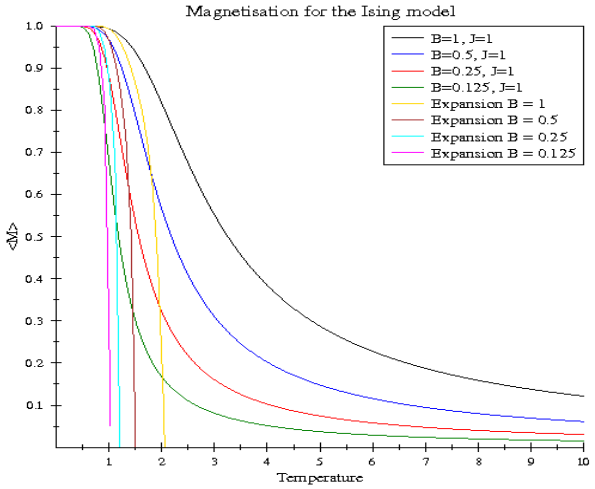

Figure 6.27: Magnetisation of the $J_1 - B$ Ising model

We now interpret the physics of the problem, and indicate how we can improve the calculation. The parameter x is required to be small for the magnetisation to be saturated. At first site, it appears that the limit $B \to 0$ prevents x from being small, but the exponential on the top means that x is small for reasonable temperature. Therefore, small fields provide a saturated magnetisation to a surprisingly high temperature.

We have neglected the effect of having multiple oppositely orientated domains, which the calculation that we would like to perform. We envisage a finite system with a *density* of these domains, whose average length is given in Eq.6.4.4. The number of these domains is optimised for a given energy to gain from the delocalisation entropy without coming into contact with one another. The parameter x may also be interpreted; the exponential on the top is the energetic cost of creating such a bound pair of domains. For the models with well defined domain walls, this energy is finite, but for the plane rotator and Heisenberg, this energy is zero and we observe

very different behaviour.

6.4.2 Summary of the Continuous-Spin Ising Model

The thermodynamics of the continuous-spin Ising model have two aspects; the phase diagram of the frustrated antiferromagnet and the magnetisation of the ferromagnet. The phase diagram is clear, and is a very simple example of order from disorder. The magnetisation is not as clear, as we have a non-perturbative dependence on the field. In other words

$$e^{-\beta B} \sim 1 - \beta B$$

is true for $\beta B \ll 1$, but not for all temperatures. This conflict means that expansions of this type are inherently difficult to control. Here, we used the parameter

$$x = \frac{e^{-\beta J}}{\sinh \beta B}$$

which is suitable for $x \ll 1$. It looks as though the limit $B \to 0$ would prohibit this, but the exponential term controls how fast x goes to zero. In other words, for any finite, but small B, there is always a temperature small enough such that x is very small and a suitable parameter for a series expansion. It then clear that this predicts a magnetisation to a relatively large temperature because when x is not small, we see the magnetisation is destroyed. For x to not be small, we require a relatively large temperature in order that the exponential is not dominantly small.

6.5 Heisenberg Model

We may calculate the same diagram for the classical Heisenberg model too. As usual, at any finite temperature thermal fluctuations, however, we may calculate the zero temperature phase diagram to see what we expect.

As said in the technique section, the J_1-J_2 and $J-B$ models are *thermodynamically* identical, but the interpretation of them is different. We could find the zero temperature phase diagram for the model with a field, and we would interpret the crossovers in the same way as the continuous spin Ising model. However, we elect to consider the J_1-J_2 model, which we have to interpret slightly differently. We first calculate where the zero temperature phase transition is and therefore begin with the model

$$H = -J_1 \sum_n \hat{\mathbf{S}}_n . \hat{\mathbf{S}}_{n+1} - J_2 \sum_n \hat{\mathbf{S}}_n . \hat{\mathbf{S}}_{n+2}$$

If we use the one dimensional Bloch transform of the form

$$\hat{\mathbf{S}}_n = \frac{1}{\sqrt{N}} \sum_k e^{ikn} \mathbf{S}_k$$

Then the Hamiltonian becomes diagonal of the form

$$H = -\sum_k \left(J_1 \cos k + J_2 \cos 2k \right) \mathbf{S}_k . \mathbf{S}_{-k}$$

We then minimise the structure factor through

$$\cos k = -\frac{J_1}{4J_2},$$

meaning we put the spin density down at the appropriate k where the equation is

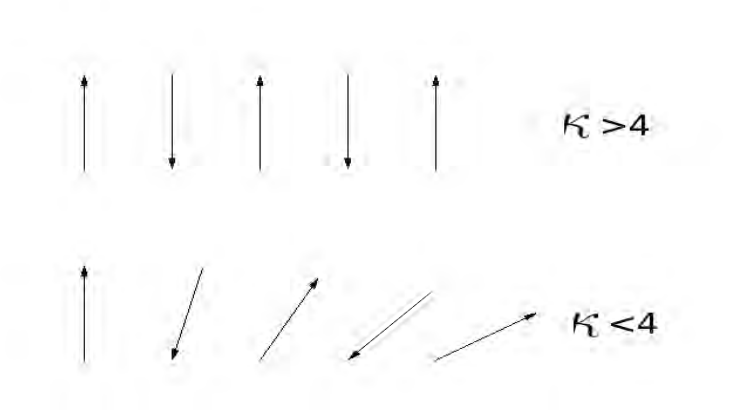

Figure 6.28: Depiction of the spiral state verses the normal anti-ferromagnet for two different values of exchange

appropriate. When $J_1 > 4J_2$, we simply have antiferromagnetism, but for $J \leq 4J_2$, we get a spiral state with pitch

$$k^* = \cos^{-1}\left[-\frac{J_1}{4J_2}\right],$$

as seen in Fig.6.28, with a state given by

$$\hat{\mathbf{S}}_n = \hat{\mathbf{e}}_0 \cos\left(k^* n + \phi\right) + \hat{\mathbf{e}}_1 \sin\left(k^* n + \phi\right)$$

for two orthonormal basis vectors $\hat{\mathbf{e}}_0$ and $\hat{\mathbf{e}}_1$. This time there is no special state with macroscopic entropy, though the state *at* $\kappa \equiv J_1/J_2 = 1/4$ is degenerate to an infinitesimal spiral. We therefore may not expect any special "shape" to the phase boundary, however, fluctuations are optimised with collinear spins. Physically one can see this by considering two spins perpendicular to one another. They cannot

fluctuate collectively in the direction parallel to either spin (due to the length constraint), which reduces the number of degrees of freedom available. Collinear spins on the other hand can fluctuate collectively in all directions, optimising the entropy. We therefore expect the antiferromagnetism to destabalise the spiral state thermally to make use of these fluctuations. In order to investigate the phase diagram, we be-

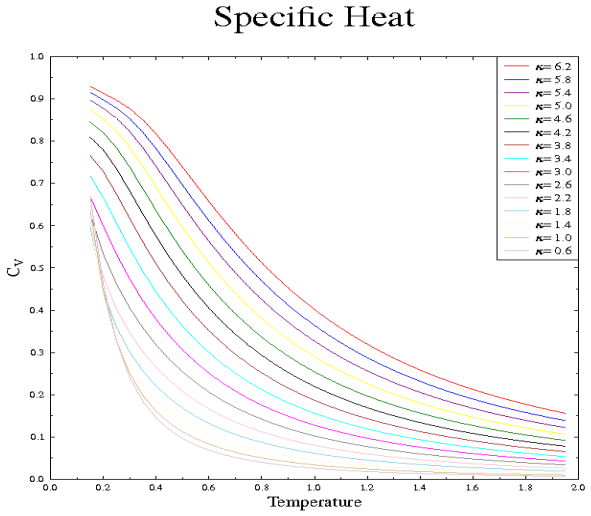

Figure 6.29: Specific heat for the Heisenberg model fig 19

gin with the specific heat, sweeping through the region of interest in parameter space, as seen in Fig.6.29. The specific heat for the Heisenberg model is particularly smooth and so it is not obvious that much is happening around $\kappa = 4$. However, if we look at the first neighbour correlation function, Fig.6.30, then we see more dramatic behaviour. For $|\kappa| \geq 4$ the correlation function is saturated at ± 1, but for $|\kappa| < 4$, we find the low temperature limit of the correlation function is given by

$$\langle \hat{\mathbf{S}}_0 . \hat{\mathbf{S}}_1 \rangle = \cos^{-1}\left(\frac{\kappa}{4}\right) \tag{6.5.1}$$

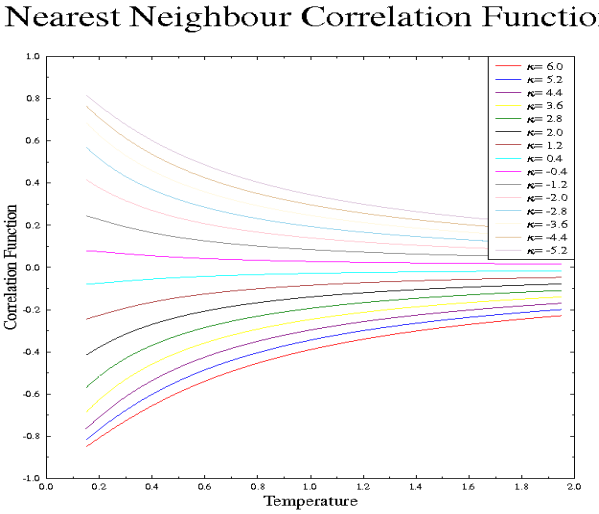

Figure 6.30: Nearest neighbour correlation functions for the Heisenberg model

as expected. One also observes this sharp change of character in the next nearest neighbour correlation function, seen in Fig.6.31. We therefore believe that the Heisenberg model has the same style of phase diagram as the continuous spin Ising model, with $\kappa = 4$ as the special state. Applying an exponentially weak field for the Heisenberg model provides exponentially weak magnetisation, unlike in the Ising models. We see this with ferromagnetic J_2 and weak ferromagnetic J_1, and observing the nearest neighbour correlation function, as seen in Fig.6.32. For $J_1 = 0$ we have two decoupled chains, which ferromagnetically order but do not co-order, providing a (very small) low temperature entropy for the relative orientation. This system is not magnetised by an infinitesimal J_1 to a large temperature, instead providing magnetisation to an infinitesimal temperature.

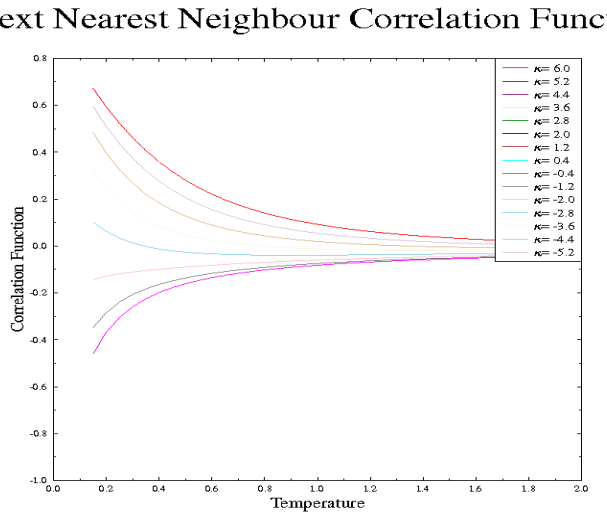

Figure 6.31: Next nearest neighbour correlation functions for the Heisenberg model

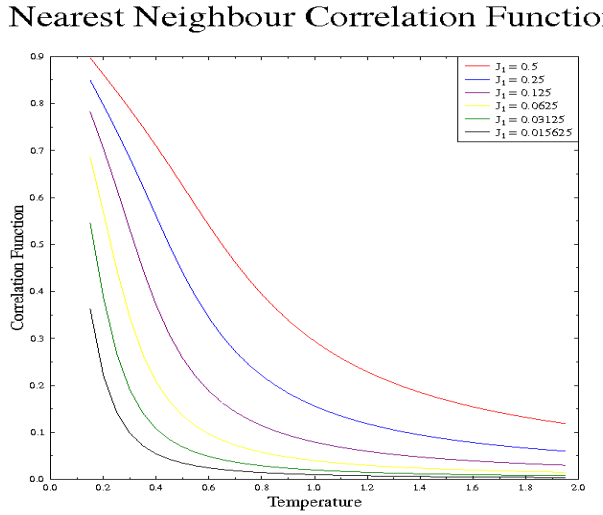

Figure 6.32: Nearest neighbour correlation functions for the ferromagnetic Heisenberg model

The reason for this behaviour is due to the isotropy of the spins clearly, where in the Ising model (and continuous Ising model) we have essentially up or down.

To examine the field dependence of the Heisenberg model, we use perturbation theory. Note that in the Ising model, we cannot perform such an expansion as the system depends exponentially on the field, and any expansion we choose truncates this strong dependence. Here however, the field dependence is not so strong, and so we may perform a standard expansion. For convenience of the expression, we will use the non-Hermitian representation of the transfer matrix, and so first we justify that we can perform the usual perturbation theory. We use the representation

$$T_{nm} = \sqrt{1+2n}\sqrt{1+2m} I_n(\beta J_1) C_{nm}(\beta B),$$

which we expand for small B, which as stated before is also a high temperature expansion. We can easily expand the function $C(x)$ for small argument using the orthogonality of the Legendre polynomials, and recursion relations, yielding the expansion for the transfer matrix as

$$\begin{aligned} T_{nm} = \sqrt{1+2n}\sqrt{1+2m} I_n(\beta J_1)\Big(\frac{\delta_{n,m}}{2n+1} + \beta B \left[\frac{n}{2n+1}\frac{\delta_{n-1,m}}{2n-1} + \frac{n+1}{2n+1}\frac{\delta_{n+1,m}}{2n+3} \right] \\ + \frac{(\beta B)^2}{2} \Big[\frac{1}{(2n+1)(2m+1)} \\ \times \Big\{ nm\frac{\delta_{n-1.m-1}}{2n-1} + n(m+1)\frac{\delta_{n-1,m+1}}{2n-1} + (n+1)m\frac{\delta_{n+1,m-1}}{2n+3} + (n+1)(m+1)\frac{\delta_{n+1,m+1}}{2n+3} \Big\} \Big] \Big) \end{aligned} \tag{6.5.2}$$

The crucial observation is that the leading order term is Hermitian, and has trivial eigenvalues and associated eigenvectors as it is diagonal. This means we can evaluate the first and second order corrections to the eigenvalue without any issue. To be

concrete, consider the first order correction to the eigenvalue given by

$$z^1 = {}_0\langle n_L|T_1|n_R\rangle_0 + {}_0\langle n_L|T_0|n_R\rangle_1 - z^0_{n0}\langle n_L|n_R\rangle_1,$$

where T_0 is the field independent term, and T_1 is the field dependent term in Eq.6.5.2. Where $|n_L\rangle$ and $|n_R\rangle$ satisfy the non-Hermitian equations

$$T|n_R\rangle = z_n|n_R\rangle$$
$$\langle n_L|T = \langle n_L|z_n$$

Given that T_0 is Hermitian, the last two terms cancel, and so we return the same result as the non-Hermitian case. We simply overlap the new matrix in the old basis to find the relative correction. First we note that the eigenvalues and eigenvectors for the unperturbed transfer matrix are given by

$$z_n = I_n(\beta J)$$
$$a^n_p = \delta_{n,p},$$

where a^n_p is the p-th coefficient of the n-th eigenvector, and is thus particularly trivial. Note that we only need the largest term from the transfer matrix as well, as we are in the thermodynamic limit, as stated before. For the Heisenberg model, we wish to calculate the magnetisation (or susceptibility), and thus we calculate

$$\langle M\rangle = -\frac{1}{\beta}\frac{\partial \log Z}{\partial B}$$
$$\chi = \frac{\partial\langle M\rangle}{\partial B}$$

The first order correction to the eigenvalue (which would give us the magnetisation) is calculated by the overlap

$$z^{(1)} = \langle n|T_1|n\rangle,$$

where T_1 is given above. It is clear that it has the form

$$\begin{pmatrix} 0 & a & 0 & \dots \\ b & 0 & c & \dots \\ 0 & d & 0 & \dots \\ \vdots & \vdots & \vdots & \ddots \end{pmatrix}$$

and therefore has no overlap with any of the groundstate eigenvectors, and thus we have no leading order correction. This provides us the proof that there is no magnetisation from the Heisenberg with (exponentially) weak fields, as is found with the exact solution. Finally we calculate the susceptibility, using the second order correction. We use the approximation

$$\begin{aligned} z^{(2)} &= \sum_{m\neq n^*} \frac{\langle m|T_1|n^*\rangle\langle n^*|T_1|m\rangle}{z_{n^*} - z_m} + \frac{1}{2}\langle n^*|T_2|n^*\rangle \\ &\approx \frac{\langle 0|T_1|1\rangle\langle 1|T_1|0\rangle}{z_1 - z_0} + \frac{1}{2}\langle 0|T_2|0\rangle \end{aligned}$$

This gives us

$$z^2 \approx \frac{1}{3}\frac{[I_0(\beta J)]^2}{I_0(\beta J) - I_1(\beta J)} + \frac{1}{6}I_0(\beta J),$$

which gives us a, strictly high temperature, expansion of the eigenvalue for the Heisenberg model, along with the zero field magnetisation (showing no long range order) and the zero field susceptibility.

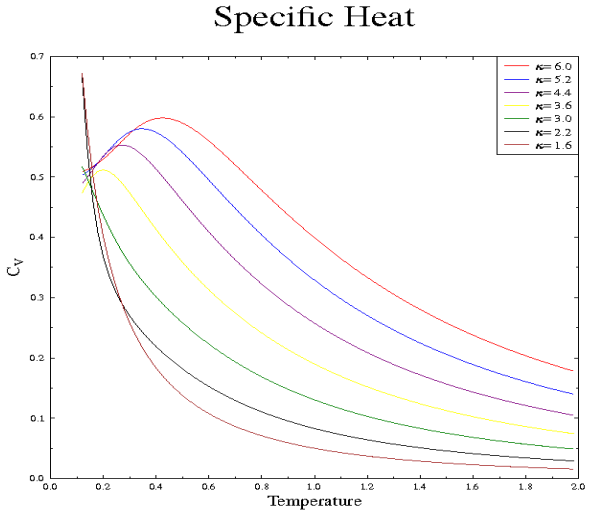

Figure 6.33: Specific heat capacity for the plane rotator near $\kappa = 0.25$

6.5.1 Summary of Results of Heisenberg Model

The phase diagram for the Heisenberg model has exactly the same form as the Ising model, but at $\kappa = 4$ rather than $\kappa = 2$. This is the first time the thermodynamics of spiral solutions has been investigated. The field dependence of the Heisenberg model is also much weaker than the Ising model, exhibiting exponentially *weak* field dependence. This is a consequence of the continuous symmetry which allows fluctuations perpendicular to the field which reduces the moment along the field direction.

6.6 Plane Rotator

We finally move on to the plane rotator model. Once again, for competing J_1 and J_2, we have two states which as shown in Fig.6.28, but with one less spin dimension to spiral in. We begin with the specific heat, given by Fig.6.33. We observe the same

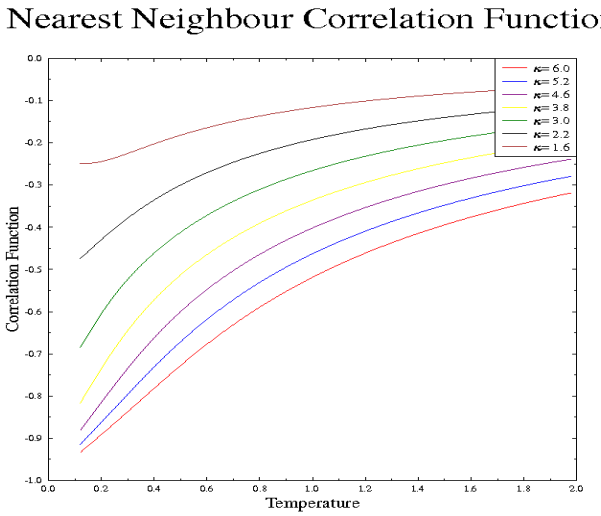

Figure 6.34: Nearest neighbour correlations for the plane rotator

characteristic change of behaviour around $\kappa \sim 4$, with the smooth peak disappearing towards the zero temperature axis. The behaviour is exemplified in the (nearest neighbour) correlation function, shown in Fig.6.34. Here, the correlations saturate at the antiferromagnetic value (-1), before increasing in line with Eq.(6.5.1). We may also look at the next nearest neighbour correlation function, seen in Fig.6.35, where the change of behaviour around $\kappa = 4$ is found once again. We therefore believe that the phase diagram is the same as the Ising and Heisenberg models. We now look at longer range correlation functions for the plane rotator. First we look at simple ferromagnetic exchange with $J_1 = J_2 = 1$, seen in Fig.6.36. We see that they strongly decay as a function of separation, though at low temperatures the correlations actually become *very* long range. We know that the correlations diverge at zero temperature, but they remain to a relatively high temperature before decaying, like the magnetisation in the continuous spin Ising model. Next we see the unfrustrated anti-ferromagnet, with $J_1 = -1.0$ and $J_2 = 1.0$. We observe exactly

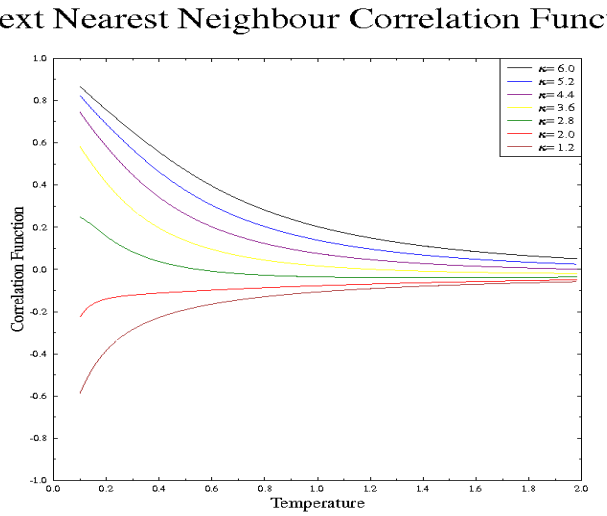

Figure 6.35: Next nearest neighbour correlations for the plane rotator

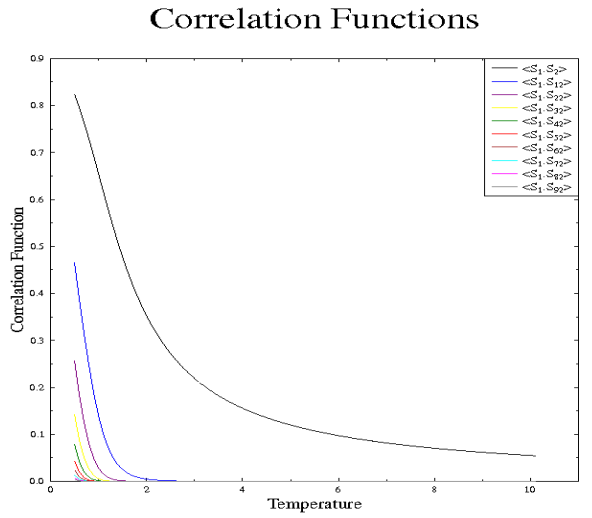

Figure 6.36: Correlation function for the plane rotator with $J_1 = 1.0$ and $J_2 = 1.0$

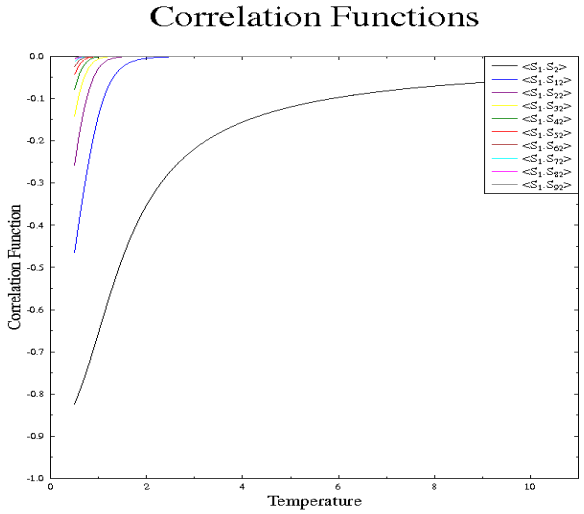

Figure 6.37: Correlation function for the plane rotator model with $J_1 = -1.0$ and $J_2 = 1.0$

the same behaviour as previously, although with the corresponding change of sign.

Classical Field Theory for the Plane Rotator

We now examine the low energy excitations of the model, just as in the continuous Ising model. To do this, we use classical continuous field theory. We write the partition function as

$$Z = \int \mathcal{D}\left[\phi(x)\right] e^{\beta J\left(\int_{-\infty}^{\infty} dx\ \cos(\phi(x)) - \cos(\phi(x+\delta)) - 1\right)}, \tag{6.6.1}$$

where we have elected to subtract off the groundstate energy. We expand the angle field to second order in δ, and expand the cosine to the same order, yielding

$$Z_{eff} = \int \mathcal{D}\left[\phi(x)\right] e^{-\beta J \int_{-\infty}^{\infty} dx\ \frac{\delta^2}{2}(\phi'(x))^2} \tag{6.6.2}$$

We solve this using the standard Euler-Lagrange, yielding

$$\frac{\partial}{\partial x}\left[\frac{\partial H}{\partial \phi'}\right] = 0 \tag{6.6.3}$$

$$\rightarrow \delta^2 \phi'(x) = C \tag{6.6.4}$$

$$\rightarrow \phi(x) \sim \frac{xC}{\delta^2} + \lambda, \tag{6.6.5}$$

which tells us that the low energy excitations (in one dimension) are *very* long range spirals. These long wave length (low energy) excitations are a consequence of the continuous symmetry of the model.

6.7 Summary of Results of all Models

We have found the low level thermodynamics of three short range one dimensional models. The continuous spin Ising model exhibits strong field dependence, while the Heisenberg and plane rotator models do not. They all have a similar phase diagram for the frustrated antiferromagnetic cases, although the distinction between states is most obvious for the continuous spin Ising model. The critical point for the continuous spin Ising model is also different to the other two models due to the inability to spiral.

6.8 Conclusion

We have studied the thermodynamics of three one dimensional models. Using transfer functions, we have reduced the problem to an eigen problem, where the thermodynamics is all contained within the largest eigenvalue of the integral operator. For the continuous spin Ising model, we use the Legendre polynomial basis to represent

the problem as a matrix, and then recursion relations to find the elements of the matrix. For the Heisenberg model we also use the Legendre basis, but we have a more explicit method of calculating matrix elements. Finally for the plane rotator, we used a Fourier basis for the eigenfunction to transform the problem to reciprocal space. Here, once again we had an explicit representation for the matrix elements. For the continuous spin Ising model, a second transfer matrix was found which provided an explicit representation for calculating matrix elements exactly. For the other models, we can approximate the integral equations with discretisation, once again turning the problem into an matrix eigenvalue problem. The approximate method works well, though quantities like specific heat, which are second derivatives, are largely limited by truncation error. The exact methods hit no such problems until significantly lower temperature when the size of the partition function itself becomes unmanageable. We may also compare our results with Monte Carlo simulations, which have been performed on the Heisenberg model.

We have used the one dimensional analogue of phase transitions in the specific heat to describe a phase diagram, allowing us to investigate how temperature affects zero-temperature phase transitions classically. For all three models with frustrated antiferromagnetic interactions, we found several states which are groundstates at zero temperature. For the continuous spin Ising model, there is the antiferromagnet, the ferromagnet, and the ferromagnetic state where half of the spins are not ordered. For the two continuous models, the three states were the nearest neighbour antiferromagnet and the spiral. If $J_2 \to \infty$ then we have a next nearest neighbour antiferromagnet seen in Fig.6.38.

We then investigated the thermal properties of this zero temperature transition. When there is a special state (the Ising model), there is much more entropy asso-

Figure 6.38: Natural state for $J_2 \to \infty$, two decoupled antiferromagnetic chains

ciated with the special state, which destabilises the antiferromagnet. For the two continuous models, the antiferromagnetism destabilises the spiral state, in order to gain from the fluctuations. Thus the phase diagram of all the models looks essentially the same for all three models and we have the simplest possible example of an order from disorder transition, or fluctuation induced crossover. Note that if we included a crystal field we would be able to investigate the simplest case of a spin flop transition, seen in Fig.6.39.

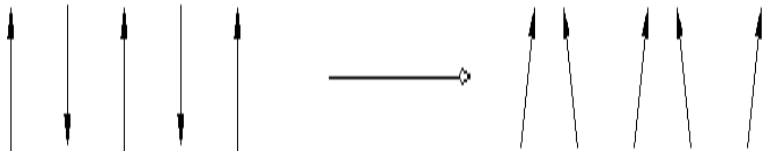

Figure 6.39: Example of applying a field to an antiferromagnetic system with a crystal field interaction

The thermodynamics of these models is clearly corrupted at low temperature by quantum mechanics; the limit $S \to \infty$ is unphysical for any real spin. However, the theory of phase transitions is believed to be classical, and therefore provided the low temperature phase is not quantum fluctuation dominated (a dimer phase on the ladder geometry), we believe that classical thermodynamics is reasonable. This method has the ability to investigate the one to two dimensional crossover using a second long range interaction. Here, phase transitions may occur in the limit of diverging the range of this second interaction (indeed, strictly in this limit only).

However, here we have no phase transitions or critical behaviour, but we have

a technique which allows investigation into the thermodynamics of such models, offering an alternative to the often used Monte Carlo.

Chapter 7

ONE TO TWO DIMENSIONAL CROSSOVER

7.1 Chapter Summary

We introduce the one to two dimensional crossover technique, that shall be explored much more fully later work [21] and [22]. We use the same transfer matrix method to solve the Ising and clock models (which are discrete). We then approximately solve the continuous spin Ising model in the two dimensional limit using direct integration of the transfer function, introduced in §.6.2. We use mean field theory to try to predict the transition in the continuous spin Ising model, and to predict the lower anomaly in the specific heat for the clock model.

The results we find are new for the models, though they amount to the results found by other techniques such as Monte Carlo. The technique of using transfer functions is partially new as has been explained, but the geometry we use to get to two dimensions is unique. It allows us to only have to integrate over one spin at a time, rather than the alternative strip geometry, in which one integrates out N spins. This makes the calculation technically much easier, but amounts to the same result in which we simply evaluate the largest eigenvalue of a transfer equation. It is important to note that the previous calculations in one dimension were exact, but

this technique is approximate as we are numerically solving the transfer equation using essentially the power method.

7.2 Introduction

Having solved several one dimensional models, (J_1-B and J_1-J_2) we now consider the one to two dimensional crossover. To achieve this, we consider models of the form

$$\begin{aligned} H &= \sum_n \left[J_1^x S_n^x S_{n+1}^x + J_1^y S_n^y S_{n+1}^y + J_1^z S_n^z S_{n+1}^z \right] \\ &+ \sum_n \left[J_N^x S_n^x S_{n+N}^x + J_N^y S_n^y S_{n+N}^y + J_N^z S_n^z S_{n+N}^z \right], \end{aligned}$$

for some given type of spin (either Ising, or classical in two or three dimensions). This type of model has partially been investigated before [76], though more usually the spiral boundary conditions are not used, in favour of cylindrical boundary conditions [1, 77, 78]. For the one dimensional models, we used exact techniques in order to turn the problem into a well specified transfer matrix. Here we abandon this mathematical control in order to include longer range interactions. In practice we use a sequence of increasing finite values for N up to some (memory limited) size. We then attempt to fit the infinite limit answer, although in reality it is not clear how to fit, and so very limited fitting will be done.

We will start with the regular Ising model, whose transition temperature is known exactly giving us a model to compare results to. For this model, the transfer matrix is exact, with the only approximation to two dimensions being N. We then generalise this model to the p-state clock model, whose spins are planar but restricted to p-evenly spaced directions around the unit circle. We regard this model as an ap-

proximation to the plane rotator, where we discretise the transfer function, though to a certain extent we study this model in it's own right, as it is equivalent to the plane rotator above some temperature. This model is known to have two transitions for $p > 4$, and we observe two anomalies in the specific heat. We also offer a mean field theory which seems to approximate the lower peak as an Ising transition reasonably well, especially for large p, though we cannot prove anything. We also study the plane Ising model, or anisotropic clock model. We see two interesting results; a *very* sharp magnetisation crossover under the application of a magnetic field which frustrates the p-fold crystal field, and the apparent destruction of the lower specific heat anomaly, which simply converges to a finite peak as a function of N in the presence of weak anisotropy. Finally we study the continuous spin Ising model, which has not been studied in two dimensions. We offer a mean field theory which seems to predict the observed specific heat anomaly reasonably well, characterising it as an Ising transition.

We will calculate the specific heat for all models, the average total magnetisation for the plane Ising model, and the long range correlation function for the regular Ising model. We will use polynomial extrapolation on the correlation function, and it is at this point it becomes clear that there is not necessarily a clear fitting procedure.

As always, we begin with the technique we will use, before moving on to the results. We essentially use the same technique throughout, though there is a slight subtlety when we calculate for the continuous spin Ising model. We then offer the results and any theories which help explain the results, for the models.

7.3 Calculation Technique

We begin with the regular Ising model. As we have seen, we may use the transfer matrix (or function) technique for these models, and we use that here. However, as was clear from the J_1-J_3 Ising model, the transfer equations necessarily grow exponentially, giving us the limiting factor for our technique. We consider

$$H = -J_1 \sum_n \sigma_n \sigma_{n+1} - J_N \sum_n \sigma_n \sigma_{n+N},$$

for a sequence of increasing N, until 2^N becomes too large. We begin with the J_1-J_3 Ising model in order to see the technique in detail, before we trivially generalise it to arbitrary N. We write the partition function as

$$\begin{aligned} Z &= \sum_{\{\sigma\}} e^{-\beta H} \\ &= \prod_{n=1}^{L} e_{\sigma_0} \sum_{\sigma_n} V_{\sigma_{n-1}\sigma_n\sigma_{n+1}} e_{\sigma_L} \end{aligned} \tag{7.3.1}$$

For a system of length L, where

$$V_{\sigma_{n-1}\sigma_n\sigma_{n+1}} \equiv e^{-\beta J(\frac{\sigma_{n-1}\sigma_n + \sigma_n\sigma_{n+1}}{2} + \sigma_{n-1}\sigma_{n+1})},$$

and e_{σ_p} is the part of the energy that we missed by factorising our Hamiltonian in the usual way (see §2.6.1) and does not contribute to the thermodynamics. We wish to turn this into matrix multiplication, but the functions V_{ijk} are not matrices. We therefore include some redundancy in the summations to turn the problem into matrix multiplication. The function V_{ijk} takes eight values, and so we arrange these

in a 4×4 matrix, with eight zeroes. We therefore define

$$T_{\sigma_1\sigma_2\tau_1\tau_2} \equiv \delta_{\tau_1\sigma_2} V_{\sigma_1\sigma_2\tau_2},$$

where the delta function controls the zeroes that we include in our new 4×4 matrix T. We now ensure that matrix of the transfer matrices is the same as producting the functions V_{ijk} together. We consider the indices of the transfer matrix as a compound label, viz

$$T_{\sigma_1\sigma_2\tau_1\tau_2} \equiv T_{ij},$$

where the indices i, j go over four values. Then matrix multiplication is

$$\sum_j T_{ij} T_{jk} = \sum_{\tau_1\tau_2} T_{\sigma_1\sigma_2\tau_1\tau_2} T_{\tau_1\tau_2\kappa_1\kappa_2}$$

in the usual way. We now check that this multiplication is the same as the product by considering

$$\begin{aligned} T_{\sigma_1\sigma_2\tau_1\tau_2} T_{\tau_1\tau_2\kappa_1\kappa_2} &= \delta_{\tau_1\sigma_2}\delta_{\kappa_1\tau_2} V_{\sigma_1\sigma_2\tau_2} V_{\tau_1\tau_2\kappa_2} \\ &= V_{\sigma_1\sigma_2\kappa_1} V_{\sigma_2\kappa_1\kappa_2} \end{aligned}$$

and we see that the index σ_2 on the functions V is being transferred in the way we desire to return the partition function. We may therefore use the transfer matrices to generate the partition function by

$$Z = Tr(T)^L \tag{7.3.2}$$

where the matrix multiplication here is over each *pair* if indices. For the case J_1-J_3 the transfer matrix is given by

$$(++,+-,-+,--)_{23}\begin{pmatrix} e^{K_1+K_3} & e^{-K_3} & 0 & 0 \\ 0 & 0 & e^{K_3-K_1} & e^{-K_3} \\ e^{-K_3} & e^{K_3-K_1} & 0 & 0 \\ 0 & 0 & e^{-K_3} & e^{-K_1-K_3} \end{pmatrix}\begin{pmatrix} ++ \\ +- \\ -+ \\ -- \end{pmatrix}_{14},$$

where $(\ldots)_{ij}$ indicates the possible states of the Ising spins σ_i and σ_j and $K_1 = \beta J_1$ and $K_3 = \beta J_3$.

It is now clear that we can generalise this for arbitrary range of interaction N, and simply include more dummy variables in the transfer matrix T. We then find the largest eigenvalue of the transfer matrix which yields the partition function in the thermodynamic limit $L \to \infty$.

This structure shall be used throughout for the transfer matrix for all models. We can also exploit two symmetries of the Hamiltonian to make the eigenfunction more symmetric, and the matrix itself smaller. We can firstly write the Hamiltonian in symmetric form

$$H = -\frac{J_1}{N}\sum_n (\sigma_n\sigma_{n+1} + \sigma_{n+1}\sigma_{n+2} + \ldots \sigma_{n+N-1}\sigma_{n+N}) - J_N \sum_n \sigma_n\sigma_{n+N},$$

and we may also use the floating basis $\tau_n = \sigma_n\sigma_{n+1}$ yielding

$$H = -\frac{J_1}{N}\sum_n (\tau_n + \tau_{n+1} + \ldots \tau_{n+N-1}) - J_N \sum_n \tau_n\tau_{n+1}\ldots\tau_{n+N-1},$$

which reduces the number of spins involved in the Hamiltonian by 1, so we can

calculate up to $N+1$ rather than N if desired. Once again we use

$$\langle E\rangle = -\frac{1}{z}\langle 0|z'|0\rangle,$$

where $z' = \frac{\partial z}{\partial \beta}$ for the exact energy, and numerical differentiation of this for the specific heat. For the long range correlation functions, we use

$$\xi = \frac{1}{\log\left(\frac{z}{\tilde{z}}\right)},$$

where z is the largest eigenvalue, and $\tilde{z}$ is the largest eigenvalue of the modified transfer matrix which contains the spin, or simply the eigenvalue of the original transfer matrix which contains the correct anti-symmetry. We only calculate this quantity for the Ising model.

For the p-state clock model, we consider the model

$$H = -J_1 \sum_n \cos(\phi_n - \phi_{n+1}) - J_n \sum_n \cos(\phi_n - \phi_{n+N}) - h_p \sum_n \cos p\phi_n,$$

where $h_p = \infty$, leading to the angles being restricted to p states. Clearly $p = 2$ is the Ising model, and $p = 1$ is trivial. Once again we use transfer matrices, which are now p^N (or p^{N-1} in the floating basis) dimensional. We set up the matrix as transferring from the set $\{\phi_n, \phi_{n+1} \ldots \phi_{n+N}\}$ to the set $\{\phi_{n+1}, \phi_{n+2} \ldots \phi_{n+N+1}\}$ using the matrix

$$T_{\phi_{n+1},\phi_{n+2}\ldots\phi_{n+N+1};\phi_n,\phi_{n+1}\ldots\phi_{n+N}}$$

exactly the same as in the Ising model, and we turn the summation over p-states for ϕ_0 into matrix multiplication.

Finally, we solve the continuous spin Ising model. We will use the same structure

as before, but we now have a truncation scheme due to the transfer function nature of the problem. We consider

$$H = -J_1 \sum \cos\theta_n \cos\theta_{n+1} - J_N \sum_n \cos\theta_n \cos\theta_{n+N}$$

which yields the transfer equation given by

$$zf(u_1, u_2 \dots u_N) = \int_{-1}^{1} \frac{du_0}{2} e^{\beta J_1 u_0 u_1 + \beta J_N u_0 u_N} f(u_0, u_1 \dots u_{N-1}),$$

which we solve using the integral equation method presented in §.6.2. Here, however, we wish to take the large N limit, and so we elect not to use the trapezium rule which requires many steps in the region $[-1, 1]$ to be accurate. Instead, we use q-step Gaussian Legendre integration, where

$$I = \int_{-1}^{1} \frac{du}{2} f(u) = \sum_{n=0}^{\infty} f(u_n) w_n \approx \sum_{n=0}^{q} f(u_n) w_n,$$

where w_n are weights, and we evaluate the q steps on a non evenly spaced grid. This integration technique uses that the integrand is well represented by a q-th order polynomial in the region $[-1, 1]$, which for our transfer function leads to a temperature above which the integral is exponentially accurate. We therefore have a q^N dimensional transfer function, where to go lower in temperature, one increases q, and therefore must reduce N.

We now move on to the results, providing the specific heat for all models, along with any relevant calculations.

7.4 Results

7.4.1 Ising Model and Clock Model

We begin with the regular Ising model. Throughout, we work with $J_1 = J_N = 1$, and ferromagnetic, and only frustrate the system with a field for the plane Ising model. After the Ising model, we study the p-state clock model, the p-state plane Ising model and the continuous spin Ising model. In Fig.7.1 we see

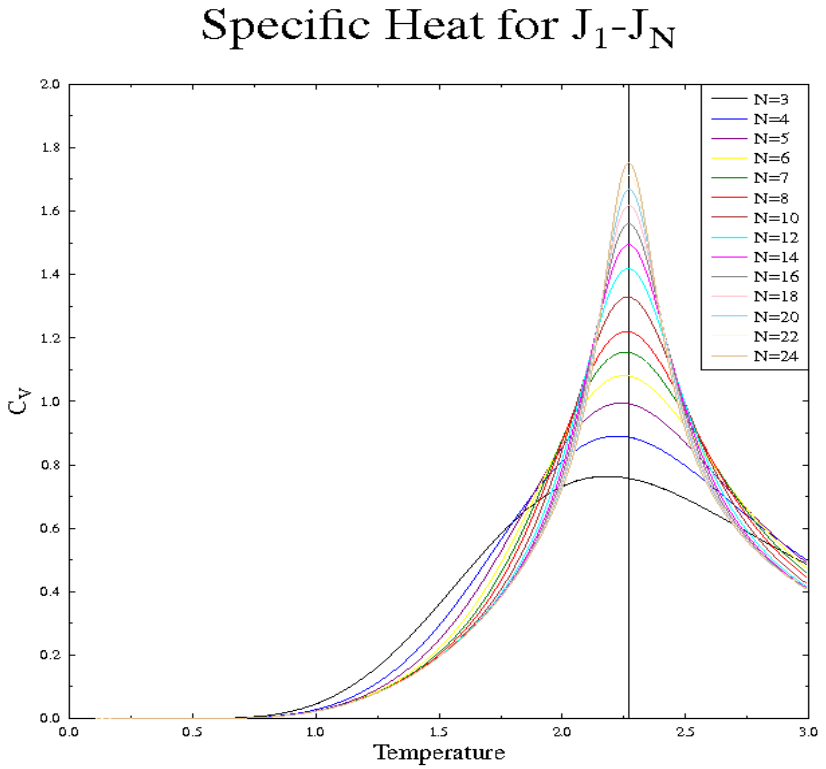

Figure 7.1: Specific heat for the Ising model on the spiral lattice.

a sequence of calculations of the specific heat for the Ising model, with $N = 3, 4, 5, 6, 7, 8, 10, 12, 14, 16, 18, 20, 22, 24$, with the exact two dimensional solution over

the top as the vertical line at [38]

$$T_I = \frac{2}{\log(1+\sqrt{2})} \approx 2.269,$$

a number which will be used extensively for other calculations. We observe that the position of the peak is in very good agreement with the exact result, and indeed grows as a function of N as expected. However, we do not know what the function is, meaning that we can not simply fit the $N \to \infty$ limit of the peak to find a sharp peak. We now look at the inverse correlation length, seen in Fig.7.2 with $N = 3, 4, 5, 6, 7, 8, 10, 12, 14, 16, 18, 20$. This correlation length should scale as

$$\xi \approx \xi_0 + \left|1 - \frac{T}{T_I}\right|^{\nu},$$

with, for the Ising model, $\nu = 1$ which is known exactly. Here, we have an anisotropic geometry which adds confusion. For a finite lattice of size $L \times L$, we expect the correlation length to be cutoff at the length scale L, which leads us to

$$T_I - T_L \approx aL^{-\frac{1}{\nu}},$$

where T_L is the finite sized pseudo-critical temperature, at which the correlations span the finite system. For us, we have a system of size $N \times \infty$, and so the full two dimensional correlations may generate down the spiral, but not perpendicular. We therefore have no simple way of extracting out the limit $N \to \infty$ as we would like. We may simply use polynomial fitting to extract out features, but we rarely expect a polynomial dependence on N. However, in Fig.7.3 we provide the inverse correlation length (up to J_1-J_8) but with the polynomial extrapolation over the top, and the

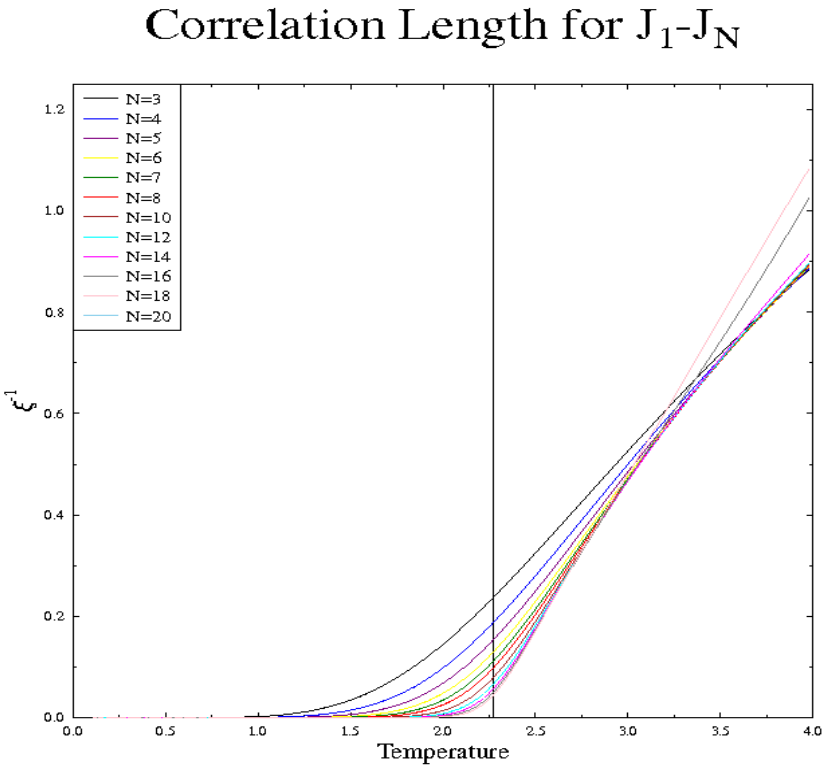

Figure 7.2: Inverse correlation length for the Ising model on the spiral lattice.

exact solution as the vertical line, which we would expect close to the transition. We see that the extrapolation agrees reasonably with the exact solution, although it goes negative, indicating that the fitting procedure is not appropriate. We next provide the results for the p-state clock model. For the cases $p = 3$ and $p = 4$, the exact solution is known [42]

$$T_{p=3} = \frac{3}{2\log(1+\sqrt{3})} \qquad T_{p=4} = \frac{T_I}{2}$$

In Fig.7.4 and Fig.7.5 we see the specific heat for a collection of spiral sizes, with

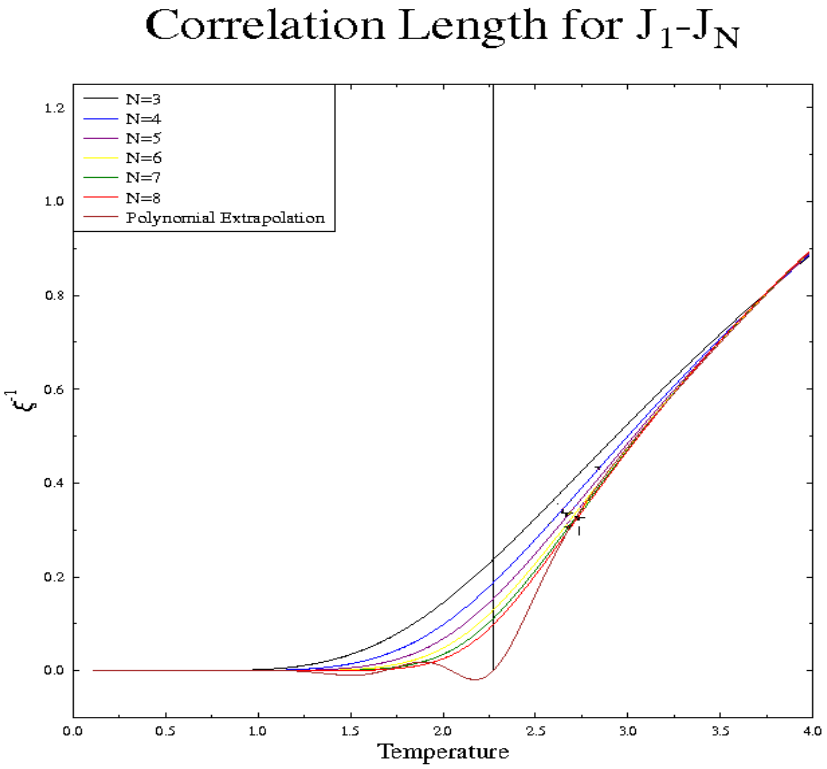

Figure 7.3: Inverse correlation length for the Ising model on the spiral lattice with polynomial extrapolation.

the exact solution over the top, and once again we see good agreement. For $p > 4$, it is known that there are two phase transitions, which are both believed to be Kosterlitz-Thouless like. In Fig.7.6, Fig.7.7, Fig.7.8 and Fig.7.9 we see the specific heat for $p = 5, 6, 7, 8$. We can see two smooth specific heat anomalies which grow as a function of N. The upper peak is p-independent while the lower one decreases in temperature with increasing p. The vertical lines on the graphs are a mean field treatment of the lower peak, which we now describe. We *reduce* our Hamiltonian to one in which neighbouring spins are either parallel or one clock tick over. This

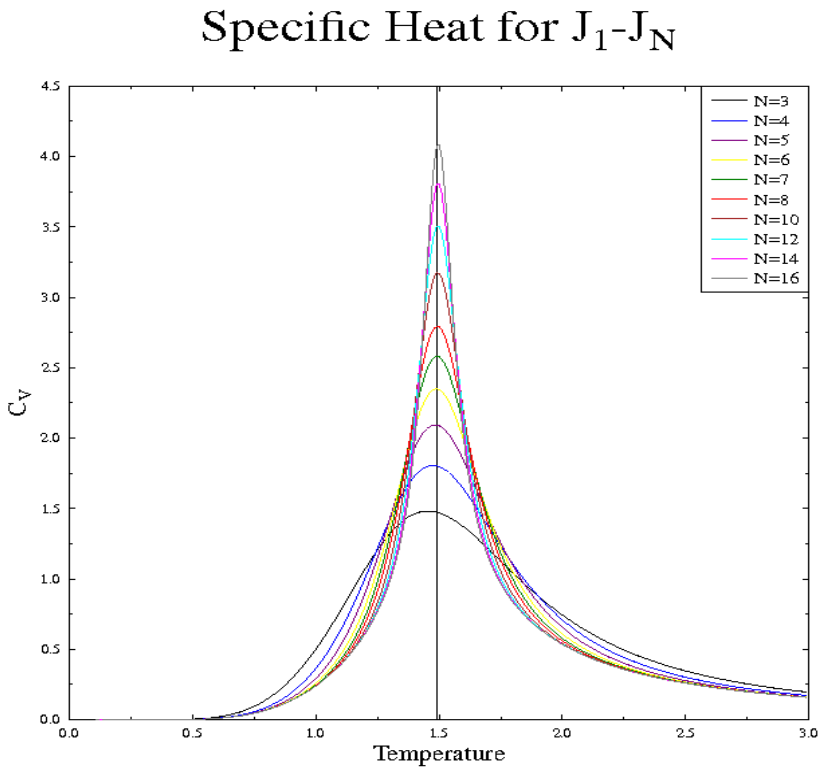

Figure 7.4: Specific heat for the $p = 3$ clock model on the spiral lattice.

turns our model into an Ising model, with two states between neighbouring spins; parallel or canted. We may write this Hamiltonian down as

$$H = -J \sum_{<ij>} \frac{\sigma_i \sigma_j + 1}{2} - \cos\left(\frac{2\pi}{p}\right) \frac{\sigma_i \sigma_j - 1}{2},$$

where the clock tick costs the energy $\cos\left(\frac{2\pi}{p}\right)$. This allows us to write

$$\begin{aligned} H &= -J \sum_{<ij>} \sigma_i \sigma_j \left(\frac{1 - \cos\left(\frac{2\pi}{p}\right)}{2} \right) + \left(\frac{1 + \cos\left(\frac{2\pi}{p}\right)}{2} \right) \\ &= -J_{eff} H_{Ising}, \end{aligned}$$

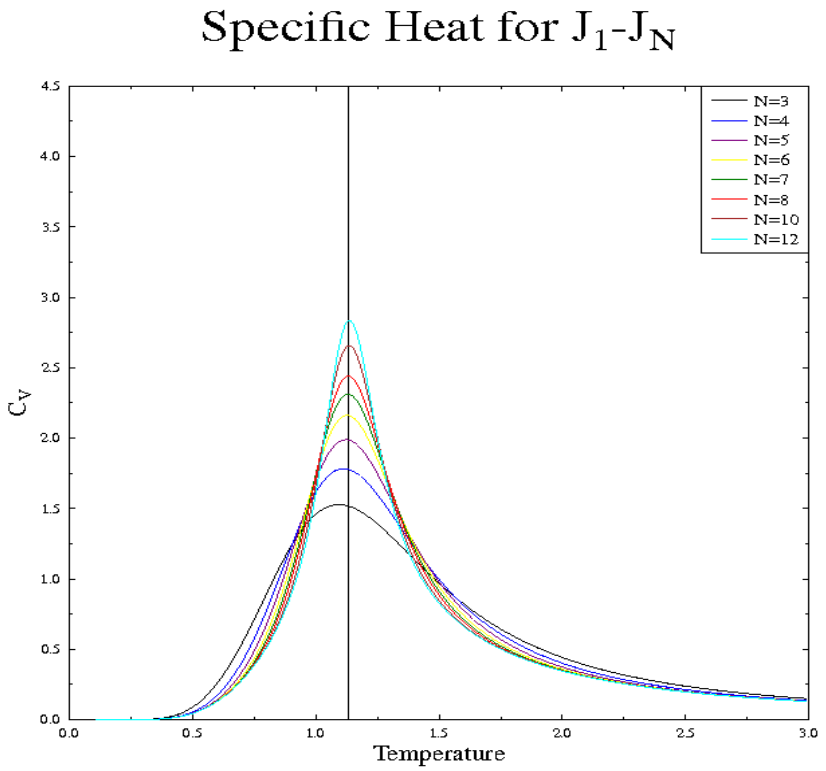

Figure 7.5: Specific heat for the $p = 4$ clock model on the spiral lattice.

which is simply the Ising model with a rescaled interaction energy. This provides us with an approximation of the lower transition given by

$$T_p = \sin^2\left(\frac{\pi}{p}\right) T_I$$

We cannot prove this to be the lower transition, although we have taken the lowest energy excitations available to the clock model, and so one would expect this to give an approximation to that transition. We note that the approximation seems agree with the peak in the specific heat with increasing p, and thus we include $p = 16$

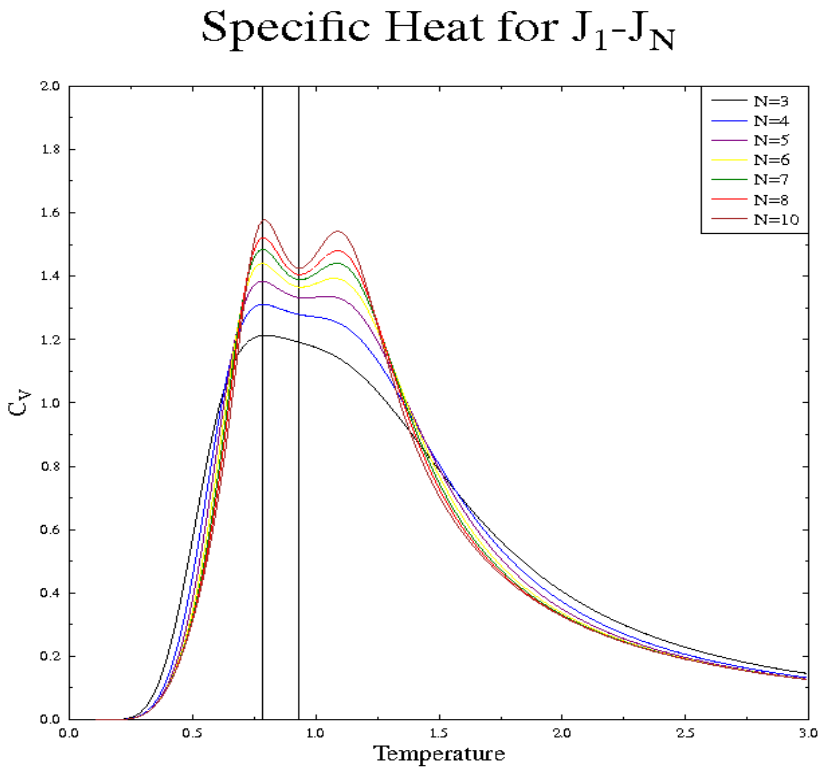

Figure 7.6: Specific heat for the $p = 5$ clock model on the spiral lattice. The lower vertical line is our mean field theory, the upper vertical line is from [1].

in Fig.7.10 to show this, where we see reasonably good agreement. Note that we expect the upper transition to be p-independent; if we regard the clock model as an approximation of the integral in the plane rotator model, then the transition cannot depend on p. We therefore expect numerical agreement above some temperature for a given p between the clock model and the plane rotator, although there could be (and is) a difference between the two which is too small to notice. For $p = 5$, the two transitions are very close, but for $p = 8$ they are well separated, showing the independence of p and the upper transition well. In Fig.7.10 we see the case

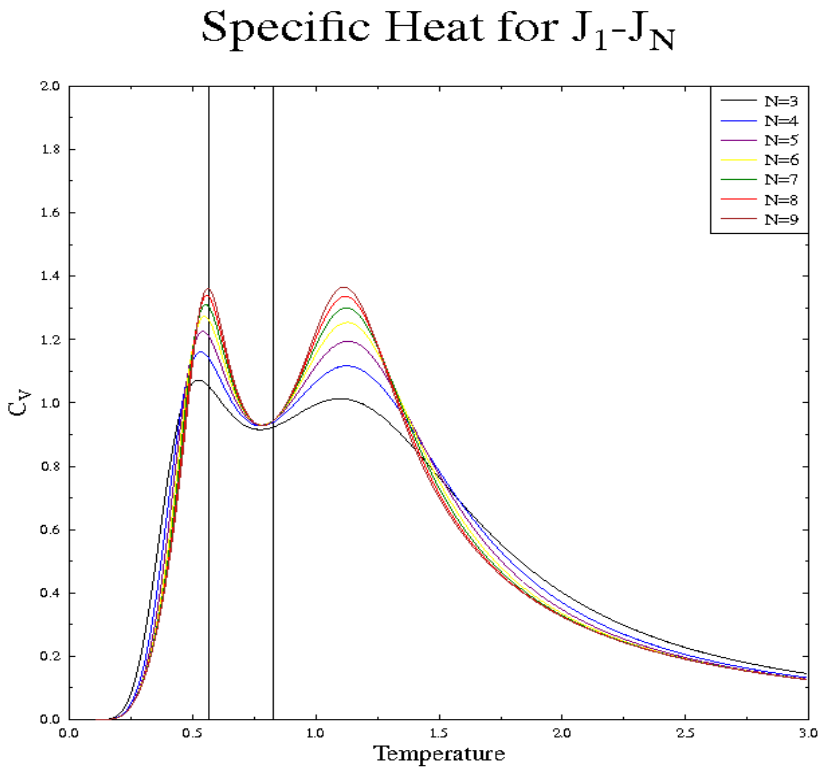

Figure 7.7: Specific heat for the $p = 6$ clock model on the spiral lattice. The lower vertical line is our mean field theory, the upper vertical line is from [1].

$p = 8$, where the lower peak has gone to very low temperature leaving only the upper peak visible. Note here we are severely limited in N due to the large p, but we can see that the upper transition is very much p independent. Note also that the specific heat anomalies both grow with increasing N, though clearly we cannot prove whether these peaks converge in the limit $N \to \infty$ as is expected.

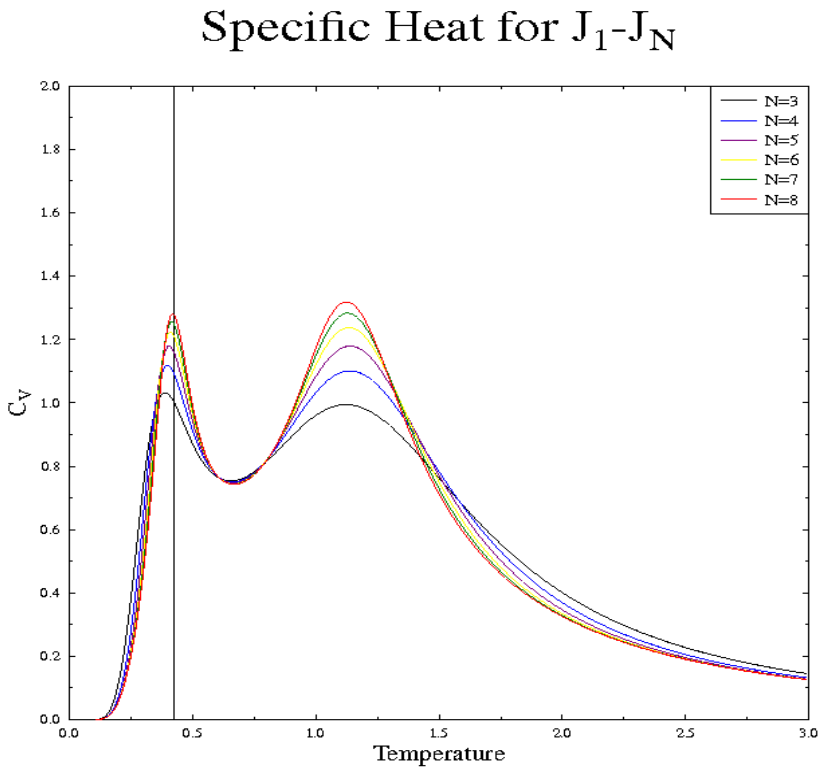

Figure 7.8: Specific heat for the $p = 7$ clock model on the spiral lattice. The lower vertical line is our mean field theory.

7.4.2 Continuous Spin Ising Model

Finally we move on to the J_1-J_N continuous spin Ising model. Here we have a parameter q; the number of integration steps. Note that this means we are studying a clock model of the continuous spin Ising model, though with unevenly spaced (and weighted) clock ticks. Here, we regard the approximation only as an error, and thus we work with sufficiently large q to investigate the temperature we are interested in. In Fig.7.11 we see the case of J_1-J_3, with $q = 6, 10, 16$ indicating how the accuracy scales with increasing the number of steps in the integration. We see that above

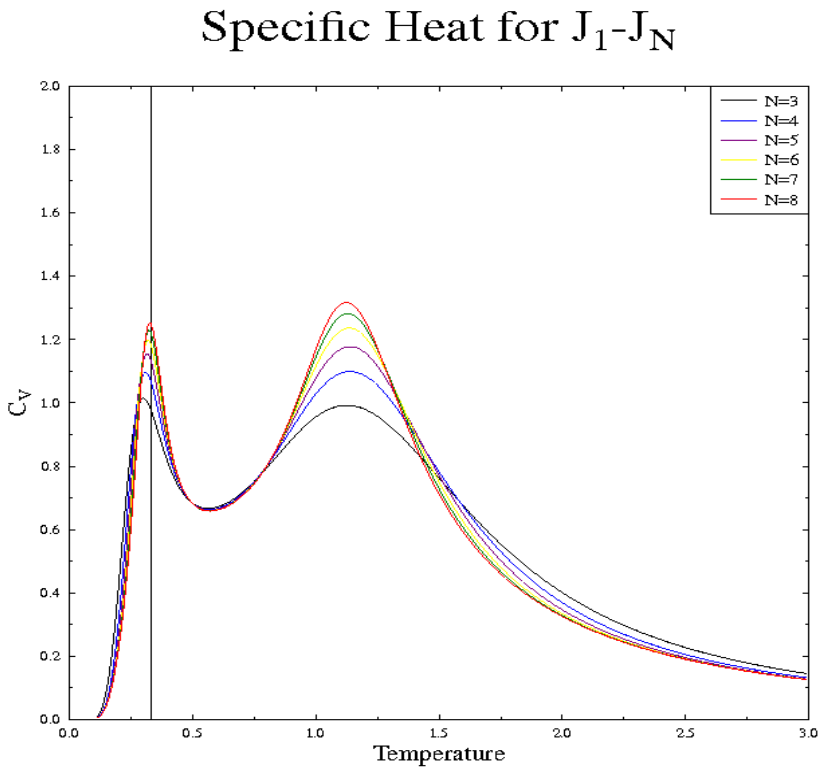

Figure 7.9: Specific heat for the $p = 8$ clock model on the spiral lattice. The lower vertical line is our mean field theory.

some temperature, all procedures agree and we therefore elect to work with $q = 6$, allowing us to calculate for $N = 3, 4, 5, 6, 7, 8$. In Fig.7.12 we see the specific heat for this sequence of increasing spiral size, where we see an increasing peak. We fully expect an Ising transition for this model, and so we perform a mean field calculation with this in mind in order to model the transition. We *assume* that the continuous spin Ising model is composed of two types of (uncoupled) fluctuations. The first is the Ising degree of freedom; the spin may either be up or down. The second is the continuous part, which allows the spin to fluctuate, but not change the Ising state.

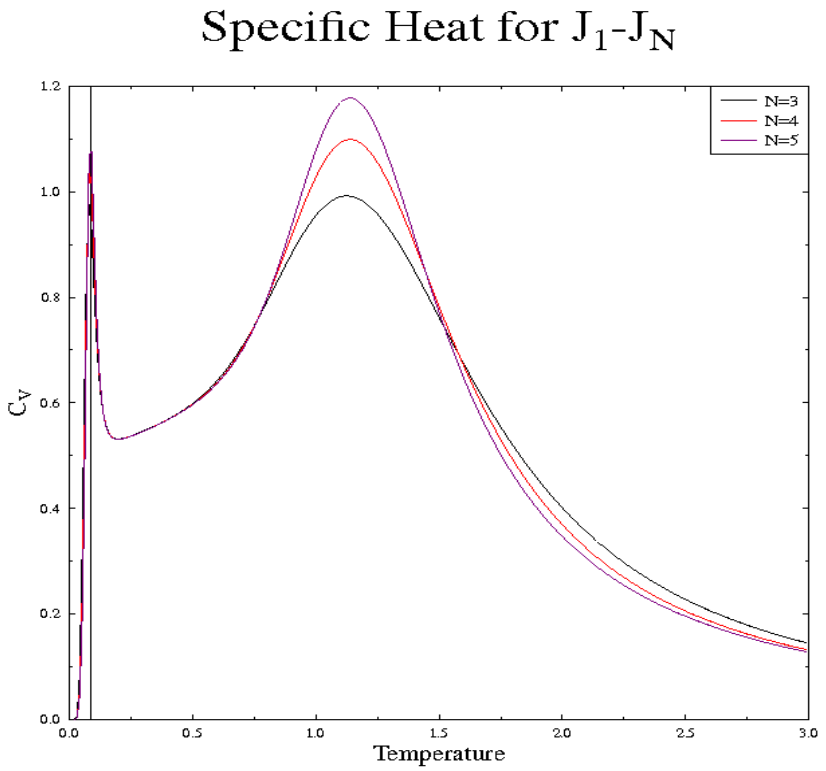

Figure 7.10: Specific heat for the $p = 16$ clock model on the spiral lattice.

We begin by simply calculating the mean field magnetisation for one spin surrounded by λ (four here) neighbours (the coordination number), each with a magnetisation m. The partition function is simply

$$Z = \int_{-1}^{1} \frac{du}{2} e^{4\beta Jum} = \frac{\sinh 4\beta Jm}{4\beta Jm}$$

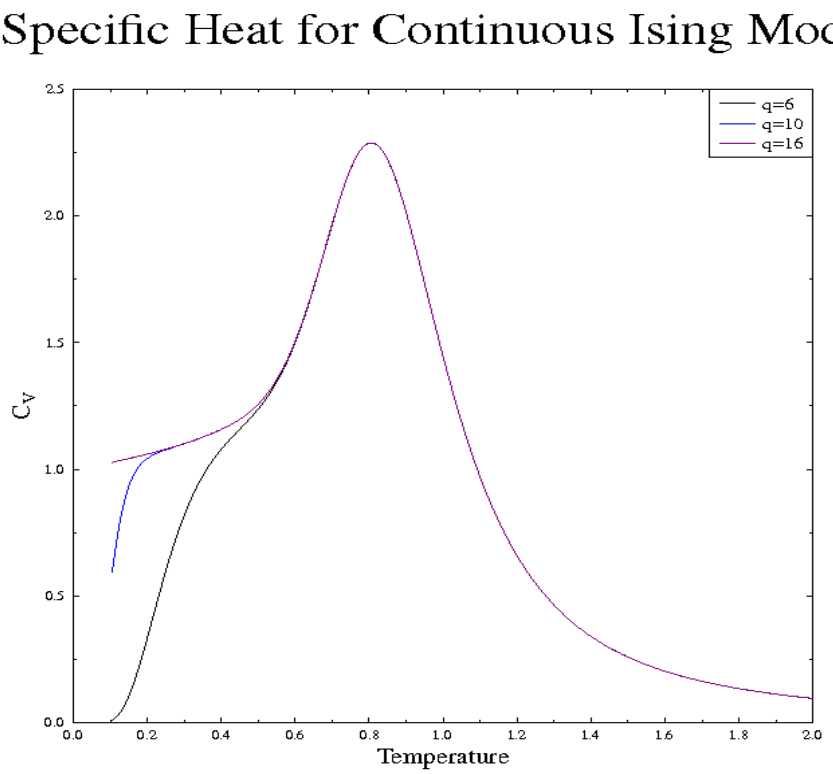

Figure 7.11: Specific heat for the continuous spin Ising model, for J_1-J_3, with increasing number of integration steps.

for two dimensions. We then calculate the magnetisation on the central site given by

$$\begin{aligned} \langle m \rangle &= \frac{\partial \log Z}{\partial(4\beta J m)} \\ &= \frac{1}{\tanh 4\beta J m} - \frac{1}{4\beta J m} \end{aligned} \tag{7.4.1}$$

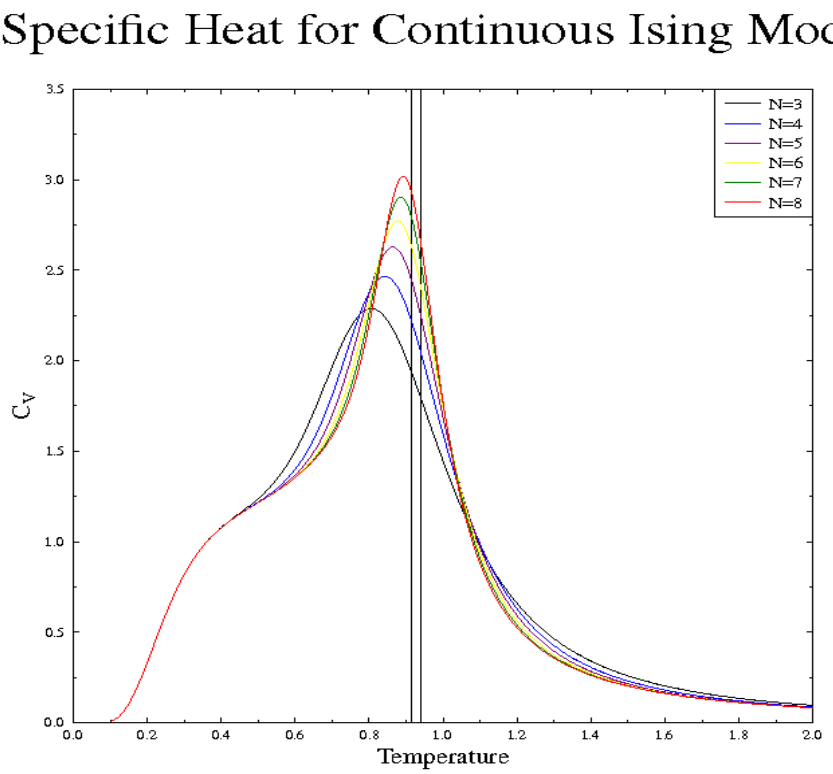

Figure 7.12: Specific heat for the continuous spin Ising model for J_1-J_N. The right vertical line is the mean field approximation and the left vertical line is the approximation from [1].

We may then self consistently solve this for m, by extracting the linear term from the right hand side, assuming that at β_c the magnetisation goes to zero

$$\rightarrow T_C = \frac{4J}{3},$$

the Curie law. We now assume, as stated before that the fluctuations decouple from the Ising degree of freedom

$$S_n^z \equiv m_n(T)\sigma_n$$

where $m(T)$ is given by Eq.7.4.1. This means our two dimensional continuous spin Ising Hamiltonian is given by

$$H = -J \sum_{<ij>} m_i(T) m_j(T) \sigma_i \sigma_j$$

If we now assume that $m_i(T) = m_j(T) = m(T)$, and that the fluctuations are site independent, then we get

$$\begin{aligned} H &= -J[m(T)]^2 \sum_{<ij>} \sigma_i \sigma_j \\ &= -J_{eff} H_{Ising}, \end{aligned}$$

allowing us to read off the two equations

$$\begin{aligned} T_{CI} &= [m(T_{CI})]^2 T_I \\ m(T) &= \frac{1}{\tanh 4\beta J m} - \frac{1}{4\beta J m} \end{aligned}$$

where T_{CI} is our expected transition temperature. We solve these (numerically) yielding

$$T_{CI} \approx 0.93932$$

$$m(T_{CI}) \approx 0.643396$$

which we have put on to Fig.7.12 as the right hand vertical line. We see that this predicts that the fluctuations reduce the moment on each site by about two thirds before the Ising transition may occur. Clearly, the two fluctuations are not decoupled, though the approximation seems reasonable if not exact. We have also

used the technique outlined in [1] to try to predict the transition temperature. They propose that the transition temperature for a two-dimensional model can be found from the crossing temperature of the energies of the J_1-J_2 and the J_1-J_3 models. For the normal Ising, this is exact, and one finds the expected T_c from duality. It must also be true that one can use the crossing of the J_1-J_2 and the J_1-J_4 models and get the same answer, as one does for the Ising model, Here, the crossing of the energies moves as a function of N, and so the technique is only approximate, so we extrapolate for the $N \to \infty$ limit of the procedure. We do not believe that it is an appropriate technique for this model, just as [78] find for other models. We also have a result from Monte Carlo analysis on the model [52], which finds that

$$T_c = 0.92 \pm 0.01$$

for a 150×150 system, in good agreement with our curves and the mean field analysis.

7.5 Conclusion

We have used the transfer function technique to solve several long range models. We have shown how this technique works for the Ising model, whose solution is fully understood. We then moved on to the p-state clock model. For $p > 5$ we find two anomalies in the specific heat, which grow as a function of N just like the Ising specific heat. We do now know whether these correspond to the phase transition, though a simple mean field theory indicates the lower peak is well predicted. The upper peak is not currently understood, and should be the remaining (invisible) Kosterlitz Thouless transition.

We then moved on the the continuous spin Ising model. We believe this to have a transition in two dimensions due to the lack of continuous symmetry. Using mean field theory, we may predict this transition as being dominated by the Ising degree of freedom. We find that although the transition may be Ising driven, the Ising fluctuations couple to the continuous degree of freedom, and so the mean field theory is insufficient here to be fully accurate.

We now comment on the technique that we have used; we are always limited by the size of our spiral. We do not know whether an $L \times L$ system is better than an $N \times \infty$ one, but our results for the Ising model indicate that our technique works well. Clearly the correlation length wrapping around the spiral is not representative of two dimensions, though periodic boundary conditions for Monte Carlo analysis on $L \times L$ lattices suffers the same problems. If nothing special happens between $N \approx 20$ and $N \to \infty$, then our calculations are very good, but we cannot be certain of this. If the maximum of the peak in the specific heat moves as a function of N, then we cannot find T_C without further fitting.

Another feature of our technique is that of convergence. We find that the thermodynamics of the two models must agree above some temperature, if we regard the clock model as an approximation of the plane rotator. This agreement is power law in temperature; the two calculations start to converge very quickly, until the error between them is not noticeable. The effect of the lower transition is washed away as a function of temperature, until we are left with the plane rotator. In order to reduce the temperature above which they agree, we may increase p, and for large values we can regard the two models the same down to relatively low temperatures. The same is true for the continuous spin Ising model; when using Gaussian Legendre Quadrature we find the same exponential convergence.

Chapter 8

MAGNETISM ON THE PYROCHLORE LATTICE

8.1 Chapter Summary

We introduce the lattice we will be studying; the pyrochlore lattice. We will show that the Heisenberg model has macroscopic zero temperature degeneracy on this geometry, following the work in [79], and then introduce the general classical model that we will study. This is not a new model, and has been looked at many times before in reference to the compounds that we study. However, it is usually only approximately solved due to the inclusion of the dipolar interaction. We then go through the experimental details for the six compounds that we wish to study, including any of the known groundstates. We have also studied the compound $Er_2Ti_2O_7$ elsewhere [80], but do not discuss it at all here as it is not in line with the classical model that we study.

8.2 Introduction

We will be working on a class of compounds, where the magnetic atoms reside on a pyrochlore lattice. The pyrochlore lattice is the most frustrated lattice experimentally available. Many frustrated lattices have been studied experimentally [81–84], due to the interesting groundstate properties and excitations. The pyrochlore lattice was first studied theoretically by Anderson [85], where the issue of zero temperature entropy was realised for the nearest neighbour Heisenberg model on this geometry. Rare-earth pyrochlores have been studied in past for the heat capacities [86], but more recently for their magnetic properties [79, 87, 88]. They may exhibit several interesting effects; interesting excitations from groundstate degeneracy [89], frustration [90], and interesting energy spectrum [91].

For the compounds that we study here, there are several interactions which control the magnetism. We find the compounds are controlled by long range forces (the dipolar interaction) [92], along with local crystal fields and Heisenberg exchange [93]. The Heisenberg interaction is frustrated on the lattice, exhibiting a finite groundstate degeneracy, and so these other interactions may lift this degeneracy. It turns out that the inclusion of the natural crystal field interaction does not lift the degeneracy completely as we shall see, and that the dipolar interaction plays a central role that we study. We will be studying a classical model which we hope captures the essential physics of the various compounds. For most of the compounds, the classical model seems to be reasonable, and for the cases of spin ice and gadolinium it does very well (as will be explained).

8.3 Pyrochlore Lattice and Frustration

We will be studying compounds of the form $R_2M_2O_7$, where R is a rare earth (or f-block) element, M is a transition metal, and O is oxygen. Before we introduce the lattice, we go through the charge counting. The oxygen will always go $2-$ due to electronegativity, while the rare earth will go $3+$, leaving the transition metal to go $4+$. There are very few transition metals which go $4+$, and consequently we may only have Ti and Sn as possible substitutions. The R^{3+} resides on a pyrochlore lattice, as does the M^{4+}, and the oxygen fills in the gaps. We begin with discussing the details of the lattice, then the crystal field, before we talk about frustration on the lattice.

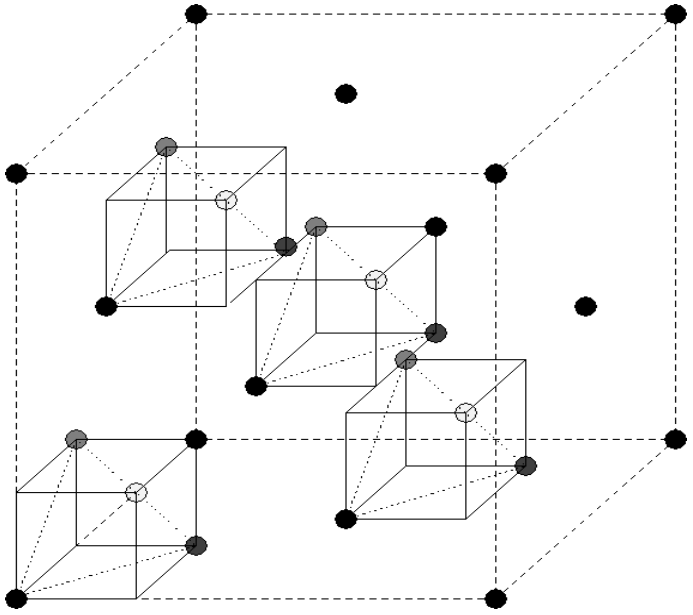

Figure 8.1: The pyrochlore lattice, showing the underlying face centered cubic lattice. Each different shade of circle depicts different sublattices.

As said before, the pyrochlore lattice is the four atoms per unit cell on an underlying face centered cubic lattice seen in Fig.8.1, which generates corner sharing tetrahedra as seen in Fig.8.2. If we view the lattice along either the (011), (101) or

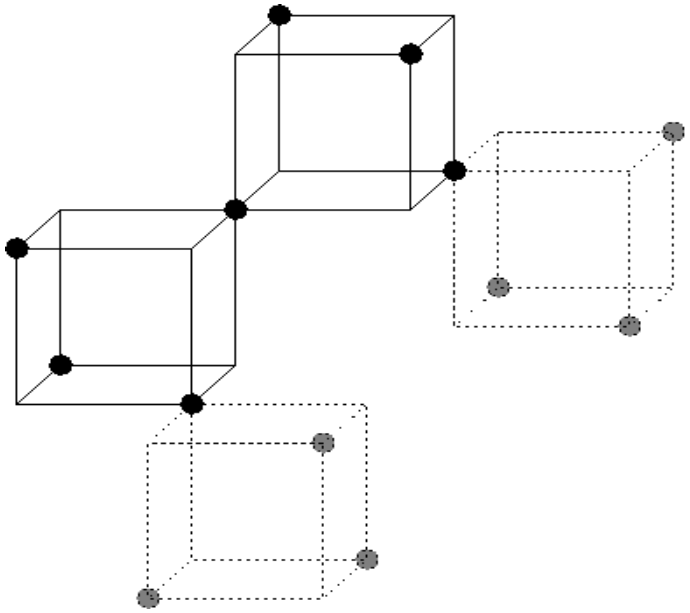

Figure 8.2: The pyrochlore lattice, showing the corner sharing tetrahedra. The shaded cubes are for clarity.

(110) directions, then we have lines of atoms along these directions and perpendicular. If we view the lattice along either (111), $(1\bar{1}\bar{1})$, $(\bar{1}1\bar{1})$ or $(\bar{1}\bar{1}1)$ we see alternating planes of sparse triangular, and Kagome lattices. When we use this projection, the sparse triangular lattices consist only of one sublattice.

It is also important to understand the *local* crystal structure around the rare earth. Each rare-earth tetrahedron has an oxygen in the center, which provides the dominant crystal field interaction to either point towards or away from the center of each tetrahedron. There are also six oxygens around the rare earth in a "puckered" hexagonal ring, depicted in Fig.8.3 which provides an azimuthal anisotropy.

In order to understand the lattice further, we first consider the nearest neighbour antiferromagnetic classical Heisenberg interaction. For the particular case of the tetrahedron (or the triangle), the nearest neighbour Heisenberg can be written as a

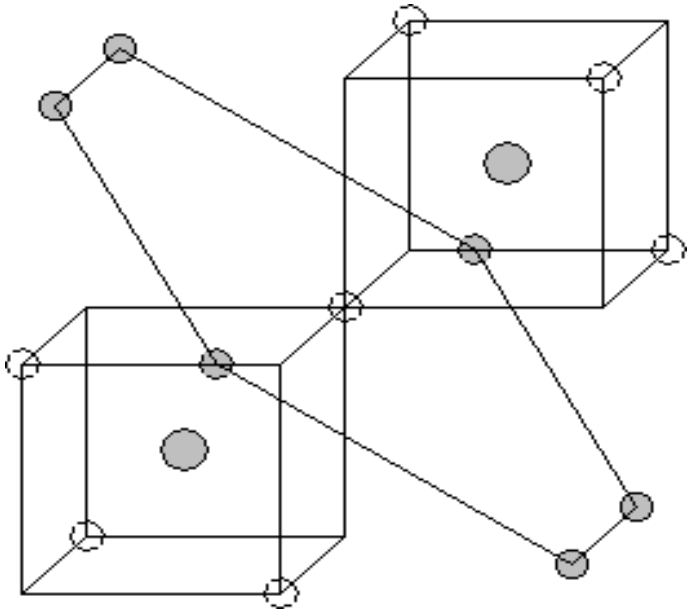

Figure 8.3: Depiction of the local crystal structure for each rare earth ion, showing the two dominant oxygens and the hexagonal ring.

sum over spins in each tetrahedron as follows

$$\begin{aligned} H &= \sum_{\langle ij \rangle} \mathbf{S}_i.\mathbf{S}_j \\ &= \sum_t \sum_{\langle ij \rangle_t} \mathbf{S}_i.\mathbf{S}_j \\ &= \sum_t \frac{1}{2} \left[(\sum_{i \in t} \mathbf{S}_i)^2 - 4 \right] \end{aligned}$$

where the sum over t is a sum over distinct tetrahedra. This energy is clearly minimised by the condition

$$\sum_{i \in t} \mathbf{S}_i = 0, \tag{8.3.1}$$

so that each tetrahedron has zero total spin. Each spin has 2 degrees of freedom per site, and so we have 4 degrees of freedom per tetrahedron (each spin lies in *two* tetrahedra). The constraint Eq.8.3.1 reduces this by 3 as the total spin has to be zero

in all three Cartesian directions, and thus we have one degree of freedom left over per tetrahedron. We are left with a *macroscopic* degeneracy, which can lead to several interesting consequences. It allows other interactions to control the groundstate of the system, and may have interesting thermodynamics and excitations as a result.

The lattice itself is also geometrically frustrated which means that one can not necessarily optimise the energy. One can measure frustration via

$$\Phi = \frac{\sum_{ij} J_{ij}\mathbf{S}_i.\mathbf{S}_j}{-\sum_{ij}|J_{ij}|},$$

where the term on the bottom is the absolute minimum of the interaction strengths J_{ij}, while the term on top is the energy that one *can* get from the interaction strengths and the spin length constraint in the groundstate. Any lattice which is bipartite is not frustrated under antiferromagnetism, and no lattice is frustrated for ferromagnetism. However, antiferromagnetism on some geometries may be frustrated, for example the antiferromagnetic Ising model on the triangular lattice has $\Phi = \frac{1}{2}$, as only two of the three bonds can gain the anti-ferromagnetism. For this case there is one spin in every three that is energetically arbitrary which provides a macroscopic degeneracy in the groundstate. The Kagome lattice is also frustrated for antiferromagnetic interactions, as is the pyrochlore. The cause of frustration in general is odd numbered loops, which can not have all bonds simultaneously anti-parallel, which means ferromagnetism is never geometrically frustrated.

When it comes to the modeling of the pyrochlore compounds, we have one major assumption; we are not dealing with a quantum mechanical model. For the rare earth systems we study, we have many J states which we believe may be *approximated* by a classical model. At finite temperature this should be reasonable, although we

are only solving this at zero temperature for the groundstates. If we ignore the quantum mechanics, then we are left with only a few types of interactions. Firstly, we may have any range classical Heisenberg interactions, and so we include some of these. Due to the tiny direct overlap of the f-electrons, the Heisenberg interaction is relatively small, and we already know that there is residual degeneracy if we have only the Heisenberg model on this lattice. We may have magnetic fields and onsite anisotropy. We will neglect magnetic fields for this study, but we include a crystal field interaction which models the oxygen which resides in the center of the tetrahedra. Finally, we are left with the long range dipolar interaction, which is present for every magnetic system, but is normally ignored as it is small. We will justify the use of the classical model more in Chap.8.5. We therefore consider the general model

$$\begin{aligned} H = \; & C \sum_j \left(1 - \left[\hat{\mathbf{z}}_{\alpha(j)}.\hat{\mathbf{S}}_j\right]^2\right) \\ & + \frac{J}{2}\sum_{j\neq j'} \frac{\hat{\mathbf{S}}_j.\hat{\mathbf{S}}_{j'} - 3\left(\hat{\mathbf{R}}_{jj'}.\hat{\mathbf{S}}_j\right)\left(\hat{\mathbf{R}}_{jj'}.\hat{\mathbf{S}}_{j'}\right)}{|\mathbf{R}_{jj'}|^3}\Big|_{\mathbf{R}_{jj'}\equiv\mathbf{R}_j-\mathbf{R}_{j'}} \\ & + \frac{J_1}{2}\sum_{\langle jj'\rangle} \hat{\mathbf{S}}_j.\hat{\mathbf{S}}_{j'} + \frac{J_3}{2}\sum_{\langle jj'\rangle_3} \hat{\mathbf{S}}_j.\hat{\mathbf{S}}_{j'}, \end{aligned} \tag{8.3.2}$$

where the first term is the local crystal-field interaction, defined in terms of $\hat{\mathbf{z}}_{\alpha(j)}$, the natural local crystallographic directions, where $\alpha(j)$ is the sublattice index, as seen in Fig.8.4. The second term is the long-range dipolar interaction between the assumed classical point-spins, $\hat{\mathbf{S}}_j$, on the pyrochlore lattice, denoted by $\mathbf{R}_j$. The third term is the nearest neighbour Heisenberg interaction and the final term is the third neighbour Heisenberg interaction. Before we go through the details of the model, we go through the experimental details of the compounds that we shall study.

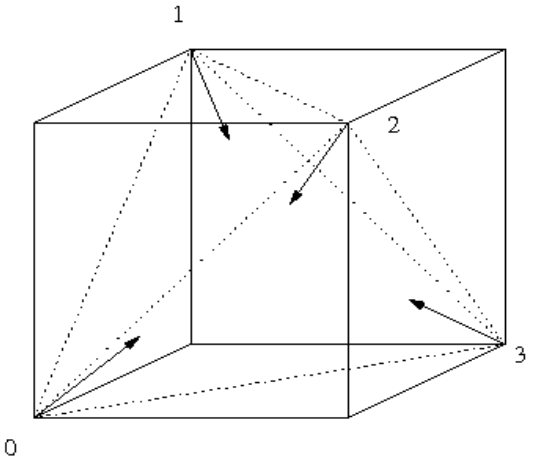

Figure 8.4: The local crystallographic axes for each of the four sublattices, yielding $\hat{\mathbf{z}}_0$, $\hat{\mathbf{z}}_1$, $\hat{\mathbf{z}}_2$ and $\hat{\mathbf{z}}_3$.

8.4 Experimental Details

We will be studying $Ho_2Ti_2O_7$, $Dy_2Ti_2O_7$, $Tb_2Ti_2O_7$, $Tb_2Sn_2O_7$, $Gd_2Ti_2O_7$ and $Gd_2Sn_2O_7$, where the first two compounds are both classed as spin ice compounds; our focus will primarily be on terbium and spin ice. We begin by discussing spin ice, then terbium which is similar, before we close with gadolinium, which motivates our modeling and provides a test of the model that we choose. All the compounds that we discuss are pure pyrochlore compounds, and we neglect any structural distortions as we believe the distortions are very small. The magnetic elements are the rare earths, and are on the right hand side of the series. The atomic physics energy scale dominates, and so we have high J_z and we wish to find the *relative* orientation of these large spins (which we think of as essentially classical).

8.4.1 Spin Ice

Spin ice was first studied as it was thought to provide a mechanism for finding magnetic monopoles [94]. This stems from a separation of energy scales which allows

a temperature regime in which magnetic monopoles may be created. Holmium and dysprosium both have very large crystal field interactions [88], which force the spins to be only parallel or anti-parallel to the local crystallographic axes seen in Fig.8.4. The spins are well modeled by only Ising variables [2], up to very high energy scales where other J_z states become relevant [88]. For holmium we have $J = \frac{15}{2}$ and for dysprosium we have $J = 8$, and both compounds are believed to be very similar. The dipolar interaction forces the so called ice rule or two-in-two-out rule [95], where out of the four spins in any tetrahedron, two point in and two point out, which we shall derive later. We see in Fig.8.5 an example of a two in two out state, which points in

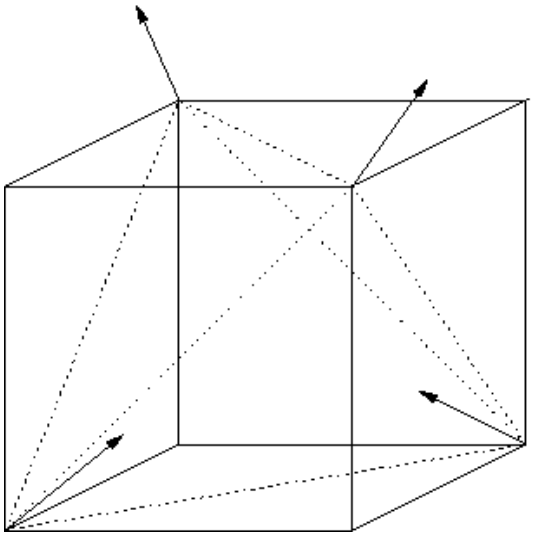

Figure 8.5: An example of a state satisfying the ice rules; two-in-two-out.

the $\hat{\mathbf{z}}$-direction. There are clearly six of these states per tetrahedron satisfying the ice rules, each pointing in either $\pm\hat{\mathbf{x}}$, $\pm\hat{\mathbf{y}}$ or $\pm\hat{\mathbf{z}}$. Experimentally, we see only one broad feature in the specific heat shown in Fig8.6, which is associated with moving from any Ising states to every tetrahedron satisfying the ice rules. This smooth peak is the reason that spin ice has the name, there is residual entropy left over after this peak and we observe no long range order. The monopole idea comes from when we

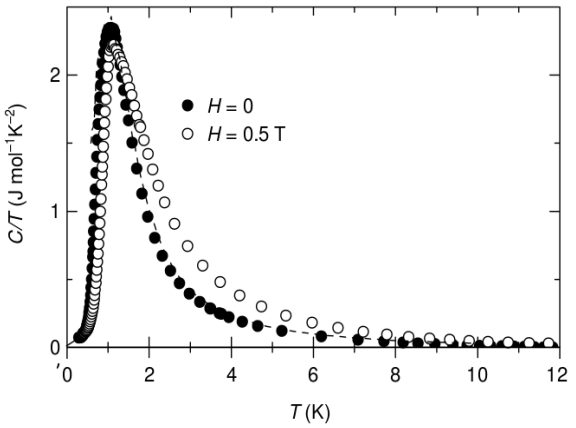

Figure 8.6: Specific heat for $Dy_2Ti_2O_7$ Ramirez et al [2]

have an excitation of the two-in-two-out subspace, which creates one tetrahedron with one-in-three-out, and another with three-in-one-out. These excitations may then separate, and interact like magnetic monopoles. We, however, will be studying the compound for the groundstate properties only, and not discuss the monopole excitations. The Curie-Weiss temperature for spin ice is $\theta_{CW} \approx 0.5K$, indicating

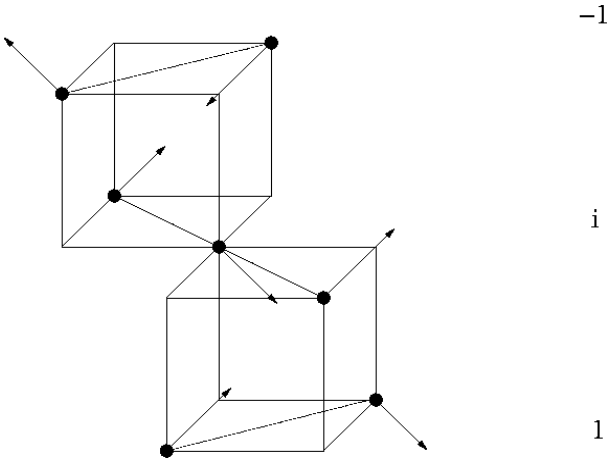

Figure 8.7: The $\mathbf{k} = (001)$ groundstate to spin ice (we refer to this as *the* spin ice state), indicating every other plane being out of phase. Dotted lines indicate the lines of spins that we refer to.

weak ferromagnetic interactions [2]. However, the groundstate to spin ice is believed

to be at $\mathbf{k} = (001)$ which is antiferromagnetic overall, and we now explain. The state at (001) cuts the lattice into planes which are in phase within the plane, but not perpendicular. We pick up a phase factor every time we move in the $\hat{\mathbf{z}}$-direction of $e^{\frac{i\pi}{2}}$ and so every other plane is exactly out of phase, and uncoupled to the nearest neighbour planes. When we put this into the context of Ising spins (pointing in or out of each tetrahedra), we see Fig.8.7 where every other line of spins is antiparallel to the next nearest neighbour in the $\hat{\mathbf{z}}$-direction, and each tetrahedron satisfies the ice rules. Monte Carlo simulations have been used to observe this state [96], and

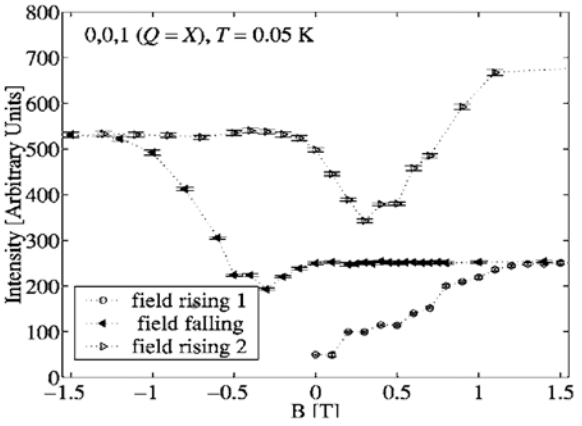

Figure 8.8: The strength of the (001) Bragg peak when applying a magnetic field in the $\pm(1\bar{1}0)$ direction and sweeping it back and forth [3].

locate the phase transition in the specific heat, though the thermalisation process is subtle, and we will discuss this later. However, experimentally the groundstate may be thermalised by the application of a (001) magnetic field [3], as seen in Fig.8.8. In this experiment, a field is applied in the $(1\bar{1}0)$ direction, which couples to half of the lines of spins seen in Fig.8.7, and is perpendicular to the other two. Of the lines that do couple to the field, half of them are parallel and half are anti-parallel in the (001) groundstate. The field therefore destroys the order in these lines as it is swept back and forth. In doing so, it creates spin flip excitations, which are frozen

at this temperature, which move around. If the excitation moves on to the lines perpendicular to the field then they may order the line into the groundstate without being affected by the field. This allows the $\mathbf{k} = (001)$ Bragg peak to grow as the field is swept back and forth.

Recent experiments have observed the upturn in the specific heat at low temperature that is expected [97] by allowing the system time to thermalise. We believe thermalisation to be a key issue in understanding spin ice, and also the terbium compounds which have similar physics.

8.4.2 Terbium Compounds

Terbium has been studied as it has a similar crystal field effect to spin ice, preferring the high J_z states ($J = 6$ for terbium), and therefore might offer some insight into spin ice. However, it turns out that the crystal field levels for terbium are around an order of magnitude smaller [98], and indeed it is more complicated. This will turn out to control the physics, and it will not be particularly spin ice like. This reduction in the crystal field means that the spins are not Ising like, and in fact relax to gain from other interactions and it has picked up the name "soft spin-ice" as a result. We study two compounds; $Tb_2Sn_2O_7$ and $Tb_2Ti_2O_7$ which have $\theta_{CW} \approx -12K$ [99] and $\theta_{CW} \approx -19K$ [100] respectively indicating antiferromagnetic interaction. For the case of the tin compound, the order is not antiferromagnetic, and is in fact a $\mathbf{k} = 0$ ferromagnet, with the spins canted away from the ferromagnetism [99], as depicted in Fig.8.9. The titanium compound however is more controversial. Originally, it was thought to be a spin liquid, dominated by quantum fluctuations [101], which could be ordered under the application of pressure [102]. However, more recent results have observed scattering at $\mathbf{k} = (\frac{1}{2}, \frac{1}{2}, \frac{1}{2})$ [4]. Just like spin ice, we believe

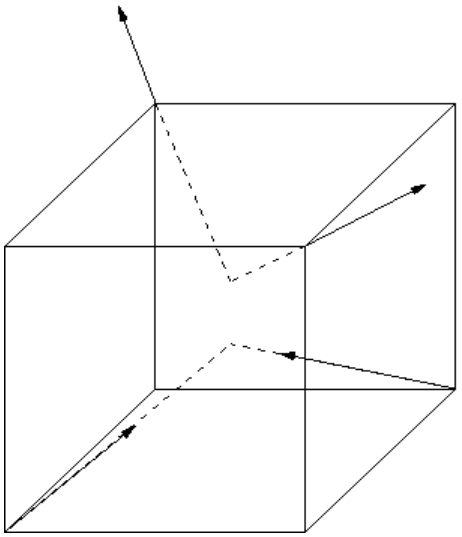

Figure 8.9: Groundstate for $Tb_2Sn_2O_7$ from neutron scattering, with the spins canted $\sim 12^\circ$ away from the ferromagnetic axis. Dotted lines are to show the canting.

thermalisation is key to the lack of order found originally. The state for the titanium compound is significantly more complicated as we require 16 spins to describe the state.

We require 16 spins due to the symmetry of the state. If we consider moving up the $\hat{\mathbf{z}}$-axis, just as we did in spin ice, then we cut the system up into planes. Each plane gains a phase factor $e^{\frac{i\pi}{4}}$. Thus every four planes is anti-phase with the next four and there is no coupling between every *other* plane, for which the phase is $e^{i\frac{\pi}{2}}$. The same is true in $\hat{\mathbf{x}}$ and $\hat{\mathbf{y}}$, and so we have a cube of spins, as depicted in Fig.8.1, containing 16 spins, which we tile in antiphase on a rocksalt superlattice. There are also therefore 16 independent Bragg peaks which describe the state.

We see the state in Fig.8.10 which is predicted from recent neutron scattering [4], though we will attempt to explain the state more clearly when we find the state from the modeling.

The only difference between the compounds is the transition metal substitution,

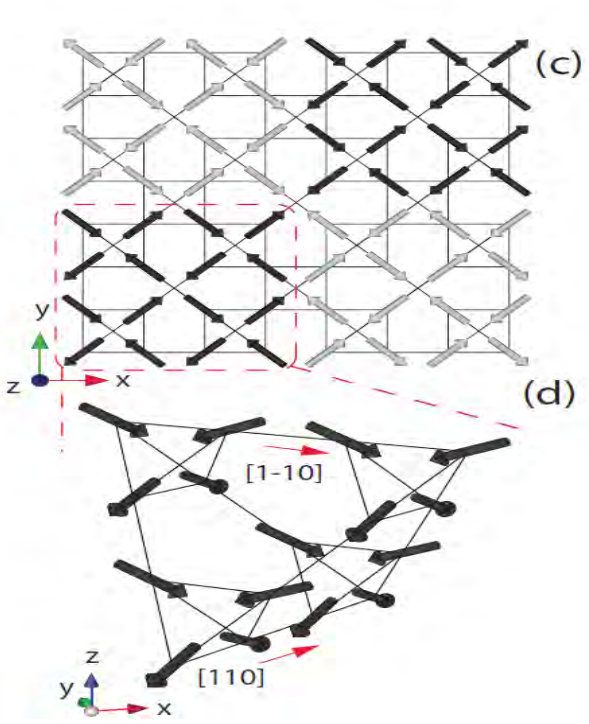

Figure 8.10: Groundstate for $Tb_2Ti_2O_7$ from neutron scattering [4].

which is clearly controlling the physics. We presume that the transition metal modifies the exchange pathway slightly, which increases the strength of a longer range bond. It is slightly easier for an electron to hop over the titanium than the tin, promoting exchange pathways through it. However, there are two natural exchange pathways through the transition metal, one being closer than the other. We show the exchange pathways in Fig8.11, where we see a closer bond J_2 which goes around a corner, and the further bond J_3 which is straight. The corner in J_2 reduces the strength compared to J_3, and so we neglect the second neighbour and only include third neighbour exchange as our longer range interactions.

The tin compound is also believed to be structurally distorted. It is thought that the tetrahedra split into two types, one of which grows slightly, and the other shrinks.

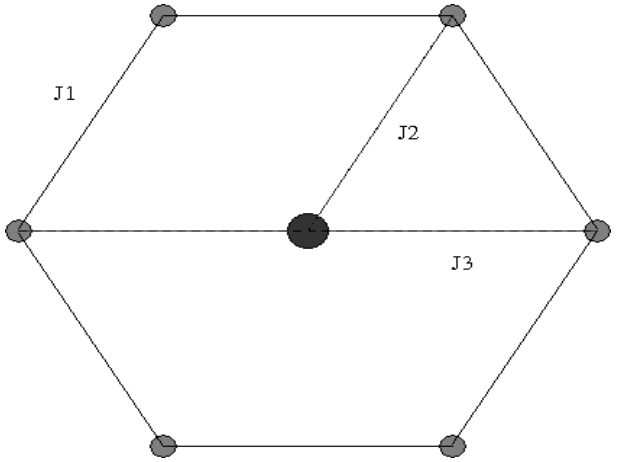

Figure 8.11: Diagram to show the exchange pathways across the transition metal. Both exchange pathways are mediated by the oxygen in the center, but the closer second neighbour bond goes round a corner (dashed line), while the longer third neighbour bond (solid line) is straight. The lighter circles are the rare-earths, and the darker circle is the transition metal.

The excitation spectrum is believed to support this picture [5], where fairly recent accurate inelastic neutron scattering results found two bands shown in Fig.8.12. The higher band, around 25K is thought to be spins waves, while the lower band is thought to be a spin flip, which has different energy due to this lattice distortion. We will interpret things slightly differently, believing that the lower excitation is indeed a spin flip, but we need not use the structural distortion to explain the energy gap. The interest in this experiment is the unusual swapping of energy scales between the crystal field and the spin waves, and this concept will be refined later.

8.4.3 Gadolinium Compounds

We finally discuss the compounds $Gd_2Ti_2O_7$ and $Gd_2Sn_2O_7$, which we include as a reference for our model. This compound has been studied previously extensively in [23], which includes theoretical modeling of the compound. We are using gadolinium as a test for our model, and therefore refer the reader to that thesis, and will

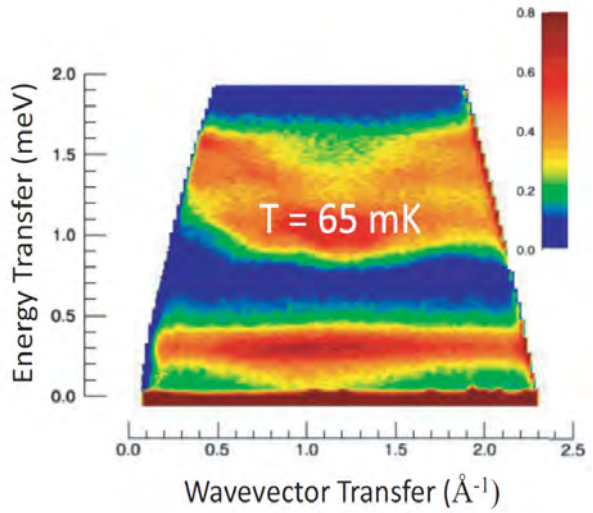

Figure 8.12: Inelastic neutron scattering off $Tb_2Sn_2O_7$ showing the two bands [5].

introduce only the basics of the compound here. Gadolinium is special as it has $\mathbf{J} = \mathbf{S} = \frac{7}{2}$ and $\mathbf{L} = 0$, and so it is isotropic. This means it does not feel any crystal field interaction, and so is interesting for two reasons. The isotropic Heisenberg interaction does not order on the pyrochlore lattice, and so we may investigate the dipolar interaction as well, but also because for our modeling we can always check taking the crystal field term to zero. It is thought to have some anisotropy [103], but we will neglect such anisotropies in the modeling, and consider the gadolinium to be isotropic only.

The Curie-Weiss temperatures for both compounds are anti-ferromagnetic, $\theta_{CW} \sim -9.9K$ for the titanium, and $\theta_{CW} \sim -8.6K$ for the tin [8]. Experimentally, the tin compound is well understood, while the titanium compound is controversial, just like the terbium compounds. $Gd_2Sn_2O_7$ is known to have order at $\mathbf{k} = \mathbf{0}$, and is the anti-ferromagnetic spiral state depicted in Fig.8.13. The large degeneracy of the anti-ferromagnetic Heisenberg interaction on the pyrochlore lattice is lifted with

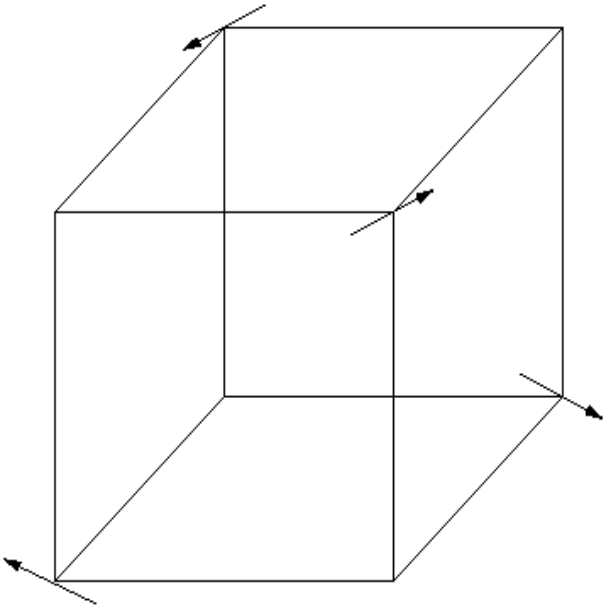

Figure 8.13: Groundstate of $Gd_2Sn_2O_7$ from [6] also known as the Palmer-Chalker state [7].

the dipolar interaction, choosing one unique state (and symmetric copies), as we shall show later. The titanate compound is much more controversial, though it is

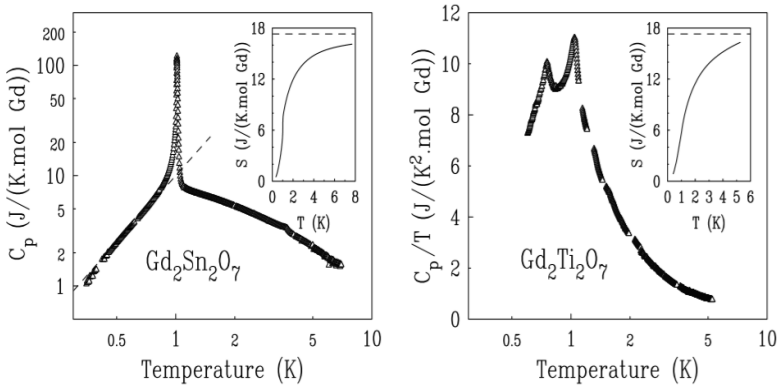

Figure 8.14: Specific heat capacity measurements from $Gd_2Sn_2O_7$ and $Gd_2Ti_2O_7$, showing the two magnetic peaks in the titanium compound from [8].

known to order at $\mathbf{k} = (\frac{1}{2}, \frac{1}{2}, \frac{1}{2})$ [104]. One of the most interesting features is the

specific heat, which indicates two magnetic transitions, seen in Fig.8.14, while the tin compound has one first order transition.

It once again requires 16 spins to describe the state for the titanium compound, and is thought to have 12 ordered spins and 4 spins which fluctuate and have zero length on average. However, this is it odds with the Mössbaur which shows that all sites have a full spin on them. We shall find a different state to this when numerically solving the classical model, where all the spins are fully ordered, but it is within the $\mathbf{k} = (\frac{1}{2}, \frac{1}{2}, \frac{1}{2})$ subspace.

8.4.4 Summary of Experiments

We have introduced the basics of the pyrochlore geometry and the experimental details to the compounds that we shall be studying. We will be studying the family of compounds $R_2M_2O_7$, with R being Ho (Dy), Tb, or Gd, and M being Ti or Sn. The spin ice compounds have interesting ordering properties which we attempt to explain using thermalisation. We will investigate the non-trivial excitations of the effective model, and explain the magnetisation properties. The terbium compound was, until recently, controversial. We will investigate the model with carefully chosen parameters, and find the groundstate for the tin and titanium compounds, which agree with the neutron scattering experiments. We will also explain the excitations of the compound using our model. Finally, we will use gadolinium as a reference for our model, setting the crystal field term to zero. We will find the well known Palmer-Chalker state for the tin compound, and a different $\mathbf{k} = (\frac{1}{2}, \frac{1}{2}, \frac{1}{2})$ state for the titanium compound. However, our focus will be more on spin ice and terbium.

8.5 Modelling

We now turn our attention to the modeling of the set of compounds that we wish to study. As said before, we are studying the model

$$\begin{aligned} H = \; & C \sum_j \left(1 - \left[\hat{\mathbf{z}}_{\alpha(j)}.\hat{\mathbf{S}}_j\right]^2\right) \\ & + \frac{J}{2}\sum_{j\neq j'} \frac{\hat{\mathbf{S}}_j.\hat{\mathbf{S}}_{j'} - 3\left(\hat{\mathbf{R}}_{jj'}.\hat{\mathbf{S}}_j\right)\left(\hat{\mathbf{R}}_{jj'}.\hat{\mathbf{S}}_{j'}\right)}{|\mathbf{R}_{jj'}|^3}\Big|_{\mathbf{R}_{jj'}\equiv\mathbf{R}_j-\mathbf{R}_{j'}} \\ & + \frac{J_1}{2}\sum_{\langle jj'\rangle_1} \hat{\mathbf{S}}_j.\hat{\mathbf{S}}_{j'} + \frac{J_3}{2}\sum_{\langle jj'\rangle_3} \hat{\mathbf{S}}_j.\hat{\mathbf{S}}_{j'} \end{aligned}$$

This is a classical model, with unit length spins which are centered on a given site with no orbital structure. The quantum version of this model has been studied before [5], although only for the spin wave spectrum and not for the possible groundstates. The classical version seems an inappropriate model to study, but we justify it in two ways. Firstly, for gadolinium we expect the model to reasonable due to the relatively small anisotropy. Secondly, the f-electrons are dominated by the atomic physics, and so we are expecting large J states (for which there are many available "directions" for the spin) to dominate. Nonetheless, this is not the true model, but we use it to investigate the classical groundstates.

In §.8.3 we studied the nearest neighbour anti-ferromagnetic Heisenberg on the pyrochlore lattice, and found a large groundstate degeneracy. In order to lift this degeneracy we include more terms, namely a longer range Heisenberg interaction, the dipolar interaction and a crystal field. The crystal field interaction is designed to promote the Ising states observed in spin ice, and does not include the hexagonal ring of oxygens, although this *could* be included.

We have not mentioned the orbital shape of the compounds that we study, apart

from gadolinium. We elect to mention it now as we have a particular form for the crystal field. Terbium has $L = 3$, and has one electron more than the spherically symmetric gadolinium. In free space, Hund's rule dominates and we find that $\mathbf{J} = \mathbf{L} + \mathbf{S}$. The crystal field interaction can then lift the large J^z degeneracy. The pure $L = 3$ state which is very "plate-like" is bad for the local oxygen environment, and so it prefers $J^z = 5$ and $J^z = 4$ states rather than the maximum $J^z = 6$ state. To see what the state may look like we consider

$$J^-|6,6\rangle = J^-|3,3\rangle|3,3\rangle = \frac{1}{\sqrt{2}}|3,2\rangle|3,3\rangle + \frac{1}{\sqrt{2}}|3,3\rangle|3,2\rangle \equiv |6,5\rangle,$$

where

$$\begin{aligned} |J,J^z\rangle &= |L,L^z\rangle|S,S^z\rangle \\ J^-|J,j\rangle &= \sqrt{(J+j)(J-j+1)}|J,j-1\rangle \end{aligned}$$

for any $-J > j \leq J$. The lower total angular momentum state is an equal linear combination of the $L = 3$ and $L = 2$ which reduces the "plate-like" shape of the orbital, allowing it to avoid the hexagonal ring of oxygens around it slightly. In the same way

$$J^-|6,5\rangle = \sqrt{\frac{5}{22}}|3,1\rangle|3,3\rangle + \sqrt{\frac{5}{22}}|3,3\rangle|3,1\rangle + \sqrt{\frac{12}{22}}|3,2\rangle|3,2\rangle \equiv |6,4\rangle,$$

which includes some of the $L = 1$ state as well, again reducing the "plate-like" shape.

Terbium is particularly simple due to the single electron picture, but the other elements have many more electrons. For example the maximum J^z state for holmium

is given by

$$|8,8\rangle = \underbrace{|2,2\rangle}_{S}\underbrace{|3,3\rangle|2,2\rangle|1,1\rangle}_{L},$$

where we have indicated the spin states by S, and the orbital states by L. Here, any reduction in the maximal J^z state will mix in the $L = 0$ orbital, which is pointing directly at the oxygen above, and so we would expect this to be very high energy. For the case of holmium (and dysprosium where the argument is similar) we therefore only expect two states $|J, \pm J\rangle$, but for terbium we expect other states to contribute. Again, we are modeling this classically, and so for holmium we think of the states as being Ising-like, and so the limit $C = \infty$ provides this. For terbium on the other hand, we use a crystal field which promotes the states pointing at the oxygens, but does not demand it. It is now clear that for gadolinium, which has $2J + 1 = 8$ states, the classical model is reasonable, as any linear combination of these 8 states is allowed, and so the large spin can point anywhere. A third

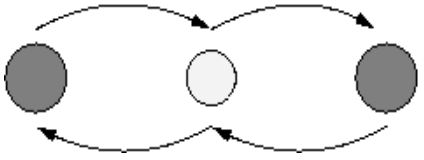

Figure 8.15: Diagram of the first neighbour exchange pathway. The larger circles are the rare earth sites, and the smaller circle is the oxygen.

neighbour Heisenberg interaction is also included, which we have discussed before as going across the hexagon. However, one can be more concrete by considering the exchange pathways, comparing J_1, J_2 and J_3 and indicating how the tin affects the pathway. We have drawn the pathways in Fig.8.11. Note that on each line drawn in Fig.8.11, there is also an oxygen. Thus for the first neighbour exchange, we require

a fourth order perturbation, drawn in Fig.8.15, and given by

$$J_1 \sim \frac{t^4}{U^2 V},$$

where t is the hopping integral from the Hubbard model, U is the penalty for occupying the oxygen site, and V is the penalty for occupying the rare earth. Next we

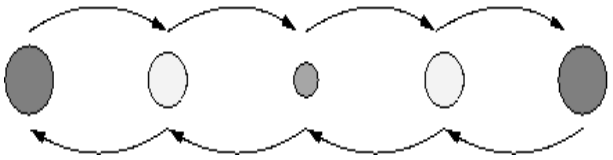

Figure 8.16: Diagram of the second and third neighbour exchange pathway. The larger circles are the rare earth sites, the smallest circle is the transition metal, and the smaller circles are the oxygens.

consider the third neighbour exchange, which is depicted in Fig.8.16, and requires ten hops. It is given by

$$J_3 \sim \frac{t^{10}}{U^2 V^4 \Delta^2} = \frac{J_1^2 t^2 U^2}{V^2 \Delta^2},$$

where Δ is the penalty for occupying the transition metal site. For the second neighbour interaction, we reduce this interaction by the overlap between the oxygen orbital and the transition metal orbital, which are at 60° to one another, giving $J_2 = \alpha^2 J_3$, where $\alpha < 1$. There is also another contribution to the second neighbour interaction, hopping across another rare earth, but once again it scales with α^2, and it contains $\frac{1}{V^6}$, which is much smaller than the transition metal penalty. We therefore ignore the second neighbour interaction, only using the third neighbour in our modeling. The contribution Δ controls how strong the third neighbour exchange is, and for titanium it turns out that Δ is smaller and it is cheaper to hop across.

Finally, we have the dipolar interaction, which is very hard to tackle. We devote §.9.3 and §.9.4 to dealing with this long range interaction, which forms a central

part of the study. For the compounds we wish to study, we may use the Curie Weiss temperatures to tell us the relative strength of the interactions. We may also use crystal field experiments to tell us the approximate energy scale of the crystal field interaction, though the interpretation of this is only approximate. This is an important issue of inelastic neutron scattering, but will be discussed more when we come to the excitations from terbium stannate.

Compound	C (K)	J_1(K)	J_D(K)	J_3(K)
$Gd_2Ti_2O_7$	0	5	~ 1	0.2
$Gd_2Sn_2O_7$	0	5	~ 1	0
$Tb_2Ti_2O_7$	30	~ 7	~ 1	0.2
$Tb_2Sn_2O_7$	30	~ 7	~ 1	0
$Dy_2Ti_2O_7$	> 500	4	~ 1	–
$Ho_2Ti_2O_7$	~ 600	1.5	~ 1	–

Table 8.1: Approximate interaction strengths for the various compounds from [90, 105–107]

We will work at zero temperature, solving the (C, J_1) phase diagram for $J_3 = 0$ and $J_3 = 0.1$, constituting tin and titanium respectively. The line $(0, J_1)$ will represent gadolinium, while the large crystal field limit will represent spin ice. Before we find the phase diagram however, we have to "solve" the dipolar interaction. There is no easy way to generate the interaction strengths as the interaction is infinite range, and so in principle we would have to sum over infinitely many spins. We therefore spend some time determining how to solve this problem, generating the interactions that we desire.

8.6 Summary

We have discussed the pyrochlore lattice and the inherent geometric frustration, and the experiments related to the compounds we want to study. We have also

introduced the model that we wish to study, which although classical, we hope captures the basic physics of the various compounds. We have also attempted to justify our use of a classical model for these systems, which for some will work very well and others only partially. Finally, we have Table.8.5 which indicates the approximate relative sizes of the interactions that feed into our model, and will allow us to place the compounds on the phase diagram that we find. Before we move on to the phase diagram itself however, we will generate the new technique we use to control the dipolar interaction.

Chapter 9

THE DIPOLAR INTERACTION

9.1 Chapter Summary

We introduce a new technique for calculating the dipolar interaction. We first discuss the physical issues with the dipolar interaction, and then offer the standard way of calculating the dipolar interaction, the Ewald technique which we may use as a comparison for the new technique. For the Ewald technique, we start by calculating the Madelung sum for NaCl, as the dipolar interaction is very related to the Coulomb interaction. We start with a simple way of using Ewald, before moving on to a new implementation of the technique. This has been used before for calculating the dipolar interaction for the pyrochlore lattice in [80, 108]. It is the same basic idea as is used elsewhere (error functions), but offers slightly more control and speed. We then provide the new real space technique, which allows us to calculate the dipolar interaction in real space rather than reciprocal space. Most importantly, it separates the short and long range parts of the dipolar interaction, allowing us to rigorously solve the local part, and leave the long range shape dependent issue separate. We work in the spherical crystal approximation for the long range part, which we summarise in Sec.9.4.1, where the shape dependence is simple (a constant

independent of position and orientation within the sphere). We generate two real space techniques, which are very similar; the cubic and anisotropic methods. The cubic method is easier to calculate, but slightly slower. For non-cubic lattices the anisotropic method is significantly faster.

9.2 Introduction

We wish to study the model given by Eq.8.3.2, which involves the long range dipole interaction. We therefore have to calculate the interaction strength of this model, which is a non-trivial task, and so we develop a new technique. We introduce Ewald first, as a technique we use to compare to, but we only use the real space technique for the later calculations as it is more direct.

The difficulties with the dipolar interaction stem from physical pathologies of the Hamiltonian [109], and we generate the physical ideas now before we discuss the details of the techniques. We will also discuss the Coulomb interaction, which seems unrelated, but in fact has all of the same issues (and mathematically turns out to be roughly equivalent) as it is long range. For the case of the Coulomb interaction, one calculates the charge sum for a crystal called a Madelung sum [110]. For a charge neutral system (of a given shape), this sum is well defined, but in general it depends *strongly* on the way in which the sum is performed and terminated [111]. For an infinite, charge neutral, lattice there are infinitely many positive and negative sites. The sum is therefore $C_- + C_+$ where $C_\pm \to \pm\infty$, which is not necessarily well specified. This is known as conditional convergence. We will use the Coulomb interaction as the first example of using the Ewald summation technique to indicate the difficulties encountered. The dipolar interaction is long range and also exhibits conditional convergence, however the consequences are a real effect and care must be

taken to deal with them. To indicate the physical issues we see that the summation depends strongly on the boundary of the sample, seen naïvely with

$$\int_{\mathcal{R}} d^3r V_d(\mathbf{r}) \sim \int_{\mathcal{R}} \Omega(\theta,\phi)\frac{d^3r}{r^3} = \Omega_d \int_{\epsilon}^{\lambda} \frac{dr}{r} \sim \log\left(\frac{\lambda}{\epsilon}\right), \tag{9.2.1}$$

where $V_d(\mathbf{r})$ is the dipolar interaction, Ω_d is the angular part of the integral, and stems from the fact that the dipole interaction scales as $\sim \frac{1}{r^3}$. Normally the angular dependence of the state means that this is not an issue, and the long range term is averaged to zero. However, for non zero values of Ω_d there is an issue. This strong dependence on the boundary of the integral is called shape anisotropy, and means that the shape of the crystal has physical consequences for the interaction. The only times when $\Omega_d \neq 0$ is for ferromagnetic $\mathbf{k} = \mathbf{0}$ states, where the spins line up and the magnetic field has to go outside the crystal which causes an energetic penalty. In this situation we must also include the shape of the crystal in the modeling. We will therefore use a *reference* for this, called the spherical crystal approximation for which the value of this penalty is a constant, independent of position and orientation within the sample (see §.9.4.1). Though Eq.9.2.1 seems to provide a divergent contribution, in fact we do not observe this for the case of the spherical crystal approximation.

We will use two techniques to calculate the dipolar interaction; Ewald and a real space summation. Ewald calculates the dipolar interaction in reciprocal space and gives us access to everywhere apart from $\mathbf{k} = \mathbf{0}$, at which point the technique fails as we have not explicitly included the crystal shape. The real space technique separates out the long range shape dependent part from the short range part, allowing us to calculate the energy of states, even at $\mathbf{k} = \mathbf{0}$. Pure ferromagnetic states at $\mathbf{k} = \mathbf{0}$ pay the long range penalty, but they may "recover" this energy by reconstructing into a $\mathbf{k} \to \mathbf{0}$ state, and become relevant. For example, a ferromagnet can have

no long range component if it has a domain wall separating two regions of opposite orientations of ferromagnetism. The energy penalty for the domain wall scales as $\sim L^2$, while the dipolar energy for the full ferromagnet scales as $\sim L^3$. Even if the coefficient of the L^3 term is small (though $\gtrsim \frac{1}{L}$), it is worth making a $\mathbf{k} \to \mathbf{0}$ state which is locally ferromagnetic, but globally an antiferromagnet.

Domain walls are created to recover the long range component of the dipolar interaction, as has been understood for a long time [112–115]. For a long thin sample, the domain walls lie across the width to minimise the area. If we apply a magnetic field, the population of the domain walls changes to magnetise the sample, (as the field is macroscopic), and so the magnetisation is proportional to the field. Once the field has created a mono-domain ferromagnet, the rate of magnetisation changes as the field must over turn the spin-spin interactions or crystal fields (which are typically larger). Moreover, if there is disorder in the sample, the (dipole necessitated) domains are pinned, and require a finite field to begin repopulating, which is known as hysteresis. More work on dipole driven domains appears in [116].

9.3 Ewald Summation

9.3.1 Introduction

Long range interactions are in general very hard to calculate [117–120]. They are either very slow to compute [121], involving summing over long range, or for special cases or dimensions, are conditionally convergent [122]. We will be interested in calculating two long range sums; Coulomb sums and dipolar sums. We will use the Coulomb sum initially for our examples, and then move on to the (related) dipolar interaction. Calculating Coulomb sums (called Madelung energies [110]) has been a

long standing problem, where the interaction comes in the form

$$I = \sum_{i \neq j} \frac{q_i q_j}{|\mathbf{r}_{ij}|},$$

where $\mathbf{r}_{ij}$ is the separation vector between the charges q_i (q_j) at the site i (j). In three dimensions, this sum is ill specified and exhibits conditional convergence. Physically, for the case of the Coulomb interaction, it means that charges at very long range still matter for charge neutrality [123], and so great care must be taken when controlling this sum.

The standard method is Madelung or Ewald [124, 125], where the summation is split into two parts; a short range part and a long range part. This splitting is a cunning way of ensuring charge neutrality. The long range part may then be Fourier transformed into a short range part in *reciprocal* space, such that it can be calculated easily. We begin with the basic mathematical idea before applying it to the specific case of the Coulomb interaction.

The Ewald technique has several stages, and so we summarise them here. We first split the sum up into two parts, a short range and a long range part. This part is the regularisation, and we must carefully choose this. The second part is the Fourier transform, which turns the long range real space part back into a short range reciprocal space part. Again, we must choose a splitting of the function such that the Fourier transform is do able, and that it decays quickly in reciprocal space. However, the greatest care must be taken with the term at $\mathbf{k} = \mathbf{0}$, which represents the long range part of the sum in real space. The sum that we start with is conditionally convergent, and depends on the boundary conditions. We therefore work within the *spherical crystal approximation* (which we calculate later) which gives us an absolutely convergent sum and a unique reference. For the case of the

Coulomb interaction, this is charge neutrality, and for the dipolar interaction it is shape dependence of the sample. These effects may be included later as extra details, but here we only work within this approximation. The term at $\mathbf{k} \to \mathbf{0}$ we will call the long range correction, and when appropriate we will extract it out.

We seek to calculate the following quantity

$$I = \sum_{\mathbf{R}} f(\mathbf{R}),$$

we may perform the summation in two ways, in real space or reciprocal space. Note here that we have an unrestricted sum, including $\mathbf{R} = \mathbf{0}$, which is not the case for the Coulomb and dipole interactions, and we take care to deal with this. We begin by re-writing our summation in two parts, such that

$$I = \sum_{\mathbf{R}} f_1(\mathbf{R}) + \sum_{\mathbf{R}} f_2(\mathbf{R})$$

We choose f_1 to be the short range part, and f_2 to be the long range part. It is also crucial that the sum over f_2 is unrestricted and includes the origin. We then Fourier transform the long range part, turning it into a short range sum in reciprocal space, giving us

$$I = \sum_{\mathbf{R}} f_1(\mathbf{R}) + \frac{1}{\Omega} \sum_{\mathbf{G}} \tilde{f}_2(\mathbf{G}),$$

where Ω is the associated reciprocal space volume, and we used the Poisson summation identity

$$\sum_{\mathbf{R}} F(\mathbf{R}) = \frac{1}{\Omega} \sum_{\mathbf{G}} \tilde{F}(\mathbf{G}),$$

where $\mathbf{G}$ is the reciprocal lattice.

9.3.2 Madelung Sum

We begin with the Coulomb interaction, calculating the Madelung sum for a given lattice. We therefore calculate

$$I = \sum_{i \neq j} \frac{q_i q_j}{|\mathbf{r}_{ij}|}$$

There are clearly many ways of splitting the sum up, and we elect to run through several schemes before generating the relevent scheme to calculate the dipolar interaction effectively. For simplicity, we elect to calculate the Madelung sum for NaCl; rock salt. This is clearly charge neutral, and the crystal structure is two interleaved FCC lattices. We first calculate the Madelung sum using a brute force approach, writing the sum as

$$I = \sum_{j \neq 0} \frac{\cos(2\pi(|r_x| + |r_y| + |r_z|))}{|\mathbf{r_j}|} \approx 1.7475645946\ldots,$$

where the sum runs over a simple cubic lattice everywhere except the origin. This brute force approach is appropriate only for a very first pass, and we must include at order 10^n sites for n decimal places of accuracy. Note that we must be very careful with the boundary of the summation. Here we choose a sphere, with equal positive and negative charges. We included the answer to 10 decimal places here, as we will compare the techniques to this answer throughout. We now run through the first example of using Ewald. We will go through the technique for a single lattice of positive charges, and then add the second negative one in at the end, as the calculation is essentially the same. The first splitting we elect to use is

$$\sum_{\mathbf{r} \neq \mathbf{0}} \frac{1}{|\mathbf{r}|} \equiv \sum_{\mathbf{r} \neq \mathbf{0}} \frac{e^{-\lambda |\mathbf{r}|}}{|\mathbf{r}|} + \sum_{\mathbf{r}} \frac{1 - e^{-\lambda |\mathbf{r}|}}{|\mathbf{r}|} - \lambda, \tag{9.3.1}$$

we recognise that the first term exponentially decays at large $\mathbf{r}$, while the second term does not. We have therefore *regularised* the real space sum. However, the second term is smooth for small $\mathbf{r}$ (where the regular interaction is not), and so we can Fourier transform it. We find

$$I = \sum_{\mathbf{r}\neq\mathbf{0}} \frac{e^{-\lambda|\mathbf{r}|}}{|\mathbf{r}|} - \lambda + \frac{4\pi}{\Omega}\sum_{\mathbf{k}} \frac{\lambda^2}{k^2(k^2+\lambda^2)}$$

We now find that this is ill defined at $\mathbf{k} = 0$, and so we include the second lattice of opposite charge in order to have charge neutrality. We include the second lattice as a copy of the first, displaced by δ, however, we must include the *average* of the second lattice which preserves the original symmetry of the lattice, and keeps the limit $\mathbf{k} \to \mathbf{0}$ analytic. We define the potential on a given site

$$V(\mathbf{r}) \equiv \sum_{\mathbf{r}'\neq\mathbf{r}} \frac{1}{|\mathbf{r}-\mathbf{r}'|} - \frac{1}{6}\sum_{\delta}\sum_{\mathbf{r}'} \frac{1}{|\mathbf{r}-\mathbf{r}'+\delta|},$$

where δ is the vector to the six nearest neighbours on the other lattice. We split this other lattice up in exactly the same way as before Eq.9.3.1, and use that

$$\int_{\mathcal{R}} d^3\mathbf{r} e^{i\mathbf{k}.\mathbf{r}} f(|\mathbf{r}+\delta|) = 4\pi e^{-ik\delta}\int_0^\infty ds e^{ik.s} f(s)$$

for spherically symmetric functions. We find that

$$I = \sum_{\mathbf{r}\neq\mathbf{0}} \frac{e^{-\lambda|\mathbf{r}|}}{|\mathbf{r}|} - \lambda + \frac{4\pi}{\Omega}\sum_{\mathbf{k}} \frac{\lambda^2}{k^2(k^2+\lambda^2)}\left[1-\gamma_k\right]$$

where

$$\gamma_k \equiv \frac{1}{6}\sum_{\delta} e^{-ik\delta}$$

For inversion symmetric systems, such as NaCl, the structure factor is real, and thus $1-\gamma_k \sim k^2$. We now find that the long range correction is well defined at $k=0$ and so *in principal* we have a reciprocal space sum which converges as k^{-2}. We extract out the term at $k=0$ as $k \to 0$, finding a constant contribution of

$$\lim_{\mathbf{k}\to 0} \frac{4\pi}{\Omega} \frac{\lambda^2}{k^2(k^2+\lambda^2)} \left[1-\gamma_k\right] \to \frac{4\pi}{\Omega}$$

If we add this correction on to the real and reciprocal space sums, then we get numerical agreement between this method and the literature answer. However, we may make the term at $k=0$ zero, and increase the rate of convergence in reciprocal space by changing the regularisation that we use and include a second exponential

$$\sum_{\mathbf{r}\neq\mathbf{0}} \frac{1}{|\mathbf{r}|} \equiv \lim_{\mu\to 0} \sum_{\mathbf{r}\neq\mathbf{0}} \frac{e^{-(\lambda+\mu)|\mathbf{r}|}}{|\mathbf{r}|} + \sum_{\mathbf{r}} e^{-\mu|r|} \frac{1-e^{-\lambda|\mathbf{r}|}}{|\mathbf{r}|} - \lambda \tag{9.3.2}$$

We now find that the $k=0$ term is 0 in this limit, and so we have correctly extracted out the long range correction, however we still only have a slow power law convergence. We see in Fig.9.1 the calculation of the Madelung constant using the first splitting in Eq.9.3.1. We see relatively good convergence compared to using 10^n spaces. Note that L is the linear size of the cube that we calculate on in real and reciprocal space, and provided we go far enough we get the correct answer independent of λ.

We now introduce the splitting that we shall use for the dipolar sums, and the most effective splitting. This is a new way of calculating using Ewald, although it is equivalent to the usual method using error functions [126–128]. We use this method as it gives us more control over the accuracy of the summation, and is much faster for doing lattice sums. We wish to have strong convergence in reciprocal space, and

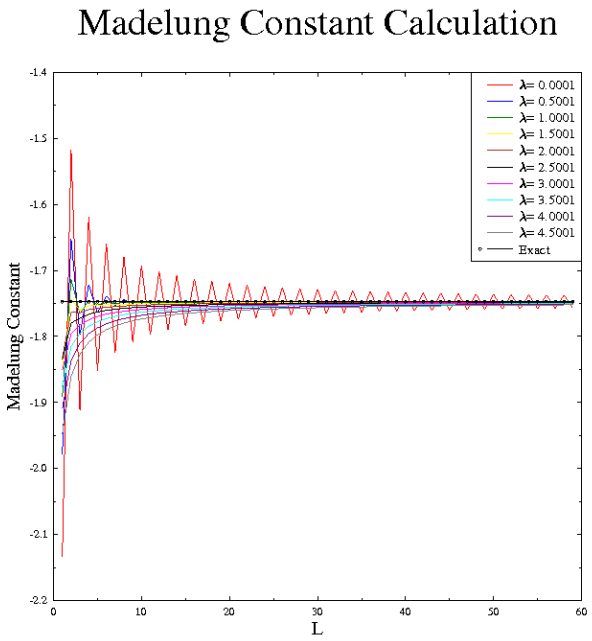

Figure 9.1: Calculation of the Madelung constant for NaCl using the splitting given in Eq.9.3.1.

so we set up the following general split

$$\frac{1}{r} = \frac{1-\theta(a-r)C(r)}{r} \equiv V(r), \tag{9.3.3}$$

where $C(0) = 1$ and $C(a) = 0$. We are making use of the fact that we are calculating a *lattice* sum, and so as long as the function matches the Coulomb interaction at lattice sites, we may choose any function between. We are also not evaluating this sum at the origin in the original sum, so if we simply make the function zero at the origin, then we may include the origin. The sum we therefore use is given by

$$\sum_{\mathbf{R}\neq 0} V(\mathbf{R}) = \sum_{\mathbf{R}} U(\mathbf{R})$$

where $U(\mathbf{0}) = 0$ which allows us to have an unrestricted sum. We now have to pick the splitting, and we want to pick a function which has strong convergence when we Fourier transform it. If we choose a smooth function $C(r)$ which is zero at the origin, and, has n zero derivatives at the origin, then it is clear that when we Fourier transform we have strong power law decay. This is seen in

$$\tilde{C}(k) = \int dx e^{ikx} C(x) = \int dx e^{ikx} \left[\frac{i}{k}\right]^n \frac{d^n C}{dx^n}(x) \tag{9.3.4}$$

and therefore, for large k, $C(k) \sim \frac{1}{k^n}$, and we have power law convergence. We therefore want a function $C(x)$ that has n derivatives at the origin and satisfies the boundary conditions, and so we elect to use the function

$$C_n(x) \equiv 1 - \frac{\int_0^x (y(a-y))^n dy}{\int_0^a (y(a-y))^n dy} \tag{9.3.5}$$

which has n zero derivatives at the origin and the point a. a is a parameter which controls how much of the sum we do in real and reciprocal space, and we choose to be the first lattice spacing here so that *none* of the sum is done in real space. Our splitting is such that the real space sum has converged *before* the first lattice spacing, and so we calculate the entire sum in reciprocal space. The parameter n should also be optimised as it controls stability and speed. Note also that we will calculate the sum fully in reciprocal space. As seen in Fig.9.2, we see that we have a function which goes to zero at the origin, with n derivatives, and matches up to the Coulomb interaction at the first lattice site smoothly.

We extract out the parameter a from the bottom integral in Eq.9.3.5, and calculate the integral

$$A_n \equiv \int_0^1 [y(1-y)]^n dy = \frac{n!n!}{(2n+1)!},$$

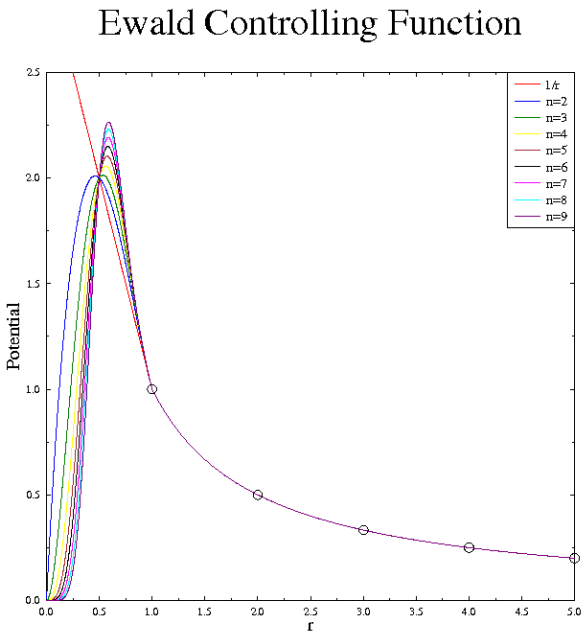

Figure 9.2: Plot of the function we use to modify the Coulomb interaction, indicating how it goes to zero at the origin for the case $a = 1$.

which will normalise our function. We use that

$$\tilde{V}(k) = 4\pi \int_0^\infty x \frac{\sin(kx)}{k} V(x) \ \ dx$$

for spherically symmetric functions. Upon substituting $V(x)$ from Eq.9.3.3, we integrate by parts in order to convert the double integral in $C(x)$ to a single one, finding

$$\tilde{V}_n(k) = \frac{4\pi}{A_n} \int_0^1 \frac{\cos kxa}{k^2} [x(1-x)]^n dx$$

From this we can calculate the Madelung sum for NaCl very quickly, using a large value of n, and setting $a = a_l$, the lattice spacing. We must also choose how far out in reciprocal space we calculate, which gives us three parameters that we

can use to optimise the summation. We see in Table.9.3.2 the calculation of the Madelung constant using the splitting given in Eq.9.3.3. We once again see very good convergence, with the particular choice $n = 20$, where L is the size of the sphere we sum upto in reciprocal space. For $L \sim 20$ we find 8 decimal places of agreement for most values of a, indicating the rate of convergence. Note that not only have we got convergence to the Madelung constant, but that for various values of the parameter a the sum is still converging. This freedom of the choice of the value a (and n) indicates that the summation is working correctly.

L	$a = 0.8$	$a = 0.85$	$a = 0.9$	$a = 0.95$	$a = 1.0$	$a = 1.05$	Exact
2	-1.829485	-2.155424	-2.436020	-2.666440	-2.842928	-2.96288	-1.747564
3	-3.004405	-2.774606	-2.486757	-2.177036	-1.878438	-1.618249	-1.747564
4	-2.220656	-1.807637	-1.464663	-1.222990	-1.095639	-1.078859	-1.747564
5	-0.9637311	-1.166118	-1.448138	-1.721505	-1.922861	-2.023281	-1.747564
6	-1.497809	-1.793449	-1.978018	-2.035497	-1.992651	-1.896521	-1.747564
7	-2.105578	-1.996440	-1.833666	-1.70586	-1.650763	-1.659465	-1.747564
8	-1.76920	-1.655090	-1.645021	-1.691355	-1.740273	-1.764966	-1.747564
9	-1.647916	-1.714469	-1.760561	-1.769760	-1.759643	-1.749190	-1.747564
10	-1.735797	-1.774402	-1.768658	-1.752280	-1.744561	-1.744842	-1.747564
11	-1.772918	-1.754260	-1.744692	-1.744985	-1.747010	-1.747679	-1.747564
12	-1.750331	-1.743708	-1.745848	-1.747549	-1.747690	-1.747584	-1.747564
13	-1.743636	-1.746583	-1.747711	-1.747629	-1.747577	-1.747577	-1.747564
14	-1.747294	-1.747705	-1.747586	-1.747578	-1.747570	-1.747565	-1.747564
15	-1.747705	-1.747582	-1.747579	-1.747568	-1.747565	-1.747564	-1.747564
16	-1.747564	-1.747579	-1.747566	-1.747565	-1.747564	-1.747564	-1.747564
17	-1.747566	-1.747566	-1.747565	-1.747564	-1.747564	-1.747564	-1.747564
18	-1.747556	-1.747565	-1.747564	-1.747564	-1.747564	-1.747564	-1.747564
19	-1.747544	-1.747564	-1.747564	-1.747564	-1.747564	-1.747564	-1.747564
20	-1.747556	-1.747564	-1.747564	-1.747564	-1.747564	-1.747564	-1.747564
21	-1.747544	-1.747564	-1.747564	-1.747564	-1.747564	-1.747564	-1.747564

9.3.3 Ewald Summation for the Dipolar Interaction

We can now use these ideas to calculate the dipolar interaction using the Ewald technique. For the Coulomb sum, we had to worry about charge neutrality, for the dipolar interaction we worry about the penalty for the ferromagnetic solution at $\mathbf{k} = 0$. This is a real penalty, and thus we can calculate safely everywhere except at the origin.

We first calculate the general form of the dipolar interaction in reciprocal space, before we show how we apply Ewald summation to help us. We write the dipolar interaction as

$$\mathcal{H} = \sum_{jj'} \mathbf{S}_j J_{jj'} \mathbf{S}_{j'}$$

We have included the origin in the summation (which would be divergent for the original dipolar interaction), and so this $J_{jj'}$ is not the same interaction, but it matches up at every non zero point. This allows us to carry the Hamiltonian into reciprocal space, which necessitates including the term at the origin. We first Bloch transform the spins in order to carry this interaction into reciprocal space

$$\mathbf{S}_j = \frac{1}{\sqrt{N}} \sum_{\mathbf{k}} e^{i\mathbf{k}.\mathbf{R_j}} \mathbf{S}_{\mathbf{k}},$$

which gives

$$\mathcal{H} = \frac{J}{N} \sum_{jj'} \sum_{\alpha\beta} \sum_{\mathbf{k}\mathbf{k}'} S^{\alpha}_{\mathbf{k}} S^{\beta}_{\mathbf{k}'} e^{i\mathbf{k}.\mathbf{R}_j} e^{i\mathbf{k}'.\mathbf{R}_{j'}} J^{\alpha\beta}_{jj'},$$

where the indices α, β represent the Cartesian directions, and we are explicitly writing the matrix structure of the dipolar interaction. For the case of the dipole interaction, the function $J_{jj'}$ is the double derivative of a function which only depends on

the separation of the spins (the Coulomb interaction). The differentials complicate matters, but are not important for now, allowing us to write

$$J_{jj'} = J(|\mathbf{R}_j - \mathbf{R}_{j'}|)$$

We rewrite the vector $\mathbf{R}_{j'}$ as $\mathbf{R}_{j'} \equiv \mathbf{R}_j + \mathbf{x}$, which gives us

$$\mathcal{H} = J \sum_{\alpha\beta} \sum_{\mathbf{k}} S^{\alpha}_{\mathbf{k}} S^{\beta}_{-\mathbf{k}} \sum_{\mathbf{x}} e^{-i\mathbf{k}.\mathbf{x}} J^{\alpha\beta}(|\mathbf{x}|)$$

We Fourier transform the potential

$$J(|\mathbf{x}|) = \int \frac{d^3\mathbf{q}}{(2\pi)^3} e^{i\mathbf{q}.\mathbf{x}} \tilde{J}(\mathbf{q})$$

which gives us

$$\mathcal{H} = \sum_{\alpha\beta} \sum_{\mathbf{k}} S^{\alpha}_{\mathbf{k}} S^{\beta}_{-\mathbf{k}} \int \sum_{\mathbf{x}} e^{i\mathbf{x}.(\mathbf{q}-\mathbf{k})} \frac{d^3\mathbf{q}}{(2\pi)^3} \tilde{J}^{\alpha\beta}(\mathbf{q})$$

We then use the Poisson identity

$$\sum_{\mathbf{r}} e^{i\mathbf{t}.\mathbf{r}} = \frac{(2\pi)^3}{\Omega} \sum_{m} \delta(\mathbf{t} - \mathbf{G}_m),$$

where $\mathbf{G}_m$ is the reciprocal lattice. This gives us

$$\mathcal{H} = \frac{J}{\Omega} \sum_{\alpha\beta} \sum_{\mathbf{k}} S^{\alpha}_{\mathbf{k}} S^{\beta}_{-\mathbf{k}} \sum_{m} \tilde{J}^{\alpha\beta}(\mathbf{k} + \mathbf{G}_m)$$

We seek to minimise this as a function of $\mathbf{k}$, and use that the minimum (eigen)value yields the groundstate. Note that this may not be consistent with the spin constraint,

and so once the eigenvector is found, it is back transformed to check. For the case of the dipolar interaction, there are two important features. The interaction term has matrix structure, and that it can be related back to the Coulomb interaction allowing us to use the previous ideas. We first note that the dipolar interaction is also given by

$$\mathcal{H} = J \sum_{i \neq j} \mathbf{S_i} . \frac{\partial}{\partial \mathbf{r}_\alpha} \mathbf{S_j} . \frac{\partial}{\partial \mathbf{r}_\beta} \mathbf{V}(|\mathbf{r_{ij}}|)$$

where α, β label the Cartesian components (as the spins are three dimensional), and

$$V(x) = \frac{1}{x} \tag{9.3.6}$$

everywhere except $x = 0$ where $V(0) = 0$. This is just the Coulomb interaction, double differentiated, and so we may make use of the Ewald technique. It is easy to see that differentiating in the Fourier transform simply yields $\mathbf{k}_\alpha$ for each, and therefore the result is modified to

$$\mathcal{H} = \frac{J}{\Omega} \sum_{\alpha\beta} \sum_{\mathbf{k}} S_k^\alpha S_{-k}^\beta \sum_m (\mathbf{k} + \mathbf{G_m})_\alpha (\mathbf{k} + \mathbf{G_m})_\beta \tilde{V}(\mathbf{k} + \mathbf{G_m}),$$

and so we define the dipolar matrix as

$$D_{\alpha\beta}(\mathbf{k}) = \sum_m (\mathbf{k} + \mathbf{G_m})_\alpha (\mathbf{k} + \mathbf{G_m})_\beta \tilde{V}(\mathbf{k} + \mathbf{G_m})$$

Once again, we must have a modified interaction such that we may include the origin, but it is clear that we may use the previous functions from the Coulomb interaction to satisfy this condition and so we use the splitting given in Eq.9.3.3. We seek to minimise the dipolar matrix as a function of $\mathbf{k}$, and find the minimum eigenvalue and eigenvector. If the eigenvector is consistent with the spin constraint,

then we have minimised the dipolar interaction.

The problem has been reduced from the full $3N \times 3N$ (for the whole N particle system) matrix to a $3p \times 3p$ matrix (for p atoms per unit cell of the underlying lattice). We have to diagonalise the matrix at every $\mathbf{k}$, though continuity means we can work on a grid in reciprocal space. We now go through the details of using this technique for the dipolar interaction.

As noted before, we may use the same function as we found the Coulomb sums, and therefore we use

$$\tilde{V}_n(k) = \frac{4\pi}{A_n} \int_0^1 \frac{\cos kxa}{k^2} [x(1-x)]^n dx,$$

which we substitute into the dipolar matrix to find explicitly

$$D_{\alpha\beta}(\mathbf{k}) = \frac{4\pi}{\Omega A_n} \sum_m (\mathbf{k} + \mathbf{G_m})_\alpha (\mathbf{k} + \mathbf{G_m})_\beta \int_0^1 \cos\left(|(\mathbf{k} + \mathbf{G_m})| xa\right) [x(1-x)]^n dx$$

We now simply have to evaluate these integrals, and sum up the contributions on the reciprocal lattice at the chosen $\mathbf{k}$. In order to calculate these integrals, we may simply integrate them directly using the trapezium rule, which works but is slow (inaccurate) on this interval. Instead, we recognise that the representation of the interaction that we have chosen is essentially a Bessel function, and so we can use the associated recursion relations for these. We wish to use relatively large n in order to make the sum converge more quickly, and so we need fast ways of calculating Bessel functions. In fact we use two ways to find the potential depending on where we are in $\mathbf{k}$-space. We use the recursion relation (by integrating by parts) for large k. We represent using

$$V_n(k) = \frac{4\pi}{k^2} B_n(bk),$$

where

$$B_n(k) = \frac{1}{A_n}\int_0^1 dx\ cos(kx)(x(1-x))^n,$$

from which we find

$$B_n(k) = 4\frac{4n^2-1}{k^2}\left(B_{n-1}(k) - B_{n-2}(k)\right)$$

However, at small k this fails, and so we Taylor expand giving

$$B_n(k) = 1 - \frac{(n+1)}{(2+2n)}\frac{k^2}{2.1}\Big(1 - \frac{(n+2)}{(3+2n)}\frac{k^2}{4.3}\Big(1 - \frac{(n+3)}{(4+2n)}\frac{k^2}{5.6}\Big(\ldots \times\Big(1 - \frac{(n+p)}{(2p+2n+1)}\frac{k^2}{2p(2p-1)}\Big)\Big)\Big)\Big)$$

We may now calculate the dipolar matrix by evaluating the integral using either a Taylor expansion or using recursion relations. In order to calculate the dipolar matrix for the pyrochlore lattice, we use Appendix.E, which simplifies the numerics. However, in general we simply find the reciprocal lattice and sum over this. For example, for FCC, we choose the $\mathbf{k}$ point we wish to calculate $D_{\alpha\beta}(\mathbf{k})$ at, and sum over the reciprocal lattice which is the BCC lattice for this example.

The technique we have used is the same as for the Madelung sums. Once again, we get the same answer for various choices of the parameters, n and a, indicating that we have summed correctly. We will provide an explicit example of the dipolar matrix in order to compare the real space technique to this answer. We choose

$\mathbf{k} = (0, 0, \delta)$ (with $\delta = 0.000001$) which gives us

$$\begin{pmatrix}
-a & 0 & 0 & 0 & 0 & 0 & 0 & 0 & -b & 0 & -b & 0 \\
0 & -a & 0 & 0 & 0 & -b & 0 & 0 & 0 & -b & 0 & 0 \\
0 & 0 & 2a & 0 & -b & 0 & -b & 0 & 0 & 0 & 0 & 0 \\
0 & 0 & 0 & 2c & 0 & 0 & 0 & b & 0 & 0 & 0 & b \\
0 & 0 & -b & 0 & -c & 0 & b & 0 & 0 & 0 & 0 & 0 \\
0 & -b & 0 & 0 & 0 & -c & 0 & 0 & 0 & b & 0 & 0 \\
0 & 0 & -b & 0 & b & 0 & -c & 0 & 0 & 0 & 0 & 0 \\
0 & 0 & 0 & b & 0 & 0 & 0 & 2c & 0 & 0 & 0 & b \\
-b & 0 & 0 & 0 & 0 & 0 & 0 & 0 & -c & 0 & b & 0 \\
0 & -b & 0 & 0 & 0 & b & 0 & 0 & 0 & -c & 0 & 0 \\
-b & 0 & 0 & 0 & 0 & 0 & 0 & 0 & b & 0 & -c & 0 \\
0 & 0 & 0 & b & 0 & 0 & 0 & b & 0 & 0 & 0 & 2c
\end{pmatrix} \tag{9.3.7}$$

with $a = 2.0944$, $b = 1.80757$ and $c = 1.08347$.

9.3.4 The full model

For solving a particular problem, we need to have the full model written in reciprocal space. We can find the energy matrix and then minimise over $\mathbf{k}$ in order find the minimum eigenvalue. However, this may not be consistent with the spin constraint, which has become significantly harder to control. For the pyrochlore lattice, and for the case of the rare-earth pyrochlores, we have a classical model as

$$\mathcal{H} = H_C + H_D + H_1 + H_3,$$

where H_C is the crystal field, H_D is the dipolar interaction, H_1 is the nearest neighbour Heisenberg interaction, and H_3 is the third neighbour Heisenberg interaction. We represent the crystal field term as

$$\begin{aligned} H_C &= C\sum_i \left[1 - (\hat{\mathbf{z}}_{\alpha(\mathbf{i})}.\hat{\mathbf{S}}_\mathbf{i})^2\right] \\ &= CN - C\sum_{i\in t} \hat{\mathbf{S}}_\mathbf{i} \left[\hat{\mathbf{z}}_{\alpha(\mathbf{i})}\hat{\mathbf{z}}^\dagger_{\alpha(\mathbf{i})}\right] \hat{\mathbf{S}}_\mathbf{i} \end{aligned}$$

As the crystal field interaction is onsite, there is no $\mathbf{k}$ dependence, and so we simply calculate the 12×12 matrix, given by

$$H_C = \begin{pmatrix} I_0 & 0 & 0 & 0 \\ 0 & I_1 & 0 & 0 \\ 0 & 0 & I_2 & 0 \\ 0 & 0 & 0 & I_3 \end{pmatrix}$$

Where

$$\begin{aligned} I_0 &= \frac{1}{3}\begin{pmatrix} 1 & 1 & 1 \\ 1 & 1 & 1 \\ 1 & 1 & 1 \end{pmatrix} \\ I_1 &= \frac{1}{3}\begin{pmatrix} 1 & -1 & -1 \\ -1 & 1 & 1 \\ -1 & 1 & 1 \end{pmatrix} \\ I_2 &= \frac{1}{3}\begin{pmatrix} 1 & 1 & -1 \\ 1 & 1 & -1 \\ -1 & -1 & 1 \end{pmatrix} \end{aligned}$$

$$I_3 = \frac{1}{3}\begin{pmatrix} 1 & -1 & 1 \\ -1 & 1 & -1 \\ 1 & -1 & 1 \end{pmatrix}$$

We Bloch transform the Heisenberg interaction to give

$$H_{J_1} = J\sum_{\langle ij\rangle}\mathbf{S}_i.\mathbf{S}_j = J\sum_{\mathbf{k}}\mathbf{S}_{\mathbf{k}}\gamma_{\mathbf{k}}\mathbf{S}_{-\mathbf{k}},$$

where $\gamma_{\mathbf{k}}$ is the nearest neighbour structure factor given by

$$\gamma_{\mathbf{k}} = \begin{pmatrix} \mathbf{0} & \mathbf{I}\gamma_{01} & \mathbf{I}\gamma_{02} & \mathbf{I}\gamma_{03} \\ \mathbf{I}\gamma_{10} & \mathbf{0} & \mathbf{I}\gamma_{12} & \mathbf{I}\gamma_{13} \\ \mathbf{I}\gamma_{20} & \mathbf{I}\gamma_{21} & \mathbf{0} & \mathbf{I}\gamma_{23} \\ \mathbf{I}\gamma_{30} & \mathbf{I}\gamma_{31} & \mathbf{I}\gamma_{32} & \mathbf{0} \end{pmatrix},$$

$\mathbf{I}$ is a 3×3 identity matrix, and

$$\begin{aligned} \gamma_{01} &= \gamma_{10} = 2\cos(k_y + k_z) \\ \gamma_{02} &= \gamma_{20} = 2\cos(k_z + k_x) \\ \gamma_{03} &= \gamma_{30} = 2\cos(k_x + k_y) \\ \gamma_{12} &= \gamma_{21} = 2\cos(k_x - k_y) \\ \gamma_{13} &= \gamma_{31} = 2\cos(k_z - k_x) \\ \gamma_{23} &= \gamma_{32} = 2\cos(k_y - k_z) \end{aligned}$$

Finally, we find the associated structure factor for the third nearest neighbour Heisenberg interaction

$$H_{J_3} = J_3 \sum_{\langle ij \rangle_3} \mathbf{S}_i . \mathbf{S}_j = J_3 \sum_{\mathbf{k}} \mathbf{S}_{\mathbf{k}} \Gamma_{\mathbf{k}} \mathbf{S}_{-\mathbf{k}},$$

where

$$\Gamma_{\mathbf{k}} = \begin{pmatrix} \mathbf{I}\Gamma_{00} & \mathbf{0} & \mathbf{0} & \mathbf{0} \\ \mathbf{0} & \mathbf{I}\Gamma_{11} & \mathbf{0} & \mathbf{0} \\ \mathbf{0} & \mathbf{0} & \mathbf{I}\Gamma_{22} & \mathbf{0} \\ \mathbf{0} & \mathbf{0} & \mathbf{0} & \mathbf{I}\Gamma_{33} \end{pmatrix},$$

and

$$\begin{aligned} \Gamma_{00} &= 4\left[\cos^2(k_y - k_z) + \cos^2(k_z - k_x) + \cos^2(k_x - k_y) - \frac{3}{2}\right] \\ \Gamma_{11} &= 4\left[\cos^2(k_y - k_z) + \cos^2(k_z + k_x) + \cos^2(k_x + k_y) - \frac{3}{2}\right] \\ \Gamma_{22} &= 4\left[\cos^2(k_y + k_z) + \cos^2(k_z - k_x) + \cos^2(k_x + k_y) - \frac{3}{2}\right] \\ \Gamma_{33} &= 4\left[\cos^2(k_y + k_z) + \cos^2(k_z + k_x) + \cos^2(k_x - k_y) - \frac{3}{2}\right] \end{aligned}$$

Note that the third neighbour Heisenberg is diagonal in reciprocal space as it only couples to its own sublattice.

We have generated the general form of the model we wish to solve in reciprocal space, given by

$$H = \sum_{\mathbf{k}} \mathbf{S}_{\mathbf{k}} \mathbf{S}_{-\mathbf{k}} J(\mathbf{k})$$

which includes the dipole, crystal field, nearest neighbour Heisenberg and next nearest neighbour Heisenberg interactions. We minimise this over $\mathbf{k}$, and use the min-

imum eigenvalue as the answer. This provides a lower bound on the energy of the Hamiltonian, although we must check that the state maintains the spin constraint. In practice, we use this technique as a cross check to the real space technique that we will develop (which automatically keeps the spin constraint).

9.3.5 Summary and Comments

We have presented the Ewald technique, an effective way of calculating long range interactions. We take the interaction and split it into a long range part and a short range part. We then Fourier transform the long range part into a short range part in reciprocal space. We may then sum up both contributions quickly to provide the answer to the original long range real space problem. The details of this splitting have been calculated in many different ways, starting with the most simple, and ending with using Bessel-like functions. We will only calculate using the most complicated method as it is the fastest. For the Coulomb interaction, we used Ewald to control charge neutrality, but for the dipolar interaction, the $\mathbf{k} = \mathbf{0}$ issue is a real issue. We now take some time to explain the consequences of this.

The dipolar interaction could (in principle) be divergent only for *ferromagnetic* states, though we will work in the spherical crystal approximation for which the penalty is finite. For antiferromagnetism, we are automatically dealing with a $\mathbf{k}$ other than the origin. The long range dipole interaction provides an energetic penalty for the ferromagnet, involved with putting the magnetism outside of the sample and paying a large amount of energy. Instead, the dipole interaction prefers to set up *domains* of opposite orientation, paying only the surface interaction between the domains, but gaining the long range dipole interaction for a *macroscopic* (scaling with the full volume) number of spins.

The spherical crystal approximation (which we will go through next) for Ewald corresponds to taking the limit $\mathbf{k} \to \mathbf{0}$ from three orthogonal directions and averaging the answer [129].

9.4 Real Space Summation

9.4.1 Shape Anisotropy and the Spherical Crystal Approximation

For this discussion, we will only be considering ferromagnetic states as all other states have no shape anisotropy and therefore the spherical crystal approximation only applies to ferromagnets. For short range interactions the *shape* of the sample is usually not important [130]. Any interactions which depend only on the surface scale as L^2, and so are irrelevant compared to any tiny interaction which scales as L^3. However, if there is an interaction which is long range, then a spin will interact with every other spin, no matter how far away the other spins are, and as such the shape of the sample becomes part of the interaction. In these situations, one must make any calculation with reference to the particular shape, hence the spherical crystal approximation [131–133]. Shape anisotropy can have several interesting effects such as anisotropic magnetisation of the sample. If the magnetisation of the sample is anisotropic, one naïvely expects an interaction of the form

$$H \sim K(\mathbf{l}.\mathbf{m})^2,$$

where K is some energy scale, $\mathbf{l}$ is a vector which characterises the shape, and $\mathbf{m}$ is the magnetisation vector. When one tries to change $\mathbf{m}$ by applying a magnetic

field, one notices the shape via $\mathbf{l}$. If one has a spherical crystal, the symmetry of the shape means that rotations of $\mathbf{m}$ or $\mathbf{l}$ cannot contribute, and so a spherical crystal can have no such shape anisotropy. However, the dipolar interaction itself knows about the underlying lattice, and so even for a spherical crystal, anisotropy from the *local* part of the dipolar interaction would still be present. However, we may calculate the shape anisotropy from the long range of the dipolar interaction, which here is in the continuum limit (as we will explain), which shows that there is no such anisotropy.

We now calculate the spherical crystal approximation, though we work in general at first. We wish to calculate the interaction between a single spin at position $\mathbf{x}$ and the entire sample in the continuum limit. The real space technique we develop involved calculating the lattice part of the dipolar interaction, and separating it from the long range part (which is turned into a continuum problem). We need a reference calculation (the spherical crystal approximation) for which the technique is unique. In the continuum limit, we *must* have an overall ferromagnetic moment left in the sample in order for this calculation to be non-zero, which we assume here. We therefore calculate

$$E_{\alpha\beta}(\mathbf{x}) = \int_{\mathcal{S}\neq\mathbf{x}} d^3\mathbf{r}\; V(\mathbf{r},\mathbf{x}), \tag{9.4.1}$$

where $V(r,x)$ is some Hamiltonian between the spin and the continuum of surrounding spin density, and we integrate over the entire sample $\mathcal{S}$ except for the single spin which we are considering. $E_{\alpha\beta}(\mathbf{x})$ is the energy of this interaction (where the indices are the relative orientations of the sample ferromagnet and the chosen test spin), and depends implicitly upon $\mathcal{S}$. For any short range interaction $V(\mathbf{r},\mathbf{x}) \approx \delta^3(|\mathbf{x}-\mathbf{r}|)$, and so it cannot depend upon the boundary. Moreover, any interaction which *only* depends on the surface is less important than any volume dependent interaction

with a coefficient $J > \frac{1}{L}$. For interactions which do extend to the boundary we can have a finite energy penalty. If the interaction can be written as a divergence of another function

$$V(\mathbf{r}, \mathbf{x}) = \nabla . U(\mathbf{r}, \mathbf{x}), \tag{9.4.2}$$

then we can turn the volume integral into a surface integral (using the divergence theorem), at which point it does explicitly depend upon the shape as well. We work with the dipolar interaction, and so we get

$$\begin{aligned} E_{\alpha\beta}(\mathbf{x}) &= \int_{\mathcal{S}\neq\mathbf{x}} d^3r \frac{\partial^2}{\partial r_\alpha \partial r_\beta} \frac{(-1)}{|\mathbf{x}-\mathbf{r}|} \\ &= \frac{\partial^2}{\partial x_\alpha \partial x_\beta} \int_{\mathcal{S}\neq\mathbf{x}} d^3r \frac{(-1)}{|\mathbf{x}-\mathbf{r}|} \end{aligned}$$

We will calculate the spherical crystal approximation, so we calculate the quantity $E_{\alpha\beta}(\mathbf{x})$ for $\mathbf{x}$ somewhere inside the sphere. We use the point $\mathbf{x}$ to define our spherical polar coordinates, and to define the $\mathbf{z}$-axis, and therefore maintain the azimuthal symmetry. We therefore calculate

$$E_{\alpha\beta}(\mathbf{x}) = -2\pi \frac{\partial^2}{\partial x_\alpha \partial x_\beta} \int_0^\pi \frac{d\theta}{2} \sin\theta \int_\epsilon^{r(\theta)} r \; dr,$$

where $r(\theta)$ describes the boundary of the circle from the point $\mathbf{x}$, and ϵ excludes the spin itself. We may carry out the integral over r trivially, and we note that

$$r(\theta) = -x\cos\theta + \sqrt{a^2 + x^2\sin^2\theta},$$

where a is the radius of the sphere we are in. Thus we find

$$E_{\alpha\beta}(\mathbf{x}) = -2\pi \frac{\partial^2}{\partial x_\alpha \partial x_\beta} \int_\epsilon^\pi \frac{d\theta}{2} \sin\theta \left(\left[-x\cos\theta + \sqrt{a^2 + x^2 \sin^2\theta} \right]^2 - \epsilon^2 \right)$$

We expand out the squared term, and change variables to $u = \cos\theta$, and note that the cross term from the squared bracket is zero. Note also that as we are taking a derivative, the term ϵ^2 can also have no effect. Thus we have

$$E_{\alpha\beta}(\mathbf{x}) = -2\pi \frac{\partial^2}{\partial x_\alpha \partial x_\beta} \int_{-1}^1 x^2 \left(2u^2 - 1\right) \frac{du}{2},$$

from which we find

$$E_{\alpha\beta}(\mathbf{x}) = \frac{4\pi}{3} \delta_{\alpha\beta}$$

Therefore the interaction between a spin and a continuum of spin density in a sphere gives a constant energy, independent of the size of the sphere and the position within that sphere. This calculation is for a ferromagnet, and indicates that the ferromagnetic penalty for a sphere is this constant contribution on every site. For any state which is not a ferromagnet, we can recover this energy penalty by using domains which do not have a macroscopic energy cost.

We now make the difference between our problem and the usual approach to the dipolar interaction clear. As said before in Eq.9.4.2, if we can write the interaction as an integral over a surface explicitly, then we can calculate the shape dependence for the dipolar interaction. However, one assumes ferromagnetism for this in the continuum limit; we have magnetism as the *variable* and we have a lattice. We must calculate the short range contributions from the dipolar interaction as these control the local magnetism, and then see whether the long range contribution modifies the answer.

9.4.2 Mathematical Procedure

Here, we provide a new way of calculating the dipolar interaction, separating out the long range boundary dependant terms from the short range interactions. We will work in the spherical crystal approximation, in which the long range contribution happens to be zero and position independent. The mathematical tool we employ is smoothing, where we end up with a discrete model for the short range part and a continuum model for the long range part.

We begin with a lattice of spins, which we assume are classical and point like. The dipolar interaction is given by

$$\begin{aligned}\mathcal{H} &= \frac{J}{2}\sum_{j\neq j'}\frac{\hat{\mathbf{S}}_j.\hat{\mathbf{S}}_{j'}-3\left(\hat{\mathbf{r}}_{jj'}.\hat{\mathbf{S}}_j\right)\left(\hat{\mathbf{r}}_{jj'}.\hat{\mathbf{S}}_{j'}\right)}{|\mathbf{r}_{jj'}|^3}\Big|_{\mathbf{r}_{jj'}\equiv\mathbf{R}_j-\mathbf{R}_{j'}} \\ &= \frac{J}{2}\sum_{j\neq j'}\hat{\mathbf{S}}_j.\frac{\partial}{\partial\mathbf{r}_{jj'}}\hat{\mathbf{S}}_{j'}.\frac{\partial}{\partial\mathbf{r}_{jj'}}\frac{(-1)}{|\mathbf{r}_{jj'}|}\Big|_{\mathbf{r}_{jj'}=\mathbf{R}_j-\mathbf{R}_{j'}},\end{aligned}$$

which we write explicitly as

$$\begin{aligned}\mathcal{H} &= \frac{J}{2}\sum_{jj'}\hat{\mathbf{S}}_j.\begin{pmatrix}\frac{1}{r^3}-\frac{3x^2}{r^5} & -\frac{3xy}{r^5} & -\frac{3xz}{r^5}\\ -\frac{3xy}{r^5} & \frac{1}{r^3}-\frac{3y^2}{r^5} & -\frac{3xy}{r^5}\\ -\frac{3xz}{r^5} & -\frac{3yz}{r^5} & \frac{1}{r^3}-\frac{3z^2}{r^5}\end{pmatrix}.\hat{\mathbf{S}}_{j'} \\ &\equiv \frac{J}{2}\sum_{jj'}\hat{\mathbf{S}}_j.D_3(\mathbf{R}_j-\mathbf{R}_{j'}).\hat{\mathbf{S}}_{j'},\end{aligned}$$

where $r^2\equiv x^2+y^2+z^2=(\mathbf{R}_j-\mathbf{R}_{j'})^2$ and $\{x,y,z\}$ are the vectors between the two spins. We assume that the states we generate have some inherent periodicity. There exists a scale over which the magnetic state repeats itself, which is smaller than the entire crystal. This is called the magnetic superlattice, on which every spin is parallel, and can enlarge the original unit cell of the crystal. The superlattice can

consist of many sublattices, which is the details of the magnetic order. We therefore break the original lattice up; we have the superlattice vectors which move between copies of parallel spins (the magnetic periodicity). We then have the sublattice vectors, which move between the sublattices which generate the magnetic order. For example, antiferromagentism on a linear chain would have the superlattice as every other site, and the sublattice vector would be the vector between a pair of sites (which are anti-parallel). Let the sublattice label be α and the sublattice vector be $\mathbf{x}_\alpha$, and the superlattice primitive vectors be $\mathbf{R}$, which consists of N sublattices. For example see Fig.9.3. This depicts two distinct sublattices, separated by the vector $\mathbf{x}$. We then sum over the cubic superlattice generated by the vectors **1**, **2** and **3** (equivalent to $\mathbf{R}$).

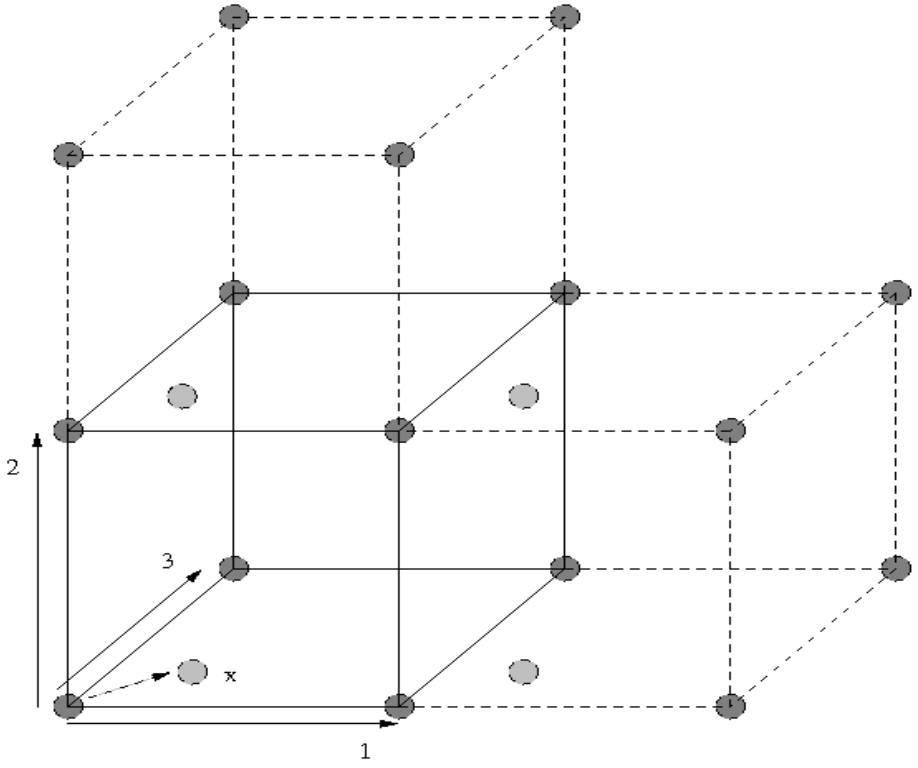

Figure 9.3: Example of splitting up a lattice with superlattice vectors **1**, **2**, **3** and the sublattice vector $\mathbf{x}$

We calculate the interaction matrix

$$J_{\alpha\beta} = \sum_{\mathbf{R}\neq 0} D_3(\mathbf{x}_{\alpha\beta} + \mathbf{R})\Big|_{\mathbf{x}_{\alpha\beta}=\mathbf{x}_\alpha - \mathbf{x}_\beta},$$

which is the interaction between sublattice α and β. We can generate the $N \times N$ interaction matrix from this, although in reality, symmetry provides most of the answer. This interaction matrix can be calculated in many ways, and here we employ real space smoothing of the spins. Note that the spins can point in arbitrary directions, as we can always rotate them, so we simply calculate the interaction matrix, and then minimise the spin directions afterwards. We will use two methods to calculate the interaction matrix. The first is called the cubic method, and is easier to understand. The second is called the anisotropic method, and while conceptually identical, it is mathematically more difficult.

9.4.3 Cubic Method

The central idea to the new technique is that of real space smoothing. We take the original point spins and smear them out over the lattice. We start with

$$\begin{aligned}\hat{\mathbf{S}}(\mathbf{r}) &= \hat{\mathbf{S}}\delta(\mathbf{r} - \mathbf{R}_{WS}) \\ &\equiv \hat{\mathbf{S}}\left[\delta(\mathbf{r} - \mathbf{R}_{WS}) - \frac{\Theta(\mathbf{r} - \mathbf{R}_{WS})}{V_{WS}}\right] + \hat{\mathbf{S}}\frac{\Theta(\mathbf{r} - \mathbf{R}_{WS})}{V_{WS}}, \end{aligned} \tag{9.4.3}$$

where WS indicates the Wigner-Seitz cell of the superlattice given by the lattice constants $\{a_x, a_y, a_z\}$, and $\hat{\mathbf{S}}$ is the direction of the spin. Note that Θ is the "top-hat" function, while δ is the usual Dirac delta-function. We have smoothed the spin over the maximum possible volume without it overlapping the next spin which is also smoothed. This creates a smooth spin density everywhere. The bracketed term

has zero average. Having zero average means that provided this term converges once we sum it up, then it cannot contribute to the long range continuum problem, so we have separated the problem into a short range part (which has no long range average) and a long range problem (the unbracketed term). We will not deal with this long range problem here, but we will work in the spherical crystal approximation for which this problem is a constant for ferromagnets.

We can substitute this into the interaction $J_{0\alpha}$, using that

$$\sum_n F(x_n) = \sum_n \int F(y)\delta(y - x_n)dy,$$

which means we turn the original sum into an integral. The parts coming from the Θ functions are therefore integrated, but the terms associated with the delta functions are simply evaluated. We therefore define and construct

$$\frac{\partial^3 D_3^I(\mathbf{r})}{\partial x \partial y \partial z} \equiv D_3(\mathbf{r}),$$

where

$$D_3^I(x,y,z) = \begin{pmatrix} \arctan\frac{yz}{xr} & \ln\frac{\sqrt{x^2+y^2}}{r+z} & \ln\frac{\sqrt{x^2+z^2}}{r+y} \\ \ln\frac{\sqrt{x^2+y^2}}{r+z} & \arctan\frac{zx}{yr} & \ln\frac{\sqrt{y^2+z^2}}{r+x} \\ \ln\frac{\sqrt{x^2+z^2}}{r+y} & \ln\frac{\sqrt{y^2+z^2}}{r+x} & \arctan\frac{xy}{zr} \end{pmatrix},$$

which comes from the smooth interaction once integrated. When we put this into Eq.9.4.3, we get

$$J_{0\alpha} = \sum_{x=X^-}^{X^+} \sum_{y=Y^-}^{Y^+} \sum_{z=Z^-}^{Z^+} A(x,y,z) + B(x,y,z) + C_0,$$

where $A(x,y,z)$ is the short range component of dipolar interaction, given by

$$\begin{aligned} A(x,y,z) &= D_3(x,y,z) - \frac{1}{a_x a_y a_z}\Big[D_3^I\left(x+\frac{a_x}{2},y+\frac{a_y}{2},z+\frac{a_z}{2}\right) \\ &- D_3^I\left(x-\frac{a_x}{2},y+\frac{a_y}{2},z+\frac{a_z}{2}\right) + D_3^I\left(x+\frac{a_x}{2},y-\frac{a_y}{2},z+\frac{a_z}{2}\right) \\ &+ D_3^I\left(x+\frac{a_x}{2},y+\frac{a_y}{2},z-\frac{a_z}{2}\right) - D_3^I\left(x-\frac{a_x}{2},y-\frac{a_y}{2},z+\frac{a_z}{2}\right) \\ &- D_3^I\left(x-\frac{a_x}{2},y+\frac{a_y}{2},z-\frac{a_z}{2}\right) - D_3^I\left(x+\frac{a_x}{2},y-\frac{a_y}{2},z-\frac{a_z}{2}\right) \\ &+ D_3^I\left(x-\frac{a_x}{2},y-\frac{a_y}{2},z-\frac{a_z}{2}\right)\Big], \end{aligned}$$

and $B(x,y,z)$ is the long range component stemming from the second Θ-function in Eq.9.4.3, C_0 is a constant term that needs compensating which we correct later.

In performing the sum over $A(x,y,z)$, the terms stemming from the smoothing add up (they were chosen to not overlap, but fill space), seen in

$$\int_a^b f(x)dx + \int_b^c f(x)dx = \int_a^c f(x)dx,$$

and so we only have to evaluate these terms at the edge of the chosen summation limit. We therefore sum over $D_3(x,y,z)$, and evaluate D_3^I at the eight edges of the chosen summation region (plus half a lattice spacing) with the appropriate phases from Eq.9.4.4. We find that compensated sum converges much more quickly than directly summing up the dipolar interaction, decaying as $\sim \frac{1}{|r|^7}$ for cubic systems (although we have to perform a fully 3-dimensional sum). We elect to stop the sum on a cube, but once we have converged the summation the final shape plays no role.

We now consider the constant term C_0 which stems from the smooth part of the interaction. In Eq.9.4.3 we are adding and subtracting a smooth contribution. We then integrate over the smooth contribution, and have a free choice in the integration

volume. We therefore choose the volume such that it corresponds to the spherical crystal approximation; a sphere with an infinitesimal puncture at the site we are considering. We have currently smoothed over the chosen spin, so we must correct the calculation by subtracting off the interaction between a spin and an infinitesimal sphere (the puncture in the spherical crystal approximation). Though this looks like a task involving a singular integral, it turns out it may still be performed. We start by writing the dipolar interaction in terms of the Green's function

$$D_d(\mathbf{r})_{ij} \propto \frac{\partial^2}{\partial x_i \partial x_j} \mathcal{G}_d(\mathbf{r}), \tag{9.4.4}$$

where $\mathcal{G}_d$ is the Green's function of the Laplacian in d dimensions. Here, we will be working with $d = 3$, but when we use the anisotropic real space method, this will not be the case. We wish to calculate

$$E_{\alpha\beta}(\mathbf{r}) = \int_{\tilde{V}} d^3\mathbf{r} \frac{\partial^2}{\partial x_i \partial x_j} \mathcal{G}_d(\mathbf{r})$$

The diagonal terms are given by

$$\frac{\partial^2}{\partial x^2} \frac{(-1)}{|\mathbf{r}|} = \frac{1}{3} \nabla_3^2 \frac{(-1)}{|\mathbf{r}|} + \frac{1}{3} \left(2\frac{\partial^2}{\partial x^2} - \frac{\partial^2}{\partial y^2} - \frac{\partial^2}{\partial z^2} \right) \frac{(-1)}{|\mathbf{r}|},$$

where ∇_d^2 is the Laplacian in d dimensions. We note that the integral of the second term vanishes for all boundaries, and that the first term may be evaluated using the identity

$$\nabla_3^2 \frac{(-1)}{|\mathbf{r} - \mathbf{R}|} = 4\pi\delta(\mathbf{r} - \mathbf{R}),$$

and so the contribution for a spin inside an infinitesimal sphere is also

$$\frac{4\pi}{3}\delta_{\alpha\beta} \tag{9.4.5}$$

We therefore make the constant term

$$C_0 = \frac{1}{a_x a_y a_z}\frac{4\pi}{3}\begin{pmatrix} 1 & 0 & 0 \\ 0 & 1 & 0 \\ 0 & 0 & 1 \end{pmatrix}$$

It turns out that the self energy is regular, and also happens to be the same as the spherical crystal approximation. We may now calculate the real space sum in the spherical crystal approximation by performing the sum over the discrete sites, adding the smooth contributions at the edge, and adding on this term which corresponds to a puncture around the chosen spin. This allows us to calculate the dipolar interaction for an arbitrary set of sublattices on a cubic or orthorhombic lattice. For the full formula that we use to calculate using this technique see Appendix.C. At the end of the next section, we compare this method to the Ewald technique. The long range smooth part of the interaction has not been controlled at all, but the *local* part of the dipolar interaction on a lattice has been calculated exactly.

9.4.4 Anisotropic Method

We now present a more efficient, but more subtle way of calculating the dipolar interaction in real space. We use the same idea, but instead of smoothing in all 3-dimensions, we split the smoothing process up and smooth in one dimension at a

time. We begin with the same $D_3(\mathbf{r})$, and smooth the spin as follows

$$\mathbf{S}(\mathbf{r}) = \hat{\mathbf{S}}\left(\left[\delta(z-Z) - \frac{1}{a_z}\Theta(z-Z)\right] + \frac{1}{a_z}\Theta(z-Z)\right)\delta(x-X)\delta(y-Y),$$

where we have smoothed over the z-axis initially. We now calculate

$$J(x,y) = \underbrace{\sum_{z=Z^-}^{Z^+} D_3(x,y,z) - \frac{1}{a_z}\int_{Z^-}^{Z^+} D_3(x,y,z)\, dz}_{D(x,y)} + \frac{1}{a_z}\int_{Z^-}^{Z^+} \Theta(z-Z^{\pm})D_3(x,y,z), \tag{9.4.6}$$

where the last term is calculated at the boundaries of the z sum, and we can find the integral exactly as

$$D_3^z(x,y,z) = \begin{pmatrix} -\frac{z}{2r^3} + \frac{z}{r}\frac{y^2-x^2}{(x^2+y^2)^2}\left[1+\frac{x^2+y^2}{2r^2}\right] & -\frac{z}{r}\frac{2xy}{(x^2+y^2)^2}\left[1+\frac{x^2+y^2}{2r^2}\right] & \frac{x}{r^3} \\ -\frac{z}{r}\frac{2xy}{(x^2+y^2)^2}\left[1+\frac{x^2+y^2}{2r^2}\right] & -\frac{z}{2r^3} + \frac{z}{r}\frac{x^2-y^2}{(x^2+y^2)^2}\left[1+\frac{x^2+y^2}{2r^2}\right] & \frac{y}{r^3} \\ \frac{x}{r^3} & \frac{y}{r^3} & \frac{z}{r^3} \end{pmatrix}$$

Note that $D_3(x,y,z)$ is ill-defined as its argument tends to zero (just as previous) but we can regularise it as we have done here using the primitive function on the boundary and ignoring the difficulty at the origin. We notice that $D(x,y)$ converges as $\frac{1}{|z|^5}$, and moreover

$$\sum_{xy} D(x,y) \tag{9.4.7}$$

converges exponentially, and so this part of the interaction is readily calculated. We now notice that the final term in Eq.9.4.6 involves several types of terms. We wish to separate out long range decaying terms from non-decaying terms, and so we find

that the only non-decaying terms are given as follows

$$\lim_{z\to\infty} D_3^z(\mathbf{r}) \equiv D_2(x,y) = \begin{pmatrix} \frac{y^2-x^2}{(x^2+y^2)^2} & -\frac{2xy}{(x^2+y^2)^2} \\ -\frac{2xy}{(x^2+y^2)^2} & \frac{x^2-y^2}{(x^2+y^2)^2} \end{pmatrix}$$

We must now deal with this. Note that there are *two* of these contributions, as D_3^z is symmetric in z, and we must include the contributions from both planes. We now use the same theory as used previously, but smooth in the x-axis. Initially we started with a full three dimensional lattice. We smoothed over the z-axis and turned the problem into a two dimensional array of *lines* of spins. Although, we only consider the ends of these lines, and so we have a two dimensional array of point spins. We therefore smooth these point spins into one dimensional lines of spins. Thus we use

$$\mathbf{S}(x,y) = \hat{\mathbf{S}}\left(\left[\delta(x-X) - \frac{1}{a_x}\Theta(x-X)\right] + \frac{1}{a_x}\Theta(x-X)\right)\delta(y-Y)$$

In the same spirit as previously, we find

$$J(y) = \underbrace{\sum_{x=X^-}^{X^+} D_2(x,y) - \frac{1}{a_x}\int_{X^-}^{X^+} D_2(x,y)\,dx}_{C(y)} + \frac{1}{a_x}\Theta(x-X^{\pm})D_2(x,y) \qquad (9.4.8)$$

Once again, $C(y)$ converges as a power law in x and exponentially in y, and we can find the integral exactly, providing

$$D_2^x \equiv \begin{pmatrix} \frac{x}{x^2+y^2} & \frac{y}{x^2+y^2} \\ \frac{y}{x^2+y^2} & -\frac{x}{x^2+y^2} \end{pmatrix},$$

and so this is readily calculated once again, and we need only the long range component from $D_2(x,y)$. Interestingly, we note that

$$\lim_{x\to\infty} D_2(x,y) \to 0,$$

but we must include the integral of these interactions, and so we have to include the interaction

$$\lim_{x\to\infty} \int_{Y^-}^{Y^+} D_2^x(x,y)\, dy = \iint dA\; D_2(x,y)$$

The subtlety here is that we are calculating the corrections to the original calculation, just as we did when we smoothed over the original spin in the cubic method. We notice that the diagonal parts of D_2^x look like the following

$$D_2^x \equiv \begin{pmatrix} \partial_x \mathcal{G}_2 & \partial_y \mathcal{G}_2 \\ \partial_y \mathcal{G}_2 & -\partial_x \mathcal{G}_2 \end{pmatrix},$$

where $\mathcal{G}_2 = \ln(\mathbf{r})$. Therefore, we find that D_2 is given by

$$D_2 \equiv \begin{pmatrix} \partial_x^2 \mathcal{G}_2 & \partial_{xy} \mathcal{G}_2 \\ \partial_{xy} \mathcal{G}_2 & -\partial_x^2 \mathcal{G}_2 \end{pmatrix},$$

and so we must correct $C(x,y)$ with the additional contribution, using Eq.9.4.4 once again,

$$\frac{1}{a_x a_y}\frac{2\pi}{2}\begin{pmatrix} 1 & 0 \\ 0 & -1 \end{pmatrix}$$

Note that there are *two* of these, just as before, as we have to compensate both planes in the limit $z \to \infty$. We must also compensate $D(x,y)$ in the same way, and

so we find

$$\iint dA\ D_2(x,y) = \lim_{z\to\infty} \iint dA\ D_3^z(x,y,z) = \iiint dV\ D_3(x,y,z),$$

and so noticing that D_3^z appears to have the form

$$\begin{pmatrix} -\frac{1}{2}\partial_z \mathcal{G}_3 & 0 & 0 \\ 0 & -\frac{1}{2}\partial_z \mathcal{G}_3 & 0 \\ 0 & 0 & \partial_z \mathcal{G}_3 \end{pmatrix}$$

means we compensate $D(x,y)$ with

$$\frac{1}{a_x a_y a_z}\frac{4\pi}{3}\begin{pmatrix} -\frac{1}{2} & 0 & 0 \\ 0 & -\frac{1}{2} & 0 \\ 0 & 0 & 1 \end{pmatrix}$$

In Appendix.C, we provide an explicit formula for both calculations, in order to exhibit the final result.

9.4.5 Summary and Comments

We have offered a new way of calculating the dipole interaction using a real space summation. We extract out the long range part from the short range part using smoothing of the spins. If we use the spherical crystal approximation, then the long range part is only a constant for ferromagnets and zero for everything else, and we may deal with simply the short range interactions other than for ferromagnets. For ferromagnets, as was discussed in the Ewald section, we should replace the energy with the appropriate domain reconstructed state. We provided two real space

calculations for calculating the interaction elements. For anisotropic systems, the cubic method is slower than the anisotropic one, but for cubic systems we see little difference between the methods. Note that we may check our interaction matrix by back transforming the structure factor from Ewald,

$$J_{\alpha\beta}(\mathbf{R}_{jj'}) \sim \sum_{\mathbf{k}}^{*} e^{i\mathbf{k}.(\mathbf{R}_{jj'}+\mathbf{c}_\alpha+\mathbf{c}_\beta)}\gamma_{\alpha\beta}(\mathbf{k})\Big|_{\mathbf{R}_{jj'}=|\mathbf{x}_j-\mathbf{x}_{j'}|},$$

up to normalisation, where $*$ means we include the term at $\mathbf{k}=\mathbf{0}$ with the average of $\mathbf{k}\to\mathbf{0}$ from the three Cartesian directions, and $\mathbf{c}_\alpha$ are the sublattice vectors. We sum over discrete $\mathbf{k}$ limited to $\frac{2\pi}{N}$ where N is the size of the cube that we want in real space.

To compare the new real space technique to Ewald, we calculate the interaction matrix for a given number of sublattices. This gives us a grid of $\mathbf{k}$ points that we can compare to by adding the real space matrices together with the appropriate phases. The technique is competitive in computer time, and provides machine accuracy, but the main advantage is that the matrix elements that we want are calculated directly, rather than having to back transform them. However, any non-trivial $\mathbf{k}$ points, or states which are larger than the periodicity that we have assumed are not included in the technique.

9.5 Summary of Methods

We have provided two methods to calculate the long range dipole interaction. The first is the standard Ewald technique, where one splits the interaction in two parts, one short range, and one long range. The long range one is then Fourier transformed to become short range in reciprocal space, and so one has two short range sums

to calculate. The new technique is to calculate the sum in real space, but limit ourselves to an inherently periodic structure. We can have as many sublattices as the computation will allow, but it is exact within this. Within the real space technique, we offered two ways of calculating; the cubic method and the anisotropic method. The anisotropic method is more subtle, and slightly harder to control numerically, but it converges slightly more quickly than the cubic method (and significantly more quickly on non-cubic lattices).

We may calculate the interaction strengths using the real space technique (rather than having to back Fourier transform them from the Ewald technique), and find the zero temperature phase diagram of the model via real space minimisation of the spins. We may also calculate using Ewald on the reciprocal lattice. We include the term at $\mathbf{k} = \mathbf{0}$ as the average of $\mathbf{k} \to \mathbf{0}$, and back transform the state to obtain numerical precision between the two techniques. We will find this phase diagram using *only* the real space technique, and we are consequently assuming mono-domains of ferromagnetism if we find ferromagnetic groundstates. We could use Ewald to find the appropriate $\mathbf{k} \to \mathbf{0}$ state instead (which would have a lower energy), which would be a multi-domain ferromagnet, but we do not here.

Chapter 10

ZERO TEMPERATURE PHASE DIAGRAM

10.1 Chapter Summary

In this chapter we provide the phase diagram to the general classical model introduced in Chap.8. This phase diagram is entirely new, and allows us to compare all the compounds that we wish to study using Tab.8.5. First we outline our minimisation technique, and depict the six relevant states for our phase diagram. We then move on to how we use our technique and the associated issues before showing the results. We provide two phase diagram; $J_3 = 0$ and $J_3 = 0.1$, though we show two of each for large and small crystal field strengths. We conclude with comments about the phase diagram, along with justifying (analytically) several of the groundstates we find. We finish with discussing the excitations of $Tb_2Sn_2O_7$, where experimental data [5] is predicted using our real space technique.

10.2 Introduction

Firstly, we introduce the technique we use in order to minimise our classical model. We have already shown the real space technique that we use to calculate the dipolar

matrix, and we shall use these matrix elements in our procedure. This justifies our focus on calculating the dipolar interaction matrix elements in real space as we are now going to use them directly. Once we are clear on the technique that we use, including the limitations, we introduce the six relevant states that we encounter in the phase diagram. We then discuss the relevant compounds placing them on our phase diagram. We elect to calculate the full phase diagram in (J_1, C) space, with fixed dipolar strength, as it allows us to see how close the compounds are to predicted phase transitions. If they are close, we cannot be fully confident of our predictions, but for most compounds the states are stable. We will find two diagrams, $J_3 = 0$ and $J_3 = 0.1$, representing the tin and titanium compounds respectively. The spin ice state (as presented in §.8.4.1) is robust to the inclusion of the third neighbour interaction, while the spiral state (§.8.4.3) and the ferromagnetic state (§.8.4.2) are easily destabalised to more exotic states which are found in the titanium compounds.

10.3 Technique

We wish to solve the following classical model at zero temperature

$$\begin{aligned} H = \; & C \sum_j \left(1 - \left[\hat{\mathbf{z}}_{\alpha(j)}.\hat{\mathbf{S}}_j\right]^2\right) \\ & + \frac{J}{2}\sum_{j\neq j'} \frac{\hat{\mathbf{S}}_j.\hat{\mathbf{S}}_{j'} - 3\left(\hat{\mathbf{R}}_{jj'}.\hat{\mathbf{S}}_j\right)\left(\hat{\mathbf{R}}_{jj'}.\hat{\mathbf{S}}_{j'}\right)}{|\mathbf{R}_{jj'}|^3}\Big|_{\mathbf{R}_{jj'}\equiv\mathbf{R}_j-\mathbf{R}_{j'}} \\ & + \frac{J_1}{2}\sum_{\langle jj'\rangle}\hat{\mathbf{S}}_j.\hat{\mathbf{S}}_{j'} + \frac{J_3}{2}\sum_{\langle jj'\rangle_3}\hat{\mathbf{S}}_j.\hat{\mathbf{S}}_{j'} \end{aligned} \tag{10.3.1}$$

The spins are classical spins, parametrised by two angles to maintain the spin length constraint as stated in Chap.2. The only term which is difficult to control is the

dipolar interaction, which we have dealt with in Chap.9.

We will work on a finite periodic lattice, and assume that the states have an inherent periodicity (which is at most the size of the lattice that we use). For example, we may start with four spins and find the $\mathbf{k} = \mathbf{0}$ phase diagram (note that pyrochlore is four atoms per unit cell and so $\mathbf{k} = \mathbf{0}$ can be anti-ferromagnetism and ferromagnetism). If we then enlarge our spin space to sixteen spins, then any state which we find again from the $\mathbf{k} = \mathbf{0}$ phase diagram, we know to be the groundstate up to 16 spins. We will *always* be restricted to a finite number of spins, and so we can never be certain of our calculations if a groundstate with a larger periodicity is relevant. We do not expect a larger periodicity to be relevant, but we cannot rule it out.

We will limit ourselves to 32 spins, finding the phase diagram limited to symmetries within this. This allows us access to $\mathbf{k} = (1/2, 1/2, 1/2)$, spin ice states and $\mathbf{k} = (1/2, 1/2, 0)$, but nothing larger. For $\mathbf{k} = (1/2, 1/2, 1/2)$ we may also use 16 spins with antisymmetry, but prefer to simply use 32 in case $\mathbf{k} = (1/2, 1/2, 0)$ were to become relevant. We use a numerical procedure to minimise our Hamiltonian, which regularly fails. We therefore have six starting conditions which are the relevant symmetries that we find throughout the phase diagram, and minimise locally from there into the groundstate. For large crystal fields, this is the only way to proceed as the optimiser never flips a spin (due to the energy barrier), but at low crystal fields the optimiser does a good job (where the landscape is much smoother). We may therefore also use random starting states at low crystal field, and locally minimise them. For details of the naming procedure and stacking procedure, see Appendix.F, but for here it is enough to know that we use 32 spins which are in two cubes of 16. We then tile this antisymmetrically, which we see in Fig.10.1, where

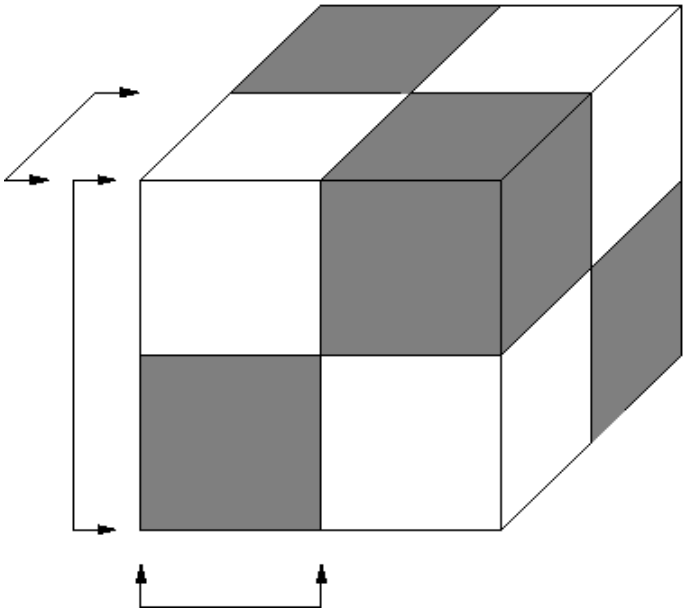

Figure 10.1: Sketch of the large cube, where each smaller cube represents 16 spins, and stacking two cubes together gives the 32 spins that we use. We also see the anti-symmetric stacking of the cubes.

one "column" is the 32 spins we depict in Fig.F.1, and the full cube contains 128 spins.

We now describe the starting states that we use, which are the simplified states that we find throughout the phase diagram, although they distort. We generate these states from some exact solutions, which appeared in [23] for the case of the line $C = 0$. For the other states, we offer some justification in Sec.10.4.1 as to why we pick these as our starting states.

We also draw them limited to 16 spins, which for $\mathbf{k} = (1/2, 1/2, 1/2)$ we tile antisymmetrically. We first examine the two natural limits of $J_1 \to \pm\infty$ in the large crystal field limit, providing the all in state and the ferromagnetic state seen in Fig.10.3 and Fig.10.2 respectively. If we have no crystal field and antiferromagnetic interactions, we generate the spiral state, seen in Fig.10.4. This optimises the local Heisenberg and dipolar energies (see Appendix.D), although is poor for crystal field

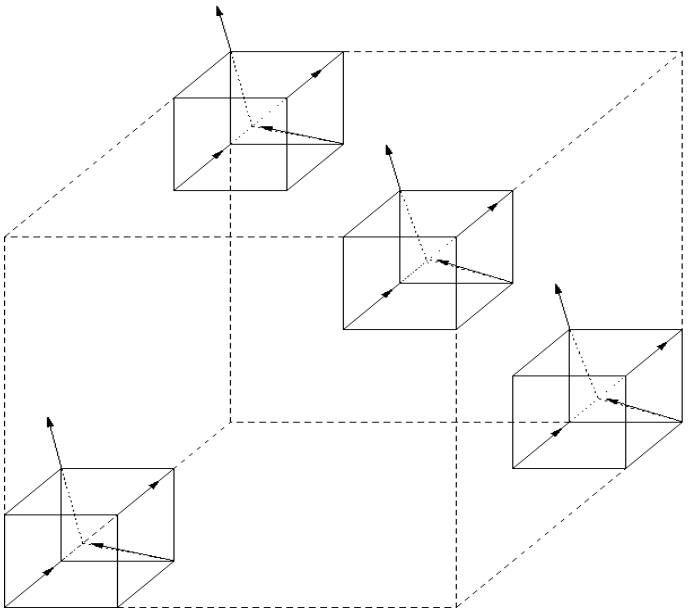

Figure 10.2: The sixteen spins making up the ferromagnetic state. Note that this is not to scale, and is drawn to make the spins easier to see.

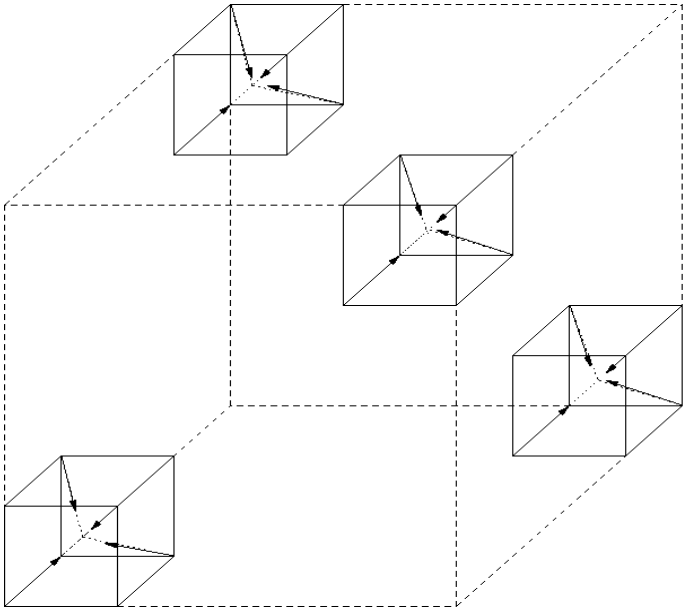

Figure 10.3: The sixteen spins making up the anti-ferromagnetic all in state

interactions. We then have the two more complicated states, the $\mathbf{k} = (001)$ spin ice state, and the $\mathbf{k} = (1/2, 1/2, 1/2)$ state. We begin with spin ice, which we depict in

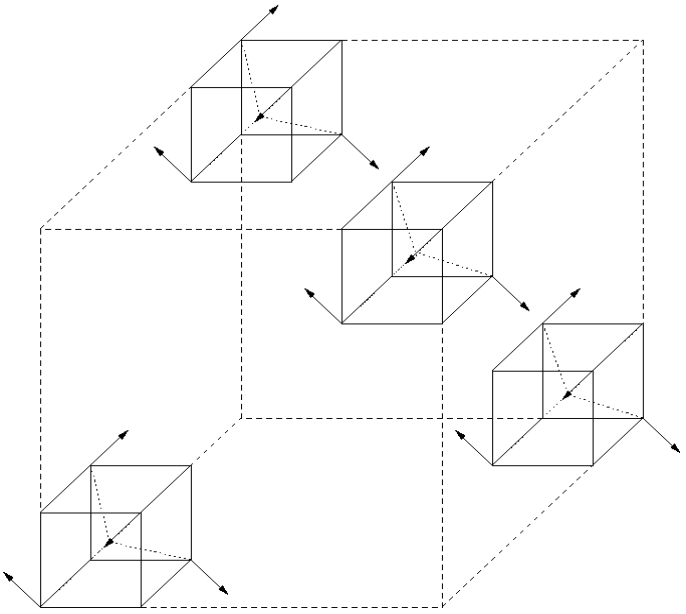

Figure 10.4: The sixteen spins making up the anti-ferromagnetic spiral state

Fig.10.5. We see the lines of spins along the (110) direction which are parallel. As we move up the $\hat{\mathbf{z}}$-axis this alternates. Finally, we show the $\mathbf{k} = (1/2, 1/2, 1/2)$ in

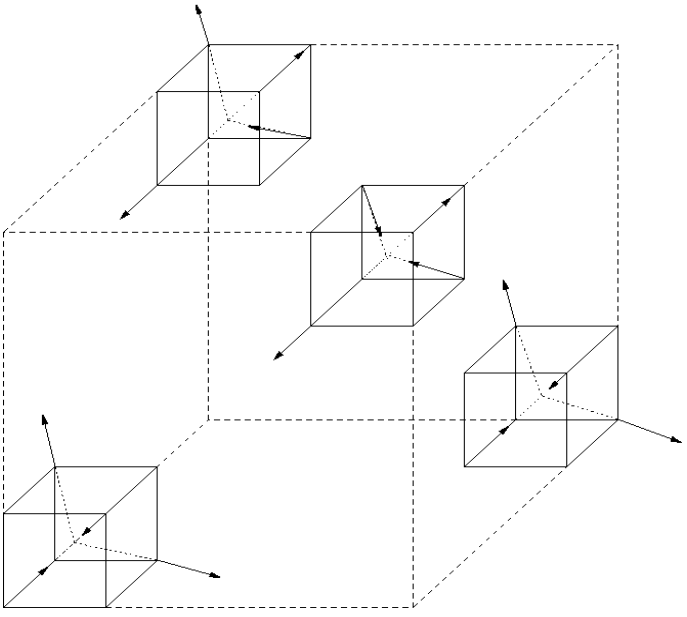

Figure 10.5: The sixteen spins making up the spin ice state

Fig.10.6. This state comprises lines of spins which are parallel along the lines, but

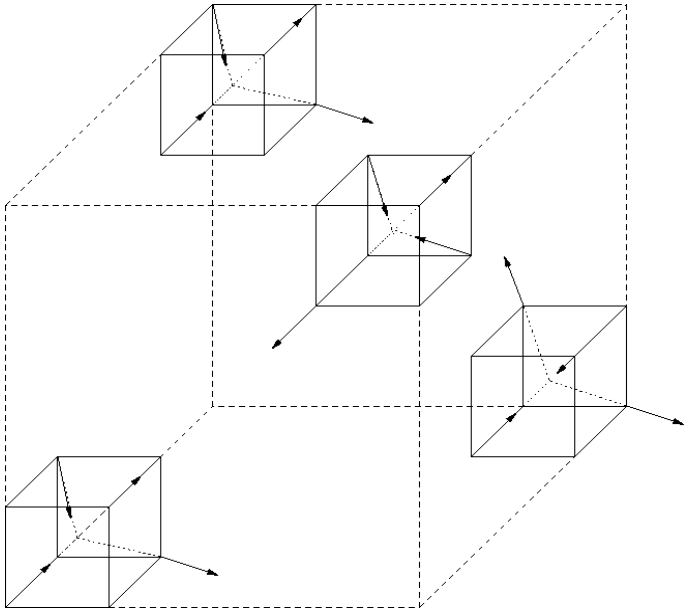

Figure 10.6: The sixteen spins making up the $\mathbf{k} = (1/2, 1/2, 1/2)$ state for $Tb_2Ti_2O_7$.

anti-parallel between neighbouring lines in all directions. We also tile this cube anti-symmetrically, and so in the next 16 spin cube, all the spins are reversed, whereas for all other states they are tiled symmetrically. These are the states we start with, and locally minimise them.

Apart from special points in phase space, these states are never the true ground-states, having small distortions to gain from the interactions which are orthogonal to the starting state. However, if we use the starting configurations, the optimiser will distort the state to the local minimum energy. We now provide an example of the type of calculation that we do in order to find the phase diagram. In Fig.10.7 we see a cut across the phase diagram at $C = 300$, varying the Heisenberg interaction. The minimum of this curve is the local groundstate, which changes as we move along. Note that the curve corresponding to the (irrelevant here) spiral state is not continuous, while the curves which become the groundstate are. This appears

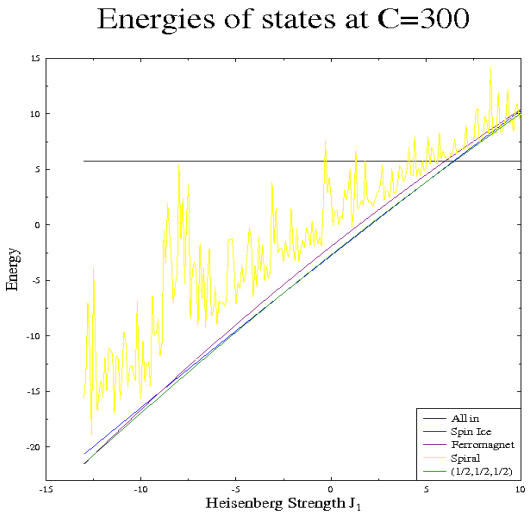

Figure 10.7: Cut across the phase diagram showing the relative energies of each starting state.

to be a consequence of the optimiser, which fails to consistently locally optimise the spiral state at large crystal field. The spiral state is totally opposed to the crystal field interaction, and so the minimiser randomly optimises this energy first, before finding the local groundstate. At low crystal field this problem goes away as the optimiser can move the spins around more freely. We may also use random starting conditions, although for us there are 2^{32} natural states, and so this procedure only works at small crystal field again. If we do use random conditions, then we find at small crystal fields, the states are reproduced in the correct regions of parameter space, although we still require many attempts. The lines that are groundstates or near groundstates however are smooth, and so we only need to find the minimum curve. Note that we work on a grid in parameter space, which leaves an inaccuracy in the point we identify as crossing. We could improve this with a finer grid, or extrapolating between the points.

10.4 Results

We now provide the $J_3 = 0$ phase diagram with $J_D = 4$ always. We begin with the large crystal field diagram, seen in Fig.10.8. To the far right labeled 4 we see the all

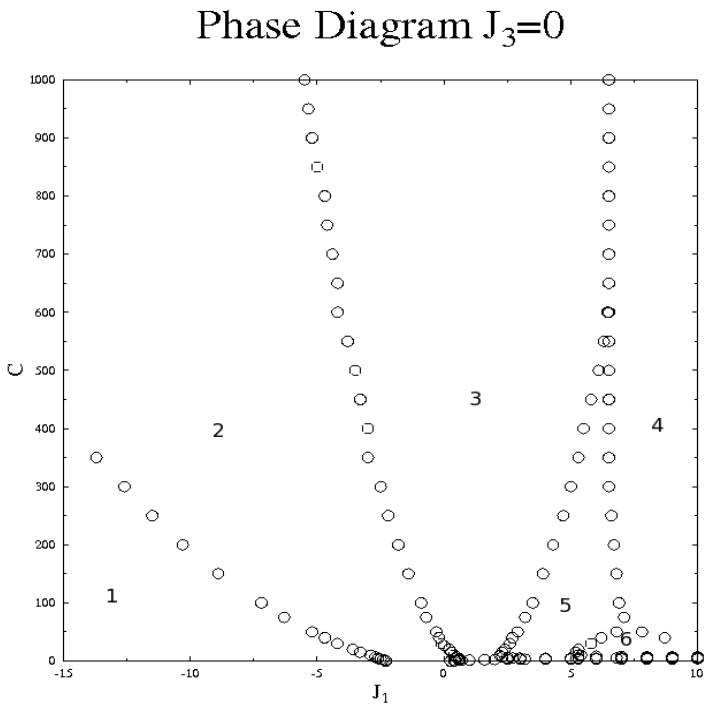

Figure 10.8: The (J_1, C) phase diagram for large crystal field with $J_3 = 0.0$. 1 is the ferromagnet, 2 is $\mathbf{k} = (1/2, 1/2, 1/2)$, 3 is spin ice, 4 is all-in-all-out, and 5 is another $\mathbf{k} = (1/2, 1/2, 1/2)$, and 6 is the terbium ferromagnet. The points are not on a smooth line due to the parameter space grid we work on.

in state, which again does well for the antiferromagnetic Heisenberg and the crystal field interactions. To the bottom left, labeled 1 we find the ferromagnet, which optimises both the ferromagnetic Heisenberg and the crystal field but does badly for the dipolar interaction. At large crystal field, the ferromagnet is along crystallographic directions, but at small crystal fields, it becomes collinear. The ferromagnetism is

destabalised by the dipolar interaction before the Heisenberg interaction becomes antiferromagnetic, to become the $\mathbf{k} = (1/2, 1/2, 1/2)$ state, labeled 2, which recovers the long range dipole and is hence the groundstate for $J < 0$. We now depict this $\mathbf{k} = (1/2, 1/2, 1/2)$ at low crystal fields. For large crystal fields, the state is the essentially the same as Fig.10.6, but with the spins distorted towards the local ferromagnetism (of each tetrahedron). However, for small crystal fields, the state is very different, though still within the $\mathbf{k} = (1/2, 1/2, 1/2)$ subspace. We depict the state at $C = 0$ and $J_1 = -1$ roughly in Fig.10.9, though there are small distortions away from this state. There is a crossover between this state and the larger crystal field

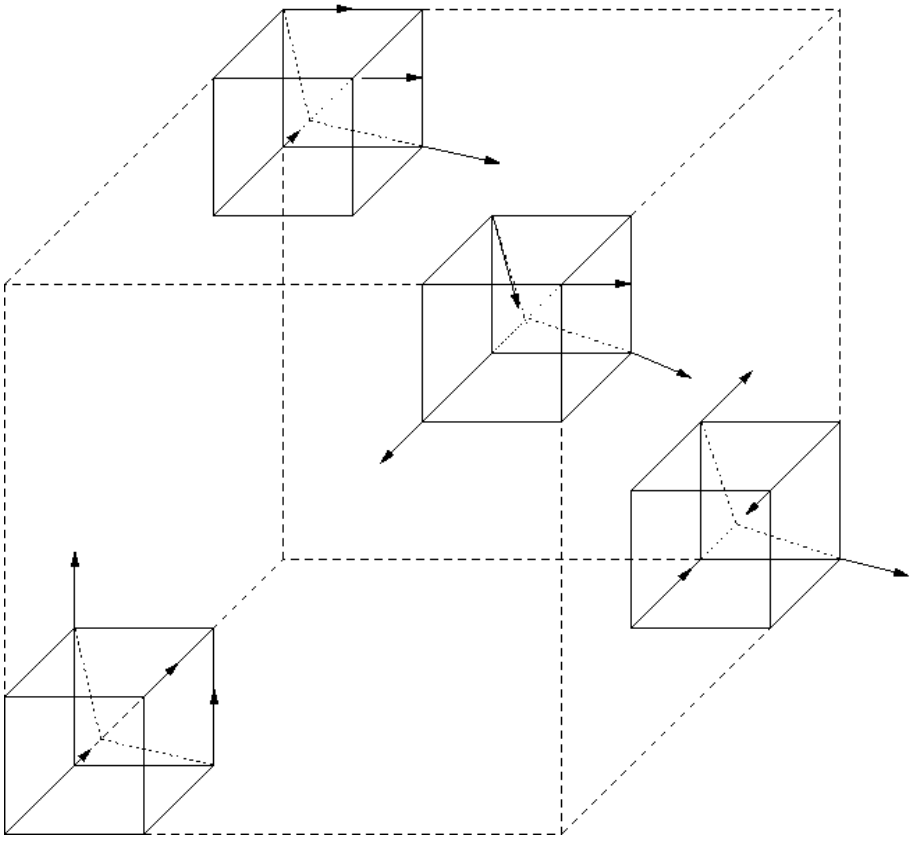

Figure 10.9: The $\mathbf{k} = (1/2, 1/2, 1/2)$ state at $C = 0$ and $J_1 = -1$, showing the dominant component of each spin.

state, although due to the lack of change of symmetry we observe no actual phase

transition. Notice the Cartesian spins, which become energetically unfavourable at relatively small crystal fields.

The next state we encounter is the spin ice state labeled 3, in our phase diagram, and is shown in Fig.10.5. This state distorts strongly as we reduce the crystal field, becoming a collinear state. We then find another $\mathbf{k} = (1/2, 1/2, 1/2)$ state, labeled 5, which is the same as 1, but the spins are distorted away from the local ferromagnetism to gain from the antiferromagnetic Heisenberg. We then find the all in state, in the region labeled 4, which is dominated by the crystal field and Heisenberg interaction, and is symmetrically prohibited from relaxing. We then find a pocket of ferromagnetism, labeled 6, which is the canted ferromagnet we expect for $Tb_2Sn_2O_7$. The spins are once again canted away from the total spin of each tetrahedron, which is ferromagnetic, but this time all the tetrahedra line up to produce a global ferromagnet.

We now move on the the small crystal field phase diagram, seen in Fig.10.10. Many of the phases are the same, except for the inclusion of the state labeled as 7, which is the spiral state. The spiral state is very opposed to the crystal field, and so only survives up to $C \sim 5$, even as $J \to \infty$, and is destabalised quickly by states which can gain the crystal field interaction. We also see that the spin ice state, labeled 3 comes down to essentially zero crystal field. We do not know whether the spin ice state also exists for $C < 0$. We also see that the second $\mathbf{k} = (1/2, 1/2, 1/2)$ labeled by 4 does not come down to $C = 0$, but does go to $J \to \infty$.

Now we include a small third neighbour interaction and find the associated phase diagram. This interaction stabalises the $\mathbf{k} = (1/2, 1/2, 1/2)$ states, as the third neighbour bonds go between sites which are anti-parallel in $\mathbf{k} = (1/2, 1/2, 1/2)$ symmetry. We find exactly this, although some states are stable to the inclusion of

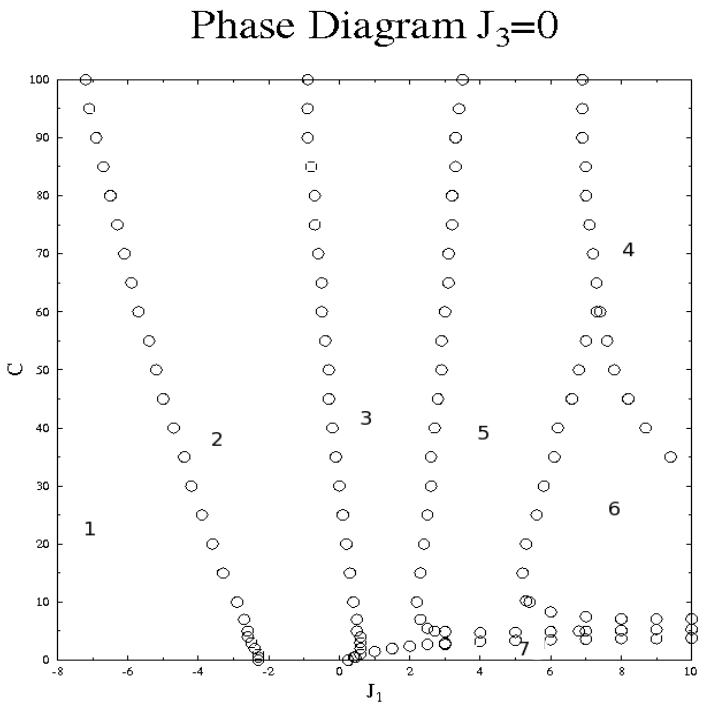

Figure 10.10: The (J_1, C) phase diagram for small crystal field with $J_3 = 0.0$. 1 is the ferromagnet, 2 is $\mathbf{k} = (1/2, 1/2, 1/2)$, 3 is spin ice, 4 is all in, 5 is another $\mathbf{k} = (1/2, 1/2, 1/2)$ state, 6 is the terbium ferromagnet, and 7 is the spiral state.

this interaction. We start with the large crystal field diagram with $J_3 = 0.1$, seen in Fig.10.11. For large negative Heisenberg interactions, we find the ferromagnetic state labeled 1, exactly the same state as was found previously. This state transits more quickly into the $\mathbf{k} = (1/2, 1/2, 1/2)$ labeled 2. We then find the spin ice state labeled 3, once again the same as before. We find another $\mathbf{k} = (1/2, 1/2, 1/2)$ state labeled 5, which destabalises the terbium ferromagnet completely so that we cannot observe it in this diagram. Finally, we still have the all in state labeled 4, which has a higher energy, and so is slightly smaller in area here.

If we move to the small crystal field phase diagram we can see another state

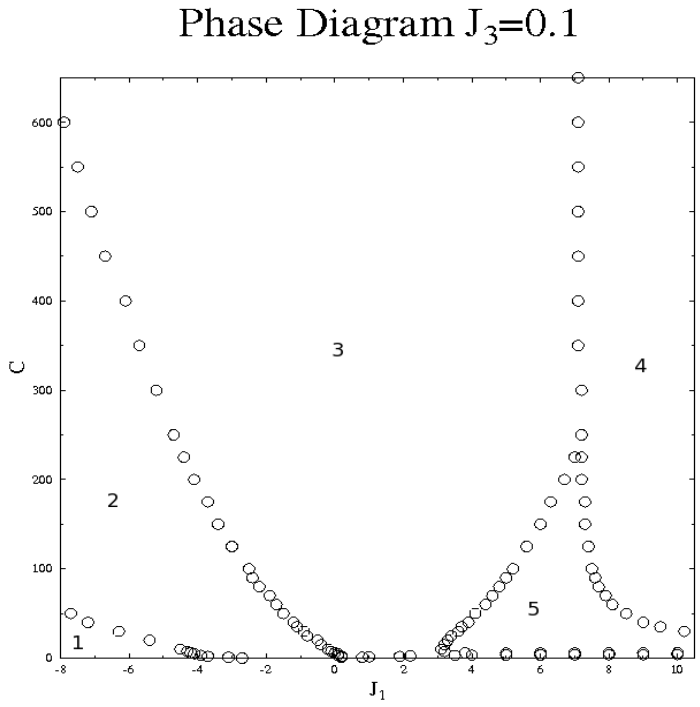

Figure 10.11: The (J_1, C) phase diagram for large crystal field with $J_3 = 0.1$. 1 is the ferromagnet, 2 is $\mathbf{k} = (1/2, 1/2, 1/2)$, 3 is spin ice, 4 is the all-in-all-out state, and 5 is a $\mathbf{k} = (1/2, 1/2, 1/2)$ state.

here, seen in Fig.10.12. Here, we find another $\mathbf{k} = (1/2, 1/2, 1/2)$, labeled by 6. This state completely destabalises the spiral state which was present for the $J_3 = 0$ phase diagram.

We have found two phase diagrams, one for $J_3 = 0$ and one for $J_3 = 0.1$. When we include a third neighbour interaction, the regions of $\mathbf{k} = (1/2, 1/2, 1/2)$ are vastly increased, indicating that the system is very frustrated in some regions of parameter space, and unstable to small perturbations. The spin ice state is robust to the interaction, while the gadolinium spiral and the terbium ferromagnet are both destabalised quickly.

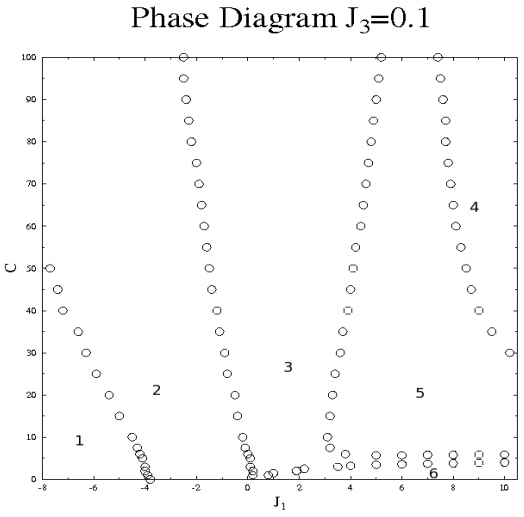

Figure 10.12: The (J_1, C) phase diagram for small crystal field with $J_3 = 0.1$. 1 is the ferromagnet, 2 is $\mathbf{k} = (1/2, 1/2, 1/2)$, 3 is spin ice, 4 is the all-in-all-out state, while 5 and 6 are both $\mathbf{k} = (1/2, 1/2, 1/2)$ states but with different local spin states.

10.4.1 Comments

Having calculated the two phase diagrams, some comments about the states that we find and the technique are in order. The phase diagrams that have been found have not been seen previously, and therefore we may only check our results by comparing Ewald and the real space technique. We have used a real space minimisation technique to solve our model numerically, which automatically maintains the spin constraint. Therefore, any state within a given periodicity is accessible. Ewald requires a non-trivial linear combination of the eigenvectors in order to maintain the spin constraint for many atoms per unit cell (in general), and therefore the states that have been found previously are energetically unfavourable [134]. We now emphasise that the phase diagrams that have been offered are modified by Ewald, and we have not included this here. An important feature is that the ferromagnetic states

are *at* $\mathbf{k} = \mathbf{0}$, and not $\mathbf{k} \to \mathbf{0}$. They all pay the long range dipole penalty therefore, and are energetically worse than they would be if we took the limit. This means that all ferromagnetic regions should be larger (in parameter space) than they are. We could use Ewald to find the phase diagram, but for every state we would have to check that the state was consistent with the spin constraint, hence the reason for using the real space technique and real space minimisation.

There is also a dramatic effect by including a relatively small third neighbour interaction. This stems from the high frustration that is present; there are many states close by in energy at any given point, and so small interactions may stabalise other states and change the phase diagram drastically. We observe this here, where the $\mathbf{k} = (1/2, 1/2, 1/2)$ states are stabalised almost everywhere.

We may now put the various compounds that we wish to study on the phase diagram. The simplest is spin ice, which has a very large crystal field, and $J_1 \sim 1.5$. This puts the spin ice state as the only possibility, even when we include the third neighbour interaction. The extensive entropy that is usually studied stems from the fact that the groundstate is stabalised by weak third neighbour *dipole* interactions, which are an order of magnitude weaker than the nearest neighbour ones which demand two in two out. The spin ice is robust against third neighbour Heisenberg interactions because for (001), the interaction cancels which means the penalty is relatively small compared to $\mathbf{k} = \mathbf{0}$ states. The gadolinium compounds live on the $C = 0$ line, with $J_1 \sim 10$, where we see the normal spiral state for $J_3 = 0$ and a rather complicated $\mathbf{k} = (1/2, 1/2, 1/2)$ state for $J_3 = 0.1$. The titanium state is a prediction from the model, to be tested against more experimental work. We see similar effects for the terbium compounds which has $C \sim 30$ and $J_1 \sim 7$. We observe a $\mathbf{k} = \mathbf{0}$ ferromagnet for the tin compound with $J_3 = 0$, and a $\mathbf{k} = (1/2, 1/2, 1/2)$

state for the titanium compound with $J_3 = 0.1$. Once again, the titanium state is a prediction. It agrees with the current experimental predictions [4], though we also predict that the spins are distorted away from the ferromagnetism (of each tetrahedron) like the tin compounds, and this needs to be verified as well.

Having provided the various states using the minimisation procedure, we now attempt to rationalise some of the states analytically. Using nearest neighbour techniques we may explain the spiral state for gadolinium, the two-in-two-out state for spin ice, and the ferromagnetism for terbium stannate. We begin with spin ice, and explain the two-in-two-out state. If we have $C = \infty$, then the spins become Ising variables, which either point in or out, yielding sixteen states per tetrahedron. If we ignore the Heisenberg interaction, which is small for the spin ice compounds, then we are left with the dipole interaction, which, in the Ising variables, is given by

$$\begin{aligned} H_{eff} &= \frac{J_D}{2} \sum_{j \neq j'} \sigma_j \sigma_{j'} \frac{\hat{\mathbf{z}}_j . \hat{\mathbf{z}}_{j'} - 3 \left(\hat{\mathbf{R}}_{jj'} . \hat{\mathbf{z}}_j \right) \left(\hat{\mathbf{R}}_{jj'} . \hat{\mathbf{z}}_{j'} \right)}{|\mathbf{R}_{jj'}|^3} \Big|_{\mathbf{R}_{jj'} \equiv \mathbf{R}_j - \mathbf{R}_{j'}} \\ &= \frac{J_D}{2} \sum_{j \neq j'} \sigma_j J_{jj'} \sigma_{j'} \end{aligned}$$

If we restrict to nearest neighbours for now, then we may calculate this exactly. We have that

$$\hat{\mathbf{z}}_j . \hat{\mathbf{z}}_{j'} = \frac{1}{3}(4\delta_{jj'} - 1)$$

for nearest neighbours, and that

$$\left(\hat{\mathbf{R}}_{jj'} . \hat{\mathbf{z}}_j \right) \left(\hat{\mathbf{R}}_{jj'} . \hat{\mathbf{z}}_{j'} \right) = -\frac{4}{\sqrt{6}},$$

where we normalise $|R_{jj'}|^2 = 1$. This interaction can be written as a sum over

tetrahedra, yielding

$$H_{eff} = -\frac{4J_D}{3} + \frac{J_D}{6}\left[6\sqrt{6}-1\right]\sum_t \left(\sigma_0+\sigma_1+\sigma_2+\sigma_3\right)^2$$

We then note that the coefficient of the squared term is positive, and so minimised by being zero, which corresponds to two spins pointing in and two pointing out. If we include the Heisenberg interaction into this, we have

$$J\sum_{jj'} \hat{\mathbf{S}}_{\mathbf{j}}.\hat{\mathbf{S}}_{\mathbf{j}'} = -J\sum_t \left(\sigma_0+\sigma_1+\sigma_2+\sigma_3\right)^2 - \frac{9}{2},$$

and so we have the stability criterion (at nearest neighbour only)

$$J < \frac{J_D}{6}(6\sqrt{6}-1),$$

for the two in two out ferromagnetic state to remain the groundstate. Note that the long range dipole interaction changes this result dramatically. The true groundstate at $\mathbf{k} = (001)$ is rather subtle to show, and requires the Ewald technique to show that the minimum in the eigenvalue is indeed at $\mathbf{k} = (001)$.

We may also justify the spiral state for gadolinium, with aid of Appendix.D. For the case of spin zero, the nearest neighbour dipolar interaction restricted to one tetrahedron reduces to

$$H = (S_0^x + S_1^x - S_2^x - S_3^x)^2 + (S_0^y + S_2^y - S_1^y - S_3^y)^2 + (S_0^z + S_3^z - S_1^z - S_2^z)^2$$

It is easy to see that this is minimised by the spiral state of gadolinium stannate,

parametrised by

$$\begin{aligned}\mathbf{S}_0 &= (-\alpha, \alpha, 0)\\ \mathbf{S}_1 &= (\alpha, \alpha, 0)\\ \mathbf{S}_2 &= (-\alpha, -\alpha, 0)\\ \mathbf{S}_3 &= (\alpha, -\alpha, 0),\end{aligned}$$

where $\alpha = \frac{1}{\sqrt{2}}$, while the Heisenberg part is optimised for any spin zero state.

We now move on to how the groundstate of terbium is ferromagnetic, despite the antiferromagnetic interactions. At large crystal field strengths, we have seen that we either have the two-in-two out state or the all in state. As we reduce the crystal field, the spins may relax to gain from the frustrated Heisenberg and dipolar interactions, but not for the all in state, which is symmetrically prohibited from relaxing. We therefore find new states at intermediate crystal fields, which can gain from the other interactions at the expense of the weakening crystal field. This is what we find for the terbium style ferromagnets. At infinite crystal fields, the two-in-two-out states may only point in one of the three Cartesian directions, and so we label these by $\hat{\mathbf{x}}_i$; the total spin in a given tetrahedron. We then calculate the local exchange field on a given site

$$\mathbf{M}_0 = J \sum_{\langle 0j \rangle} \mathbf{S}_j$$

Assuming that the spins are roughly along crystallographic directions, we can maximise the component *perpendicular* to the spin 0, which allows the spin to distort maximally. Note that all "2-in-2-out" states are the same energy at order of nearest neighbour exchange, and the field coming from a general such state is along a

Cartesian direction $\hat{\mathbf{x}}_j$. We let

$$\mathbf{S}_j \rightarrow \hat{\mathbf{z}}_{\alpha(j)}\sigma_j + \mathbf{d}_j,$$

where σ_j are the Ising variables, and $\hat{\mathbf{z}}_{\alpha(j)}$ are the local crystallographic axes, and $\mathbf{d}_j$ are the distortions away from this state, and for spin ice $\mathbf{d} = 0$. A small linear change in a spin can gain from perpendicular distortions and lose nothing from the parallel component as it scales as $\mathbf{d}^2$. The local field on a given site is given by the sum of the (Cartesian) fields coming from the two tetrahedra that the chosen spin lies in. We therefore find that

$$M_0 = J(\hat{\mathbf{x}}_i + \hat{\mathbf{x}}_j),$$

and therefore the component perpendicular to the chosen spin is given by

$$\mathbf{B}_\perp = \mathbf{S}_0 \wedge (\hat{\mathbf{x}}_i + \hat{\mathbf{x}}_j)$$

To maximise this, we want $|\hat{\mathbf{x}}_i + \hat{\mathbf{x}}_j|$ to be as large as possible, which means we want the two fields to add in parallel giving rise to the ferromagnetism. The ferromagnetism allows the spins to relax away from the crystallographic directions and gain energy from the interactions perpendicular to this direction. Therefore, the antiferromagnetism is maximised by aligning the two-in-two-out tetrahedra, and allowing the spins to relax away from the magnetic direction to gain from perpendicular interactions.

We may also investigate metastable states; for the case terbium stannate we have the experiment [5] where inelastic neutrons are used to investigate the excitations.

We may use our numerical procedure to locally minimise the state with a single spin flipped around in the ground state, and compare the *flat* band in [5] to the energy of such an excitation. However, to understand the excitation itself, we first refine the notion of excitations and spin waves, and their unusual ordering in rare earths. We call the application of the operator $\mathbf{S}^-$ a spin reduction. Spin waves correspond to creating a single delocalised spin reduction, in the form

$$\mathbf{S}_k = \frac{1}{N}\sum_j e^{i\mathbf{k}.\mathbf{r_j}}\mathbf{S}_j,$$

with a corresponding probability of finding this spin flip on each site given by the associated Bloch phase. This changes the J_z state minimally on each site, while the dispersion corresponds to how this locally orthogonal distortion moves through the system. However, although the distortion may be "small" the energy penalty can be high.

Crystal field excitations are local creatures, and correspond to flipping the spin a large amount, though the energy for such an event can be much smaller. This reversal of energy scales comes from the large number of J states in rare-earths; there are sufficiently many for the states to approximate the classical minima while spin waves are not minima. For example, in a cubic environment, there are 6 natural directions towards the cube corners. If $2J+1$ is not large enough, then the spins cannot notice the cubic symmetry. For more on rare-earths in cubic environments, see [21].

At high temperature in $Tb_2Sn_2O_7$, there are two low lying doublets, then a gap to the higher lying crystal field states [135]. It is thought that these correspond to $J_z = \pm 5$ and $J_z = \pm 4$, although the extra hexagonal symmetry will couple in more states, so this picture is not exact. The groundstate doublet is thus some linear

combination of J_z states, $|\phi^{\pm}\rangle$. This doublet cannot couple to itself as it is not a Kramer's doublet, and therefore the states are orthogonal

$$\langle\phi^{\pm}|\mathbf{J}|\phi^{\mp}\rangle = 0,$$

where $\mathbf{J}$ is the total angular momentum operator. Thus for the excitation to exist, the state we excite to must not be ϕ^{-}. It is thought that the degeneracy of this doublet is not lifted, but at low temperature the lowest degenerate doublet is split into two energy levels; the groundstate itself and an excited state, caused by the local exchange field stemming from the interactions. Previously a crystal distortion was required to break the degeneracy, but here the local interactions are sufficient to describe the physics. The observed spin flip is associated with flipping the spin between the groundstate linear combination $|\phi_0\rangle$ and a *different* linear combination corresponding to the spin pointing in a different direction to the exact inverse. Excitations to the higher states correspond to the spin waves, as the spin only cants over a small amount between the $J_z = 4$ and $J_z = 5$ for example. Again, the spin waves and spin flips are energetically in the opposite order from normal.

Using the real space technique, we can flip a single spin and let it relax, indicating the energy scale of this excitation. It is this relaxation which is crucial to understanding the low energy excitations. We find that a system with 16 spins is insufficient to describe the physics, as the spin which we have reversed is coupled to itself via the long range dipolar interaction fairly strongly. Hence, we begin with 32 spins. The relaxation of the spin causes the new state *not* to be exactly opposite to the old one; if it were then the two states would become a doublet, and there could be no coupling between the two states. As the spin relaxes the new state becomes permitted, and we find that the energy scale of the interaction accounts

very accurately for the low lying excitation observed in inelastic neutron scattering.

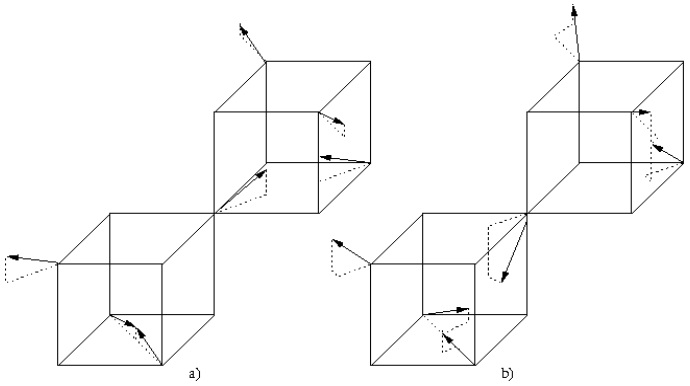

Figure 10.13: Depiction of local distortion around flipped spin sited in the center. a) corresponds to the groundstate spin configuration, while b) has the center spin flipped, indicating the relaxation of the six nearest neighbours.

We depict the distortion around the spin flip in Fig.10.13, which shows the groundstate with the ferromagnetic moment in the $\hat{\mathbf{y}}$-direction with dotted arrows, and the new distorted state with solid arrows. Local to the flipped spin are six nearest neighbours. In the terbium ground-state there exists a special ferromagnetic direction parallel to a Cartesian direction. Once the spin is flipped, it relaxes to become more anti-parallel to this direction to gain from the anti-ferromagnetic exchange. The six nearest neighbours also relax to gain from the flipped spin. The two spins which lie in the plane perpendicular to the ferromagnetic direction relax differently from the other four; they become more parallel to this direction, gaining once again from the antiferromagnetic exchange. The other four spins also increase their component parallel to the special Cartesian directions, but the components perpendicular to this are controlled be the dipolar interaction. The perpendicular component of the spin, parallel to the vector between the relevant spin and the flipped spin, is increased, gaining from the anisotropic part of the dipolar interaction.

10.5 Conclusion

We have used a numerical technique to find the zero temperature phase diagram to our classical model. In chapter 9 we showed how to generate the dipolar matrix elements, technically the most difficult part of the technique.

Our phase diagram has many groundstates, some of which are relevant to the compounds that we study. We find the spin ice state at large crystal field, as expected, which is very robust to the inclusion of a weak third neighbour interaction. We find the ferromagnetic state (in the antiferromagnetic parameter region) for $Tb_2Sn_2O_7$ which is destabalised to a $\mathbf{k} = (\frac{1}{2}, \frac{1}{2}, \frac{1}{2})$ state by a weak third neighbour interaction in agreement with experiment. We also find gadolinium has the same property; a $\mathbf{k} = \mathbf{0}$ spiral state at $J_3 = 0$ and $\mathbf{k} = (\frac{1}{2}, \frac{1}{2}, \frac{1}{2})$ for $J_3 = 0.1$. However, for gadolinium titanate the actual state we predict is not the same as the experimentally predicted state. We force the spin constraint by solving the problem in real space (which we believe to be the most important energy scale) while the experimentally obtained state does not. However, all other states are in agreement with experimentally confirmed states.

We have justified many of the states from nearest neighbour arguments, although without Ewald, groundstates to the long range dipolar interaction are rare. We have also investigated the metastable spin flip excitation in $Tb_2Sn_2O_7$ finding excellent agreement with experiment. We predict the lower band to be such an excitation, while the upper band is spin waves (in agreement with experiment).

Chapter 11

CONCLUSION

We have used two new techniques to investigate magnetism in various contexts. Transfer functions have been used to solve the thermodynamics of various one dimensional models and the one to two dimensional crossover. We have also used a new real space technique to calculate the dipolar interaction on the pyrochlore lattice. We will conclude these sections separately starting with the thermodynamics.

11.1 Thermodynamics Conclusion

We have solved the thermodynamics of several one dimensional models; the plane rotator (J_1-J_2 and B-J_1), the continuous spin Ising (B-J_1) and the Heisenberg model (J_1-J_2 and B-J_1). We have used transfer functions, the continuous version of transfer matrices, to solve these models. This technique has been used before for the nearest neighbour analogue of some of these models, although not extended to second neighbour interactions, and not at all for the continuous spin Ising model.

Having solved the models, we investigated the temperature effects on the zero temperature phase transition. Infinitesimal temperature turns this transition into a crossover immediately, but it still has the character of a transition. The two di-

mensional order is still present, but is necessarily not long range due to entropic arguments, but it may extend over a very long distance. We found an asymmetry around the zero temperature transition, which when temperature is increased destablises one of the phases more than the other. We found that fluctuations in collinear states always destabalised states which were "less" collinear (spiral states). We believe that the three models have qualitatively the same phase diagram, although the critical point is not the same. It is also clear that for isotropic models (ones for which the spin symmetry is the same as the symmetry of the Hamiltonian), the J_1-J_2 model is thermodynamically identical to a B-J_1 model, even though the details of the model (correlation functions, magnetisation) are very different.

We also investigated the magnetisation of the three models under a weak field. We believe that the Heisenberg and plane rotator are not *strongly* magnetised by weak fields, but that the continuous spin Ising model is strongly magnetised. A very small field produces a large magnetisation to a temperature much larger than the applied field. We attempted to parametrise this idea, although the behaviour is Arrhenius and is therefore not Taylor expandable, we found a expansion scheme which relates the three energy scales; β, B, J_1. Provided that $1 \gg \beta B \gg e^{-\beta J}$, the magnetisation is expandable, and we observe a strong magnetisation.

We then used the transfer function technique to investigate the one to two dimensional crossover by studying J_1-J_N models for increasing N. For the Ising model this technique works well, showing a peak in the specific heat at the expected transition temperature. We then investigated the p-state clock model, finding two anomalies in the specific heat. The lower peak is well modeled by a mean field theory, indicating it may be an Ising transition, although we can not prove it. The upper transition is not understood, although it is associated with the underlying Kosterlitz Thouless

transition, which would be which is not a divergent peak in the specific heat.

We finally investigated the J_1-J_N continuous spin Ising model. We believe there to be a transition in this model due to the lack of a continuous symmetry which breaks inversion symmetry. We see a peak around $T_C \lesssim 1$. Using mean field theory we find $T_C \approx 0.93932$, in good agreement with [52]. We use the idea that the transition is controlled by the Ising character of the spins, not the continuous degree of freedom, and found the result to be in agreement but an overestimate. Although we cannot prove there to be a transition, comparisons to the Ising model mean we are confident that there is a transition, which is unsurprising given that the symmetry of the *model* (but not spins) is the same as the Ising model.

Our use of transfer functions offers a complementary technique to Monte Carlo simulations or high temperature expansions. It is exact on the geometry that we work on (for discrete models), but has unconventional boundary conditions, with one infinite dimension and one finite one. It is not clear how this affects the results compared to square lattice Monte Carlo simulations, but we view it as an alternative technique to investigate thermodynamics in the one to two dimensional crossover. We also believe, using the regular Ising model as the basis, that short range interacting models do not depend on the boundary conditions strongly, and so we believe the technique provides a good limit to two dimensions.

11.2 Phase Diagram Conclusion

We have calculated the dipolar interaction using a new real space technique. It separates out the long range part of the dipolar interaction (which is a constant for the spherical crystal approximation), from the short range contribution. Using this technique, we may use numerical minimisation to find the groundstate of the dipole

interaction.

We want to investigate several rare earth pyrochlore compounds; $Tb_2Sn_2O_7$, $Tb_2Ti_2O_7$, $Ho_2Ti_2O_7$ ($Dy_2Ti_2O_7$), $Gd_2Sn_2O_7$ and $Gd_2Ti_2O_7$. The first compound is a ferromagnet (with antiferromagnetic interactions). The second has $\mathbf{k} = (\frac{1}{2}, \frac{1}{2}, \frac{1}{2})$. The third (and fourth) compounds are spin ice compounds with very large crystal field interactions. The tin compound for Gd is an antiferromagnetic spiral, while the titanium compound once again has $\mathbf{k} = (\frac{1}{2}, \frac{1}{2}, \frac{1}{2})$.

We generate a classical model which we numerically minimise, using nearest neighbour Heisenberg, dipolar, crystal field interactions along with third neighbour Heisenberg interactions, which are zero for tin and small for titanium. We get agreement with all the experiments in various parameter regimes, indicating that our model is in agreement with the experimentally determined groundstates for the compounds, apart from $Gd_2Ti_2O_7$ where our state has the same symmetry but is not the same state. We believe the experimental state to be incorrect as the spin constraint is not maintained, whereas the state we find has the correct symmetry, and all the spin lengths are the same. We found the phase diagram for the model in the (J_1, C) plane with two values for J_3. The third neighbour exchange *significantly* affects the groundstates indicating the degree to which the model is frustrated. The $\mathbf{k} = \mathbf{0}$ states are strongly penalised by this interaction, driving the system into $\mathbf{k} = (\frac{1}{2}, \frac{1}{2}, \frac{1}{2})$ states. Note however that we do not subtract the long range penalty of $\mathbf{k} = \mathbf{0}$ ferromagnetic states, which are unphysically penalised due to the formation of domains over long range.

Nearest neighbour interactions were used to justify the groundstate for $Tb_2Sn_2O_7$, $Gd_2Sn_2O_7$ and the two-in-two out state for spin ice. More subtle groundstates may only be "proved" using numerical techniques (and rigorously proved if the energy

agrees with the Ewald lower bound).

11.3 Further Work

This work can be extended in many different ways. The one dimensional exact thermodynamics can be extended to include the plane Ising model, to investigate the zero temperature phase transition with respect to different degrees of freedom in spin space. Mainly however, the thermodynamics can be extended by looking further in to two dimensions, as will be done in [21]. The clock model (and therefore presumably the plane rotator model as well) appears to have divergent peaks in the specific heat, in contradiction to previous thoughts. This would be investigated much more thoroughly. The continuous spin Ising model is fairly clearly understood, but again, comparisons to the plane Ising model offer insight in to the transition, especially including the anisotropy parameter Δ. Moreover, one could investigate a general $O(n)$ model with interactions which have Z_2 Ising symmetry. Finally, no work has been done in this thesis regarding the Heisenberg model in two dimensions, for which the transition temperature is believed to be zero.

The work on the phase diagram should also be extended to the $C < 0$ portion, for which the compound $Yb_2Ti_2O_7$ is believed to be relevant. Thermodynamics of the model can be investigated using Monte Carlo, and low energy excitations of the model can be examined numerically [136].

Appendix A

APPENDIX A

A.1 Special Functions

In this appendix, we define the special functions that will be used as some are non-standard notation and normalisation. We begin with the Legendre polynomials, with the orthogonality relation

$$\int_{-1}^{1} \frac{du}{2} P_n(u) P_m(u) = \frac{\delta_{nm}}{2n+1} \tag{A.1.1}$$

These are the polynomials which are orthogonal on the measure

$$\int_{-1}^{1} \frac{du}{2} \tag{A.1.2}$$

Which are order n for P_n,

$$P_n(u) = a_n u^n + a_{n-1} u^{n-1} + \ldots + a_0 \tag{A.1.3}$$

This also defines the Rodriguez formula for us

$$P_n(u) = \frac{1}{2^n n!}\frac{d^n}{du^n}(u^2-1)^n \tag{A.1.4}$$

which, with integration by parts makes the polynomials automatically orthogonal on the given measure. We also have the recursion relation

$$uP_n(u) = \frac{1}{2n+1}(nP_{n-1}(u) + (n+1)P_{n+1}) \tag{A.1.5}$$

We also use the associated Legendre Polynomials given by

$$P_l^m(u) = \frac{(-1)^m}{2^l l!}\frac{\sqrt{(l+m)!}}{\sqrt{(l-m)!}}(1-u^2)^{-\frac{m}{2}}\frac{d^{l-m}}{du^{l-m}}(u^2-1)^l \tag{A.1.6}$$

From which

$$P_l^m(u)P_l^m(u) = P_l^{-m}(u)P_l^{-m}(u) \tag{A.1.7}$$

We may use these polynomials as a basis to build the plane wave expansion. Consider two unit vectors $\hat{\mathbf{a}}_1$ and $\hat{\mathbf{a}}_2$. If we define the local $\hat{\mathbf{z}}$-axis as $\hat{\mathbf{a}}_1.\hat{\mathbf{a}}_2 = \cos\theta$, then we may expand the following

$$e^{x\hat{\mathbf{a}}_1.\hat{\mathbf{a}}_2} \equiv e^{x\cos\theta} = \sum_{l=0}^{\infty}(2l+1)I_l(x)P_l(\cos\theta) \tag{A.1.8}$$

Which clearly defines the coefficients as

$$I_l(x) \equiv \int_{-1}^{1}\frac{du}{2}P_l(u)e^{xu} \tag{A.1.9}$$

which are the modified spherical Bessel functions of the first kind. We can use the addition theorem for spherical harmonics to relate this to the associated Legendre

Polynomials, in which we keep track of the global $\hat{\mathbf{z}}$-axis, to see

$$e^{x\hat{\mathbf{S}}_0.\hat{\mathbf{S}}_1} = \sum_{l=0}^{\infty} I_l(x)(2l+1) \sum_{m=-l}^{l} P_l^m(u_0)P_l^m(u_1)e^{im(\phi_0-\phi_1)} \tag{A.1.10}$$

The spherical Bessel functions have the following identities

$$I_0(x) = \frac{\sinh x}{x} \tag{A.1.11}$$

$$\frac{dI_n(x)}{dx} = \frac{1}{2n+1}\left[nI_{n-1}(x) + (n+1)I_{n+1}(x)\right] \tag{A.1.12}$$

and

$$\frac{I_n(x)}{x} = \frac{1}{2n+1}\left[I_{n-1}(x) - I_{n+1}(x)\right] \tag{A.1.13}$$

and are related to the modified Bessel functions of the first kind

$$I_n(x) = \sqrt{\frac{\pi}{2x}}B_{n+\frac{1}{2}}(x) \tag{A.1.14}$$

We also use $B_n(x)$, which are controlled by

$$B_n(x) = \int_0^{2\pi} \frac{d\theta}{2\pi} e^{x\cos\theta}\cos(n\theta) \tag{A.1.15}$$

and have no closed form representation, and come from expanding

$$e^{x\cos\theta} = \sum_{m=-\infty}^{\infty} B_m(x)e^{im\theta} \tag{A.1.16}$$

They satisfy

$$\frac{dB_n(x)}{dx} = \frac{B_{n+1}(x) + B_{n-1}(x)}{2} \tag{A.1.17}$$

$$\frac{2n}{x}B_n(x) = B_{n-1}(x) - B_{n+1}(x) \tag{A.1.18}$$

Appendix B

APPENDIX B

B.1 Deriving the recursion relations for the Continuous-Spin Ising Model

Here we derive the recurssion relations for the continuous spin Ising model transfer matrix elements. We use two recursion relations Eq.(A.1.5) and Eq.(A.1.13) extensively. We begin with the zero field case, and consider the integral

$$H_n^m = \int_{-1}^{1} \frac{du}{2} P_n(u) I_m(xu)$$

with $x = \beta J$. Along the edge of the matrix ($m = 0$) we find

$$H_n^0 = \int_{-1}^{1} \frac{du}{2} P_n(u) \frac{\sinh xu}{xu}$$

Using Eq.(A.1.5) we find

$$H_n^0 = \frac{1}{n} \int_{-1}^{1} \frac{du}{2} \left((2n+1) P_{n-1}(u) \frac{\sinh xu}{x} - (n-1) P_{n-2}(u) \frac{\sinh xu}{xu} \right)$$

We then use our definition for the Bessel function given by Eq.(A.1.9) to see this gives us (after re-arranging)

$$H^0_{n-2} = \frac{(2n-1)}{(n-1)}\left(xI_{n-1}(x)\right) - \frac{n}{n-1}H^0_n \tag{B.1.1}$$

For the rest of the matrix we use two recursion relations (Eq.(A.1.5) and Eq.(A.1.13)) simultaneously giving the identity

$$\begin{aligned} P_n(u)I_m(xu) = \frac{x}{(2n+1)(2m+1)}\Big[&nP_{n-1}(u)I_{m-1}(xu) - nP_{n-1}(u)I_{m+1}(xu) + \\ &(n+1)P_{n+1}(u)I_{m-1}(xu) - (n+1)P_{n+1}(u)I_{m+1}(xu)\Big] \end{aligned}$$

Which we write in terms H^m_n. Then we use that $H^m_n = H^n_m$ (which means we cannot use the recursion relations for $m = n$) along with simply relabelling $n \leftrightarrow m$ to find

$$\begin{aligned} &mH^{n-1}_{m-1} - mH^{n+1}_{m-1} + (m+1)H^{n-1}_{m+1} - (m+1)H^{n+1}_{m+1} \\ &= nH^{n-1}_{m-1} - nH^{n-1}_{m+1} + (n+1)H^{n+1}_{m-1} - (n+1)H^{n+1}_{m+1} \end{aligned}$$

which gives us

$$H^{n-1}_{m+1} = H^{m+1}_{n-1} - \frac{(n-m)}{(n+m+1)}\left(H^{m-1}_{n-1} - H^{m+1}_{n+1}\right) \tag{B.1.2}$$

We run Eq.(B.1.1) backwards from the edge, starting the first term with $H^N_0 = 0$ for some N. We then use Eq.(B.1.2) to fill in the rest of the matrix. When we include a field, we use the same analysis, only the algebra is slightly more involved. We have the matrix given by

$$H^m_n = \int_{-1}^{1} \frac{du}{2} P_n(u) I_m\left(xu + y\right) e^{yu}$$

We once again start by calculating the edge terms, given by H_n^0

$$H_n^0 = \int_{-1}^{1} \frac{du}{2} P_n(u) \frac{\sinh(xu+y)}{(xu+y)} e^{yu}$$

Once again we use Eq.(A.1.5) giving us

$$H_n^0 = \frac{2n+1}{xn} \int_{-1}^{1} \frac{du}{2} P_{n-1}(u) \sinh(xu+y) e^{yu}$$
$$-\frac{(2n+1)y}{xn} \underbrace{\int_{-1}^{1} \frac{du}{2} P_{n-1}(u) \frac{\sinh(xu+y)}{(xu+y)} e^{yu}}_{H_{n-1}^0} - \frac{n-1}{n} H_{n-2}^0$$

Finally, to calculate the leftover integral, we use the identity of the Bessel function Eq.(A.1.9)

$$\begin{aligned}
\frac{2n+1}{xn} \int_{-1}^{1} \frac{du}{2} P_{n-1}(u) \sinh(xu+y) e^{yu} &= e^{y} \frac{2n+1}{xn} \int_{-1}^{1} \frac{du}{2} P_{n-1}(u) e^{u(y+x)} \\
&- e^{-y} \frac{2n+1}{xn} \int_{-1}^{1} \frac{du}{2} P_{n-1}(u) e^{u(y-x)} \\
&= \frac{2n+1}{xn} \left[e^{y} I_{n-1}(y+x) - I_{n-1}(y-x) e^{-y} \right]
\end{aligned}$$

Finally giving us the answer for the first recurssion relation after rearranging

$$H_{n-2}^0 = \left(\frac{2n-1}{n-1} \right) \left(\frac{(I_{n-1}(y+x)e^{y} - I_{n-1}(y-x)e^{-y} - H_{n-1}^0 y)}{x} \right) - \left(\frac{n}{n-1} \right) H_n^0 \tag{B.1.3}$$

When we include a field, we couple in the other matrix elements, so we need another 'edge" recursion relation, for H_n^1, given by

$$H_n^1 = \int_{-1}^{1} \frac{du}{2} P_n(u) \left[\frac{\cosh(xu+y)}{xu+y} - \frac{\sinh(xu+y)}{(xu+y)^2} \right] e^{yu}$$

We once again use Eq.(A.1.5) yielding

$$H_n^1 = \frac{(2n+1)}{xn}\int_{-1}^{1}\frac{du}{2}P_{n-1}(u)\cosh(xu+y)e^{yu} - \frac{y(2n+1)}{xn}\int_{-1}^{1}\frac{du}{2}P_{n-1}(u)\frac{\cosh(xu+y)}{(xu+y)}e^{yu}$$
$$-\frac{(2n+1)}{xn}\int_{-1}^{1}\frac{du}{2}P_{n-1}(u)\frac{\sinh(xu+y)}{(xu+y)}e^{yu} + \frac{y(2n+1)}{xn}\int_{-1}^{1}\frac{du}{2}P_{n-1}(u)\frac{\sinh(xu+y)}{(xu+y)^2}e^{yu}$$
$$-\frac{n-1}{n}H_{n-2}^1$$

We use can calculate the integral for the first term, while the other terms can be related to other matrix elements, finally giving us the second recursion relation after some algebra

$$\begin{aligned} H_1^{m-2} &= \frac{\left(\frac{y-1}{y}\right)I_{m-1}(y+x)e^{y} - \left(\frac{y+1}{y}\right)I_{m-1}(y-x)e^{-y}}{x}\frac{2m-1}{m-1} \\ &+ \frac{(m-1)H_0^{m-2}+mH_0^m}{y(m-1)} - \frac{y(2m-1)}{x(m-1)}H_1^{m-1} - \frac{m}{m-1}H_1^m \end{aligned} \quad \text{(B.1.4)}$$

It is now clear how to obtain the third recursion relation, using Eq.(A.1.5 and Eq.(A.1.13)). We find the (modified identity)

$$P_n(u)I_m(xu) = \frac{x}{(2n+1)(2m+1)}\Big[nP_{n-1}(u)I_{m-1}(xu) - nP_{n-1}(u)I_{m+1}(xu) +$$
$$(n+1)P_{n+1}(u)I_{m-1}(xu) - (n+1)P_{n+1}(u)I_{m+1}(xu)\Big]$$
$$\frac{y}{u(2n+1)(2m+1)}\Big[nP_{n-1}(u)I_{m-1}(xu) - nP_{n-1}(u)I_{m+1}(xu) +$$
$$(n+1)P_{n+1}(u)I_{m-1}(xu) - (n+1)P_{n+1}(u)I_{m+1}(xu)\Big]$$

We then notice that the last term can be re-written using Eq.(A.1.5) to give

$$P_n(u)I_m(xu) = \frac{x}{(2n+1)(2m+1)}\Big[nP_{n-1}(u)I_{m-1}(xu) - nP_{n-1}(u)I_{m+1}(xu) +$$

$$(n+1)P_{n+1}(u)I_{m-1}(xu) - (n+1)P_{n+1}(u)I_{m+1}(xu)\Big]$$
$$\frac{y}{(2m+1)}\Big[P_n(u)I_{m-1}(xu) - P_n(u)I_{m+1}(xu)\Big]$$

We then use the symmetry $H_n^m = H_m^n$ and equate, yielding

$$H_{n+1}^{m-1} = H_{n-1}^{m+1} - \frac{n-m}{n+m+1}(H_{n-1}^{m-1} - H_{n+1}^{m+1})$$
$$-\frac{y(2n+1)}{x(n+m+1)}(H_n^{m-1} - H_n^{m+1}) + \frac{y(2m+1)}{x(n+m+1)}(H_{n-1}^m - H_{n+1}^m) \qquad \text{(B.1.5)}$$

which we may use everywhere apart from $n = m$.

Appendix C

APPENDIX B

C.1 Explicit Formulae for the Real Space Dipole Interaction

We provide explicit formula for the two methods. As always, we work in the spherical crystal approximation, and any long range, shape dependent, aspects can be included if required. We provide the interaction between sublattice 0 and α. The cubic method is given by

$$\begin{aligned}
\mathbf{J}_3^{0\alpha} &= \sum_{x=-X}^{X}\sum_{y=-Y}^{Y}\sum_{z=-Z}^{Z}\mathbf{D}_3(x+c_x^\alpha, y+c_y^\alpha, z+c_z^\alpha) \\
&- \frac{1}{a_x a_y a_z}\Big(\mathbf{G}\left[X+\frac{a_x}{2}+c_x^\alpha, Y+\frac{a_y}{2}+c_y^\alpha, Z+\frac{a_z}{2}+c_z^\alpha\right] \\
&- \mathbf{G}\left[-X-\frac{a_x}{2}+c_x^\alpha, Y+\frac{a_y}{2}+c_y^\alpha, Z+\frac{a_z}{2}+c_z^\alpha\right] \\
&- \mathbf{G}\left[X+\frac{a_x}{2}+c_x^\alpha, -Y-\frac{a_y}{2}+c_y^\alpha, Z+\frac{a_z}{2}+c_z^\alpha\right] \\
&- \mathbf{G}\left[X+\frac{a_x}{2}+c_x^\alpha, Y+\frac{a_y}{2}+c_y^\alpha, -Z-\frac{a_z}{2}+c_z^\alpha\right] \\
&+ \mathbf{G}\left[-X-\frac{a_x}{2}+c_x^\alpha, -Y-\frac{a_y}{2}+c_y^\alpha, Z+\frac{a_z}{2}+c_z^\alpha\right] \\
&+ \mathbf{G}\left[-X-\frac{a_x}{2}+c_x^\alpha, Y+\frac{a_y}{2}+c_y^\alpha, -Z-\frac{a_z}{2}+c_z^\alpha\right]
\end{aligned}$$

$$
\begin{aligned}
&+ \quad \mathbf{G}\left[X + \frac{a_x}{2} + c_x^\alpha, -Y - \frac{a_y}{2} + c_y^\alpha, -Z - \frac{a_z}{2} + c_z^\alpha\right] \\
&- \quad \mathbf{G}\left[-X - \frac{a_x}{2} + c_x^\alpha, -Y - \frac{a_y}{2} + c_y^\alpha, -Z - \frac{a_z}{2} + c_z^\alpha\right]\Big) \\
&- \quad \frac{1}{a_x a_y a_z}\frac{4\pi}{3}\mathbf{I}_3
\end{aligned}
$$

Where $\mathbf{I}_n$ is an n-dimensional identity matrix, and X, Y, Z are the edges of the summation region, chosen to be large enough to converge the interaction, and c_i^α is the i-th component of the vector between sublattice 0 and sublattice α. Note that if $\mathbf{c}^\alpha = 0$, then we must not include the origin in the summation.

The anisotropic method is not as straight forward, due to the choice of regions to sum over.

$$
\begin{aligned}
\mathbf{J}_3^{0\alpha} &= \sum_{z=-Z}^{Z}\sum_{x=-A_1}^{A_1}\sum_{y=-A_1}^{A_1}\mathbf{D}_3(x + c_x^\alpha, y + c_y^\alpha, z + c_z^\alpha) \\
&- \sum_{x=-A_1}^{A_1}\sum_{y=-A_1}^{A_1}\frac{1}{a_z}\left(\mathbf{D}_3^z\left[x + c_x^\alpha, y + c_y^\alpha, Z + c_z^\alpha + \frac{a_z}{2}\right] - \mathbf{D}_3^z\left[x + c_x^\alpha, y + c_y^\alpha, -Z + c_z^\alpha - \frac{a_z}{2}\right]\right) \\
&- \mathbf{T}_3 \\
&+ \frac{2}{a_z}\sum_{x=-X}^{X}\sum_{y=-A_2}^{A_2}\mathbf{D}_2(x + c_x^\alpha, y + + c_y^\alpha) \\
&- \frac{2}{a_z}\sum_{y=-A_2}^{A_2}\frac{1}{a_x}\left(\mathbf{D}_2^x\left[X + c_x^\alpha + \frac{a_x}{2}, y\right] - \mathbf{D}_2^x\left[-X + c_x^\alpha - \frac{a_x}{2}, y\right]\right) - \frac{4}{a_z}\mathbf{T}_2
\end{aligned}
$$

Where $\mathbf{T}_3$ is the 3 dimensional self interaction to be subtracted given by

$$
\mathbf{T}_3 = \frac{1}{a_x a_y a_z}\frac{4\pi}{3}\begin{pmatrix} -\frac{1}{2} & 0 & 0 \\ 0 & -\frac{1}{2} & 0 \\ 0 & 0 & 1 \end{pmatrix}
$$

and $\mathbf{T}_2$ is the 2-dimensional self interaction, given by

$$\mathbf{T}_2 = \frac{1}{a_x a_y}\frac{2\pi}{2}\begin{pmatrix} 1 & 0 \\ 0 & -1 \end{pmatrix}$$

We also have to choose all the parameters for the summation carefully. We are taking the limit that $Z >> X$, and $Z >> A_1$, and $X >> A_2$. These must all be chosen to calculate the interaction to the desired accuracy. Again, when $\mathbf{c}^\alpha = 0$, we must not include the origin in the summation.

Finally, we set the dipolar interaction up as

$$E = \sum_{\alpha\beta} \hat{\mathbf{S}}_\alpha \cdot \mathbf{J}_3^{\alpha\beta} \cdot \hat{\mathbf{S}}_\beta \tag{C.1.1}$$

Where $\mathbf{J}_3^{\alpha\beta}$ is a $3N \times 3N$ matrix where N is the number of sublattices.

Appendix D

APPENDIX D

D.1 Showing the nearest neighbour dipole interaction as a sum of 7 quadratics

We now show that the dipole interaction, restricted to nearest neighbours may be written as a sum of seven quadratics. We define the total spin in a tetrahedron by

$$\mathbf{T} \equiv \frac{\mathbf{1}}{\mathbf{2}} \left(\mathbf{S_0} + \mathbf{S_1} + \mathbf{S_2} + \mathbf{S_3} \right) \tag{D.1.1}$$

Which allows us to write the Heisenberg interaction as

$$\mathcal{H}_H = \tilde{J} \sum_{\langle ij \rangle} \mathbf{T_i}.\mathbf{T_j} \tag{D.1.2}$$

The dipolar interaction is given by

$$\mathcal{H}_d = \frac{J}{2} \sum_{j \neq j'} \frac{\hat{\mathbf{S}}_j.\hat{\mathbf{S}}_{j'} - 3\left(\hat{\mathbf{R}}_{jj'}.\hat{\mathbf{S}}_j\right)\left(\hat{\mathbf{R}}_{jj'}.\hat{\mathbf{S}}_{j'}\right)}{|\mathbf{R}_{jj'}|^3}\Big|_{\mathbf{R}_{jj'} \equiv \mathbf{R}_j - \mathbf{R}_{j'}} \tag{D.1.3}$$

We subsume the "Heisenberg" part of this interaction into the Heisenberg interaction, and simply renormalise the strength. The residual part, restricted to a single tetrahedron, we write as

$$\tilde{\mathcal{H}} = -\frac{3J}{2}\Big[\quad (\quad S_0^y + S_0^z)(S_1^y + S_1^z) + (S_2^y - S_2^z)(S_3^y - S_3^z) \tag{D.1.4}$$

$$(\quad S_0^z + S_0^x)(S_2^z + S_2^x) + (S_1^z - S_1^x)(S_3^z - S_3^x) \tag{D.1.5}$$

$$(\quad S_0^x + S_0^y)(S_3^x + S_3^y) + (S_1^x - S_1^y)(S_2^x - S_2^y)\Big] \tag{D.1.6}$$

We now expand this out, and collect together terms to write it in a more convenient way, as follows

$$\tilde{\mathcal{H}} = -\frac{3J}{2}\Big\{\Big[S_0^x S_3^x + S_1^x S_2^x + S_0^x S_2^x + S_1^x S_3^x\Big] \tag{D.1.7}$$

$$\Big[S_0^y S_1^y + S_2^y S_3^y + S_0^y S_3^y + S_1^y S_2^y\Big] \tag{D.1.8}$$

$$\Big[S_0^z S_1^z + S_2^z S_3^z + S_1^z S_3^z + S_0^z S_2^z\Big] \tag{D.1.9}$$

$$\Big[S_0^y S_1^z + S_0^z S_1^y - S_2^y S_3^z - S_2^z S_3^y\Big] \tag{D.1.10}$$

$$\Big[S_0^z S_2^x + S_0^x S_2^z - S_1^z S_3^x - S_1^x S_3^z\Big] \tag{D.1.11}$$

$$\Big[S_0^x S_3^y + S_0^y S_3^x - S_1^x S_2^y - S_1^y S_2^x\Big]\Big\} \tag{D.1.12}$$

We shall consider the first three terms separately to the second three terms. The first three terms, we re-write again

$$\Big\{\Big[(S_0^x + S_1^x)(S_2^x + S_3^x)\Big] \tag{D.1.13}$$

$$\Big[(S_0^y + S_2^y)(S_1^y + S_3^y)\Big] \tag{D.1.14}$$

$$\Big[(S_0^z + S_3^z)(S_1^z + S_2^z)\Big]\Big\} \tag{D.1.15}$$

We then use the idea

$$(S_0^x+S_1^x) \equiv \frac{1}{2}\left((S_0^x+S_1^x+S_2^x+S_3^x)+(S_0^x+S_1^x-S_2^x+S_3^x)\right) = \frac{1}{2}\left(T_x+(S_0^x+S_1^x-S_2^x+S_3^x)\right) \tag{D.1.16}$$

For all three terms, which allows us to write the first three terms as

$$\frac{1}{4}\left[(S_0^x+S_1^x-S_2^x-S_3^x)^2+(S_0^y+S_2^y-S_1^y-S_3^y)^2+(S_0^z+S_3^z-S_1^z-S_2^z)^2-T_x^2-T_y^2-T_z^2-2\right]$$

Where we have used that the spins are normalised

$$(S_\alpha^x)^2+(S_\alpha^y)^2+(S_\alpha^z)^2 = 1 \tag{D.1.17}$$

We now have to deal with the final three terms, which we re-write as

$$\begin{aligned}
-\frac{1}{2}\Big\{\Big[\quad (\quad & \overbrace{S_0^y+S_1^y)(S_0^z+S_1^z)+(S_2^y+S_3^y)(S_2^z+S_3^z)}^{A} && \text{(D.1.18)}\\
(\quad & S_0^z+S_2^z)(S_0^x+S_2^x)+(S_1^z+S_3^z)(S_1^x+S_3^x) && \text{(D.1.19)}\\
(\quad & S_0^x+S_3^x)(S_0^y+S_3^y)+(S_1^x+S_2^x)(S_1^y+S_2^y)\Big] && \text{(D.1.20)}\\
- \quad & S_0^yS_0^z-S_1^yS_1^z-S_2^yS_2^z-S_3^yS_3^z && \text{(D.1.21)}\\
- \quad & S_0^zS_0^x-S_1^zS_1^x-S_2^zS_2^x-S_3^zS_3^x && \text{(D.1.22)}\\
- \quad & S_0^xS_0^y-S_1^xS_1^y-S_2^xS_2^y-S_3^xS_3^y\Big\} && \text{(D.1.23)}
\end{aligned}$$

We use the same idea as previous Eq.D.1.16, when considering the first term (A) to give

$$\begin{aligned}
\frac{1}{4}\Big\{ \quad & [\quad T_y+(S_0^y+S_1^y-S_2^y-S_3^y)][T_z+(S_0^z+S_1^z-S_2^z-S_3^z)] && \text{(D.1.24)}\\
- \quad & [\quad T_y-(S_0^y+S_1^y-S_2^y-S_3^y)][T_z-(S_0^z+S_1^z-S_2^z-S_3^z)]\Big\} && \text{(D.1.25)}
\end{aligned}$$

Which gives the following answer, for all three terms

$$
\begin{aligned}
-\frac{1}{2}\Big\{\Big[\quad & T_y \quad (S_0^z + S_1^z - S_2^z - S_3^z) + T_z(S_0^y + S_1^y - S_2^y - S_3^y) && \text{(D.1.26)}\\
+ \quad & T_x \quad (S_0^z - S_1^z + S_2^z - S_3^z) + T_z(S_0^x - S_1^x + S_2^x - S_3^x) && \text{(D.1.27)}\\
+ \quad & T_x \quad (S_0^y - S_1^y - S_2^y + S_3^y) + T_y(S_0^x - S_1^x - S_2^x + S_3^x)\Big] && \text{(D.1.28)}\\
- \quad & S_0^y S_0^z - S_1^y S_1^z - S_2^y S_2^z - S_3^y S_3^z && \text{(D.1.29)}\\
- \quad & S_0^z S_0^x - S_1^z S_1^x - S_2^z S_2^x - S_3^z S_3^x && \text{(D.1.30)}\\
- \quad & S_0^x S_0^y - S_1^x S_1^y - S_2^x S_2^y - S_3^x S_3^y\Big\} && \text{(D.1.31)}
\end{aligned}
$$

Finally, we notice that this is equivalent to

$$
\begin{aligned}
\frac{1}{2}\Big[& (S_0^x + S_0^y + S_0^z - T_x - T_y - T_z)^2 && \text{(D.1.32)}\\
& + (S_1^x - S_1^y - S_1^z - T_x + T_y + T_z)^2 && \text{(D.1.33)}\\
& + (-S_2^x + S_2^y - S_2^z + T_x - T_y + T_z)^2 && \text{(D.1.34)}\\
& + (-S_0^x - S_3^y + S_3^z + T_x + T_y - T_z)^2\Big] - 2T^2 && \text{(D.1.35)}
\end{aligned}
$$

And so, we can rewrite the dipolar interaction on a single tetrahedron as

$$
\begin{aligned}
\tilde{\mathcal{H}} \;=\; & \frac{3J}{2}\Big[\frac{1}{2}\big[(S_0^x + S_0^y + S_0^z - T_x - T_y - T_z)^2 + (S_1^x - S_1^y - S_1^z - T_x + T_y + T_z)^2\\
+ \; & (-S_2^x + S_2^y - S_2^z + T_x - T_y + T_z)^2 + (-S_0^x - S_3^y + S_3^z + T_x + T_y - T_z)^2\big] - 2T^2\Big]\\
+ \; & \frac{3J}{2}\Big(\frac{1}{4}\big[(S_0^x + S_1^x - S_2^x - S_3^x)^2 + (S_0^y + S_2^y - S_1^y - S_3^y)^2 + (S_0^z + S_3^z - S_1^z - S_2^z)^2\\
- \; & T_x^2 - T_y^2 - T_z^2 - 2\big]\Big)
\end{aligned}
$$

The first four quadratics act like a local crystal field, while the last three promote the spiral state.

Appendix E

APPENDIX E

E.1 Application of Ewald to the Pyrochlore lattice

The application of this is simple for FCC, but for the pyrochlore we can make use of the superlattice. As stated before, the compounds we discuss, of the form $R_2M_2O_7$ have *two* interleaved pyrochlore lattices, one for the rare earth and one for the transition metal. If we simply add both lattices together, then we create an FCC lattice, with half of the sites as non-magnetic. We therefore include titanium into the lattice which provides a small scale FCC lattice with one atom per unit cell. We can use eight reciprocal lattice points to set up the full FCC lattice, as follows

$$\mathbf{K}_0 = (111) \tag{E.1.1}$$

$$\mathbf{K}_1 = (1\bar{1}\bar{1}) \tag{E.1.2}$$

$$\mathbf{K}_2 = (\bar{1}1\bar{1}) \tag{E.1.3}$$

$$\mathbf{K}_3 = (\bar{1}\bar{1}1) \tag{E.1.4}$$

$$\mathbf{Q}_0 = (000) \tag{E.1.5}$$

$$\mathbf{Q}_1 = (200) \tag{E.1.6}$$

$$\mathbf{Q}_2 = (020) \tag{E.1.7}$$

$$\mathbf{Q}_3 = (002) \tag{E.1.8}$$

We then recognise that these are structure factor related spots, which gives us four *constraints*, allowing us to write the linear combinations

$$\mathbf{S_{k+K_0}} = \frac{1}{2}\left[-\mathbf{S_{k+Q_0}} + \mathbf{S_{k+Q_1}} + \mathbf{S_{k+Q_2}} + \mathbf{S_{k+Q_3}}\right] \tag{E.1.9}$$

$$\mathbf{S_{k+K_1}} = \frac{1}{2}\left[\mathbf{S_{k+Q_0}} - \mathbf{S_{k+Q_1}} + \mathbf{S_{k+Q_2}} + \mathbf{S_{k+Q_3}}\right] \tag{E.1.10}$$

$$\mathbf{S_{k+K_2}} = \frac{1}{2}\left[\mathbf{S_{k+Q_0}} + \mathbf{S_{k+Q_1}} - \mathbf{S_{k+Q_2}} + \mathbf{S_{k+Q_3}}\right] \tag{E.1.11}$$

$$\mathbf{S_{k+K_3}} = \frac{1}{2}\left[-\mathbf{S_{k+Q_0}} + \mathbf{S_{k+Q_1}} + \mathbf{S_{k+Q_2}} - \mathbf{S_{k+Q_3}}\right] \tag{E.1.12}$$

We write the dipolar interaction as follows

$$E_{\alpha\beta} = \sum_{\mathbf{k}} \sum_{m\in\mathcal{G}} \mathbf{S}^{*\alpha}_{\mathbf{k+Q_m}} D_{\alpha\beta}(\mathbf{k}+\mathbf{Q_m}) \mathbf{S}^{\beta}_{\mathbf{k+Q_m}} + \sum_{\mathbf{k}} \sum_{m\in\mathcal{G}} \mathbf{S}^{*\alpha}_{\mathbf{k+K_m}} D_{\alpha\beta}(\mathbf{k}+\mathbf{K_m}) \mathbf{S}^{\beta}_{\mathbf{k+K_m}} \tag{E.1.13}$$

We can substitute in the relations for the structure factors, and then only calculate *half* the number of matrices. We can rotate back to sub-lattice representation using the transformation

$$U = \frac{1}{2}\begin{pmatrix} \mathbf{I} & \mathbf{I} & \mathbf{I} & \mathbf{I} \\ \mathbf{I} & \mathbf{I} & -\mathbf{I} & -\mathbf{I} \\ \mathbf{I} & -\mathbf{I} & \mathbf{I} & -\mathbf{I} \\ \mathbf{I} & -\mathbf{I} & -\mathbf{I} & \mathbf{I} \end{pmatrix} \tag{E.1.14}$$

Where $\mathbf{I}$ are 3×3 identity matrices.

Appendix F

APPENDIX F

F.1 Details of the pyrochlore lattice

We use the following naming procedure on the pyrochlore lattice, given in Fig.F.1. This generates two cubes of sixteen spins, which we stack on top of one another.

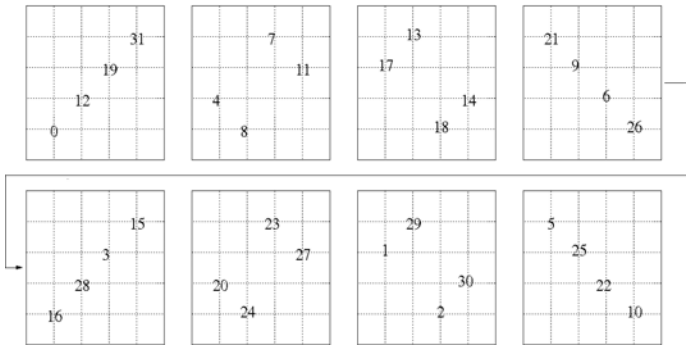

Figure F.1: Drawing of the pyrochlore lattice to show the nomenclature we use to label our sites. The arrow indicates how we "stack" the cubes of spins.

If we have four of these blocks of spins, we have a cube of 128 spins. We then use periodic boundary conditions on the column of 32 spins, and tile it in *antiphase* in the larger cube.

List of References

[1] J Wosiek. Locating analytically critical temperatures in some statistical systems. *Physical Review B*, 49(21):15023, 1994.

[2] A. P. Ramirez, A. Hayashi, R. J. Cava, S. T. Bramwell, R. Siddharthan, and B. S. Shastry. Zero-point entropy in "spin ice". *Nature*, 399, 1999.

[3] T. Fennell, O. A. Petrenko, B. Fåk, S. T. Bramwell, M. Enjalran, T. Yavors'kii, M. J. P. Gingras, R. G. Melko, and G. Balakrishnan. Neutron scattering investigation of the spin ice state in $dy_2ti_2o_7$. *Phys. Rev. B*, 70:134408, Oct 2004.

[4] K Fritsch, KA Ross, Y Qiu, JRD Copley, T Guidi, RI Bewley, HA Dabkowska, and BD Gaulin. Antiferromagnetic spin ice correlations at (1 2, 1 2, 1 2) in the ground state of the pyrochlore magnet tb 2 ti 2 o 7. *Physical Review B*, 87(9):094410, 2013.

[5] Sylvain Petit, Pierre Bonville, Isabelle Mirebeau, Hannu Mutka, and Julien Robert. Spin dynamics in the ordered spin ice $tb_2sn_2o_7$. *Phys. Rev. B*, 85:054428, Feb 2012.

[6] AS Wills, ME Zhitomirsky, B Canals, J P Sanchez, P Bonville, P Dalmas de Réotier, and A Yaouanc. Magnetic ordering in gd2sn2o7: the archetypal heisenberg pyrochlore antiferromagnet. *Journal of Physics: Condensed Matter*, 18(3):L37, 2006.

[7] SE Palmer and JT Chalker. Order induced by dipolar interactions in a geometrically frustrated antiferromagnet. *Physical Review B*, 62(1):488, 2000.

[8] P Bonville, JA Hodges, M Ocio, JP Sanchez, P Vulliet, S Sosin, and D Braithwaite. Low temperature magnetic properties of geometrically frustrated gd2sn2o7 and gd2ti2o7. *Journal of Physics: Condensed Matter*, 15(45):7777, 2003.

[9] Michael E. Fisher. Magnetism in one-dimensional systemsthe heisenberg model for infinite spin. *American Journal of Physics*, 32(5):343–346, 1964.

[10] Daniel C Mattis. Transfer matrix in plane-rotator model. *Physics Letters A*, 104(6):357–360, 1984.

[11] A.M. Cave, A.K.R Briffa, R.J. Mason, and M.W. Long. To submitted; ferromagnetism in random geometries close to the percolation threshold: Y_2crsbo_7. 2015.

[12] G Chaboussant, PA Crowell, LP Lévy, O Piovesana, A Madouri, and D Mailly. Experimental phase diagram of cu 2 (c 5 h 12 n 2) 2 cl 4: A quasi-one-dimensional antiferromagnetic spin-heisenberg ladder. *Physical Review B*, 55(5):3046, 1997.

[13] M Steiner, J Villain, and CG Windsor. Theoretical and experimental studies on one-dimensional magnetic systems. *Advances in Physics*, 25(2):87–209, 1976.

[14] H Chaker, A Kabadou, M Toumi, and R Ben Hassen. Rietveld refinement of the gadolinium strontium oxide srgd2o4. *Powder Diffraction*, 18(04):288–292, 2003.

[15] O Young, G Balakrishnan, MR Lees, and OA Petrenko. Magnetic properties of geometrically frustrated srgd 2 o 4. *Physical Review B*, 90(9):094421, 2014.

[16] OA Petrenko. Low-temperature magnetism in the honeycomb systems srln2o4. *arXiv preprint arXiv:1403.0877*, 2014.

[17] Sudip Chakravarty, Bertrand I Halperin, and David R Nelson. Low-temperature behavior of two-dimensional quantum antiferromagnets. *Physical review letters*, 60(11):1057, 1988.

[18] Assa Auerbach and Daniel P Arovas. Spin dynamics in the square-lattice antiferromagnet. *Physical review letters*, 61(5):617, 1988.

[19] M Greven, RJ Birgeneau, Y Endoh, MA Kastner, M Matsuda, and G Shirane. Neutron scattering study of the two-dimensional spins= 1/2 square-lattice heisenberg antiferromagnet sr2cuo2cl2. *Zeitschrift für Physik B Condensed Matter*, 96(4):465–477, 1995.

[20] Jürg Fröhlich and Thomas Spencer. Kosterlitz-thouless transition in the two-dimensional plane rotator and coulomb gas. *Physical Review Letters*, 46(15):1006, 1981.

[21] A.M. Cave. Thesis to be submitted. 2015.

[22] M. Robson. Thesis to be submitted. 2017.

[23] Amy KR Briffa. *Low temperature magnetic ordering of frustrated rare-earth pyrochlores*. PhD thesis, University of Birmingham, 2012.

[24] A.K.R Briffa, Cave. A.M, R.J Mason, and M.W. Long. To submitted; μ-sr does not work in truely gapless magnets. 2015.

[25] John Hubbard. Electron correlations in narrow energy bands. *Proceedings of the Royal Society of London. Series A. Mathematical and Physical Sciences*, 276(1365):238–257, 1963.

[26] Antoine Georges and Gabriel Kotliar. Hubbard model in infinite dimensions. *Physical Review B*, 45(12):6479, 1992.

[27] John C Slater and George F Koster. Simplified lcao method for the periodic potential problem. *Physical Review*, 94(6):1498, 1954.

[28] NF Mott. Metal-insulator transition. *Reviews of Modern Physics*, 40(4):677, 1968.

[29] Elliott H Lieb. Two theorems on the hubbard model. In *Condensed Matter Physics and Exactly Soluble Models*, pages 55–58. Springer, 2004.

[30] Jozef Spalek. tj model then and now: a personal perspective from the pioneering times. *arXiv preprint arXiv:0706.4236*, 2007.

[31] PW Anderson. Antiferromagnetism. theory of superexchange interaction. *Physical Review*, 79(2):350, 1950.

[32] Charles L Cleveland and Rodrigo Medina. Obtaining a heisenberg hamiltonian from the hubbard model. *American Journal of Physics*, 44(1):44–46, 1976.

[33] R.J. Mason. Midterm assessment. 2011.

[34] Rudolf Peierls. On ising's model of ferromagnetism. In *Mathematical Proceedings of the Cambridge Philosophical Society*, volume 32, pages 477–481. Cambridge Univ Press, 1936.

[35] Mariana J. Whitaker and Colin Greaves. Magnetic ordering in the pyrochlore ho2crsbo7 determined from neutron diffraction, and the magnetic properties of other {RE2CrSbO7} phases (re=y, tb, dy, er). *Journal of Solid State Chemistry*, 215(0):171 – 175, 2014.

[36] Ernst Ising. Beitrag zur theorie des ferromagnetismus. *Zeitschrift fr Physik*, 31(1):253–258, 1925.

[37] Hendrik A Kramers and Gregory H Wannier. Statistics of the two-dimensional ferromagnet. part i. *Physical Review*, 60(3):252, 1941.

[38] Lars Onsager. Crystal statistics. i. a two-dimensional model with an order-disorder transition. *Phys. Rev.*, 65:117–149, Feb 1944.

[39] C.N. Yang. The spontaneous magnetization of a two-dimensional ising model. *Physical Review*, 85(5), 1952.

[40] Elliott H. Lieb. Residual entropy of square ice. *Phys. Rev.*, 162:162–172, Oct 1967.

[41] Rodney J Baxter. Eight-vertex model in lattice statistics. *Physical Review Letters*, 26(14):832, 1971.

[42] Renfrey Burnard Potts. Some generalized order-disorder transformations. In *Mathematical Proceedings of the Cambridge Philosophical Society*, volume 48, pages 106–109. Cambridge Univ Press, 1952.

[43] MA Moore. Additional evidence for a phase transition in the plane-rotator and classical heisenberg models for two-dimensional lattices. *Physical Review Letters*, 23(15):861, 1969.

[44] John Michael Kosterlitz and David James Thouless. Ordering, metastability and phase transitions in two-dimensional systems. *Journal of Physics C: Solid State Physics*, 6(7):1181, 1973.

[45] P Butera and M Comi. Quantitative study of the kosterlitz-thouless phase transition in an xy model of two-dimensional plane rotators: High-temperature expansions to order β 20. *Physical Review B*, 47(18):11969, 1993.

[46] Seiji Miyashita, Hidetoshi Nishimori, Akira Kuroda, and Masuo Suzuki. Monte carlo simulation and static and dynamic critical behavior of the plane rotator model. *Progress of Theoretical Physics*, 60(6):1669–1685, 1978.

[47] Jorge V José, Leo P Kadanoff, Scott Kirkpatrick, and David R Nelson. Renormalization, vortices, and symmetry-breaking perturbations in the two-dimensional planar model. *Physical Review B*, 16(3):1217, 1977.

[48] N David Mermin and H Wagner. Absence of ferromagnetism or antiferromagnetism in one-or two-dimensional isotropic heisenberg models. *Physical Review Letters*, 17(22):1133, 1966.

[49] PC Hohenberg. Existence of long-range order in one and two dimensions. *Physical Review*, 158(2):383, 1967.

[50] N David Mermin. Crystalline order in two dimensions. *Physical Review*, 176(1):250, 1968.

[51] George A Baker Jr and John M Kincaid. Continuous-spin ising model and λ: ϕ 4: d field theory. *Physical Review Letters*, 42(22):1431, 1979.

[52] PA Serena, N Garci, A Levanyuk, et al. Monte carlo calculations on the two-dimensional anisotropic heisenberg model. *Physical Review B*, 47(9):5027, 1993.

[53] Garrett S Sylvester. Inequalities for continuous-spin ising ferromagnets. *Journal of Statistical Physics*, 15(4):327–341, 1976.

[54] Piotr Bialas, Philippe Blanchard, Santo Fortunato, Daniel Gandolfo, and Helmut Satz. Percolation and magnetization in the continuous spin ising model. *Nuclear Physics B*, 583(1):368–378, 2000.

[55] AD Bruce. Universality in the two-dimensional continuous spin model. *Journal of Physics A: Mathematical and General*, 18(14):L873, 1985.

[56] GS Joyce. Classical heisenberg model. *Physical Review*, 155(2):478, 1967.

[57] KH Fischer. Static properties of spin glasses. *Physical Review Letters*, 34(23):1438, 1975.

[58] Maria Axenovich and Marshall Luban. Exact ground state properties of the classical heisenberg model for giant magnetic molecules. *Physical Review B*, 63(10):100407, 2001.

[59] Christian Holm and Wolfhard Janke. Critical exponents of the classical three-dimensional heisenberg model: A single-cluster monte carlo study. *Physical Review B*, 48(2):936, 1993.

[60] Freeman J Dyson, Elliott H Lieb, and Barry Simon. Phase transitions in the quantum heisenberg model. *Physical Review Letters*, 37(3):120, 1976.

[61] Jürg Fröhlich, Barry Simon, and Thomas Spencer. Infrared bounds, phase transitions and continuous symmetry breaking. *Communications in Mathematical Physics*, 50(1):79–95, 1976.

[62] OliverA. McBryan and Thomas Spencer. On the decay of correlations inso(n)-symmetric ferromagnets. *Communications in Mathematical Physics*, 53(3):299–302, 1977.

[63] IAkov Grigorevich Sinaĭ. *Theory of phase transitions: rigorous results*, volume 108. Pergamon, 1982.

[64] HE Stanley and TA Kaplan. Possibility of a phase transition for the two-dimensional heisenberg model. *Physical Review Letters*, 17(17):913, 1966.

[65] P Chandra, P Coleman, and AI Larkin. Ising transition in frustrated heisenberg models. *Physical review letters*, 64(1):88, 1990.

[66] M Blume, P Heller, and NA Lurie. Classical one-dimensional heisenberg magnet in an applied field. *Physical Review B*, 11(11):4483, 1975.

[67] SH Liu. Critical temperature of pseudo-one-and-two-dimensional magnetic systems. *Journal of magnetism and magnetic materials*, 82(2):294–296, 1989.

[68] MP Kawatra and LJ Kijewski. Exact solution of a one-dimensional magnetic lattice gas with an ising interaction. *Physical Review*, 183(1):291, 1969.

[69] Jrg Frhlich and Thomas Spencer. The kosterlitz-thouless transition in two-dimensional abelian spin systems and the coulomb gas. *Communications in Mathematical Physics*, 81(4):527–602, 1981.

[70] Viktor Szalay. The overlap integral of associated legendre functions. *Journal of Physics A: Mathematical and General*, 23(12):2689, 1990.

[71] John Couch Adams. On the expression of the product of any two legendre's coefficients by means of a series of legendre's coefficients. *Proceedings of the Royal Society of London*, 27(185-189):63–71, 1878.

[72] A.M. Cave, A.K.R Briffa, R.J. Mason, and M.W. Long. To submitted; static thermal correlations in the j_1-j_2 heisenberg model. 2015.

[73] David P Landau and Kurt Binder. *A guide to Monte Carlo simulations in statistical physics*. Cambridge university press, 2009.

[74] P Butera, M Comi, and AJ Guttmann. Critical exponents of the three-dimensional classical plane-rotator model on the sc lattice from a high-temperature-series analysis. *Physical Review B*, 48(18):13987, 1993.

[75] Matteo Calandra Buonaura and Sandro Sorella. Numerical study of the two-dimensional heisenberg model using a green function monte carlo technique with a fixed number of walkers. *Physical Review B*, 57(18):11446, 1998.

[76] George A. Baker. Ising model with a long-range interaction in the presence of residual short-range interactions. *Phys. Rev.*, 130:1406–1411, May 1963.

[77] D. Wilms, A. Winkler, P. Virnau, and K. Binder. Monte carlo simulations of the 2d-ising model in the geometry of a long stripe. *Computer Physics Communications*, 182(9):1892 – 1895, 2011. Computer Physics Communications Special Edition for Conference on Computational Physics Trondheim, Norway, June 23-26, 2010.

[78] Ivo Souza, Carlos Lobo, and João Seixas. Testing a simple criterion for the critical temperature. *Phys. Rev. B*, 55:6356–6359, Mar 1997.

[79] M. J. Harris and M. P. Zinkin. Frustration in the pyrochlore antiferromagnets. *Modern Physics Letters B*, 10:417–438, 1996.

[80] M. I. Brammall, A. K. R. Briffa, and M. W. Long. Magnetic structure of $gd_2ti_2o_7$. *Phys. Rev. B*, 83:054422, Feb 2011.

[81] JS Helton, K Matan, MP Shores, EA Nytko, BM Bartlett, Y Yoshida, Y Takano, A Suslov, Y Qiu, J-H Chung, et al. Spin dynamics of the spin-1/2 kagome lattice antiferromagnet zncu 3 (oh) 6 cl 2. *Physical review letters*, 98(10):107204, 2007.

[82] Rajiv RP Singh and David A Huse. Ground state of the spin-1/2 kagome-lattice heisenberg antiferromagnet. *Physical Review B*, 76(18):180407, 2007.

[83] N Elstner and AP Young. Spin-1/2 heisenberg antiferromagnet on the kagome´ lattice: High-temperature expansion and exact-diagonalization studies. *Physical Review B*, 50(10):6871, 1994.

[84] David A Huse and Andrew D Rutenberg. Classical antiferromagnets on the kagomé lattice. *Physical Review B*, 45(13):7536, 1992.

[85] P. W. Anderson. Ordering and antiferromagnetism in ferrites. *Phys. Rev.*, 102:1008–1013, May 1956.

[86] H.W.J. Blte, R.F. Wielinga, and W.J. Huiskamp. Heat-capacity measurements on rare-earth double oxides r2m2o7. *Physica*, 43:549–568, 1969.

[87] et al. Bramwell, S. T. Bulk magnetization of the heavy rare earth titanate pyrochlores-a series of model frustrated magnets. *Journal of Physics: Condensed Matter*, 12:483, 2000.

[88] Y. M. Jana and D. Ghosh. Crystal-field studies of magnetic susceptibility, hyperfine, and specific heat properties of a $ho_2ti_2o_7$ single crystal. *Phys. Rev. B*, 61:9657–9664, Apr 2000.

[89] R. Moessner and J. T. Chalker. Properties of a classical spin liquid: The heisenberg pyrochlore antiferromagnet. *Phys. Rev. Lett.*, 80:2929–2932, Mar 1998.

[90] M. J. Harris, S. T. Bramwell, D. F. McMorrow, T. Zeiske, and K. W. Godfrey. Geometrical frustration in the ferromagnetic pyrochlore $ho_2ti_2O_7$. *Phys. Rev. Lett.*, 79:2554–2557, Sep 1997.

[91] Roger G Melko, Byron C den Hertog, and Michel JP Gingras. Long-range order at low temperatures in dipolar spin ice. *Physical review letters*, 87(6):067203, 2001.

[92] Olivier Cépas and B Sriram Shastry. Field-driven transitions in the dipolar pyrochlore antiferromagnet gd 2 ti 2 o 7. *Physical Review B*, 69(18):184402, 2004.

[93] SV Isakov, K Gregor, R Moessner, and SL Sondhi. Dipolar spin correlations in classical pyrochlore magnets. *Physical review letters*, 93(16):167204, 2004.

[94] C. Castelnovo, R. Moessner, and S. L. Sondhi. Magnetic monopoles in spin ice. *Nature*, 451:42–45, Jan 2008.

[95] M JP Gingras and Byron C den Hertog. Origin of spin-ice behavior in ising pyrochlore magnets with long-range dipole interactions: an insight from mean-field theory. *Canadian journal of physics*, 79(11-12):1339–1351, 2001.

[96] M. J. Harris, S. T. Bramwell, P. C. W. Holdsworth, and J. D. M. Champion. Liquid-gas critical behavior in a frustrated pyrochlore ferromagnet. *Phys. Rev. Lett.*, 81:4496–4499, Nov 1998.

[97] D Pomaranski, L. R. Yaraskavitch, S. Meng, K. A. Ross, H. M. L. Noad, H. A. Dabkowska, B. D. Gaulin, and J. B. Kycia. Absence of pauling/'s residual entropy in thermally equilibrated dy2ti2o7. *Nature*, 9, 2013.

[98] I. Mirebeau, I. Goncharenko, H. Cao, and A. Forget. Magnetic order in $tb_2sn_2o_7$ under high pressure: From ordered spin ice to spin liquid and antiferromagnetic order. *Phys. Rev. B*, 80:220407, Dec 2009.

[99] I. Mirebeau, A. Apetrei, J. Rodriguez-Carvajal, P. Bonville, A. Forget, D. Colson, V. Glazkov, J. P. Sanchez, O. Isnard, and E. Suard. Ordered spin ice state and magnetic fluctuations in $tb_2sn_2o_7$. *Phys. Rev. Lett.*, 94:246402, Jun 2005.

[100] P Bonville, I Mirebeau, A Gukasov, S Petit, and J Robert. Low temperature phase diagram for the pyrochlore compound tb2ti2o7. In *Journal of Physics: Conference Series*, volume 320, page 012006. IOP Publishing, 2011.

[101] H Cao, A Gukasov, I Mirebeau, P Bonville, and G Dhalenne. Field-induced spin-ice-like orders in spin liquid tb 2 ti 2 o 7. *Physical review letters*, 101(19):196402, 2008.

[102] I Mirebeau, IN Goncharenko, G Dhalenne, and A Revcolevschi. Pressure and field induced magnetic order in the spin liquid t b 2 t i 2 o 7 as studied by single crystal neutron diffraction. *Physical review letters*, 93(18):187204, 2004.

[103] Aksar Ali Biswas, Yatramohan Jana, and Jahangir Alam. Crystal field studies of magnetic susceptibility and specific heat properties of geometrically frustrated gd2sn2o7. In *American Institute of Physics Conference Series*, volume 1349, pages 1119–1120, 2011.

[104] JR Stewart, G Ehlers, AS Wills, St T Bramwell, and JS Gardner. Phase transitions, partial disorder and multi-k structures in gd2ti2o7. *Journal of Physics: Condensed Matter*, 16(28):L321, 2004.

[105] Byron C den Hertog and Michel JP Gingras. Dipolar interactions and origin of spin ice in ising pyrochlore magnets. *Physical review letters*, 84(15):3430, 2000.

[106] Adrian Del Maestro and Michel J. P. Gingras. Low-temperature specific heat and possible gap to magnetic excitations in the heisenberg pyrochlore antiferromagnet $gd_2sn_2o_7$. *Phys. Rev. B*, 76:064418, Aug 2007.

[107] Jason S. Gardner, Michel J. P. Gingras, and John E. Greedan. Magnetic pyrochlore oxides. *Rev. Mod. Phys.*, 82:53–107, Jan 2010.

[108] A.K.R Briffa and M.W. Long. To submitted; $gd_2sn_2o_7$ subjected to a magnetic field. 2015.

[109] Y Yafet, J Kwo, and EM Gyorgy. Dipole-dipole interactions and two-dimensional magnetism. *Physical Review B*, 33(9):6519, 1986.

[110] von E Madelung. Das elektrische feld in systemen von regelmäßig angeordneten punktladungen. *Phys. Z*, 19:524–532, 1918.

[111] MW Deem, John M Newsam, and SK Sinha. The h= 0 term in coulomb sums by the ewald transformation. *Journal of Physical Chemistry*, 94(21):8356–8359, 1990.

[112] D.C. Jiles and D.L. Atherton. Theory of ferromagnetic hysteresis. *Journal of Magnetism and Magnetic Materials*, 61(12):48 – 60, 1986.

[113] DC Jiles and DL Atherton. Ferromagnetic hysteresis. *Magnetics, IEEE Transactions on*, 19(5):2183–2185, 1983.

[114] William Fuller Brown Jr and Anton E LaBonte. Structure and energy of one-dimensional domain walls in ferromagnetic thin films. *Journal of Applied Physics*, 36(4):1380–1386, 1965.

[115] Charles Kittel. Theory of the structure of ferromagnetic domains in films and small particles. *Physical Review*, 70(11-12):965, 1946.

[116] A.M. Cave, A.K.R Briffa, R.J. Mason, and M.W. Long. To published; emplying phase boundaryies to predict phase transitions. 2015.

[117] Michael E Fisher, Shang-keng Ma, and BG Nickel. Critical exponents for long-range interactions. *Physical Review Letters*, 29(14):917, 1972.

[118] Glenn J Martyna and Mark E Tuckerman. A reciprocal space based method for treating long range interactions in ab initio and force-field-based calculations in clusters. *The Journal of chemical physics*, 110(6):2810–2821, 1999.

[119] Helmut Grubmüller, Helmut Heller, Andreas Windemuth, and Klaus Schulten. Generalized verlet algorithm for efficient molecular dynamics simulations with long-range interactions. *Molecular Simulation*, 6(1-3):121–142, 1991.

[120] Alessandro Campa, Thierry Dauxois, and Stefano Ruffo. Statistical mechanics and dynamics of solvable models with long-range interactions. *Physics Reports*, 480(3):57–159, 2009.

[121] Axel Arnold and Christian Holm. Efficient methods to compute long-range interactions for soft matter systems. In *Advanced computer simulation approaches for soft matter sciences II*, pages 59–109. Springer, 2005.

[122] SV Isakov, R Moessner, and SL Sondhi. Why spin ice obeys the ice rules. *Physical review letters*, 95(21):217201, 2005.

[123] R Magri, S-H Wei, and Alex Zunger. Ground-state structures and the random-state energy of the madelung lattice. *Physical Review B*, 42(17):11388, 1990.

[124] Paul Peter Ewald. Ewald summation. *Ann. Phys*, 369:253, 1921.

[125] Roger G Melko and Michel JP Gingras. Monte carlo studies of the dipolar spin ice model. *Journal of Physics: Condensed Matter*, 16(43):R1277, 2004.

[126] Juan J. Cerd, V. Ballenegger, O. Lenz, and C. Holm. P3m algorithm for dipolar interactions. *The Journal of Chemical Physics*, 129(23):–, 2008.

[127] Tom Darden, Lalith Perera, Leping Li, and Lee Pedersen. New tricks for modelers from the crystallography toolkit: the particle mesh ewald algorithm and its use in nucleic acid simulations. *Structure*, 7(3):R55 – R60, 1999.

[128] John Lekner. Summation of dipolar fields in simulated liquid-vapour interfaces. *Physica A: Statistical Mechanics and its Applications*, 157(2):826 – 838, 1989.

[129] CD Marquard and RB Stinchcombe. Spin-wave calculations for ferromagnetic gdcl3. *Proceedings of the Physical Society*, 92(3):665, 1967.

[130] Z. Sabsabi, F. Vernay, O. Iglesias, and H. Kachkachi. Interplay between surface anisotropy and dipolar interactions in an assembly of nanomagnets. *Phys. Rev. B*, 88:104424, Sep 2013.

[131] Charles Kittel and JK Galt. Ferromagnetic domain theory. *Solid State Physics*, 3:437–564, 1956.

[132] Soshin Chikazumi. *Physics of Ferromagnetism 2e*. Number 94. Oxford University Press, 2009.

[133] Alex Hubert, Rudolf Schafer, Alex Hubert, and R Schafer. *Magnetic domains*, volume 21. Springer, 1998.

[134] J. D. M. Champion, A. S. Wills, T. Fennell, S. T. Bramwell, J. S. Gardner, and M. A. Green. Order in the heisenberg pyrochlore: The magnetic structure of $gd_2ti_2o_7$. *Phys. Rev. B*, 64:140407, Sep 2001.

[135] J. S. Gardner, B. D. Gaulin, A. J. Berlinsky, P. Waldron, S. R. Dunsiger, N. P. Raju, and J. E. Greedan. Neutron scattering studies of the cooperative paramagnet pyrochlore $tb_2ti_2o_7$. *Phys. Rev. B*, 64:224416, Nov 2001.

[136] A.M. Cave, A.K.R Briffa, R.J. Mason, and M.W. Long. To submitted; employing domain boundaries to predict phase transitions. 2015.